František Havel

Creep in soft soils

Trondheim, May 2004

Doctoral thesis for the degree of doktor ingeniør

Norwegian University of Science and Technology
The Faculty of Engineering Science and Technology
Department of Civil and Transport Engineering

URN:NBN:no-3497

URN:NBN:no-3497

Creep in soft soils

František Havel

Thesis submitted to the Faculty of Engineering, Science and Technology,
Norwegian University of Science and Technology, in partial fulfilment of the
requirements for the degree of Doktor ingeniør

Geotechnical Division
Department of Civil and Transport Engineering
Norwegian University of Science and Technology

May 2004

URN:NBN:no-3497

The committee for the appraisal of this thesis
was comprised of the following members:

Dr. ing. Marta Doležalová, Dolexpert Geotechnika
Praha, Czech republic

Dr. ing. Bård Bostrøm, Statoil Forskningssenter
Trondheim, Norway

Professor II Dr. ing. Corneliu Athanasiu (Administrator)
Geotechnical Division
Department of Civil and Transport Engineering
Norwegian University of Science and Technology, Trondheim, Norway

URN:NBN:no-3497

Acknowledgements

Franz Kafka wrote in The Diaries (Tagebücher) that life is not one wide straight road but a lot of small ones, which are connected to each other. Almost four years ago I was at the junction of the several roads in my life and I was lucky that one of these roads led to Trondheim. I will always remember my first trip to Norway when I came to the interview and the first time I met people working in the geotechnical group at NTNU. A lot of things have changed from then, I am not so nervous and probably a bit different as a person, but this comfortable feeling I had with these people is still here and I am happy about this. I want to thank them for this special feeling. Especially I would like to mention Professor Lars Grande for his help with my whole PhD study, but also with a lot of other things connected with life in a foreign country. Mainly because of him I had the possibility to be in Trondheim and finished my PhD thesis. Our long discussions were extremely interesting and important for me and I really appreciate all the time we spend together. I would like to thank him for all the help and support he gave me, and I want to say that it was a pleasure to work with such a great person.

Human life is full of the happy but unfortunately also sad and difficult moments. During my stay in Trondheim I experienced both of them and I really appreciate that I could share these moments with my wife Kamila. All the time she stood next to me and she has played a big part in this PhD thesis. I would like to thank her for her support, love and especially her patience.

All this work was a part of the research training network co-funded by the European Commission project - Soft Clay Modelling for Engineering Practice (SCMEP). The training network was initiated at the University of Glasgow and contained cooperation among five European Universities. I want to thank all the people concerned with this project, mainly Dr Minna Karstunen as a network coordinator.

As a part of the SCMEP cooperation I had a chance to spend one month at the University of Stuttgart (USTUTT), Germany. I would like to thank Professor Pieter Vermeer for the invitation and hospitality. Special thanks are given to Marcin Cudny (Dr ing.). He helped me a lot with the understanding of many things in mathematical modelling in geotechnics, and taught me implementation of the constitutive

laws to the PLAXIS 8.1. Besides learning all these things I found a very good friend and I really appreciate it.

Much of this study was done in the geotechnical laboratory at NTNU, Department of Civil and Transport Engineering, Geotechnical Division. I would like to thank Associate Professor Rolf Sandven for the help with the special Creep Triaxial apparatus. My laboratory work would have been impossible without Jan Jønland. He helped me a lot of with the practical part of laboratory tests and I want to thank him very much for this. Special thanks are given to Kjell Roksvåg for the help with computers and calibration of the all apparatus. Additionally I want to thank Shaoli Yong for her help with the evaluation of the data from triaxial compression tests.

I would like to thank Jiri Svancara for the arrangement of the meeting with executives of Povodi Odry a.s., Czech Republic. As a result of this meeting it was possible for me to perform analysis of the Terlicko clayey shale material and Terlicko dam. I would like to thank Povodi Odry a.s. for this possibility. Especially I want to thank Tomas Skokan for the help with in-situ and case record data. Special thanks are given to my parents not just for the transport of the Terlicko clayey shale samples from the Czech Republic to the Norway but also for their support and love.

Geotechnical work is sometimes closely connected with geology. Investigation of the Terlicko clayey shale material also contained identification of the soil minerals. This work was performed in the Department of Geology and Mineral Resources Engineering by Dr Geert-Jan L.M. de Haas and Dr Toril Sørløkk. It was fantastic cooperation which helped me a lot with my work and I would like to thank both of them for their help and good will.

Thanks to Professor Corneliu Athanasiu I had possibility to spend one week in NOTEBY, Oslo, which I dedicated to the study of the in-situ creep behaviour. I would like to thank him for this opportunity and for the interesting and inspiring discussions.

Once again I would like to thank all the people from our department. For the rest of my life I will remember all of these beautiful moments we spent together. Especially I want to thank my PhD colleagues for the excellent atmosphere and friendship. Thanks to them I had chance to learn Norwegian, Ethiopian, Nepalese and Chinese cultures and I really appreciate it. Besides our department I would also like to thank the SINTEF geotechnical group, especially Geir Svanø (Dr ing.) for his help and inspiration.

The language correction of the “first edition” of this thesis was done by my friend from the UK, Adam Robinson. I would very like to thank him for this. I can imagine it has to be pretty tough job for the “non-geotechnics” person to read all this work. I would also like to thank Stewart Clark, NTNU for his editing work on the final version of this thesis.

During my stay in Trondheim I met a lot of new people and I made a lot of new friends from many different countries. Finally I would like to thank them for the beautiful time we spent together. Especially I want to thank my Polish and Czech friends which made me sometimes feel like I am still in my town of birth - Ostrava. It is sometimes important to have someone with the same cultural background.

Frantisek Havel

Trondheim, Norway, May 2004

Abstract

As more and more constructions are concentrated in densely populated urban areas, there is an increasing need to construct buildings and geotechnical structures on soft clay materials, which usually produce significant creep deformation. Although a lot of research work has been related to the creep behaviour of a natural clay material, there are still many questions about this phenomenon. Even today, prediction of the time dependent deformation is generally very problematic. Detailed laboratory, in-situ and numerical studies of soft soil creep are necessary for the better understanding and, consequently, better prognosis of this behaviour. All these studies were performed and will be presented in this thesis.

The long-term, one-dimensional consolidation has been investigated by oedometer tests on undisturbed Norwegian Kvenild quick clay, undisturbed Norwegian Glava clay, undisturbed and remolded Norwegian Onsøy clay and undisturbed Czech Terlicko clayey shale. All tests have been performed in an incremental loading oedometer apparatus with a lever arm, where, in the case of the Glava clay and the Terlicko clayey shale, two sizes of oedometer rings have been used. Detailed means of evaluating the stress-strain-time oedometer behaviour using a time resistance concept introduced by Professor Nilmar Janbu [46,48] is described. The application of the Soft-soil-creep model is presented. This is implemented in the geotechnical finite element program PLAXIS 8.1, for the mathematical modelling of the long-term oedometer test, with emphasis on the correct choice of the input parameters based on the oedometer test results, and their influence to the model's behaviour.

The undrained and drained deviatoric creep behaviour of the Norwegian Glava clay and the Czech Terlicko clayey shale have been studied under triaxial compression. Two different triaxial apparatuses have been used in the study - standard triaxial apparatus made by Wille Geotechnik Gmbh and unique Creep Triaxial apparatus made at NTNU. A large number of undrained and drained deviatoric creep tests under different conditions have been carried out on 100x50 mm (1:2) and 50x50 mm (1:1) cylindrical specimens. Evaluation of the deviatoric creep behaviour based on the time resistance concept together with detailed description of tests conditions is reported. Data is presented showing the relation between stress level, i.e. degree of shear mobilisation at the start of the creep, time, pore pressure develop-

URN:NBN:no-3497

ment and accumulated axial creep strain. Significant effort has been put into the study of the undrained triaxial tests on 1:1 clay specimens in general and undrained deviatoric creep triaxial tests on 1:1 clay specimens in particular. The problem connected with the pore pressure development and measurement is presented. A 2D numerical study of the undrained triaxial deviatoric creep tests has been done on 1:1 and 1:2 specimens using the finite element program PLAXIS 8.1. There is also a comparison of the laboratory and numerical behaviour.

Study of the viscosity and creep behaviour of a natural clay has been performed with modular compact rheometer. The MCR 300 rheometer has been used for the rheological investigation of the Norwegian Glava clay. Oscillatory, rotational and creep tests have been done with this apparatus. The basic characterisation of these tests is presented together with their evaluation. Deviatoric creep tests on modular compact rheometer have been evaluated based on the time resistance concept and compared with deviatoric creep tests on a standard triaxial apparatus.

The analysis of the Czech Terlicko dam with emphasis on the creep behaviour has been performed based on the cooperation with the Povodi Odry, a.s., Czech Republic. A detailed investigation of the undisturbed clayey shale from the Terlicko dam substratum has been done in the geotechnical and geological laboratory. The characterisation of Terlicko clayey shale is reported base on the laboratory tests results. The in-situ behaviour of the Terlicko dam with emphasis to the uplift of the right-hand slope hillside is described. In order to understand the in-situ behaviour a numerical study of the Terlicko dam has been done with PLAXIS 8.1 and Soft-soil-creep model. Results from this 2D numerical test together with recommendations and suggestions are presented.

URN:NBN:no-3497

List of symbols and abbreviations

Symbols:

A list of the most frequently used symbols in this thesis is presented. A description of the other used symbols which are not introduced in this list can be found in the text.

Greek:

δ	Deformation
ε	Normal strain
ε_e	Elastic strain
ε_f	Failure strain
ε_p	Primary consolidation strain
ε_s	Secondary consolidation strain
ε_t	Time dependent strain
ε_v	Volumetric strain
ε_{vs}	Viscous strain
γ, ε_q	Shear strain
γ	Unit weight
γ_d	Dry unit weight
γ_s	Unit weight of solid particles
γ_w	Unit weight of water
η	Dynamic viscosity
η^*	Complex viscosity
φ	Friction angle
κ^*	Modified swelling index
λ^*	Modified compression index
M	Inclination of critical state line
μ^*	Modified creep index
σ	Total normal stress

σ'	Effective normal stress
σ_c'	Preconsolidation pressure
σ_t	Time dependent strass
τ	Shear stress
ψ	Dilatancy angle

Latin:

A	Area
c	Cohesion
c_α	Coefficient of secondary consolidation
c_c	Compression index
c_r	Swelling or recompression index
c_v	Coefficient of consolidation
D	Diameter
e	Void ratio
E	Young's modulus (modulus of elasticity)
E_{oed}	Oedometric modulus
f	Degree of shear mobilisation
F	Safety factor
H	Height of the soil (sample)
k	Permeability
M	Compression modulus by Janbu
m	Modulus number
n	Porosity
p'	Effective volumetric stress
q	Deviatoric stress
r_s	Creep resistance number
S	Saturation
S	Settlement potential
s_u	Unit strength
t	Time
u	Pore water pressure
w	Moisture content
w_L	Liquid limit
w_p	Plastic limit

Abbreviations:

FEM	Finite element method
ICD	Isotropically consolidated drained triaxial test
ICD-C	Isotropically consolidated drained deviatoric creep triaxial test
ICU	Isotropically consolidated undrained triaxial test
ICU-C	Isotropically consolidated undrained deviatoric creep triaxial test
NC	Normally consolidated
NTH	Norges tekniske høgskole Norwegian Institute of Technology - before 1. January 1996
NTNU	Norges teknisk-naturvitenskapelige universitet Norwegian University of Science and Technology
OC	Over-consolidated

List of publications and presentations

List of publications performed during the PhD study:

I. Havel, F., 2000. Micromechanical modelling of the granular materials - use of the PFC2D code for modelling particular materials, Grant 103/00/1043, Report No. 2, (Scientific coordination: M. Doležalová), Praha, Czech Republic, (in Czech), 108 p.

II. Havel, F., 2001. Creep of Norwegian natural clays, SCMEP workshop 2, Graz University of Technology, TUG, Austria

III. Havel, F., 2003. Laboratory investigation of the stress-strain-time behaviour of the clayey shale material from the Terlicko dam substratum, Proceedings of the International Workshop on Geotechnics of Soft Soils - Theory and Practice, Noordwijkerhout, The Netherlands, Published by Verlag Glückauf GmbH, pp. 435-439

IV. Havel, F., 2003. Investigation of the viscosity and creep behaviour of a natural clay with modular compact rheometer, Proceedings of the International Workshop on Geotechnics of Soft Soils - Theory and Practice, Noordwijkerhout, The Netherlands, Published by Verlag Glückauf GmbH, pp. 427-433

V. Havel, F., 2003. Terlicko dam - laboratory, in-situ and numerical study, report for the Povodi Odry a.s., Czech Republic, Trondheim, Norway, 77 p.

List of presentations:

1. Havel, F. Creep of Norwegian natural clays, SCMEP workshop 2, September 2001, Graz University of Technology, TUG, Austria
2. Havel, F. Deviatoric creep - laboratory behaviour and modelling possibility, SCMEP workshop 3, August 2002, Helsinki University of Technology, HUT, Finland
3. Havel, F. Young researcher's report, SCMEP Mid-term review meeting, May 2002, Glasgow, Scotland, UK
4. Havel, F. Proposal for performance of the laboratory tests of clayey shale material, Povodi Odry a.s., September 2002, Ostrava, Czech Republic
5. Havel, F. Stress-strain-time behavior of the clay material, 25. November 2002, NTNU workshop, Department of Geotechnical Engineering, NTNU, Norway
6. Havel, F. Investigation of the viscosity and creep behaviour of a natural clay with modular compact rheometer, Proceedings of the International Workshop on Geotechnics of Soft Soils - Theory and Practice, 17-19 September 2003, Noordwijkerhout, The Netherlands

Author's contribution

The author had an active role in all stages of the work published in this thesis. The author performed the following tests by himself in the geotechnical laboratory at NTNU, Department of Civil and Transport Engineering, Geotechnical Division. There were oedometer deformation tests and triaxial deformation tests with emphasis to the volumetric and deviatoric creep behaviour, soil-particle size analyses, evaluation of the content of organic material and all general index tests (moisture content, unit weight, unit weight of the solid particles etc.). In cooperation with Professor Harald Justnes, SINTEF, Cement and Concrete laboratory, a measurement of the natural viscosity of the Norwegian Glava clay was performed with the compact rheometer MCR 300. The author made all reported numerical analysis with the finite element program for geotechnical applications - PLAXIS 8.1. As for the published in-situ behaviour, a compiling of the existing field data together with analysing of the laboratory and in-situ behaviour was performed. However, the reported X-ray diffraction analysis of the Terlicko clayey shale material was performed by Dr Geert-Jan L.M. de Haas, and differential thermal analysis (DTA) of the same material was made by Dr Toril Sørløkk, both from the Department of Geology and Mineral Resources Engineering. Sampling of the Norwegian Glava clay was performed by the laboratory staff, Department of Civil and Transport Engineering, Geotechnical Division. Sampling of the Czech Terlicko clayey shale was made by the Czech firm hired by Povodi Odry a.s.

Contents

Acknowledgements i
Abstract iv
List of symbols and abbreviations vi
List of publications and presentations ix
Author's contribution xi

1 Introduction 1

1.1 Background of the thesis 1
1.2 General information 2
1.3 Aim of the thesis 4
1.4 Scope of work 4

2 Creep theories and the basic models 6

2.1 Rheological models 7
2.1.1 Maxwell rheological model 9
2.1.2 Kelvin and Voight rheological model 11
2.1.3 Bingham rheological model 12
2.2 Phenomenological models 14
2.2.1 Application to stress-strain behaviour 14
2.2.2 Application to strain-time behaviour 16
2.2.3 Time resistance concept developed at NTNU 30
2.2.3.1 Application to stress-strain behaviour 31
2.2.3.2 Application to strain-time behaviour 34
2.3 Numerical models 39
2.4 Micro-rheology 47

3 Volumetric creep behaviour - One-dimensional consolidation of clay 51

3.1 Historical resumé 52
3.2 Introduction to the laboratory investigation of consolidation 55
3.2.1 Simulation of consolidation - oedometer apparatus 55
3.2.2 Compression curves 56
3.3 Evaluation of results from oedometer tests 59
3.3.1 Norwegian quick clay 62
3.3.1.1 Evaluation of the oedometer test 62

3.3.1.2 Mathematical modelling of the oedometer test with PLAXIS 68
3.3.2 Glava clay 73
3.3.3 Onsøy clay 76
3.3.4 Terlicko clayey shale 80

4 Deviatoric creep behaviour 86

4.1 Theoretical background 87
4.1.1 Direct shear test 88
4.1.2 Triaxial test 93
4.2 Evaluation of creep Triaxial tests performed by the author 97
4.2.1 Glava clay 101
4.2.2 Terlicko clayey shale 127

5 Investigation of the natural clay's viscosity with compact rheometer 133

5.1 Characterisation of the test material 134
5.2 Modular compact rheometer tests. 135
5.2.1 Amplitude sweep test with controlled shear strain 136
5.2.2 Rotational controlled shear stress test. 139
5.2.3 Creep test. 142

6 Analysis of the Czech Terlicko dam 145

6.1 Basic characterisation of the Terlicko dam 146
6.2 Laboratory investigation of the Terlicko shale 148
6.2.1 Description of the specimens 148
6.2.2 Laboratory test programme 148
6.2.3 Determination of the soil composition 148
6.2.4 General index tests. 150
6.2.5 Consolidation and strength tests 152
6.3 Mathematical modelling of the Terlicko dam 152
6.3.1 Geometry and material properties. 152
6.3.2 Initial conditions. 155
6.3.3 Stability analysis. 155
6.3.4 Study of the slope hillside uplift 157
6.4 Summary 160

7 Summary, conclusions and recommendations 162

7.1 Summary and conclusions 162
7.2 Recommendations for the further work 165

References **167**

Appendices

A1 Interpretation of Triaxial tests data **176**

A1.1 Introduction 176
A1.2 Evaluated parameters 176
A1.3 Area correction after consolidation and during shearing 177
A1.4 Piston and membrane correction 178

A2 Evaluation of Triaxial creep tests on Glava clay **180**

A2.1 Characterisation of the performed tests 180
A2.2 Undrained deviatoric creep tests under triaxial compression 180
A2.3 Drained deviatoric creep tests under triaxial compression. 185

Chapter 1 Introduction

1.1 Background of the thesis

This PhD study has been a part of the research training network (HPRN-CT-1999-00049) funded by the European Commission through the programme "Improving the human research potential and the socio-economic knowledge base" - Soft Clay Modelling for Engineering Practice (SCMEP). The training network was initiated at University of Glasgow (GU), and resulted in cooperation among five European universities with following research tasks:

- Norwegian University of Science and Technology (NTNU), Norway - creep (compilation of existing data, laboratory testing, creep models, application)
- Helsinki University of Technology (HUT), Finland - anisotropy and destructuration, stabilised soil (laboratory testing, model development)
- University of Glasgow (GU), United Kingdom - anisotropy and destructuration (development of constitutive model, numerical implementation and verification, practical application)
- University of Stuttgart (USTUTT), Germany - creep, anisotropy, destructuration (combined effect of anisotropy, destructuration and creep, constitutive mode, implementation and practical application)
- Technical University Graz (TUG), Austria - Anisotropy (multilaminate model for clay, development, numerical implementation and practical application)

The research teams in the network collaborated both at global level and task level. A web site was set up, where the information about participants including the young researchers was introduced. A special web site only for the SCMEP's members was established for the better communication between participants. Collaboration at global level involved meetings and workshops where ideas were discussed, planed and shared. The task level collaboration was related to specific tasks, in which more than one team contributed. This collaboration involved meetings and, particularly, short visits, where the typical duration was from one week to three months. SCMEP training network was completed at International Workshop on Geotechnics of Soft Soils - Theory and Practice, in September 2003, where the final results were presented by the young researchers, together with many other "external" contributions covering the topic of the workshop.

1.2 General information

Clayey soils are extremely complex natural materials containing a significant amount of finely dispersed clayey particles less than 0.002 mm in diameter, which have the greatest influence on the difficult physical, mechanical and physicochemical processes inside these materials. Clayey soils exhibit all the rheological properties, where the creep is the most typical, pronounced and readily observed. Because of the difficult nature of these materials there are a lot of aspects influencing their creep behaviour such as composition (i.e. content of the clayey particles), stress history, change in temperature, biochemical environment and transformations. In comparison with sandy material, clayey soils usually display large creep deformations seen for instance in the form of prolonged settlements, tilts and horizontal shifts of buildings and geotechnical structures, or slow slippage of the natural slopes and embankments.

Based on the visual observation of deformations of ancient structures and natural slopes, the existence of a creep in clayey soils is known since time immemorial. Nevertheless the real investigation of this phenomenon started in the middle of 19'th century due to the intensive building activities. Creep of clayey soils started to be interesting for scientists and specialists after the observation of unacceptably large prolonged deformations, affecting normal exploitation of structures and roads. The first highlighting of the creep's phenomenon in clayey soils can be found in "Bases and Foundation" by V. Karlovich from 1869. It is possible to say that during the last century, and mainly during the last few years that creep deformations in clayey soils started to be one of the most important problems of soil mechanics.

Today one can find a lot examples of in-situ creep behaviour. A classical one is the uneven settlement of the Tower of Pisa in Italy [44]. Construction on the tower was started in 1173 and completed in 1360. The height of the tower is 58 m from the foundation and 54.58 m from the ground, weight has been calculated as 14 453 tones, the area of the annular foundation is 285 m^2 and the mean pressure on the base is 0.514 MPa. Due to the creep deformation of clays deposited in the form of lenses in the sandy base, the tower settled and tilted to one side. The mean settlement of the structure according to one of the many evaluations is 1.5 m, and the tower still continues to settle. The tilt of the tower is 5.58 m, i.e. the inclination is about 5.5^o. An illustration of the tower's section with the geological situation below the structure together with the tower's mean settlement with mass of structure can be found in Figure 1–1 a) and b). There are a lot of other documented examples of in-situ creep behaviour, where some of them finished with the total failure of construction. One of biggest disasters was the catastrophe at the Vayont reservoir in Italy. Sliding of the reservoir's side due to the gravitational creep of the slope in

1963 resulted in the loss of 3000 lives, although the 265.5 m high thin arch dam stood unaffected [5]. Gravitational creep of slope creating the reservoir side occurred during 1961-1963, where in 1963 the creep rate was 1 cm per week, which increased in October to 1 cm per day. Late evening on 9 October more than 240 m^3 million soil slid with a speed 15-30 m/s into the reservoir creating a wave that rose 270 m above the reservoir level. A 70 m high wave hit the town of Longaron situated downstream.

a) Section of Tower of Pisa together with geological situation below the structure.

b) Illustration of the tower's mean settlement with mass of the structure.

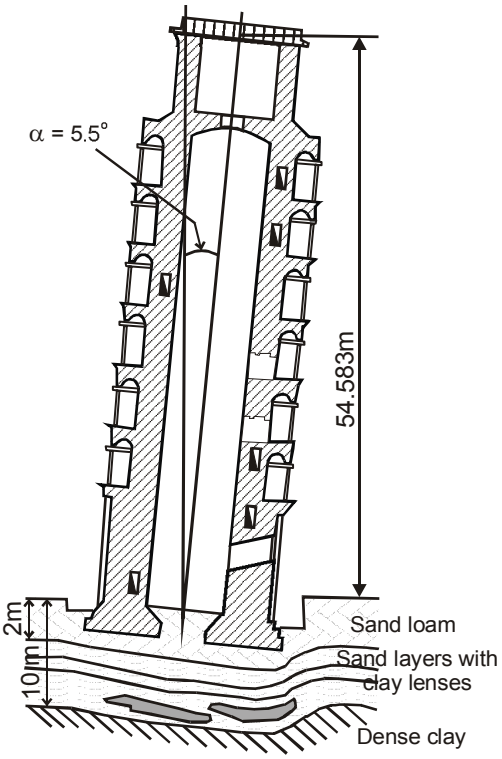

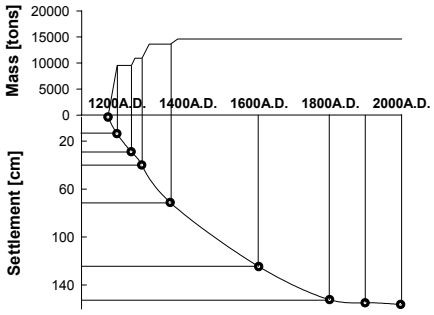

Figure 1–1: Example of the in-situ creep deformation - Tower of Pisa, Italy.

One can see that the study of the creep behaviour of soils in general and creep behaviour of clayey soils in particular is extremely important for a better prediction of in-situ behaviour. This work is also necessary to avoid the problems with significant prolonged deformations which can result in the construction's failure. Although a lot of research work related to the creep behaviour of a natural clay material has been done since this time, there are still many questions about this phenomenon. Even today, the prediction of the time dependent deformation in natural clay material is usually very problematic. Detailed laboratory, in-situ and numerical

studies of soft soil creep are necessary for the better understanding and, consequently, adequate prognosis of this behaviour.

1.3 Aim of the thesis

The main goal of this thesis has been theoretical and practical study of soft soil creep behaviour, involving the study of the creep theories, laboratory and numerical investigations and application of the knowledge used to in-situ behaviour. Main emphasis was placed on volumetric and deviatoric creep behaviour under different laboratory conditions. Oedometer and triaxial tests on different clayey materials are closely studied together with later application of mathematical modelling. Additionally attention is given to viscosity and creep behaviour of a natural clay with a modular compact rheometer.

1.4 Scope of work

The second chapter is a theoretical one. An introduction to the creep theories and models, involving the overview of a basic rheological, phenomenological and numerical creep models is presented here. Special attention is paid to the so-called time resistance concept developed at NTNU mainly by Professor Nilmar Janbu. Application of this concept to the stress-strain and strain-time behaviour is described. Finally a short description of the micro-rheological approach is presented.

Volumetric creep behaviour of the clayey soils with emphasis on the laboratory investigation is studied and discussed in Chapter three. After theoretical background evaluation and examination of results is presented based on oedometer tests performed on Norwegian Kvenild quick clay, Glava clay, Onsøy clay and Czech Terlicko clayey shale. Detailed means of evaluating the stress-strain-time oedometer behaviour are described using a time resistance concept. The application of the Soft-soil-creep model, implemented in the geotechnical finite element program PLAXIS 8.1, to the mathematical modelling of the long-term oedometer test is presented. The emphasis is placed on the right choice of the input parameters based on the oedometer test results, and their influence on the model's behaviour.

Chapter four is dedicated to the deviatoric creep behaviour of the clayey soils in laboratory conditions. As a first part, the theoretical description of the deviatoric creep behaviour under different laboratory conditions is introduced together with explanation of the different shear apparatuses. The main part of Chapter four involves a study of the undrained and drained deviatoric creep behaviour of the Norwegian Glava clay and Czech Terlicko clayey shale under triaxial compression

with using two different triaxial apparatuses. A large number of undrained and drained deviatoric creep tests carried out on 100x50 mm (1:2) and 50x50 mm (1:1) cylindrical specimens are evaluated and investigated. Particular effort is put into the study of the undrained triaxial tests on 1:1 clay specimens in general and undrained deviatoric creep triaxial tests on 1:1 clay specimens in particular. There is also a 2D numerical study of the undrained triaxial deviatoric creep tests on 1:1 and 1:2 specimens with the finite element program PLAXIS 8.1. A comparison is given between the laboratory and numerical behaviour.

Investigation of the viscosity and creep behaviour of the natural clay with a modular compact rheometer is presented in Chapter five. After characterisation of the viscosity as one of the main factors influencing the clay's creep behaviour, oscillatory, rotational and creep tests performed with the MCR 300 rheometer on Norwegian Glava clay are presented and studied. Finally deviatoric creep tests on a modular compact rheometer are evaluated based on the time resistance concept. A basic comparison with triaxial deviatoric creep tests is introduced based on the reached values of the dynamic viscosity.

Chapter six describes the analysis of the Czech Terlicko dam with emphasis on the creep behaviour. At the start of the chapter there is a basic description of the dam from the geological and geotechnical points of view. The following part contains a description of the detailed investigation of the undisturbed clayey shale from the Terlicko dam substratum performed in the geotechnical and geological laboratory at NTNU. Based on the laboratory tests the characterisation of Terlicko clayey shale is reported. The in-situ behaviour of the Terlicko dam with emphasis to the uplift of the right-hand slope hillside is investigated through 2D numerical study with PLAXIS 8.1 and Soft-soil-creep model. The results from this numerical test together with recommendations and suggestions are presented.

The final chapter, Chapter seven, summarizes the main conclusions and comments based on the Chapters three, four, five and six. The new improved findings which can be helpful for the other creep studies are presented. Finally some recommendations are given for further work.

Chapter 2 Creep theories and the basic models

The fundamental problem of creep's theories is the determination of the stress-strain-time relationship. Because of the complexity of the creep phenomenon and the large number of factors influencing it, several creep theories have been developed to describe creep behaviour in a wide range of real materials. These theories differ in one way in the equations of state correlating stress, strain and time,

$$\varepsilon_t = f(\sigma_t, t), \quad \text{or} \quad \sigma_t = f(\varepsilon_t, t), \tag{2.1}$$

and in another in the way about how to achieve these equations or how to describe creep phenomena (which is more or less connected). From this point of view it is possible to divide creep theories into different groups.

N.N. Maslov has identified two approaches, the phenomenological and the physicomechanical [63]. The physicomechanical approach is described as "the method based on investigation into the nature of the observed phenomena and the related laws, and utilisation of certain physical properties of soil and typical parameters of the process". A typical quantity introduced in the physicomechanical approach is viscosity according to Maslov. This decomposition seems to be logical. However, after analysing of several creep theories from these two groups one can find the incorrectness of this conclusion. The problem is that after mathematical modification and parameters' substitution of some creep theories from the phenomenological group, the same creep theory can be physicomechanical.

Jaroslav Feda has generally divided all rheological problems into macro and micro-rheology [33], where macro-rheology is subdivided into the method of rheological models and method of integral representation. It is obvious from the names of groups that the mathematical modelling of the real material's structure is defined as micro-rheology issue whereas in macro-rheology the structure of material is not represented.

A similar structure as introduced by Feda will be used for the description of the basic creep theories. The present author has divided creep theories into the four groups - rheological models, models based on phenomenological behaviour (for

simplicity the term “phenomenological models” will be used here, although there are not phenomenological from the Maslov’s point of view), numerical models and micro-rheology.

2.1 Rheological models

All materials possess properties of elasticity, plasticity and viscosity. These properties can act in different combinations depending on the current material and situation. The behaviour of the real material is extremely complex and a description of the deformation often becomes a questionable task. Hence deformation of the real materials are described here by their simplified models known as rheological models (also models of ideal bodies).

Qualitatively there is similarity between rheological properties of various materials. The rheological study of one material can be extremely useful for carrying out experimental and theoretical studies of another. Theoretically one can say that rheological models for the viscous soil behaviour are historically based on the viscous behaviour of fluids, gases, metals and lately mainly concrete.

The foundation of the science of rheology was laid by Newton in 1687, in his laws of motion of an ideal viscous fluid, today known as Newtonian fluid. Newton found a linear relation that existed between the flow rate and flow resistance of an ideal viscous fluid. The viscosity of the Newtonian ideal viscous fluid can be determinated by a relation between stress and the rate of flow, shown in Eq. (2.2),

$$\sigma = \eta \frac{d\varepsilon_{vs}}{dt} = \eta \cdot \dot{\varepsilon}_{vs} \tag{2.2}$$

where ε_{vs} is the viscous strain, t time, η the coefficient of viscosity (dynamic or effective viscosity) and $\dot{\varepsilon}_{vs}$ the rate of viscous strain. In rheological models the Newtonian fluid is simulated as a viscous element, consisting of a cylinder with a perforated piston filled with a viscous fluid. Illustration of this element can be found in Figure 2–1, c). Generally the relation between stress and rate of flow is considered to be linear or non-linear, see Figure 2–2.

In rheological models the properties of elasticity are described through the ideal elastic Hook medium simulated as an elastic spring, as shown in Figure 2–1, a). The characteristic feature of the ideal elastic Hook medium is a linear relation between stress and strain,

$$\sigma = E \cdot \varepsilon_e \tag{2.3}$$

where E is Young's modulus or modulus of elasticity and ε_e is the elastic strain. However, in rheological models this relation can be non-linear as well, as shown in Figure 2–2. Eq. (2.3) represents the simplest equation of state, which can be written both in differential and integral form.

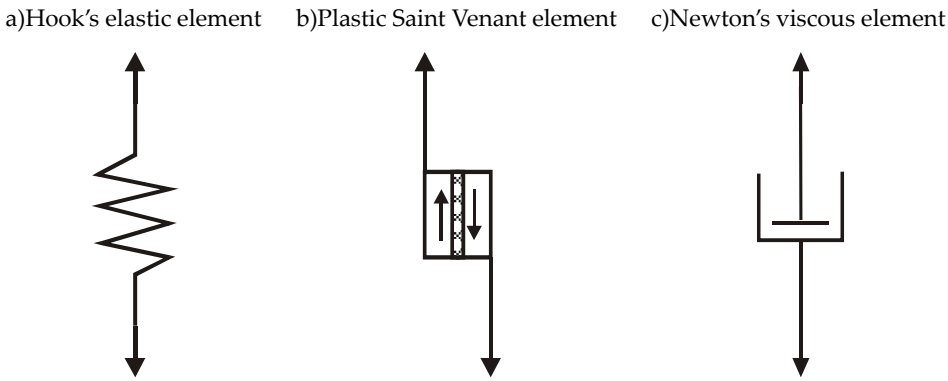

Figure 2–1: Basic types of elements used in rheological models.

The ideal rigid plastic Saint Venant body is used for the description of plastic behaviour. The body is simulated by the dry Coulomb friction that appears on a rough surface when a load is moved on it under the action of a horizontal force producing a stress equal to the plastic flow limit σ_{yp}. When $\sigma<\sigma_{yp}$ the deformation of rigid plastic body is zero while at $\sigma=\sigma_{yp}$ it experiences unlimited plastic strain. Illustration of the plastic Saint Venant element can be found in Figure 2–1, b).

The rheological behaviour of an ideal body is determined by the rheological equation of state includes stress and strain and their derivatives with respect to time,

$$\Phi\left(\sigma, \varepsilon, \frac{d\sigma}{dt}, \frac{d\varepsilon}{dt} \ldots\right) \tag{2.4}$$

This equation combines Newton's viscous, Hook's elastic and Saint Venant's plastic elements, depending on the given rheological model.

As mentioned above, the rheological models are constructed by combining the constitutive behaviour of these three basic elements. Mathematical relations of rheological models can then be depicted in graphical forms, using the symbols of the elementary materials described above. Such a visualisation serves well as an introduction into the problems and defines the problems in a clear manner.

A lot of different rheological models have been introduced for the mathematical description of the stress-strain-time behaviour of soils. Nevertheless, the basic

behaviour of the soils can be described according to three elementary rheological models - Maxwell, Kelvin and Voight, and Bingham. All these models will be introduced in the following sections.

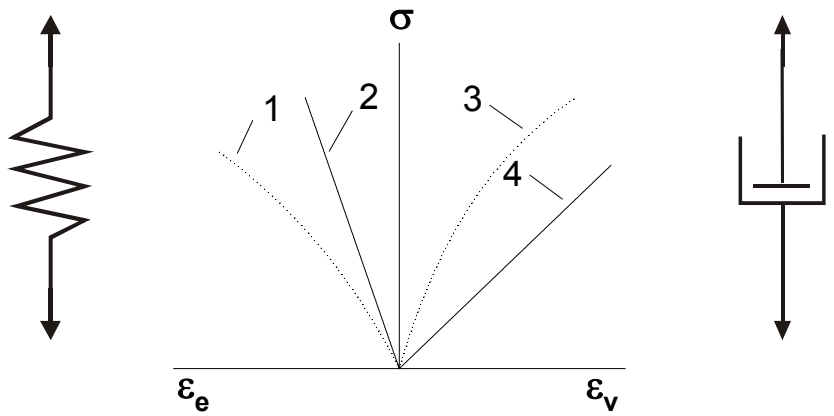

Figure 2–2: Rheology curves of the Hook's and Nowten's elements: 1 - non-linear Hook's element; 2 - linear Hook's element; 3 - non-linear Newton's element; 3 - linear Newton's element

2.1.1 Maxwell rheological model

The Maxwell visco-elastic rheological model (Maxwell body) was first presented in 1868 by James C. Maxwell. The model consists of Hook's elastic element connected in series with Newton's viscous element, see Figure 2–3. After the application of a certain stress, the elastic spring will produce immediate strain in contradiction to the viscous element where the immediate strain will be zero. As the stress continues to act, viscous flow due to the movement of the performed piston in the viscous fluid will occur and so-called delayed strain will be produced. The total strain will be the sum of immediate and delayed strains (primary and secondary strains respectively), and the stress will be equal on both the basic elements.

$$\varepsilon = \varepsilon_e + \varepsilon_{vs} \tag{2.5}$$

$$\sigma = \sigma_e = \sigma_{vs} \tag{2.6}$$

The same relation as shown in Eq. (2.5) can be also applied to the strain rates. Hence the total strain rate $\dot{\varepsilon}$ is the sum of the strain rates of Newton's viscous and Hook's elastic elements,

$$\dot{\varepsilon} = \dot{\varepsilon}_e + \dot{\varepsilon}_{vs} \tag{2.7}$$

which leads, after combination with Eq. (2.2) and Eq. (2.3), to the following differential equation according to Maxwell,

$$\dot{\varepsilon} = \frac{\dot{\sigma}}{E} + \frac{\sigma}{\eta} \tag{2.8}$$

or, after rearrangement,

$$\sigma + \dot{\sigma} \cdot \frac{\eta}{E} = \sigma + \dot{\sigma} \cdot \lambda_M = \dot{\varepsilon} \cdot \eta \tag{2.9}$$

The parameter λ_M is the time constant called relaxation time, which determined the time-dependent behaviour of the serially connected components of the Maxwell model. After calculation of this differential equation for the initial condition $\sigma=\sigma_0$ for time t=0 one can obtained the time-dependent stress relaxation function, formulated as

$$\sigma(t) = \sigma_0 \cdot \exp\left(-\frac{t}{\lambda_M}\right) \tag{2.10}$$

At the time $t=\lambda_M$, the following relation can be found,

$$\sigma(\lambda_M) = \sigma_0 \cdot 0,368 = 36,8\% \cdot \sigma_0 \tag{2.11}$$

It means that in the time corresponding to the relaxation time λ_M of the Maxwell model the σ value has decreased to 36.8% of the initial stress σ_0, i.e. the stress has already decreased to 63.2% of the initial value. Based on the previous equation one can see that the parameter λ_M can characterise speed of the relaxation of given material. Example of very small molecules with extremely short relaxation time can be, for example, water with λ_M=1E-12 s.

Deformation of the Maxwell body for a constant stress σ_0, i.e. for the creep behaviour, can be determined from the relation based on Eq. (2.8),

$$\varepsilon(t) = \frac{\sigma_0}{E} + \frac{\sigma_0}{\eta} t = \varepsilon_0 + \dot{\varepsilon}_{vs} \cdot t \tag{2.12}$$

where $\varepsilon(t)$ is strain of the body at time t and ε_0 is a strain at time t=0.

The creep behaviour of the Maxwell rheological model during loading and subsequent unloading, with linear viscosity, is shown in Figure 2–3.

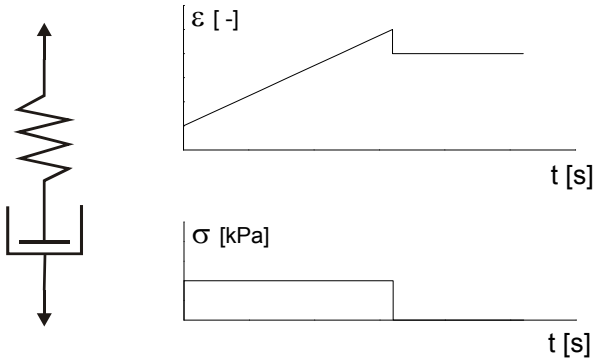

Figure 2–3: Maxwell rheological model with demonstration of the stress and strain behaviour.

2.1.2 Kelvin and Voight rheological model

Kelvin and Voight rheological model is visco-elastic model consists of Hook's elastic element connected in parallel with Newton's viscous element, see Figure 2–4. Some authors describe this model as the Kelvin model, and others as the Voight model or visco-elastic solid model. In this model, elastic and viscous elements can only be deformed together and to the same extent. Hence instantaneous deformation of this rheological model is zero. Stress will be distributed between both model components,

$$\varepsilon = \varepsilon_e = \varepsilon_{vs} \tag{2.13}$$

$$\sigma = \sigma_e + \sigma_{vs} \tag{2.14}$$

After the combination of equations, the differential equation according to Kelvin and Voight will be,

$$\sigma = E \cdot \varepsilon + \eta \cdot \dot{\varepsilon} \tag{2.15}$$

Solving this equation for the constant stress one arrives at the relation, also called the creep function,

$$\varepsilon(t) = \frac{\sigma}{E}\left[1 - \exp\left(-\frac{E}{\eta} \cdot t\right)\right] = \frac{\sigma}{E}\left[1 - \exp\left(-\frac{t}{\lambda_K}\right)\right] \tag{2.16}$$

where λ_K is a constant called the time of retardation which determines the time-dependent deformation behaviour of the parallel connected components of the Kelvin and Voight model. Solving this equation at the time point $t=\lambda_K$ leads to the result,

$$\varepsilon(\lambda_K) = \frac{\sigma}{E} \cdot \left(1 - \frac{1}{e}\right) = 63,2\% \cdot \frac{\sigma}{E} = 63,2\% \cdot \varepsilon_{max} \tag{2.17}$$

This means that in the creep phase at the time corresponding to the retardation time the value of the creep strain has increased to 63.2% of the maximum strain ε_{max}, which will be finally reached at the end of the load interval. Similarly like relaxation time λ_M for relaxation tests, the retardation time λ_K is relevant in creep tests and is unique for all materials.

The creep behaviour in the Kelvin and Voight rheological model for the linear viscosity is illustrated in Figure 2–4.

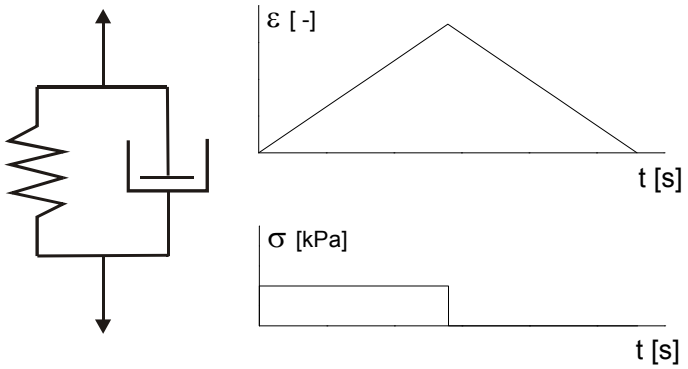

Figure 2–4: Kelvin and Voight rheological model with demonstration of the stress and strain behaviour.

2.1.3 Bingham rheological model

The Bingham visco-plastic rheological model consists of a Saint Venant rigid plastic element connected in parallel with Newton's viscous element, see Figure 2–5. This model introduces a yield point, often called a "Bingham yield point", which describes the transition from the state of rest to the state of flow. The state equation of this model, the Bingham model equation is then,

$$\sigma = \sigma_y + \eta_B \cdot \dot{\varepsilon}_{vs} \tag{2.18}$$

where σ_y is the yield stress and η_B is so called "Bingham viscosity". It is important to note, that the "Bingham viscosity" is not a physical viscosity value of the investigated sample, but in this case it is no more than a calculated coefficient used for the curve approximation (sometimes also called "Bingham flow coefficient").

The Bingham model was often used for its simplicity requiring only a ruler. After computers became widely used, this rheological model is not used so often mainly because of problems with the physical meaning of the introduced parameters. Besides the "Bingham viscosity" also "Bingham yield point" describes the transition from the state of rest to the state of flow relatively inaccurately. It means that this model should only be used for very simple quality control tests.

Flow curve according to the Bingham model for the linear "Bingham viscosity" is shown in Figure 2–5.

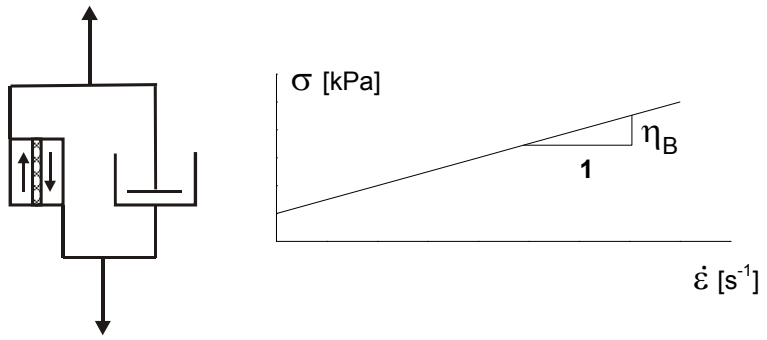

Figure 2–5: Bingham rheological model with demonstration of the flow curve.

There are a lot of different rheological models which more or less combine or use the basic ideas of Maxwell, Kelvin/Voight and Bingham bodies. Some rheological models proposed for the characterisation of the stress-strain-time soil behaviour are Murama and Shibata model (1958), Schiffman model (1959), Christensen and Wu model (1964), Abdel-Hady and Herrin model (1966) or modified Komamura-Huang model (1974). A lot of other rheological models with more details can be found in [11,33,69,77].

The advantages and disadvantages of the different rheological models are neatly recapitulated in [33]. According to Jaroslav Feda, the method of rheological models is flexible in modelling different time effects. In such a way, even complex mechanical behaviour may be fitted by a complicated rheological model. One is, however,

forced to use different models for loading and unloading, for volumetric and deviatoric creep and their cross-effects, etc. The dependence of the mechanical behaviour of geomaterials on the stress and strain paths has the consequence that for different paths different models must be used. There are also other inconsistencies, such as the effect of the time being treated as a stress effect. Rheological models are, therefore, not a visualisation of the structural changes to which the material is subjected in the deformation process, but rather they serve only as a formal description of its phenomenological behaviour. The main advantage of the rheological models is that they illustrate different constitutive relations in a graphical, accessible form and allow their transformation by changing the position of various rheological elements in the total scheme.

2.2 Phenomenological models

Observation of experimental creep curves obtained by testing a number of identical specimens under creep or relaxation conditions has led to many theories of creep, which can be described as phenomenological models. Generally speaking, these models are based on the study of phenomenological stress-strain-time soil behaviour (stress vs. "instantaneous" strain, strain vs. time and stress vs. time curves) in various laboratory conditions. This behaviour is finally described by an aforementioned equation of state, see Eq. (2.1), which can be purely empirical, physical or combined.

The simplest phenomenological models were the first models that tried to explain the creep behaviour of the soil material. These models were purely empirical, trying to characterise the stress-strain or strain-time curves by regression. Application of these models were obviously possible only for given conditions. Modern models based on phenomenological soil behaviour are using physical quantities or trying to introduce physical meaning to the used parameters. This makes them more usable in various cases.

2.2.1 Application to stress-strain behaviour

Stress-strain history plays a significant role in creep behaviour. The type of the creep behaviour is fully connected with the stress-strain situation and boundary conditions, e.g. in the case of the oedometric stress-strain conditions the volumetric creep, without secondary and tertiary creep phases will be expected. From this point of view it is necessary to understand and evaluate the stress-strain situation for estimating and understanding the following creep behaviour. Typical stress-strain curves plotted for a specific instant of time in a case of the consolidation and deviatoric behaviour together with the connection between stress-strain and strain-

time (creep) curves at instant time for a case of the deviatoric creep tests are shown in Figure 2–6.

a) Typical stress-strain diagram in the case of: 1 - deviatoric behaviour, 2 - consolidation.

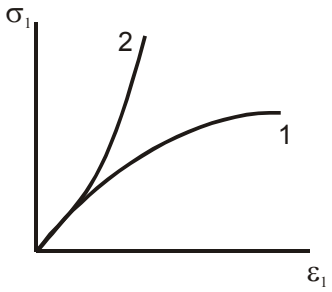

b) Set of creep curves connected with ε_t-σ curve at instant time t_x for a case no. 1 (deviatoric creep tests).

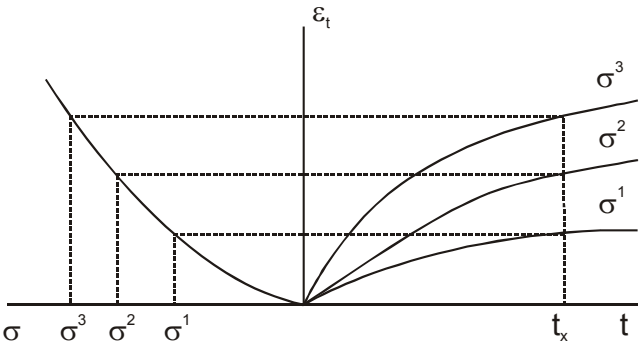

Figure 2–6: Examples of the stress-strain behaviour under different conditions together with illustration of the connection with creep curves [69].

One can find a lot of relations between stress and strain, based on approximations with power, exponential, logarithmic, hyperbolic or other empirical functions. One of the first relation between stress and strain was proposed by Bernoulli in 1694 as a simple power function,

$$\varepsilon_t = B \cdot \sigma^n \tag{2.19}$$

where the parameter n is non-dimensional without any physical meaning, while parameter B represents the strain of the body at stress σ=1. Detailed discussion

about this approximation can be found in [91]. A more general power function was derived by P. Dupen in 1811, as,

$$\varepsilon_t = \alpha \cdot \sigma \mp \beta \cdot \sigma^n \tag{2.20}$$

where α and β are constants. This function describes the deformation of specimens under uniaxial compression and tension, but is also applicable for the determination of the shear deformation.

Different phenomenological models for stress-strain behaviour have been proposed by many authors. Beside power functions, exponential functions were used by J. Riccati or later by S.R. Meschyan, logarithmic functions were used by J. Lesslie, hyperbolic functions by S.P. Timoshenko, etc. A lot of different stress-strain relations based on approximation of the stress-strain curves are described in [69]. A more complex model proposed by Janbu, will be discussed in Section 2.2.3.

2.2.2 Application to strain-time behaviour

According to the acting stress it is possible to divide creep behaviour into volumetric and deviatoric (or shear) creep. Here, volumetric creep is caused by the constant volumetric stress and deviatoric creep is caused by the constant deviatoric stress. There is also a different way of dividing the creep behaviour, shown in Figure 2–7, which is based on the type of the strain-time behaviour. According to the shape of the strain-time curve, one can divide creep into the primary, secondary and tertiary phases. The primary phase, in some literature also called transient or fading, can be defined as a creep deformation during which the strain rate decreases continuously with time. Deformation at a constant rate (material flow) is denoted as the secondary phase, and sometimes also called non-fading [69]. In the case of the tertiary or the accelerated phase the strain rate is continuously increasing and this leads to the creep rupture. Generally, volumetric creep consists only of the primary phase of the creep deformation, i.e. it tends to stabilise. Deviatoric creep may or may not consist all three phases, depending on the shear mobilisation. If the deviatoric stress is low, then only primary creep phase will appear, but after crossing some level of the shear mobilisation primary phase will be followed by the secondary phase which can lead to the tertiary phase and creep rupture.

According to the classical theory consolidation of saturated soils is divided into the primary and secondary phase, where the primary phase deals with the pore pressure dissipation with time after a load application, whereas secondary phase is mainly connected to the rearrangement and better packing of the soil mineral particles and aggregates. More detailed description of general consolidation is given in Chapter 3, so only strain-time relations will be introduced here.

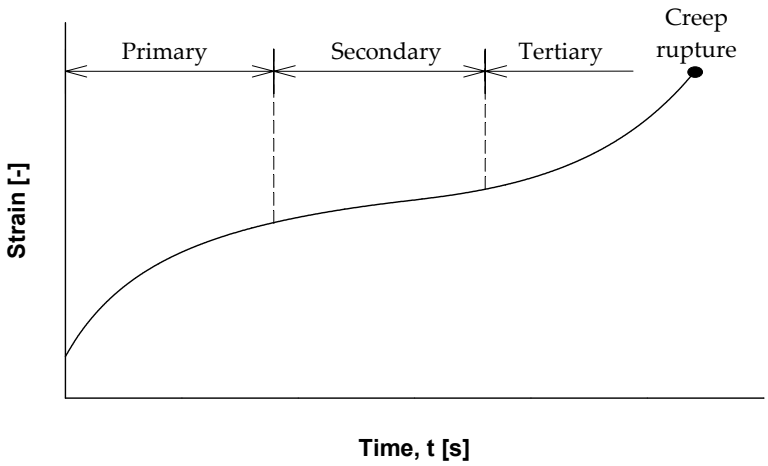

Figure 2–7: Illustration of the primary, secondary and tertiary phases of the creep.

Based on the classical theory of consolidation, described in Section 3.1, one can express the primary phase with the strain-based differential equation proposed by Janbu,

$$\frac{\partial \varepsilon}{\partial t} = \frac{\partial}{\partial z}\left(C\frac{\partial \varepsilon}{\partial z}\right) \tag{2.21}$$

where z is depth and C is coefficient of strain diffusivity [49]. The strain based degree of primary consolidation U_p is then defined as

$$U_p = \frac{\int_0^1 \varepsilon(t)d\xi}{\int_0^1 \varepsilon_p d\xi} \tag{2.22}$$

where ε_p is strain in time $t = \infty$.

Equation Eq. (2.11) was numerically solved in 1965 for three different primary strain distributions with depth [45]. Based on the solution, one can write a general

equation for the strain-based degree of primary consolidation U_p,

$$U_p = 1 - 2 \cdot (1 + r) \cdot \sum_{n=1}^{\infty} \frac{1}{N^2} \cdot \left(1 - \frac{r \cdot \sin N^r}{N^r} \right) \cdot e^{-(N^2 \cdot T_v)} \tag{2.23}$$

where T_v is time factor defined by Eq. (3.6), and n is an integer connected with N through Eq. (3.5). Three different primary strain distributions are defined by value r as,

r=0	$\varepsilon_p = \varepsilon_0 = \text{const.}$	= rectangle, case A
r=1	$\varepsilon_p = \varepsilon_0 \, \xi$	= triangle, case B
r=2	$\varepsilon_p = \varepsilon_0 \, \xi^2$	= parabola, case C

The solution in graphical form of the relation between degree of primary consolidation U_p and time factor T_v is shown in the Figure 2–8.

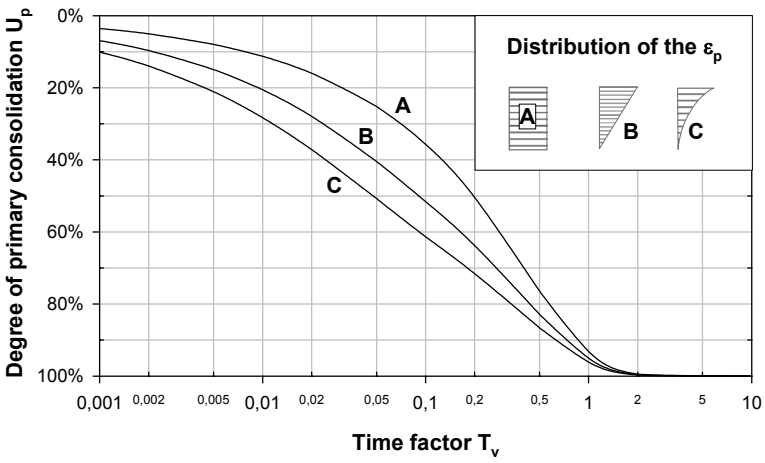

Figure 2–8: Solution of the strained-based differential equation in the form of relation between degree of primary consolidation U_p and time factor T_v.

It is possible to write for the time dependent primary strain in the given point,

$$\overline{\varepsilon}_p(t) = \frac{\sigma'}{E} \cdot U_p \tag{2.24}$$

After simplification of the relation between U_p and T_v one can write two approximations for different degree of primary consolidation,

$$\bar{\varepsilon}_p(t) = \frac{2\sigma'}{E_{oed}}\sqrt{\frac{T_v}{\pi}} = \frac{2\sigma'}{E_{oed}}\sqrt{\frac{C_v \cdot t}{H \cdot \pi}} \quad \text{for} \quad U_p=0\text{-}60\% \tag{2.25}$$

and

$$\bar{\varepsilon}_p(t) = \frac{\sigma'}{E_{oed}}\left(100 - 10^{\frac{1.781-T_v}{0.933}}\right) \quad \text{for } U_p>60\%. \tag{2.26}$$

where E_{oed} is oedometric modulus, C_v is coefficient of consolidation and H is the height of the soil.

The simplest models of the secondary phase of consolidation (volumetric creep) or generally the primary creep phase (according to the creep strain-time behaviour) are based on the approximation of strain-time curves. In this case the strain-time curves can be approximated by exponential or logarithmic functions,

$$\varepsilon_s(t) = C_0[1 - \exp(-\Delta_0 \cdot t^{\chi_0})] \tag{2.27}$$

$$\varepsilon_s(t) = L \cdot \ln(\lambda_0 \cdot t + 1) \tag{2.28}$$

where C_0, Δ_0, χ_0, L and λ_0 are experimentally determined parameters. Eq. (2.27) was proposed by F. Kohlrausch in 1863 for the description of the glass-reinforced fibre creep. Later it was widely used in the theory of the concrete [65] and clayey soils [69] creep. Logarithmic equation, Eq. (2.28), was suggested by K. Buisman.

For the evaluation of the secondary consolidation, the coefficient of secondary compression C_α has been very often used. The coefficient C_α can be defined from the variation of the void ratio e with time t for a given load increment, see Figure 2–9,

$$C_\alpha = \frac{\Delta e}{\log t_2 - \log t_1} = \frac{\Delta e}{\log\left(\frac{t_2}{t_1}\right)} \tag{2.29}$$

where Δe is change of void ratio and t_1 and t_2 is time. The magnitude of the secondary deformation can be calculated as,

$$S_s = C_\alpha' \cdot H \cdot \log\left(\frac{t_1}{t_2}\right) \tag{2.30}$$

where

$$C_\alpha' = \frac{C_\alpha}{1 + e_p}, \tag{2.31}$$

e_p is void ratio at the end of primary consolidation and H is thickness of clay layer.

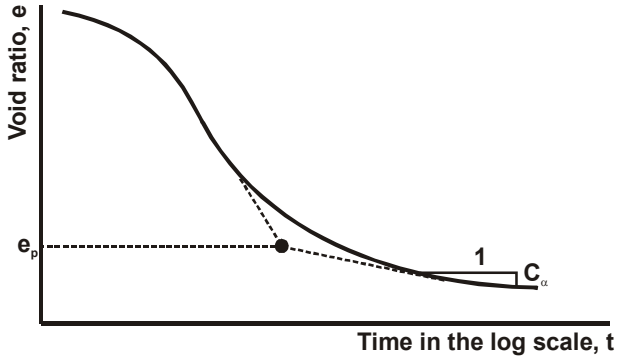

Figure 2–9: Variation of e with log t under a given load increment, and definition of coefficient of secondary compression.

A lot of creep curves based on the incremental loading oedometer tests were analysed by the author. The results suggested the following approximations - sigmoid function, see Eq. (2.32), for the primary consolidation and logarithmic function, see Eq. (2.33), for the secondary consolidation. With a little less accuracy (coefficient of determination $R_{sqr} \cong 0.9$) it is possible to use only the first function (Eq. (2.32)) for both types of consolidation.

$$\varepsilon_p(t) = y_{p0} + \frac{a_p}{1 + \left(\frac{t}{x_{p0}}\right)^b} \tag{2.32}$$

$$\varepsilon_s(t) = y_{s0} + a_s \cdot \ln(|t - x_{so}|) \tag{2.33}$$

y_{p0}, a_p, x_{p0}, y_{s0}, a_s and x_{s0} are experimentally determined constants. More information about these approximations will be described in Section 3.3.1.1.

In 1942, Taylor introduced the so-called hypothesis B [104]. This theory assumed that, for the given load step, secondary consolidation occurs due to plastic resistance and appears only after the completion of primary consolidation, which is influenced by the continuing effect of the previous load step. So, after application of

a load step, deformation is determined by primary consolidation due to the current load step and secondary consolidation due to the effect of the previous step [69]. The total effective stress may then be represented as,

$$\sigma' = \sigma_g + \sigma_b + \sigma_{vr} \tag{2.34}$$

σ_g is "static strength", i.e. stress in the soil skeleton at the end of primary consolidation due to the given load step, and $\sigma_b+\sigma_{vr}$ is "plastic strength", which is governed by secondary consolidation due to the effect of the previously applied load, where σ_b, also called the "bond", is the plastic resistance and σ_{vr} is the viscous structural resistance. Hypothesis B has been followed by many authors, e.g. Koppjan, Tan Tjong-Kie, B. Hansen, L. Aplan, G.A. Leonards and P.A. Girault.

Following Taylor's idea, the theory of isotaches was presented by L. Suklje in 1957. Suklje constructed isotaches σ′-e (were e is the void ratio) for various specific consolidation speeds v, derived from the consolidation curves of an oedometer tests, carried out for a given load increment, see Figure 2–10. Determination of the isotaches together with their possible practical use can be found in [99]. Later he developed this model for the non-linear viscous soil and extended the model to a third dimension [98].

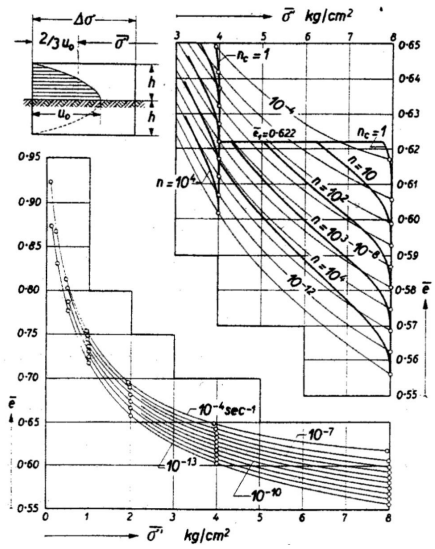

Figure 2–10: System of isotaches according to the Suklje [99].

Ten years later L. Bjerrum introduced his theory of isochrones, i.e. the system of lines, where each line represents the equilibrium void ratio for different values of

effective overburden pressure at a specific time of constant loading, Figure 2–11 a). Bjerrum introduced the terms instant and delayed compression to describe the behaviour of the soil skeleton in the absence of the pore pressure effect [15]. According to Bjerrum, the instant compression occurs simultaneously with the increase in effective pressure and causes a reduction in the void ratio until an equilibrium value is reached at which the structure effectively supports the overburden pressure. Delayed compression according to the definition represents the reduction in volume at an unchanged effective stress. The definition of instant and delayed compression compared with primary and secondary consolidation is shown in Figure 2–11, b).

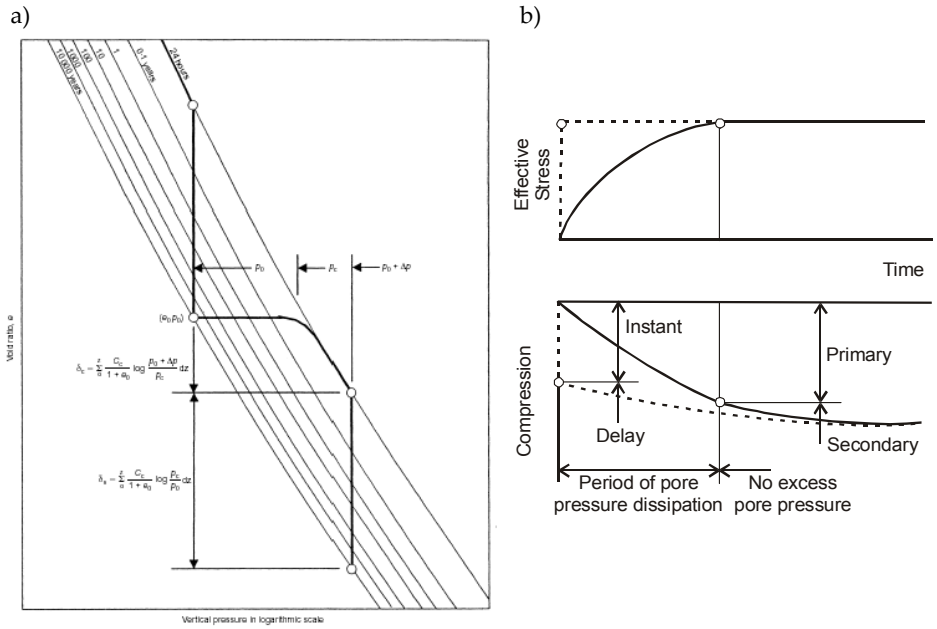

Figure 2–11: System of isochrones according to the Bjerrum, together with the definition of the instant and delayed compression [15].

According to Bjerrum's theory, delayed compression leads to the certain overconsolidation, i.e. for additional loads smaller than some critical value the instant deformation will be limited to an elastic compression. Based on this information, one can write the following equations for the instant and total compression,

$$\varepsilon_i = \frac{C_c}{1+e_0} \cdot \log \frac{p_c + [\Delta p - (p_c - p_0)]}{p_c} \tag{2.35}$$

$$\varepsilon_{to} = \frac{C_c}{1+e_0} \cdot \log \frac{p_0 + \Delta p}{p_0} \tag{2.36}$$

were ε_i (ε_{to}) is instant (total) compression, C_c is inclination of the isochores, e_0 is the starting value of the void ratio, p_0 is overburden pressure, p_c is a critical pressure showing overconsolidation and Δp is the additional stress. Bjerrum's ideas were expressed mathematically by Garlanger (1972), Magnan et al. (1979) using a stress-strain-strain rate model in one-dimensional consolidation analysis CONMULT [82], and partly by Vermeer in PLAXIS.

Even though there is a lot of difference between volumetric and deviatoric creep behaviour, some approaches can be applied to both. In [69] one can find several general approaches to the evaluation of the strain-time behaviour.

The above-mentioned Taylor's hypothesis B can be denoted as the theory of ageing for the case of consolidation. The general feature of the theory of ageing (in some literature also called the theory of time hardening) is, according to Soberberg [69], the constant relation between strain and time,

$$\Phi(\sigma, \varepsilon, t) = 0 \tag{2.37}$$

The total strain is then the sum of the elastic instantaneous strain ε_e and time dependent or creep strain ε_t, which is a function of the time t and stress σ,

$$\varepsilon(t) = \varepsilon_e + \varepsilon_t = \frac{\sigma}{E} + \varepsilon_t(\sigma, t) \tag{2.38}$$

Based on the system of isochronic ε–σ curves shown in Figure 2–12 and the theory of similarity (possibility of obtaining one set of curves by multiplying the ordinates of another set of curves with a constant factor [69]), Y.N. Rabotnov proposed a more general form of the stress-strain-time relation,

$$\sigma = \varphi(\varepsilon) \cdot \nu(t), \tag{2.39}$$

where $\varphi(\varepsilon)$ is a function of strain and $\nu(t)$ is a time dependent function.

A modified theory of ageing, so called flow theory, was introduced by K. Davenport in 1938 and later developed by L.M. Kachanov. In this theory, the relation between the rate of creep strain, stress and time, is suggested as,

$$\dot{\varepsilon}_t = \dot{\varepsilon}_t(\sigma, t) \tag{2.40}$$

Based on the theory of similarity one can write the following equation,

$$\dot{\varepsilon}_t = F(\sigma) \cdot \frac{d}{dt} C(t) \tag{2.41}$$

where F(σ) is a stress function and C(t) is creep function of time.

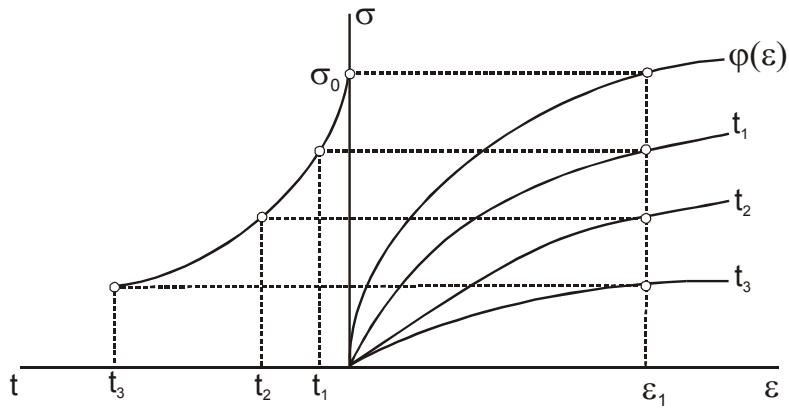

Figure 2–12: System of isochronic ε–σ curves and σ-t curve at fixed strain ε_1=constant, [69].

The theory of strain hardening, formulated by P. Ludwik, A. Nadai and Davenport and later developed by Rabotnov, supposes a constant relation between the rate of the creep strain, stress and creep strain accumulated in the material up to the given instant of time,

$$\Phi(\dot{\varepsilon}_t, \sigma, \varepsilon_t) = 0 \tag{2.42}$$

This theory is based on the idea that the rate of the creep increases with stress σ and decreases with accumulated strain, i.e. this theory is valid within the limit of primary creep. According to this assumption one can write the following equation,

$$\dot{\varepsilon}_t = \frac{f_1(\sigma)}{f_2(\varepsilon_t)} \tag{2.43}$$

Various expressions for $f_1(\sigma)$ and $f_2(\varepsilon_t)$ are given in [69].

The graphical construction of the creep curves according to these theories of ageing and hardening, compared with the experimental creep curves obtained from the testing of identical specimens under constant stress of several magnitudes is shown in Figure 2–13.

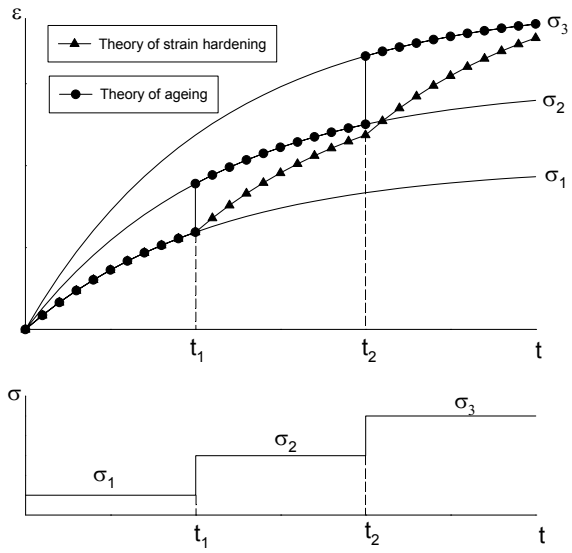

Figure 2–13: Graphical construction of creep curves under step-wise incremental stress in the theories of ageing and hardening, based on experimental creep curves, [69].

G.N. Maslov introduced the linear version of the theory of an elastically creeping body based on the Boltzmann-Volterra theory [69]. Maslov supposed in this theory that material is isotropic, a relation between stress, instantaneous strain and creep strain is linear, it is possible to superimpose creep strain, strain is independent of the sign of stress, all types of unit strains are identically dependent on time, it is possible to neglect creep recovery upon unloading an element, and creep and instantaneous strain depend on age. The total strain of a compressed element at constant unit stress σ=1 may then be given by,

$$\varepsilon(t, \nu_t) = \varepsilon_e(\nu_t) + \varepsilon_t(t, \nu_t) \tag{2.44}$$

where $\varepsilon_e(\nu_t)$ is the instantaneous elastic strain and $\varepsilon_t(t,\nu_t)$ is the creep strain at time t due to the unit stress applied a instant of time ν_t. Strain due to the action of constant stress $\sigma(\nu_{t0})$ is expressed by the relation,

$$\varepsilon(t) = \varepsilon(t, \nu_{t0}) \cdot \sigma(\nu_{t0}) \tag{2.45}$$

More information about this theory can be found in [65].

Mitchell and Singh supposed that a characterisation relationship between strain rate and time exists for most soils, at least for simple stress state and drainage conditions [79]. The general relationship between the strain rate and time was proposed by them as

$$\ln\frac{\dot{\varepsilon}}{\dot{\varepsilon}(t_1, D)} = -m_m \cdot \ln\left(\frac{t}{t_1}\right) \tag{2.46}$$

or

$$\ln\dot{\varepsilon} = \ln\dot{\varepsilon}(t_1, D) - m_m \cdot \ln\left(\frac{t}{t_1}\right) \tag{2.47}$$

where $\dot{\varepsilon}(t_1, D)$ is the axial strain rate at unit time and is a function of stress intensity D, m_m (originally called only m) is the absolute value of the slope of the straight line on the log strain rate vs. log time plot, and t_1 is a reference unit of time, e.g. 1 min. In the case of triaxial test, values of m_m generally fall in the range of 0.7 to 1.3 [79]. Stress intensity D can be taken as the deviatoric stress, a shear stress or stress level.

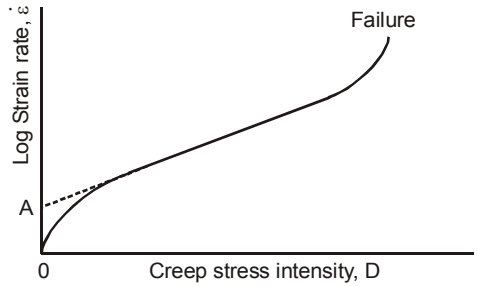

Figure 2–14: Illustration of the relation between stress intensity D and logarithm of the creep strain rate [79]

Another equation is suggested for the data plotted in the form of the logarithm of axial strain rate vs. stress intensity D,

$$\ln(\dot{\varepsilon}) = \ln\dot{\varepsilon}(t, D_0) + \alpha \cdot D \tag{2.48}$$

where $\dot{\varepsilon}(t, D_0)$ is a value of the strain rate at D=0, as a function of time after the start of creep, and α is the slope of the linear part of a log strain rate vs. stress plot. After the combination of Eq. (2.47) and Eq. (2.48), one can write for the stress intensity D=0,

$$\ln\dot{\varepsilon}(t, D_0) = \ln\dot{\varepsilon}(t_1, D_0) - m_m \cdot \ln\left(\frac{t}{t_1}\right) \tag{2.49}$$

where $\dot{\varepsilon}(t_1, D_0)$ is denoted as A and described by Singh and Mitchell like the value of the strain rate obtained by projecting the straight line portion of the relationship between the logarithm of the strain rate and stress intensity at unit time to a value of D=0. Illustration of the relation between logarithm of the strain rate and stress intensity together with demonstration of the value A can be found in Figure 2–14.

After the substitution of Eq. (2.49) into Eq. (2.48) the final strain rate equation can be obtained as,

$$\dot{\varepsilon} = A \cdot e^{\alpha \cdot D} \cdot \left(\frac{t_1}{t}\right)^{m_m} \tag{2.50}$$

which, after integration, leads to the two relations between strain and time,

$$\varepsilon = \varepsilon_1 + \frac{A}{1 - m} \cdot e^{\alpha \cdot D} \cdot (t^{1 - m_m} - 1) \qquad \text{for} \quad m_m \neq 1 \tag{2.51}$$

and

$$\varepsilon = \varepsilon_1 + A \cdot e^{\alpha \cdot D} \cdot \ln t \qquad \text{for} \quad m_m = 1 \tag{2.52}$$

where $\varepsilon=\varepsilon_1$ for t=1. Shape of the creep curves for different values of m_m are possibly to be found in Figure 2–15.

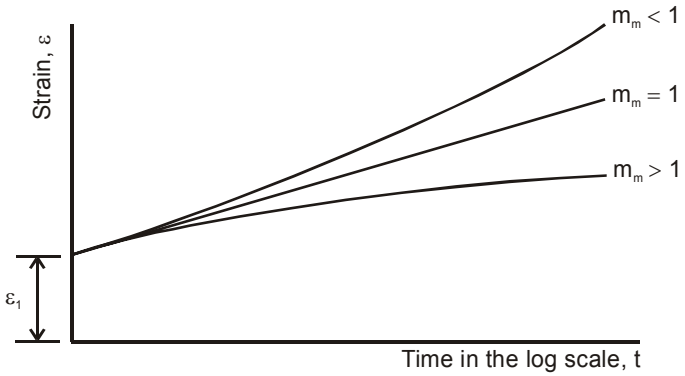

Figure 2–15: Creep curves shapes predicted by the Mitchell's stress-strain-time function for the different value of the coefficient m_m, [79].

If the value of the coefficient m_m is less than one, the high potential of the strength loss and eventual failure during creep can be indicated. In this case the time to failure (creep rupture) can be computed according to Singh and Mitchell as,

$$t_f = \frac{C}{\dot{\varepsilon}_{min}} \tag{2.53}$$

where $\dot{\varepsilon}_{min}$ is the minimum strain rate before occurrence of the tertiary or accelerated creep phase (see Figure 2–16) and C is a constant evaluated for the laboratory tests. Values of the parameter C for different clays can be found in [79].

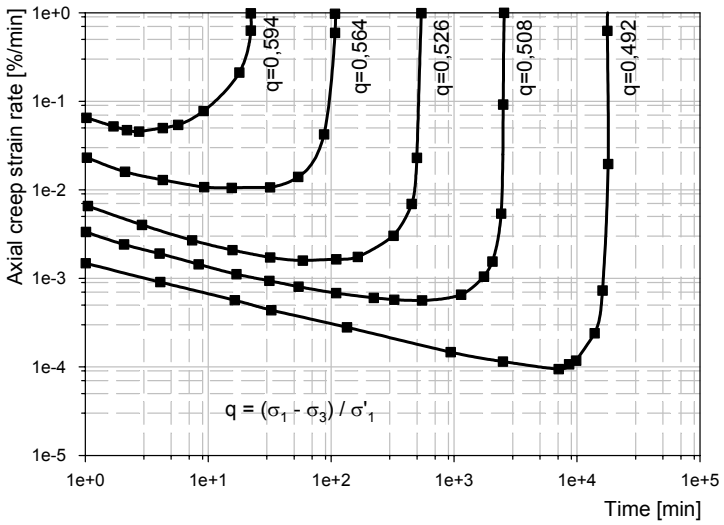

Figure 2–16: Axial creep strain rate vs. time behaviour of K_0-consolidated, undisturbed Haney clay under axisymmetric loading [108].

Singh and Mitchell supposed that the strain at failure is a constant, independent of stress level and corresponding to the minimum strain rate $\dot{\varepsilon}_{min}$. Thus at the point of minimum strain rate the failure strain becomes,

$$\varepsilon_f = \text{Constant} = \frac{1}{1 - m_m}(\dot{\varepsilon}_{min} \cdot t_f) = \frac{C}{1 - m_m} \tag{2.54}$$

and the constant C can be evaluated from the following equation,

$$C = (1 - m_m)\varepsilon_f \tag{2.55}$$

After evaluation of the C value according to the laboratory tests results one can compute the time to failure from the combination of Eq. (2.50) and Eq. (2.53) as,

$$\ln t_f = \frac{1}{1 - m_m}\left(\ln\left(\frac{C}{A}\right) - \alpha \cdot D\right) \tag{2.56}$$

More detailed information about creep rupture can be found in [79].

For the case of the simple shear one can find in [69] several equations based on the afore-mentioned theory of ageing, Eq. (2.38),

$$\gamma(t) = \frac{\tau}{G_0} + \omega(t) \cdot f(\tau), \tag{2.57}$$

the theory of hardening, Eq. (2.43),

$$\gamma(t) = \frac{\tau}{G_0} + [(1 + \alpha)\chi \cdot \tau^{\beta} \cdot t]^n, \tag{2.58}$$

or the theory of elastically creeping body, Eq. (2.44),

$$\gamma(t) = \frac{\tau}{G_0} - \int_{\nu_0}^{t} f[\tau(\nu)] \cdot \frac{\partial \omega(t - \nu)}{\partial \nu} d\nu \tag{2.59}$$

where $\omega(t)$ is a creep measure in simple shear, $f(\tau)$ is the shear stress function with condition that $f(\tau=1)=1$, χ, n and β are experimentally determined parameters and G_0 is the modulus of instantaneous deformation under simple shear. The rest of the notations are explained above.

There are a lot of other phenomenological methods for the evaluation of the primary, secondary or tertiary creep. Neat recapitulations of these methods are presented by [69] and [33].

2.2.3 Time resistance concept developed at NTNU

The time resistance concept has been developed mainly by Professor Nilmar Janbu over the last 40 years. Development of the concept was based on the interpretation of the creep tests in an oedometer but it is possible to extend it to the deviatoric creep behaviour. Basic features of this concept will be described here for volumetric and deviatoric creep.

The resistance concept is widely used in almost all engineering disciplines. Essentials to this concept can be found in the Newton's laws of motion from the 17th century. In 1822 Fourier's relation was introduced which expresses as the conduction of heat in two-dimensional objects. Modification of this relation is known as the thermal resistance concept, or just the resistance concept, described as,

$$Q = A \cdot \frac{(\Delta T)}{R_t} \tag{2.60}$$

where Q is the rate of flow of heat, A is the area through which heat flows, ΔT is the difference between the temperature of the warm and cold faces of the material and R_t is the thermal resistance [93]. In 1827 Ohm introduced a relation between the potential difference V, or voltage, and the rate of flow of charge I, or current, today known as Ohm's law, in the form of,

$$\frac{V}{I} = R_e \tag{2.61}$$

where R_e is electric resistance, defined as the opposition offered to the passage of a steady electric current through a body, circuit, or substance (according to "The New Penguin English Dictionary"). Besides this example one can find many forms of resistance, e.g. dynamic resistance, hydraulic resistance, and elastic resistance.

By virtue of these relations, it is possible to say that all media possess resistance against a forced change of existing equilibrium conditions. The resistance of a medium, or of an isolated part of it, can therefore be determined by measuring the incremental response to a given incremental action, see Figure 2–17, [48]. The general definition of the resistance can be then written as,

$$\text{Resistance, } R_x = \frac{\text{Incremental action, dx}}{\text{Incremental responce, dy}} \tag{2.62}$$

For the non-linear response, like in a most soils, the resistance is defined as the tangent to the action-response curve. The definition of the resistance concept in a graphical form is shown in Figure 2–17.

The biggest advantage of the resistance concept is the basic and simple approach to the soil stress-strain-time behaviour evaluation, which makes it a powerful tool for practical engineering. Janbu's resistance concept can be used not only for clay but also for other granular media, such as silts, sands, moraine, fractured rocks and sedimentary rocks, see Figure 2–18.

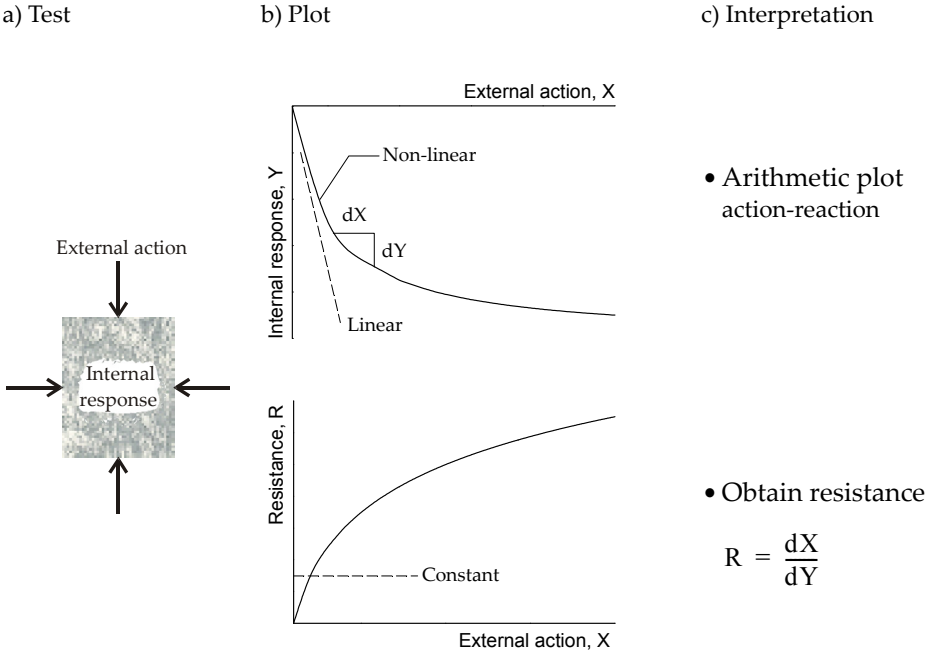

Figure 2–17: Definition of the resistance concept [48].

2.2.3.1 Application to stress-strain behaviour

If one applies the resistance approach to the soil stress-strain behaviour, the stress-strain curves from the laboratory or in-situ testing are action-response measurements, where stress is action and strain is response. Then, according to Janbu, the soil sample resistance against deformation, M, under oedometric conditions is,

$$M = \frac{d\sigma'}{d\varepsilon} \tag{2.63}$$

M is called the compression modulus, and the swelling modulus, for loading and unloading, respectively. Generally M will be called the tangent modulus in the following text. The development of the tangent modulus M with stress σ' together with stress-strain curves from oedometer tests are plotted in Figure 2–18. Four sets of diagrams represent: a) an over-consolidated clay, b) a silty sand at in-situ porosity, c) an intact sample of a cemented moraine, a shale or sedimentary rock and d) a

sample of the intact, fairly undisturbed quick clay, or an extra-sensitive soil in general, with loose, porous structure, easily collapsible for increasing stress σ′ around preconsolidation pressure [48]. All diagrams are plotted in an arithmetic scale. The samples for all four cases were obtained from natural deposits with as little disturbance as possible. Hundreds of laboratory oedometer tests were done with a similar shapes of the σ′-ε and M-σ′ curves for the presented material categories.

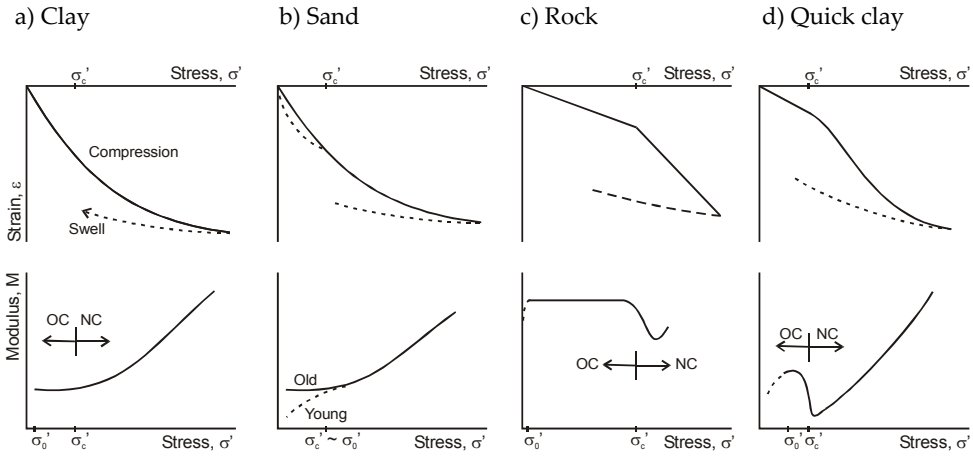

Figure 2–18: Typical σ′-ε and M-σ′ curves obtained by oedometer tests [48].

The great advantage of the M-σ′ curves is that one can clearly distinguish the overconsolidated (OC) and normally consolidated (NC) range, i.e. the preconsolidation stress σ_c' causes a significant change in the M-σ′ curve's shape. The most dramatic change between these two areas is typical for the extra-sensitive soil material due to the grain structure collapse caused by the breakage of contact points between mineral particles.

According to Janbu, it is possible to use in practical engineering the simple equation for the tangent modulus M as a function of the effective stress σ′, to cover all variations indicated in Figure 2–18. The idealized formula used since 1963 is then,

$$M = m\,\sigma_a \left(\frac{\sigma'}{\sigma_a}\right)^{1-\alpha}, \tag{2.64}$$

where σ_a is reference stress (100 kPa), σ′ is effective stress (kPa), m is the modulus number (dimension less) and α is the stress exponent (dimension less). After the combination of this equation with Eq. (2.63) one can write the general definition of the strain as,

$$\varepsilon = \int_{\sigma'_c}^{\sigma' = \sigma'_c + q'} \frac{1}{M} d\sigma' , \tag{2.65}$$

where the starting value of the stress increase q′ is supposed to be σ_c'.

Different types of the M-σ′ behaviour can be described by Eq. (2.64) using various values of the stress exponent α. According to Janbu there are four main categories of the M-σ′ variations, introduced in the following points.

i The over-consolidated soils ($\sigma'<\sigma_c'$) denoted OCS or EE (equivalent elastic), where the stress exponent α=1. In this case,

$$M = m\sigma_a = M_{OC} = \text{const.} \tag{2.66}$$

$$\varepsilon = \frac{q}{M_{OC}} \tag{2.67}$$

ii The normally consolidated sand (NCS) with α=0.5. In silty sandy soils (NC) the α-value may range typically between 0.4 to 0.65, so 0.5 should be considered as an average choice for practical purposes only. The forms for the tangent modulus M and strain ε then are,

$$M = m\sqrt{\sigma'\sigma_a} \tag{2.68}$$

$$\varepsilon = \frac{2}{m}\left[\sqrt{\frac{\sigma'_c + q'}{\sigma_a}} - \sqrt{\frac{\sigma'_c}{\sigma_a}}\right] \tag{2.69}$$

iii The normally consolidated clays, NCC. For this material α=0, and

$$M = m\sigma' \tag{2.70}$$

$$\varepsilon = \frac{1}{m}\ln\frac{\sigma'_c + q'}{\sigma_c} \tag{2.71}$$

iv The normally consolidated quick clays (NCQC) or extra sensitive soils (NCES), which can described by α=-0.5. For Scandinavian quick clays the α-value may range from -0.3 to -0.5, while Canadian quick clays seem to have lower values of α, say down to -0.7. M and ε can be then defined as,

$$M = m\sigma'\sqrt{\frac{\sigma'}{\sigma_a}} \tag{2.72}$$

$$\varepsilon = \frac{2}{m}\left[\sqrt{\frac{\sigma_a}{\sigma'_c}} - \sqrt{\frac{\sigma_a}{\sigma'_c + q'}}\right] \quad \text{for} \quad \alpha = -0.5 \tag{2.73}$$

Demonstration of all these categories in graphic form can be found in Figure 2–19 a). Figure 2–19 b) shows typical values of the modulus number m for different material and porosity. Generally, for normally-consolidated clay the typical value of the modulus number m is m=8-25. In the case of normally-consolidated sand, and silt, the m=50-100 (silt) and 100-500 (sand), respectively. More information can be found in [48].

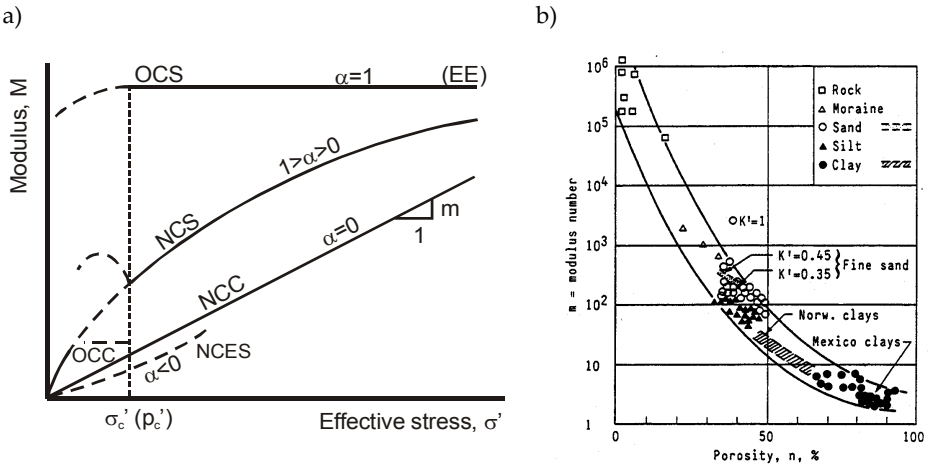

Figure 2–19: Idealised M-σ'curves and demonstration of the typical values of the modulus number m.

2.2.3.2 Application to strain-time behaviour

The previous section has already described the application of the resistance concept to stress-strain behaviour. In the same way one can apply the resistance concept to the soil strain-time behaviour. In this case the time is considered as an action and strain as a response. Hence, the time resistance of the soil R can be defined as,

$$R = \frac{dt}{d\varepsilon} = \frac{1}{\dot{\varepsilon}} \tag{2.74}$$

For most granular media the time resistance generally increases with time for one-dimensional compression. During the primary consolidation the R-t curve has the characteristic parabolic shape. Nevertheless, after crossing to the certain time t_0, the R-t relation starts to be linear. Experience has shown that t_0 is usually much smaller than the duration of the primary phase, t_p. This means that creep (under stationary

stress) occurs already from $t=t_0$, i.e. using Janbu's words, for $t \geq t_0$ it is likely that the gradients and hence the seepage forces, $i\gamma_w$, are so small that the time-delayed compression for all practical purposes is governed by the intergranular shear stress and shear strains only. So, based on the R-t relation, one can define three parts of the consolidation, primary consolidation for the time $t<t_0$, linked process for the time $t_0 \leq t \leq t_p$ and pure creep for the time $t>t_p$, see Figure 2–20.

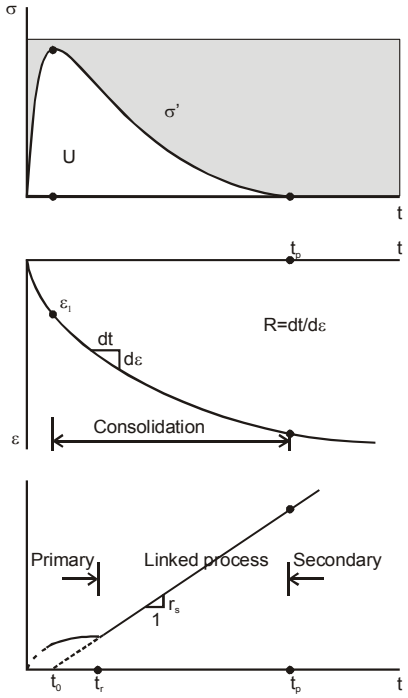

Figure 2–20: Definition of the time resistance R and creep resistance number r_s for the incremental loading oedometer, [48].

The slope of the linear relation between time resistance R and time t, after crossing time t_0, can be described with creep resistance number r_s (or only creep resistance or creep number),

$$r_s = \frac{dR}{dt} \tag{2.75}$$

It has been proved, by a large amount of oedometer tests, that the creep resistance number depends on the level of the effective stress. Figure 2–21 shows the typical relation between the creep resistance number r_s and effective stress σ' for the Norwegian undisturbed soft clay. Generally, the creep resistance is very large in the OC

range ($\sigma'<\sigma_c'$) and drops radically when the effective stress σ' approaches the preconsolidation pressure σ_c'. The minimum value of the creep resistance r_s is at $\sigma'=\sigma_c'$ and thereafter increases slightly with increasing σ'. One can see that the preconsolidation σ_c' can be clearly identified from the r_s-σ' curve for natural clays. Typical values of the creep resistance r_s for the normally-consolidated, saturated clays lie in the range r_s=100-500 for the in-situ water content w=30-60%.

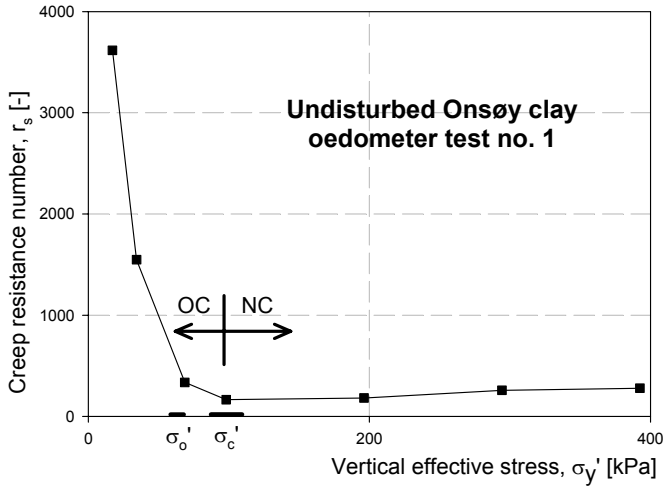

Figure 2–21: Example of the creep resistance number r_s variation depends on the effective vertical stress σ'. Oedometer test of the Norwegian Onsøy clay performed by the author.

The settlement potential, S, was introduced by Janbu as a diagnostic tool for the evaluation of the case records data as,

$$S = \dot{\delta} \cdot t \tag{2.76}$$

where $\dot{\delta}$ is the rate of observed deformation obtained as a tangent to the δ-t curve, and t is time. The shape of the S-t curve for the primary consolidation, i.e. $t < t_0$, is for most cases parabolic, like R-t curve. During the creep behaviour, i.e. $t \geq t_0$, the settlement potential is constant. Evaluation of the settlement potential together with the typical shape of the S-t curve can be seen in Figure 2–22.

The settlement potential evaluated only for the creep phase is sometimes denoted by Janbu as a creep potential S_c. The creep potential of a layer of thickness H is then, according to the definition,

$$S_c = \dot{\delta}_c \cdot t = \dot{\varepsilon}_c \cdot H \cdot t \tag{2.77}$$

If the creep resistance number r_s is constant over the whole layer, then the relation between R and r_s is supposed to be

$$R = r_s \cdot t \tag{2.78}$$

then one can write, based on Eq. (2.74),

$$S_c = \frac{H}{r_s} = \text{const.} \tag{2.79}$$

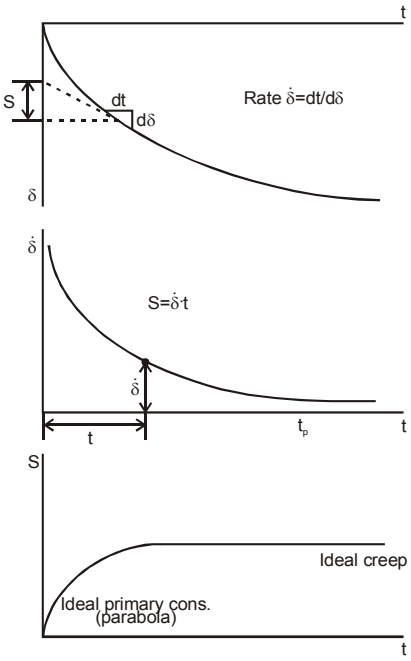

Figure 2–22: Definition of the settlement potential [50].

If r_s is not constant over the layer, i.e. for layered soils, the creep settlement S_c can be computed as

$$S_c = \sum_{i=1}^{n} \frac{\Delta H_i}{(r_s)_i}, \tag{2.80}$$

or,

$$S_c = \frac{H}{r_b - r_0} \ln \frac{r_b}{r_0}, \tag{2.81}$$

if r_s increases linearly with depth from r_0 at the base (z=0) to r_b at z=H.

Based on the previous information one can write equation for the total strain ε, which is supposed to be a function of the effective stress σ′ and time t,

$$\varepsilon = f(\sigma', t) \tag{2.82}$$

The total differential of the strain dε can be then written as,

$$d\varepsilon = \frac{\partial \varepsilon}{\partial \sigma'} d\sigma' + \frac{\partial \varepsilon}{\partial t} dt = \frac{d\sigma'}{M} + \frac{dt}{R} \tag{2.83}$$

After the combining of Eq. (2.83) with Eq. (2.63) and Eq. (2.74), and integration for three different time phases, including the integration initial ε_i for t=0, there is,

$$\varepsilon = \varepsilon_i + \int_{\sigma'_0}^{\sigma'_0 + q} \frac{1}{M} d\sigma' + \int_{t_p}^{t} \frac{1}{R} dt = \varepsilon_i + \varepsilon_p + \varepsilon_c \tag{2.84}$$

where ε_i is initial strain, caused by $\Delta\sigma'$ at a very small time t_i, ε_p is primary consolidation over time t_p, and ε_c is creep strain, after time t_p. In this idealization no overlap is encountered.

A series of drained and undrained triaxial creep tests with Norwegian Eberg clay were carried out by S. Christensen [23]. The extended time resistance concept was used for the evaluation. If one would suppose that the creep strain ran through all creep phases displayed in Figure 2–7, then, from an extension of Janbu's resistance concept, the following equations emerge for strain,

$$\varepsilon = \left(\frac{t}{t_c}\right)^{1 - n_c} \cdot \frac{1}{r_c \cdot (1 - n_c)} \tag{2.85}$$

where $0 < t < t_c$,

$$\varepsilon = \frac{1}{r_c \cdot (1 - n_c)} + \frac{1}{r_s} \cdot \ln\left(\frac{R_c + r_c \cdot (t - t_c)}{R_c}\right) \tag{2.86}$$

where $t_c \le t < t_{si}$, and

$$\varepsilon = \varepsilon_c + \frac{1}{r_s} \cdot \ln\left(\frac{R_c + r_c \cdot (t - t_c)}{R_c}\right) + \frac{t - t_{si}}{R_{max}} \tag{2.87}$$

where $t_{si} \le t < t_{sf}$. The parameters used above have the following meaning: t_c is initial response time, r_c is initial creep response number, n_c is initial time response exponent, t_{si} is the starting time of the secondary creep, r_s is the creep resistance number for the primary creep, R_c is time resistance at t_c, ε_c is initial creep strain, t_{sf} is starting time of the tertiary creep and R_{max} is the time resistance in the secondary creep. A complete R-t curve for the strain going through all creep phases is shown in Figure 2–23.

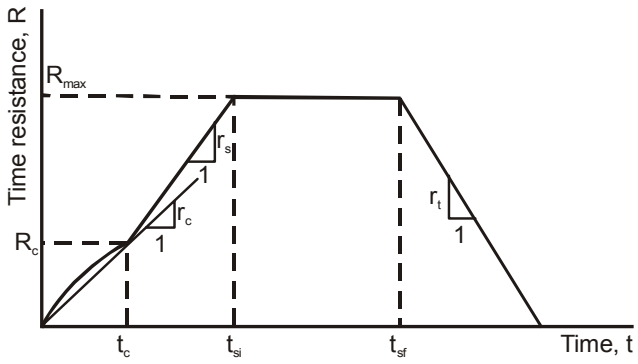

Figure 2–23: Definition of the time resistance R for the triaxial behaviour.

More information about the time resistance concept together with a numerical example of its application can be found in [100], for example. Application of the resistance concept to case records is presented in [47, 51].

2.3 Numerical models

Numerical analysis can be defined as a general study of methods for solving complicated mathematical problems using the basic arithmetic operations. In the case of modelling the behaviour of geotechnical materials, the continuum with infinitely many degrees of freedom is replaced by a set of points or elements with a finite number of interconnections. Instead of unknown continuous functions, the numerical values of these functions are determinated in a set of discrete points. So finally the governing system of differential or integral equations is replaced by a large system of linear of nonlinear algebraic equations (according to M. Dolezalova in [33], or according to [117]). It is of course necessary to use computers to solve these equations. From this point of view it is possible to say that the development of numerical

models is directly connected with the development of computers. Today numerical models can be divided into three large groups: finite element method (FEM), boundary element method as a part of integral methods (BEM) and the distinct element method (DEM). In-depth information about these methods can be found in [29, 31, 33, 41, 56] etc.

Based on the above introduction to the numerical models, one can see that numerical analysis is the only tool for solving differential or integral equations. The main background of the numerical models used in geotechnics are constitutive relations, i.e. relations between stress and strain, and in the case of the rheology also time. These relations are based on the previously explained rheological and phenomenological models or on the micro-rheology. There are a lot of constitutive relations for modelling of the creep, or, more generally, rheological behaviour of the soil materials. In [33] one can find a division into the four main groups - linear viscoelastic, non-linear viscoelastic, elastic-viscoplastic and rate-type viscoplastic relations.

In 1966 Perzyna presented an elastic-viscoplastic model based on his theory of overstress, which has become more or less a standard basis for the further development of viscoplastic models [54]. In this type of model, the strain is decomposed into two parts - an elastic one and a viscoplastic one,

$$\dot{\varepsilon}_{ij} = \dot{\varepsilon}^{e}_{ij} + \dot{\varepsilon}^{vp}_{ij} \tag{2.88}$$

The viscoplastic strain is assumed to be time-dependent, where the viscoplastic strain rate intensity depends on the distance between the position of the stress state, which defines the position of the so-called loading or dynamic yield surface, and the static yield surface, see Figure 2–24. The value of the viscoplastic strain rate increase with the increasing distance between static and loading yield surfaces.

From the numerical point of view one can write the following equation for the viscoplastic strain,

$$\dot{\varepsilon}^{vp}_{ij} = \gamma^{0} \cdot \langle \phi(F) \rangle \cdot \frac{\partial F}{\partial \sigma_{ij}}, \tag{2.89}$$

where F is a yield function defined as,

$$F = \frac{f}{k_s} - 1, \tag{2.90}$$

f is a valid yield function of plasticity in the stress space, k_s is a fixed material parameter or it can be a function of hardening with the accumulation of viscoplastic

strain, e.g. $k_s = g(\varepsilon_{ij}^{vp}, \varepsilon_{ij}^{vp})$, $\phi(F)$ is a scalar function and <> are the Macaulay brackets defined as,

$$\langle \phi(F) \rangle = \begin{cases} 0, & \phi(F) \le 0 \\ \phi(F), & \phi(F) > 0 \end{cases}, \tag{2.91}$$

and γ^0 is a constant, influenced by the material viscosity.

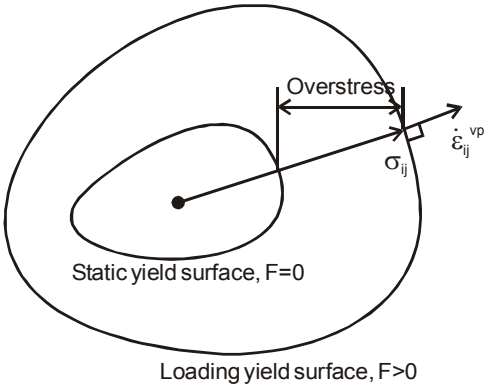

Figure 2–24: Demonstration of the Perzyna's overstress concept.

A one-dimensional viscoelastic model for the creep behaviour of clays has been developed at NTNU and SINTEF by Svanø, Christensen and Nordal [102] and implemented to the one dimensional finite element program for the soil consolidation analysis KRYKON developed by Svanø [32, 101]. The program couples soil compression and Darcy water flow in an integrated set of equations, where the soil permeability k is used for the water flow. Although the program is 1D, the radial drainage can be added by specifying a horizontal permeability different from zero. The soil constitutive law of the viscoelastic model is based on Janbu's time resistance concept explained in Section 2.2.3 and PhD work by Nowacki [84]. The creep strain rate is here assumed to be a function of the current strain and effective stress,

$$\dot{\varepsilon}_c = f(\sigma', \varepsilon). \tag{2.92}$$

After integration of Eq. (2.74) and assumption that the time resistance R can be defined as,

$$R = R_0 + r_s \cdot t, \tag{2.93}$$

where R_0 is a reference value of the time resistance in the time t_0 which conforms to the start of the secondary consolidation, the strain at any time t can be described as,

$$\varepsilon = \varepsilon_0 + \frac{1}{r} \cdot \ln \frac{R}{R_0} . \tag{2.94}$$

The ε_0 is a reference value of the strain in time t_0 and corresponds to the strain at the end of the primary consolidation, and r_s is a creep resistance number. From Eq. (2.94) one can describe the time resistance R as a function of the current strain,

$$R = R_0 \cdot e^{r_s \cdot (\varepsilon - \varepsilon_0)} . \tag{2.95}$$

The basic assumption for this model is that for the current effective stress Eq. (2.95) will be valid also at a strain lower than the reference value ε_0. A set of parameters ε_0, R_0 and r_s can be defined for each load step σ' in the oedometer. The creep function at a stress between two load steps can be found by interpolation of these parameters. The variation of the creep resistance number r_s with effective stress σ' can be represented by a bilinear curve, see Figure 2–21. A similar law may be defined for the reference time resistance R_0. The reference strain ε_0 is modelled with Janbu's stress dependent tangent modulus M as,

$$\varepsilon_0 = \frac{\sigma' - p_i'}{M_{oc}} \qquad \text{for} \quad \sigma' \le p_c' \tag{2.96}$$

$$\varepsilon_0 = \frac{p_c' - p_i'}{M_{oc}} + \frac{1}{m} \cdot \ln \frac{\sigma' - p_r'}{p_c' - p_r'} \qquad \text{for} \quad \sigma' > p_c' , \tag{2.97}$$

where p_c' is preconsolidation stress defined from the oedometer test, p_i' is the in-situ effective stress and M_{oc} is the corresponding constant modulus below p_c'. The rest of the parameters correspond to Section 2.2.3. Going back to Eq. (2.74) using time resistance according to Eq. (2.95) one can see that time itself does not enter the equation describing the strain rate.

The system of time resistance isotaches in the stress-strain diagram is shown in Figure 2–25. One can see a different behaviour before and after the crossing of the in-situ preconsolidation stress, p_c'. Practical application of this model to the Skå-Edeby test fill and Oslo railroad customs building can be found in [102].

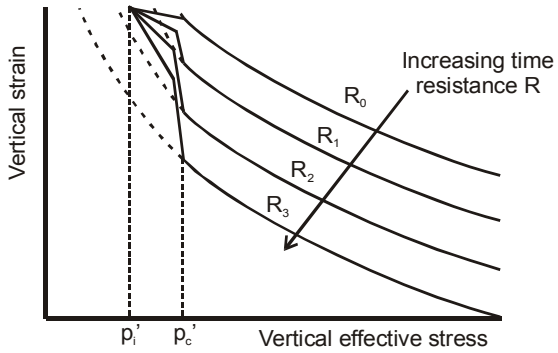

Figure 2–25: Contours of the time resistance in the stress-strain diagram, [102].

The logarithmic creep law for the secondary consolidation was transformed into a differential form and then extended towards general 3D states of stress and strain by Vermeer et al. [89, 110, 111]. This elastic-viscoplastic model was implemented to the PLAXIS as a Soft-soil-creep model. The basic idea of this model is connected with Bjerrum's and Janbu's approaches. Total strain is supposed to be sum of a time independent elastic part and a time dependent creep (viscoplastic) part. So if the effective stress σ' will be applied to the soil sample then one can write the following equation for the total strain in accordance with the time resistance concept,

$$\varepsilon = \varepsilon_e + \varepsilon_c = A \cdot \ln\frac{\sigma'}{\sigma_0'} + C \cdot \ln\frac{t_r + t}{t_r} \tag{2.98}$$

where t_r is a time defined in Figure 2–22, t is time of the creep, C is a creep parameter and A is a "deformation" parameter defined as,

$$C = \frac{C_\alpha}{(1 + e_0) \cdot \ln 10} = \frac{1}{r_s}, \tag{2.99}$$

$$A = \frac{C_r}{(1 + e_0) \cdot \ln 10}, \tag{2.100}$$

C_α is coefficient of secondary compression, C_r is swelling index, e_0 is the initial void ratio and r_s is the creep resistance number. For the same strain it is possible to write the following equation,

$$\varepsilon = \varepsilon_e + \varepsilon_c = A \cdot \ln\frac{\sigma'}{\sigma_0'} + B \cdot \ln\frac{\sigma_p'}{\sigma_{p0}'} \quad \rightarrow \quad \sigma_p' = \sigma_{p0}' \cdot e^{\left(\frac{\varepsilon_c}{B}\right)} \tag{2.101}$$

where B is the parameter connected with the compression index C_c and swelling index C_r through equation,

$$B = \frac{C_c \cdot C_r}{(1 + e_0) \cdot \ln 10} \tag{2.102}$$

In equations Eq. (2.101) and Eq. (2.102) σ_0' represents the initial effective pressure before loading, σ_{p0}' represents the preconsolidation pressure before loading and σ_p' is the preconsolidation pressure after creep. Figure 2–26 shows a stress-strain situation with the total strain divided into the elastic and creep part.

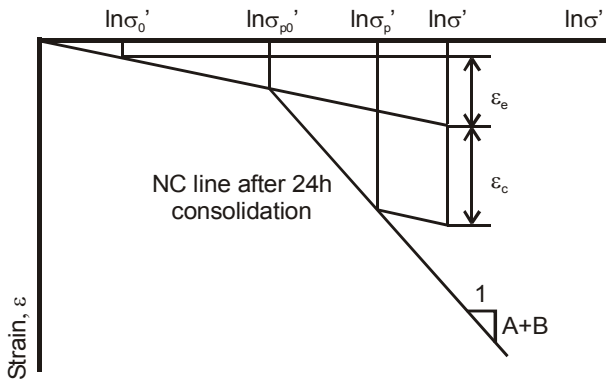

Figure 2–26: Visualisation of the model's idea in 1D.

The time dependency of the preconsolidation pressure may be found by combining Eq. (2.98) and Eq. (2.101),

$$B \cdot \ln\frac{\sigma_p'}{\sigma_{p0}'} = C \cdot \ln\frac{t_r + t}{t_r} \tag{2.103}$$

For time $t_r + t = \tau_d = 24h$ the preconsolidation pressure $\sigma_p' = \sigma'$. If one can suppose that $t = \tau_d - t_r$ then,

$$B \cdot \ln\frac{\sigma'}{\sigma_{p0}'} = C \cdot \ln\frac{\tau_d}{t_r} \quad \text{for} \quad OCR=1 \tag{2.104}$$

and

$$\frac{\tau_d}{t_r} = \left(\frac{\sigma'}{\sigma_{p0}'}\right)^{\frac{B}{C}} \tag{2.105}$$

For the strain rate it is possible to get from Eq. (2.98)

$$\dot{\varepsilon} = \dot{\varepsilon}_e + \dot{\varepsilon}_c = A \cdot \frac{\dot{\sigma}'}{\sigma'} + \frac{C}{t_r + t} \tag{2.106}$$

where t_r+ t can be eliminated using Eq. (2.103),

$$\dot{\varepsilon} = \dot{\varepsilon}_e + \dot{\varepsilon}_c = A \cdot \frac{\dot{\sigma}'}{\sigma'} + \frac{C}{t_r} \cdot \left(\frac{\sigma_{p0}'}{\sigma_p'}\right)^{\frac{B}{C}} \tag{2.107}$$

Finally, using Eq. (2.105), it is possible to eliminate t_r and σ_{p0}' and obtain the final differential equation for the 1D situation,

$$\dot{\varepsilon} = \dot{\varepsilon}_e + \dot{\varepsilon}_c = A \cdot \frac{\dot{\sigma}'}{\sigma'} + \frac{C}{\tau_d} \cdot \left(\frac{\sigma'}{\sigma_p'}\right)^{\frac{B}{C}} \quad \text{where} \quad \sigma_p' = \sigma_{p0}' \cdot e^{\left(\frac{\varepsilon_e}{B}\right)} \tag{2.108}$$

One can see, that the strain rate is fully connected with an overconsolidation ratio. With increasing OCR the strain rate will also be increasing and vice versa.

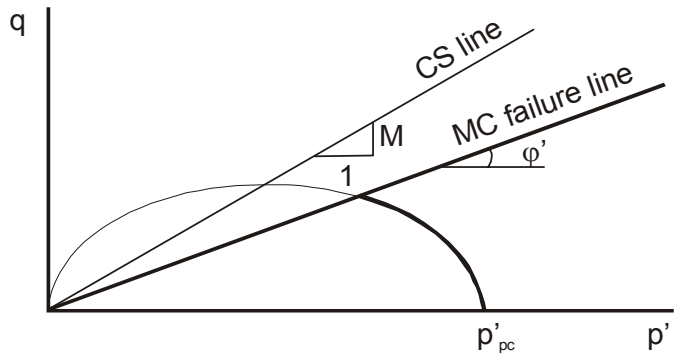

Figure 2–27: Visualisation of the SSC model in p'-q diagram.

Extension of this approach to the general, three-dimensional state of stress and strain one can find in [110, 89]. In fact, this general 3-D model is partly based on the Modified Cam-Clay constitutive model introduced by Roscoe and Burland in 1968, i.e. the Cam-Clay ellipse is used here as a yield surface for the volumetric harden-

ing, so-called "cap". The shape of this cap (and creep behaviour close to the failure) is then controlled by the slope of the so-called "critical state line" represented in PLAXIS by the parameter M (do not mix with Janbu's tangent modulus). The failure criterion is based on the Mohr-Coulomb constitutive model. Visualisation of this model in the p'-q diagram is shown in Figure 2–27.

The main disadvantage of the Soft-soil-creep model is the problem of modelling the deviatoric creep behaviour, e.g. lacking possibility of modelling the real deviatoric creep behaviour of the over-consolidated soil.

One can find a lot of more sophisticated models for the modelling of the soil creep behaviour. For instance, an elastic-viscoplastic model with incorporated damage law was introduced by Aubry, Kodaissi and Meimon [8]. Kachanov's type isotropic damage variable has been incorporated into the model, that allowed numerical reproduction of all creep phases, i.e. primary, secondary and tertiary. Oka, Adachi and Mimura [87] presented two elastic-viscoplastic constitutive models for normally-consolidated and over-consolidated clays, based on the generalised Perzyna's overstress concept and the Cam-clay model in the case of the normally-consolidated clay, and non-associated flow rule and Perzyna's concept in the case of the over-consolidated clay. Both proposed models are able to simulated an acceleration creep failure, i.e. creep rupture after tertiary creep. A non-associated Cam-clay plasticity model containing creep was introduced by Kavazanjian [54], for the modelling of the stress-strain-time behaviour of normally-consolidated to lightly over-consolidated soft clay. A second, horizontal yield surface was used by Kavazanjian within the modified Cam-clay yield ellipse, where for the both yield surfaces isotropic hardening under immediate, time-independent strains and delayed, time-dependent strains was used. Maleki, Cambou, Farsi and Ph. Dubujet developed an elastoplastic-viscoplastic model, where the viscous behaviour is defined by internal viscous variables and a viscous yield surface [62]. The expansion of the viscous yield surface is governed by so called "viscous hardening". The secondary creep surface is included making the boundary between primary and secondary creep. An advance elastic-viscoplastic model based on the Desai's hierarchical approach was presented by Vulliet and Desai [114]. An elastic-viscoplastic model of normally-consolidated clays in undrained creep was introduced by Matsui and Abe [68], Elastic-viscoplastic model with creep rupture was presented by Abe [2], or a Creep and stress relaxation model was introduced by Borja [19].

2.4 Micro-rheology

In the previous approaches the effect of the soil structure can be involved indirectly through to the additional "phenomenological" parameters. Soil material was supposed to be continuous and only the relations of its input and output data were investigated. In the case of the micro-rheology (in some literature also called the structural approach) the evaluation of the soil behaviour is connected with the physical ideas about their structure. In other words, exploration of the soil behaviour starts with structural conceptions which leading to the general soil behaviour. A strong advantage of this approach is a better understanding of the essence of the soil's stress-strain-time behaviour. According Feda [33] one can divide micro-rheology to the two concepts - micromechanical approach and particle-based conception (mesomechanical approach). Although the investigation of the creep in soft soils performed by the author did not contain the effect of the soil structure, the main micro-rheological methods have to be introduced. In spite of the complexity and strong physical background of these methods only a brief description will be presented here.

The source of the micromechanical approach is the consideration of Boltzmann's (statistical) law governing the movement of so-called flow units and its phenomenological consequences [33, 34]. Based on this law, in 1941 Eyring, Glasstone and Laidler developed a theory of absolute reaction rates, and applied this theory at the atomic and molecular levels [38]. Soon after its introduction the theory of absolute reaction rates was modified and applied to the wild spectrum of processes in which a time-dependent rearrangement of matters occurs. Adaptations to the study of soil behaviour was performed by e.g. Murayama and Shibata [80, 81], Christensen and Wu [22], Mitchell [78, 79], Abdel-Handy and Herrin [1], Andersland and Douglas [4] among others.

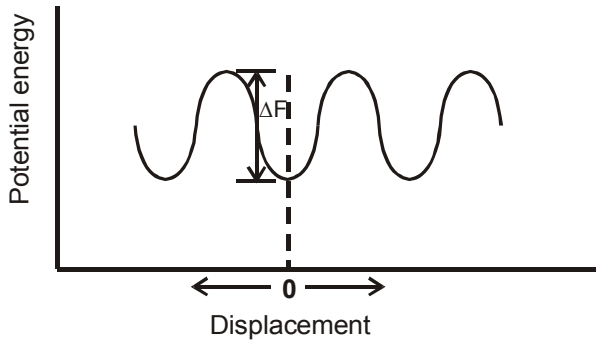

Figure 2–28: Energy barriers and activation energy, [79].

The basic idea of the rate process theory is that atoms, molecules and/or particles, termed "flow units", are separated by energy barriers which fix their equilibrium positions, distinguished by the minimum potential energy. The displacement to new positions has to be initiated by the introduction of a free energy of activation, ΔF, of sufficient magnitude to cross the barrier, see Figure 2–28. The source of the activation energy is represented by the energy of thermal vibrations of flow units, modified by various potentials. The value of activation energy depends on the material and the type of process. After crossing a barrier, the flow units occupies new free positions, formed by itself or by a defect in the crystalline lattice. So, such a deformation may be described as a sequence of displacements of flow units, made possible by the presence of various defects in the structure of the materials [33].

The mechanism of a thermally activated process is shown in Figure 2–29. Curve A represents material at rest, where A-C represent stable (equilibrium) position of flow units at a distance λ. The frequency of activation k' for the curve A is, according to [79],

$$k' = \frac{k_b \cdot T}{h_p} \exp\left(\frac{-\Delta F}{N k_b T}\right) \tag{2.109}$$

where k_b is Boltzmann's constant (=1.38E-23 JK^{-1}), T is the absolute temperature [K], h_p is Planck's constant (=16.625E-34 Js^{-1}) and N is Avogadro's number (=6.02E+23). In the absence of a directional potentials the energy barrier is crossed by the flow units in all directions and no deformation takes place.

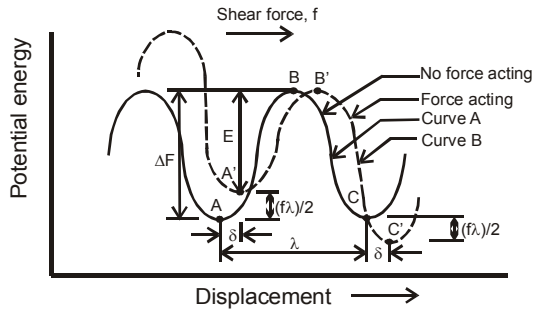

Figure 2–29: The effect of the shear force on energy barriers, [79].

After application of the shear stress, the original energy barrier becomes deformed (curve B). If one denotes the shear force acting on flow units as f, then the barrier height is reduced by an amount (fλ)/2 in the direction of the force and raised an equal amount in the opposite direction. The value of δ equals the elastic distortion of the material structure. The reduced energy barrier in the direction of shear force, according to the rate process theory, will then be

$$\vec{k}' = \frac{k_b \cdot T}{h_p} \exp\left(-\frac{\left(\frac{\Delta F}{N} - \frac{f \cdot \lambda}{2}\right)}{k_b T} \right), \tag{2.110}$$

and in the opposite direction

$$\vec{\underset{\sim}{k}}' = \frac{k_b \cdot T}{h_p} \exp\left(-\frac{\left(\frac{\Delta F}{N} + \frac{f \cdot \lambda}{2}\right)}{k_b T} \right). \tag{2.111}$$

The net frequency of activation in the direction of the shear force gives the relation,

$$\vec{k}' - \vec{\underset{\sim}{k}}' = 2 \cdot \frac{k_b \cdot T}{h_p} \exp\left(-\frac{\Delta F}{R_g T}\right) \sinh\left(\frac{f \cdot \lambda}{2 k_b T}\right) \tag{2.112}$$

where R_g is the universal gas constant. If then the displacement of the flow units in a given direction will be multiplied by the number of successful jumps per unit time, the rate of movement per unit time can be computed according to the equation,

$$\dot{\varepsilon} = 2 \cdot X \cdot \frac{k_b \cdot T}{h_p} \exp\left(-\frac{\Delta F}{R_g T}\right) \sinh\left(\frac{f \cdot \lambda}{2 k_b T}\right) \tag{2.113}$$

where X is a proportion of successful barrier crossing and may be both time and structure dependent.

In-depth information about micromechanical approaches together with practical experience and applications to real soil can be found in [33] or [79].

Particle-based conceptions consider soil particles as the principal structural element. Creep is then explained as a mechanically activated process which depends on the stress level [33. This mechanically activated process is combined with the previously described one by some investigators. Generally, the particle-based conception is more frequently applied to the granular materials than to the clayey soils.

The distinct element method was developed as a particle-based approach. Numerical experimentation with two-dimensional granular assemblies was performed by Cundall and Strack in 1982 [28]. Based on their experience they developed a distinct-element method [29] which was later extended to 3D. Interesting results obtained in this way question the phenomenological definition of strain and stress. They show, among other things, the discontinuous nature of the internal deformation of such assemblies [33]. Today the distinct element methods are used and modified by many researchers.

Chapter 3 Volumetric creep behaviour - One-dimensional consolidation of clay

In engineering practice consolidation is one of the main features of the behaviour of the clayey soils. The compressibility of the soil plays an important role in the variation of the soil strength and deformation characteristics with time, and is extremely important to the design of foundations and soil structures based on the secondary limit state, i.e. limiting strain. From this point of view volumetric creep as a part of the soil consolidation is an extremely important part of the behaviour of the clayey soils and has to be taken into consideration and carefully investigated.

The soil consolidation is a long and extremely complex process, governed by a large number of natural and external factors, such as mineral composition, grain-size distribution, moisture content, density, structural strength, permeability, collapsibility, sensitivity, swelling, shrinkage on drying, magnitude, rate and method of load application, duration of the loading, temperature and chemical changes inside sample [79, 112, 113]. In nature, soil consolidation can be simple or complex, depending on the thickness of the deposit and the type of loading. In the case of the simple consolidation, soil is compressed only in the direction of the maximum principal normal stress σ_1, while in the case of the complex consolidation, compression occurs in two or three directions [69]. Simple consolidation is denoted as one-dimensional consolidation or consolidation without lateral expansion. In engineering practice, the one-dimensional consolidation is assumed to represent the compression of a soil layer, provided that the foundation base is at least two times the thickness of the soil layer.

Generally the soil consolidation can be divided to the primary and secondary phases, where secondary consolidation can be denoted volumetric creep. Laboratory investigation of the volumetric creep deformation during one-dimensional consolidation was studied by the author. After the literature review, the several oedometer tests with different clayey materials and different tests' conditions were performed and evaluated with emphasis on creep behaviour. Detailed investigation of these tests together with a comparison of the results of the tests obtained under different conditions are presented in this chapter. Before the description of the experimental work, the basic theoretical background of the one-dimensional consolidation, containing historical resumé, introduction to the laboratory investiga-

tion and evaluation of the one-dimensional consolidation, will be introduced in the next sections.

3.1 Historical resumé

The pioneering work on the stress-strain behaviour during one-dimensional consolidation was performed by K. Terzaghi. In 1923 he published his theory of one-dimensional consolidation [107], which became the foundation for later investigations. This theory is today known as a classical theory or theory of seepage consolidation. Terzaghi's theory, developed for the prediction of long-term settlement of structures, considers that the deformation of a layer of saturated soil is determined only by the rate of seepage of pore water under the action of external load. The skeleton is considered to be a linearly deformable body with the property of instantaneous deformation [69]. Terzaghi's theory is based on the following assumptions:

- The soil is fully saturated.
- The soil-water system is homogeneous and isotropic.
- The water is supposed to be incompressible.
- The compressibility of mineral particles is neglected.
- A linear relation between the normal effective stress and void ratio is assumed.
- The flow of the water is only in one direction.
- Darcy's law of laminar seepage is valid.
- A constant coefficient of permeability during the consolidation is assumed.

Based on these assumptions and using an analogy between the theory of consolidation and the theory of heat transfer, Terzaghi proposed the pore pressure based differential equation,

$$\frac{\partial u}{\partial t} = C_v \cdot \frac{\partial^2 u}{\partial z^2} \tag{3.1}$$

where u is the pore water pressure, t is time, z is the depth and C_v is the coefficient of consolidation connected to the permeability k as,

$$C_v = \frac{k}{\gamma_w \cdot m_v} \tag{3.2}$$

m_v is the coefficient of volume compressibility defined as the volume change per unit volume per unit increase in effective stress, i.e.

$$m_v = \frac{1}{1 + e_0} \cdot \frac{\Delta e}{\Delta \sigma'} \tag{3.3}$$

Solution of Eq. (3.1) for the two-way drainage situation, i.e. boundary conditions,

z=0 u=0,
z=2H u=0,
t=0 $u=u_0$,

yields to,

$$u = \sum_{n=0}^{\infty} \left[\frac{2 \cdot u_0}{N} \cdot \sin\left(\frac{N \cdot z}{H}\right) \right] \cdot e^{-(N^2 \cdot T_v)} \tag{3.4}$$

where n is an integer,

$$N = \frac{\pi}{2} \cdot (2 \cdot n + 1), \text{ for } n = 1, 2, 3, \text{ etc.} \tag{3.5}$$

H is the height of the sample, u_0 is the initial excess pore pressure and T_v is the time factor defined as,

$$T_v = \frac{C_v \cdot t}{H^2} \tag{3.6}$$

Finally the average degree of consolidation U_z for the entire depth of the clay layer at any time t can be defined as,

$$U_z = 1 - \frac{\left(\frac{1}{2 \cdot H_{dr}}\right) \cdot \int_0^{2H_{dr}} u_z dz}{u_0} \tag{3.7}$$

More information about the classical theory of consolidation can be found in [30, 105, 106]. Even though the theory of seepage consolidation makes several unrealistic assumptions and does not involve secondary consolidation, it is still widely used in engineering practice to forecast compression rates and pore-water pressure in clays. According to the Terzaghi's classical theory, the strain-based consolidation theory was developed by Janbu in the 1960s. One can find an explanation of this theory in Section 2.2.2.

General theory of the three-dimensional consolidation was proposed by Biot, [13], in 1941. Biot supposed that soil is a porous skeleton filled with pore fluid, where the porous skeleton is assumed to be an isotropic elastic medium and pore fluid is

incompressible. The following equations of equilibrium have to be satisfied for the total normal and shear stresses,

$$\begin{aligned}
\frac{\partial \sigma_x}{\partial x} + \frac{\partial \tau_{xy}}{\partial y} + \frac{\partial \tau_{zx}}{\partial z} + w_x &= 0 \\
\frac{\partial \tau_{xy}}{\partial x} + \frac{\partial \sigma_y}{\partial y} + \frac{\partial \tau_{yz}}{\partial z} + w_y &= 0 \\
\frac{\partial \tau_{zx}}{\partial x} + \frac{\partial \tau_{yz}}{\partial y} + \frac{\partial \sigma_z}{\partial z} + w_z &= 0
\end{aligned} \tag{3.8}$$

where w_x, w_y, and w_z are the body force component per unit volume. These equations have to be coupled to the Biot's equation of the flow continuity, which is based on the Darcy's law,

$$\frac{k_x}{\gamma_w} \cdot \frac{\partial^2}{\partial x^2}\bar{u} + \frac{k_y}{\gamma_w} \cdot \frac{\partial^2}{\partial y^2}\bar{u} + \frac{k_z}{\gamma_w} \cdot \frac{\partial^2}{\partial z^2}\bar{u} + \frac{\partial \varepsilon_v}{\partial t} = 0 \tag{3.9}$$

where, ε_v is volumetric strain, γ_w is unit weight of water, $\bar{u} = u + z \cdot \gamma_w$, u is pore pressure and z is depth. Detailed information about this theory is possible to find in [13]. Finite element formulation of the consolidation for coupled problems based on the Bion's theory can be found in [90].

In 1938, Pokrovsky performed consolidation tests with saturated soil specimens with different heights - 1 and 4 cm. Based on these tests he found that duration of deformation did not differ much in these two cases, i.e. the height of the specimen had almost no effect on the time of consolidation [69]. This fact contradicts Terzaghi's classical theory. Taylor and Merchant, as mentioned earlier, re-examined the classical theory and solved the problem of one-dimensional consolidation of saturated clayey soils with the incorporation of the secondary consolidation, i.e. prolonged deformation of the soil's skeleton [104]. In 1953, Florin published his theory of the consolidation of porous creeping saturated soil, which assumed a simultaneous action of seepage and skeleton creep from the beginning of consolidation, proceeding in accordance with the linear theory of hereditary creep for ageing materials. This theory was later confirmed by several experimental studies by Gibson and Lo [37], Lo [58] etc.

The time resistance concept was developed at NTH by Janbu for the evaluation of the stress-strain-time soil behaviour. More information about this concept is presented in Section 2.2.3. Based on this concept the complex study of the creep behaviour of the Norwegian Eberg and Troll clays using oedometer tests was performed by Christensen at SINTEF. Evaluation of these tests can be found in [25, 26].

Detailed description of the application of the Janbu's theory will be described in the following sections.

A lot of different investigations were performed by many authors. Unfortunately there is not enough space in this thesis to describe all of them. Briefly one can mention work by Mesri [72], Mesri and Rokhsar [76], Mesri and Choi [73, 74], Mesri and Godlewski [71], investigation of the primary and secondary consolidation of the Finnish clays by Naatanen, Lojander and Puumalainen [85], study of the consolidation of clay and peat by Barden [10], work by Leroueil, such as [57], or the unique explanation of secondary consolidation of clay as a local dehydration process with the suggestion of a new model by Navarro and Alonso [83]. The effect of the secondary consolidation on the undrained shear strength of clay was introduced by Bjerrum and Lo [17]. Similar investigation combined with the influence of the long-term consolidation to the K_0 value can be found in [117].

3.2 Introduction to the laboratory investigation of consolidation

In 1910, the first equipment for the one-dimensional consolidation test was constructed in France by Frontar. In 1919, the Swedish Geotechnical Commission performed the one-dimensional consolidation test of clayey soil by squeezing out water through sand layers on two sides [69]. This method was later used by Terzaghi [107] to design the consolidometer, today known as the consolidation apparatus or oedometer.

3.2.1 Simulation of consolidation - oedometer apparatus

An oedometer test is one of the simplest and most widely used test in soil mechanics. Its results for the relevant conditions find a direct application in the calculation of the settlement and is extremely useful for a basic understanding of soil behaviour. A schematic diagram of the oedometer apparatus is shown in Figure 3–1. The soil specimen is placed inside a steel rigid ring to avoid an occurrence of lateral expansion. The height of the ring should be at least 2 cm and the diameter/height ration should be at least two (e.g. according to the British Standards BS1377 the diameter/height ratio must lie between three and four). Drainage is achieved by two porous discs, located at the top and bottom. The bottom disc functions as a base and the top as a piston, transmitting an external load to the specimen. During the test, the soil specimen is covered with water. The load is usually applied through a lever arm, and the compression is measured by a micrometer dial gauge.

The main problem of the oedometer apparatus is friction between the specimen and the wall of the metal ring. Frictional forces reduce the transmission of the external load to the soil specimen, which can lead to a non-homogenous state of stress and physical non-linearity in the soil. Lower soil density from the top downwards and from the centre to side of the specimen is then observed. This defect can be reduced by an increase in the D/H ratio (where D is the diameter of the specimen and H is the height of the specimen) and using industrial Vaseline or a Teflon film in the internal surface of the ring. There are also other methods, like using rings with a special design. One example can be a floating ring with the double-ended compression, i.e. both porous discs serve as a piston. The results from such a test will be presented below, see Section 3.3.4.

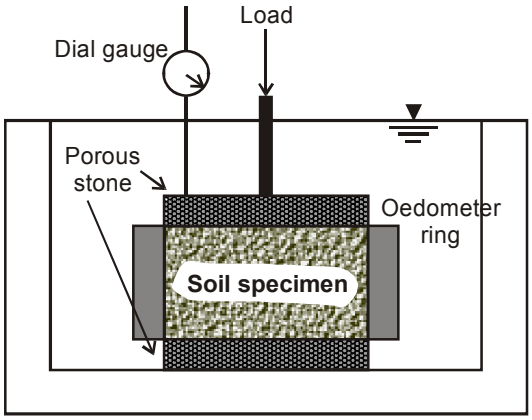

Figure 3–1: Basic scheme of the oedometer, [30].

Today one can find many types of oedometer test apparatus. Besides the classical incremental loading test, the constant rate of strain (CRS) test is now widely used [97, 116]. The loading is controlled by a fixed rate of strain $\dot{\varepsilon}_v$ in this test. As an alternative to the CRS test, the constant pore pressure ratio (CPR) test was introduced by Janbu and Tokheim [52]. In the CPR test a fixed ratio of bottom pore pressure in the sample to the total stress is controlled. The fixed ratio is normally 20-30%. For the CRS and CPR test it is typical that the porous disc is applied only on top of the specimen and the bottom part is impervious with the excess pore pressure measurement.

3.2.2 Compression curves

Terzaghi represented the results of his tests in the form of curves, denoted as compression curves, which depict the variation of void ratio e of the soil with the inter-

granular pressure σ′ in an arithmetic scale. Later on, the international geotechnical society started to use the curve e vs. log σ′, which is widely used to the present day. This idealised curve is shown in Figure 3–2. The constructed slope of the curve for the over-consolidated range was denoted as a recompression index, C_r, and the normally consolidated range compression index, C_c. Then one can write the following general equations,

$$e_0 - e = C_r \cdot \log\frac{\sigma'}{\sigma_0'}; \quad \sigma' \le \sigma_0' \tag{3.10}$$

$$e_0 - e = C_r \cdot \log\frac{\sigma_c'}{\sigma_0'} + C_c \cdot \log\frac{\sigma'}{\sigma_c'}; \quad \sigma' \ge \sigma_c' \tag{3.11}$$

where e_0 is the initial void ratio and σ_c' is the preconsolidation effective stress.

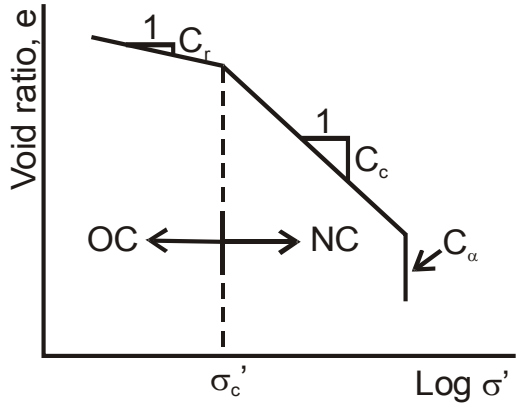

Figure 3–2: Idealised relationship between void ratio e and logarithm of the effective stress σ′.

Terzaghi and Peck [105] suggested empirical expressions of C_c for the undisturbed and remolded clay as,

$$C_c = 0,009 \cdot (w_L - 10) \tag{3.12}$$

for the undisturbed clay, and

$$C_c = 0,007 \cdot (w_L - 10) \tag{3.13}$$

for the remolded clay, where w_L is the liquid limit in%. Using the compression index for normally consolidated clay, the strain becomes,

$$\varepsilon = \frac{C_c}{1 + e_0} \cdot \log \frac{\sigma'}{\sigma_c'} \tag{3.14}$$

The coefficient of secondary consolidation, C_α, explained in Section 2.2.2 with Eq. (2.29), is usually used for the evaluation of the creep behaviour.

Regardless of its wide use, the e-logσ' method seems to be quite complicated and illogical in comparison with the natural, ε–σ' curve. The "philippic" against the e-logσ' method, based on the logical aspects, was made by Janbu in [48], quote: "It remains a mystery why the international profession still uses the awkward e-logσ' plots, and the incomplete and useless coefficient C_c, which is not even determined on measured data, but rather taken from a constructed "line" outside a measurements, for which no plausible explanation is yet available". Janbu suggested the resistance concept, explained in Section 2.2.3, which has a physical background and as an input use ε–σ' and ε-t curves. The following advice was given by Janbu for the interpretation of stress-strain,

- Use effective stress consistently, $\sigma'=\sigma-u$.
- Use engineering strain, $\varepsilon=\Delta H/H_0$.
- Plot ε vs. σ' in arithmetic scale.
- Obtain the tangent modulus M, Eq. (2.63), for the each load step.
- Plot M vs. effective stress σ'.
- Obtain the preconsolidation pressure σ_c' directly by inspecting the ε–σ' and/or M-σ' curve, when σ_c' is identified by a change in the curve.
- Determine the modulus M_{oc} for the OC-range and modulus number m for the NC-range.

The following advice for the interpretation of the stress-strain-time oedometric behaviour is suggested by the present author,

- Plot ε vs. time t in arithmetic scale.
- Obtain the time resistance R, Eq. (2.74).
- Plot the time resistance R vs. time t in arithmetic scale and obtain the creep resistance number r_s, Eq. (2.75).
- Plot creep resistance number r_s vs. effective stress σ'.
- Obtain the preconsolidation pressure σ_c' directly by inspecting the r_s-σ' curve, and compare it with σ_c' from the stress-strain interpretation.

Because the time resistance concept has been used by the present author for the evaluation of all oedometer tests, the following correlations have to be presented.

C_c can be transferred to the modulus number m for the normally consolidated clays by the relationship from 1963, as,

$$m = \frac{(1 + e_0) \cdot \ln 10}{C_c} \tag{3.15}$$

where, according to Eq. (2.70) and Eq. (2.71),

$$m = \frac{M}{\sigma'} = \frac{1}{\varepsilon} \cdot \ln\left(\frac{\sigma' + \Delta\sigma'}{\sigma'}\right) \tag{3.16}$$

The relation between the coefficient of secondary consolidation C_α and creep resistance number r_s can be written in the form,

$$r_s = \frac{(1 + e_0) \cdot \ln 10}{C_\alpha} \tag{3.17}$$

3.3 Evaluation of results from oedometer tests

As a part of this PhD study, several oedometer tests were performed and evaluated or, in the case of Norwegian quick clay, only evaluated, with emphasis on the volumetric creep behaviour. Four different materials have been chosen - Norwegian quick clay, Onsøy clay, Glava clay and Czech Terlicko clayey shale.

Oedometer tests were carried out in the geotechnical laboratory at NTNU with the incremental loading oedometer apparatus with lever arm, Figure 3–3 a). Generally, two types of oedometer rings were used. The classical oedometer ring, as shown in Figure 3–3 b), with height of the sample H=2 cm and the sample's cross section area 20 cm^2, i.e. with diameter D=5 cm, was chosen for most of the tests. In the case of the Terlicko clayey shale material, two tests were performed with floating ring, see Figure 3–3 c), with height of the sample H=3.2 cm and cross section are 50 cm^2, i.e. D=8 cm. Double drainage path with length H/2 was used for all tests. Deformation was measured by a micrometer dial gauge connected to the computer and all measured data were recorded by a computer program developed at NTNU, Department of Civil and Transport Engineering, Geotechnical Division.

As mentioned above, the time resistance concept was used for the evaluation of the tests, i.e. the advice suggested by Janbu and the author for the evaluation of the stress-strain and stress-strain-time oedometer behaviour with time resistance concept, introduced in the end of Section 3.2.2, was implemented. It means, that the following plots were made for all tests and their load steps,

- Square root of time t vs. deformation δ, $\sqrt{t} - \delta$.
- Time t vs. strain ε, t-ε.
- Time t vs. time resistance R, t-R.
- Time t vs. strain potential S, t-S.
- Effective stress σ′ vs. strain ε, σ′-ε.
- Effective stress σ′ vs. tangent modulus M, σ′-M.
- Effective stress σ′ vs. coefficient of consolidation C_v, σ′-Cv.
- Effective stress σ′ vs. permeability k, σ′-k.
- Effective stress σ′ vs. creep resistance number r_s, σ′-r_s.

For the construction and interpretation of these curves Microsoft Excel and SigmaPlot 8.0 were used.

Two sets of the σ′-M curves were made for all oedometer tests. The first set were plotted in accordance with the time corresponding to the end of the primary consolidation, and the second in accordance with the end of the load step (mostly 24 h).

Time corresponding to the end of the primary consolidation, t_{100}, was evaluated according to Taylor's "square root of time" method, e.g. [30], applied to each of the load steps. Based on Taylor's method, the coefficient of consolidation C_v, [m^2/year], was computed according to the equation,

$$C_v = \frac{0,848 \cdot H_{dr}^2}{t_{90}} \tag{3.18}$$

where H_{dr} is the length of the drainage path, and t_{90} is time corresponding to 90% of the primary consolidation. In addition, the permeability k, [m/day], was calculated from the coefficient of consolidation, according to the formula,

$$k = \frac{\gamma_w \cdot C_v}{M} \tag{3.19}$$

where γ_w is the unit weight of water.

Details of the oedometer test's evaluation with the time resistance concept will be described in the following sections.

a) Incremental loading oedometer with lever arm.

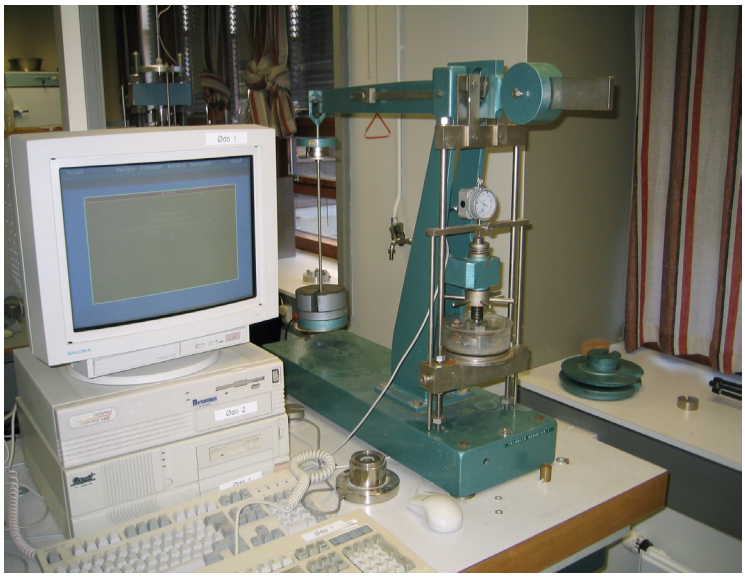

b) “Classical” oedometer ring.

c) Floating oedometer ring.

Figure 3–3: Photos of the incremental loading oedometer apparatus together with metal rings used at NTNU by the author.

3.3.1 Norwegian quick clay

Norwegian clays are encountered most frequently in the regions below and close to the marine level at the last glaciation. These clays are usually very sensitive, losing the greater part of their strength when mechanically disturbed. The most sensitive types, with remolded shear strength s_r<0.5 kPa, are called quick clays.

An example of the typical oedometer test results of the Norwegian quick clay will be presented in the following section. Detailed ways of evaluating the stress-strain-time behaviour will be described. Finally, the application of the Soft-soil-creep model, implemented in the PLAXIS, to the mathematical modelling of the oedometer test will be presented in Section 3.3.1.2. The best fit of the input parameters, based on the oedometer test results will be shown as well as their influence on the behaviour of the model.

3.3.1.1 Evaluation of the oedometer test

Data from the oedometer test performed by Schmidt as a part of her diploma thesis, [93], were used by author for the evaluation of the volumetric creep behaviour of Norwegian quick clay. During her studies at NTNU, Schmidt did seventeen oedometer tests with quick clays from the Kvenild and Frosta areas, which are close to Trondheim. A summary of the basic geotechnical parameters of these clays is shown in Table 3–1. Detailed specification and evaluations of the tests are presented in [93].

Parameters	Units	Typical value
Moisture content, w	%	45
Unit weight of solid particles, γ_S	kN/m^3	27.44
Unit weight, γ	kN/m^3	18.33
Liquid limit, w_L	%	21.50
Plastic limit, w_p	%	17.54
Void ratio, e	-	1.19
Porosity, n	%	54.24
Saturation, S	%	100
Undrained shear strength, s_u	kPa	19.9
Remolded shear strength, s_r	kPa	0.2
Friction angle, φ	°	26.56
Cohesion, c	kN/m^2	5

Table 3–1:Description of the Norwegian quick clay according to index, consolidation and strength tests results, [93].

The incremental, long-term oedometer test of the Kvenild clay, with a 24 h load step duration, was chosen by author for the following study. During test, the Kvenild clay material was fully saturated and placed into the classical oedometer ring. The basic characterisation of the tests is shown in Table 3–2.

Test	Depth	Type of the sample		Load step duration		Applied load steps
no.	[m]	Undisturbed	Remolded	1 h	24 h	[kPa]
19.	13.35	X			X	12.5-25-50-100-200 300-400-500-700

Table 3–2:Characterisation of the used Kvenild clay oedometer test.

As a first part of the quick clay investigation, the stress-strain behaviour was evaluated. After identification of the end of primary consolidation for each load step, two sets of ε-σ′ and M-σ′ curves were constructed, see Figure 3–4 a) and b). One can see the typical shape of the M-σ′ curve for Norwegian quick clay with recognisable grain structure collapse around preconsolidation pressure. As was mentioned earlier, this is the moment the specimen loses most of its internal rigidity due to breakage of the contact points between mineral grains. Based on the ε-σ′ and M-σ′ curves, the preconsolidation pressure σ_c' was found between 100 and 150 kPa. The value of the modulus number m, evaluated for the M-σ′ relation is approximately 19.

a) b)

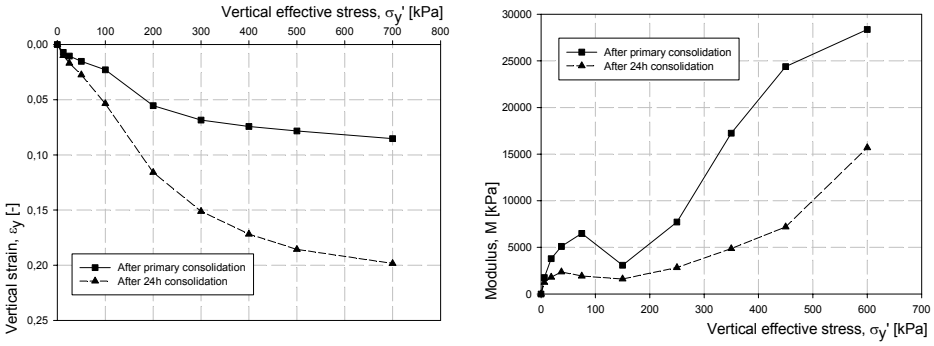

Figure 3–4: Norwegian quick clay - evaluation of the stress-strain behaviour.

Relations between the coefficient of consolidation C_v and vertical effective stress σ′, and permeability k and vertical effective stress are shown in Figure 3–5 a), b). The average value of the coefficient of consolidation was found to be around 10 m^2/year, and the average value of the permeability 2e-5 m/day. These values indicate longer time of the primary consolidation. The preconsolidation pressure σ_c' is discernible

between 100 and 150 kPa, from the shape's change of the C_v-σ′ and k-σ′ curves. This is in accordance with the conclusions, based on Figure 3–4.

a) b)

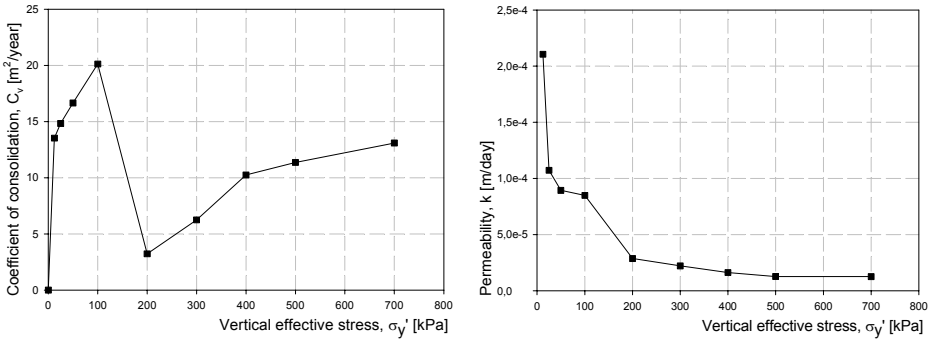

Figure 3–5: Development of the coefficient of consolidation C_v and permeability k during oedometer test.

As a second part of the study, the evaluation of the volumetric creep behaviour was performed. During the evaluation of the time resistance R one can find problem with small oscillation of the vertical strain, which causes large oscillation of time resistance, what is apparent from definition of the time resistance, see Eq. (2.74). This problem can be solved by smoothing the t-ε curve or using suitable approximations. Based on the experience, the second method seems to be easier and more sophisticated then the first one. Several approximations were performed by the author with the computer program Sigma Plot 8.0. For the secondary consolidation the logarithmic function, Eq. (3.20), was chosen as a best approximation of the t-ε curve,

$$\varepsilon(t) = y_{s0} + a_p \cdot \ln(t - x_{s0}) \tag{3.20}$$

where a_p, y_{s0} and x_{s0} are constants. Unfortunately this function is not suitable for the primary consolidation. As a best approximation of the primary part of the t-ε curve according to the coefficient of determination R_{sqr}, the following four sigmoid functions,

$$\varepsilon(t) = y_{p0} + \frac{a_p}{1 + \left(\frac{t}{x_{p0}}\right)^{b_p}} \tag{3.21}$$

$$\varepsilon(t) = y_{p0} + a_p \cdot \left(1 - \exp\left(- \left(\frac{t - x_{p0} + b_p \cdot \ln 2^{\frac{1}{c_p}}}{b_p} \right)^{c_p} \right) \right) \tag{3.22}$$

$$\varepsilon(t) = y_{p0} + \frac{a_p \cdot t^{b_p}}{(c_p^{b_p} + t^{b_p})} \tag{3.23}$$

$$\varepsilon(t) = y_{p0} + a_p \cdot (1 - e^{(-b_p \cdot t)})^{c_p} \tag{3.24}$$

and one hyperbolic function

$$\varepsilon(t) = a_p - \frac{b_p}{(1 + c_p \cdot t)^{\frac{1}{d_p}}} \tag{3.25}$$

were chosen, where a_p, b_p, c_p, d_p, x_{p0} and y_{p0} in these equations are constants. After plotting of t-ε curves based on the approximation together with the original one (see Figure 3–6 a)), sigmoid function represented by Eq. (3.24) was eliminated because of the worst fit into the original curve in comparison with other functions. The rest of functions were used for the evaluation of the time resistance R and settlement potential S, shown in Figure 3–6 b), c). Based on the long experience with using Janbu's time resistance approach at NTNU, and comparison of shape of the laboratory and in-situ R-t and S-t curves evaluated mainly by Janbu [47, 48, 51] with Figure 3–6 b) and c) the sigmoid function represented by Eq. (3.22) seems to be the best approximation of the investigated primary consolidation. Anyway finally the sigmoid function represented by Eq. (3.21), which is still a quite accurate approximation, was chosen by the author. One can see that Eq. (3.22) is more complex, i.e. contained a lot of parameters which have to be evaluated, in comparison with chosen Eq. (3.21). There is not so significant difference in accuracy between these two functions and using a less complex function is easier and faster. As was mentioned in Section 2.2.2, according to the author's investigation the function represented by Eq. (3.21) can be even used, with a little less accuracy, as an approximation curve for the all consolidation in contradiction to Eq. (3.22). Finally all incremental load steps were evaluated by the author based on Eq. (3.21) and Eq. (3.20).

Figure 3–6 c) shows boundaries between primary and secondary consolidations. This was apparent in all load steps with applied effective stress σ′ smaller then preconsolidation pressure σ_c'. After crossing the preconsolidation pressure, the shape of the t-R and t-S curves are close to the theoretical one, described in Section 2.2.3.

a) Time vs. vertical strain curves.

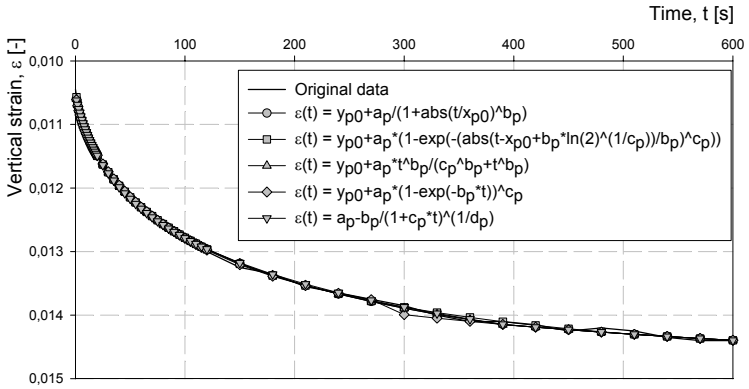

b) Time vs. time resistance curves.

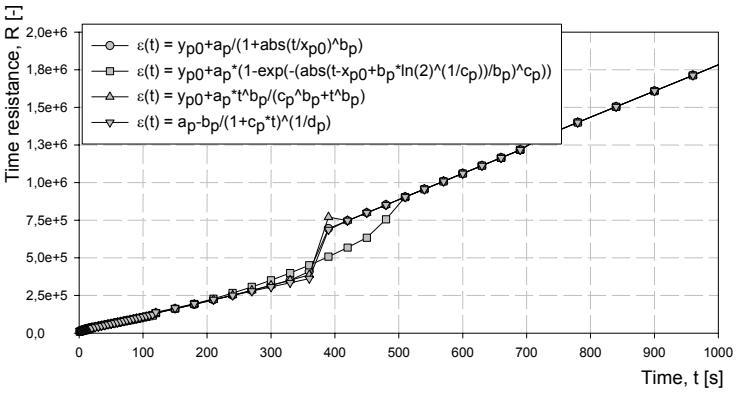

c) Time vs. settlement potential curves.

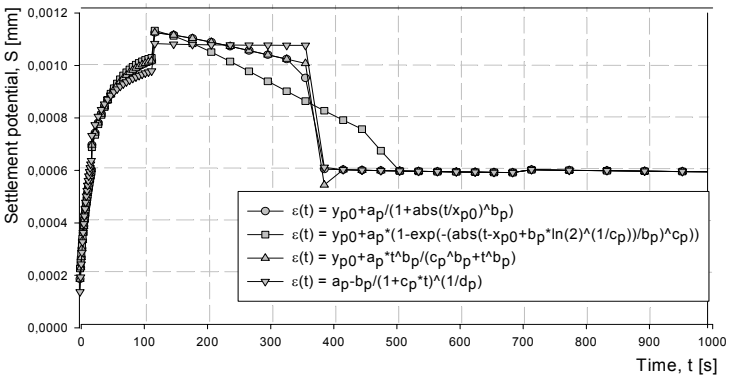

Figure 3–6: Evaluation of the creep behaviour based on the different t-ε curve approximations.

The development of the creep resistance number r_s with increasing effective stress σ' was evaluated based on the t-R relations. It is convenient to use only Eq. (3.20) for this evaluation. Using the definition of the time resistance R introduced in Section 2.2.3 and Eq. (3.20) one can write the following relation,

$$R = \frac{1}{\dot{\varepsilon}(t)} = \frac{(t - x_{s0})}{a_s} \tag{3.26}$$

From this equation it is very easy to define the creep resistance number as,

$$r_s = \frac{dR}{dt} = \frac{1}{a_s} \tag{3.27}$$

Based on the evaluation of the creep resistance number for each loading oedometer step the σ'-r_s relation for the Norwegian quick clay is shown in Figure 3–7. The average value of the creep resistance number for the normally consolidated range (see Figure 2–20) can be found to be around 300. Change of the shape, discernible in the σ'-r_s curve, defines the preconsolidation pressure σ_c' between 100 and 150 kPa. This result is in accordance with the previous investigation.

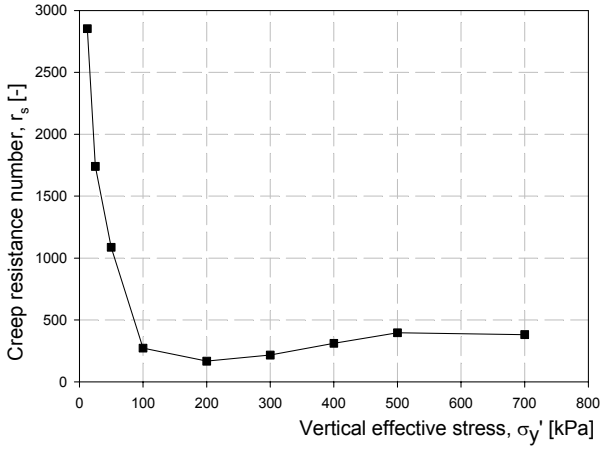

Figure 3–7: Development of the creep resistance number with effective stress for the Norwegian quick clay.

3.3.1.2 Mathematical modelling of the oedometer test with PLAXIS

After evaluation of the Norwegian quick clay oedometer test, described above, the finite element program for geotechnical application PLAXIS was chosen for the simulation of this test. Because of the emphasis placed on the creep behaviour, the Soft-soil-creep constitutive model was used. The theoretical explanation of this model can be found in Section 2.3, and only practical aspects of the use of the model will be introduced here.

As mentioned in the Section 2.3, the Soft-soil-creep model is based on the Modified Cam-clay model and Mohr-Coulomb failure criterion, what is reflected in the input parameters. Besides basic parameters, introduced in Table 3–3, one can define advance input parameters as an Poisson's ratio for unloading-reloading ν_{ur}, $\sigma'_{xx}/\sigma'_{yy}$ ratio for the normal consolidation K_0^{NC}, and inclination of the critical state line M_c (in PLAXIS only as a M), related to the K_0^{NC}.

Values of failure parameters of the Norwegian quick clay are presented in Table 3–1. The dilatancy angle, which is not involved in the table, was supposed to be zero.

Failure parameters as in the MC model	Basic stiffness parameters
Cohesion, c [kN/m^2]	Modified swelling index, κ^* [-]
Friction angle, φ [^{o}]	Modified compression index, λ^* [-]
Dilatancy angle, ψ [^{o}]	Modified creep index, μ^* [-]

Table 3–3:Overview of the basic parameters in the SSC model.

The results from the oedometer test **after 24h consolidation** were used for the evaluation of the stiffness parameters. The value of the modified swelling index can be easily computed from the average modulus number m, evaluated according to Eq. (3.16) for the overconsolidated range. Modified compression index and modified creep index are connected with the modulus number m and creep resistance number r_s through the following equations,

$$\lambda^* = \frac{1}{m} \tag{3.28}$$

$$\mu^* = \frac{1}{r_s} \tag{3.29}$$

After evaluation of these parameters for all load steps larger than preconsolidation pressure one can see, that modified compression index λ^* and modified creep index μ^* are not constant. Generally it is possible to say, that especially the modified compression index is decreasing with increasing vertical effective stress in the case of

the sensitive clays. This fact will be probably connected with the difficult structure of the Norwegian quick clay and such a kind of destructuralisation of this material.

The default setting of the advance parameters was used, where ν_{ur} is equal to 0.15, K_0^{NC} is connected with the friction angle φ through Jaky's formula,

$$K_0^{NC} = 1 - \sin\varphi \tag{3.30}$$

and M_c can be computed with equation introduced by Brinkgreve in 1994,

$$M_C = \sqrt[3]{\frac{(1-K_0^{NC})^2}{(1+2\cdot K_0^{NC})^2} + \frac{(1-K_0^{NC})\cdot(1-2\cdot\nu_{ur})\cdot\left(\frac{\lambda^*}{\kappa^*}-1\right)}{(1+2\cdot K_0^{NC})\cdot(1-2\cdot\nu_{ur})\cdot\frac{\lambda^*}{\kappa^*}-(1-K_0^{NC})\cdot(1+\nu_{ur})}} \tag{3.31}$$

More detailed information about input parameters one can find in [89].

As a second step, the finite element mesh consists 578 six-noded triangular elements was generated, see Figure 3–8. Based on the symmetry, the plain strain model with the width of the mesh 25 mm was used. The height of the mesh was in accordance with oedometer ring size, i.e. 20 mm. Mesh was horizontally restrained at lateral boundaries and fixed in both directions at bottom boundary. On the top of the mesh the distributed load 200 kN/m^2 was applied in vertical direction.

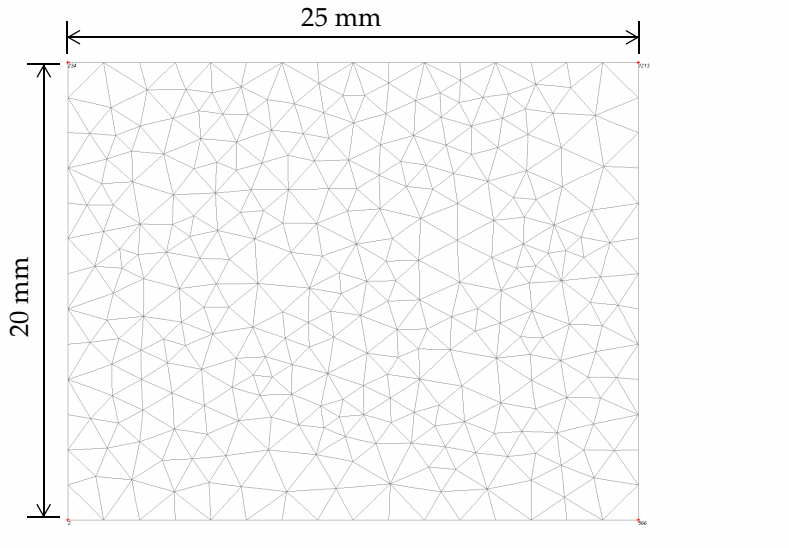

Figure 3–8: Finite element mesh used for the oedometer test simulation.

After material definition and construction of the finite element mesh, the initial conditions were generated. Pore water pressure was generated according to the ground water phreatic level, placed on the top of the modelling sample. Lateral boundaries were defined as closed consolidation boundaries, to avoid creation of the zero excess pore pressure at the boundaries during consolidation analysis. K_0 procedure was used for the generation of the initial stress conditions, with defined pre-overburden pressure POP=180 kPa.

From the laboratory investigation and in-situ observation it is discernible that the over-consolidated soil mainly exhibits primary consolidation and the creep behaviour is not significant. Based on this knowledge only the normally consolidated range was modelled, i.e. the load steps with the vertical effective stress larger than the preconsolidation pressure. Load steps with σ_y' = 300 and 400 kPa were chosen for the modelling. As a first stage, the static load with magnitude 200 kN/m^2 was activated and four days of consolidation were computed with the input parameters corresponding to the laboratory results from the load step σ_y' = 300 kPa. After this calculation the model was prepared for the application of the following load steps, i.e. modelling of the oedometer test in a normally consolidated range. Displacements were reset to zero and the static load was increased to 300 kN/m^2 in the zero time interval. Then, with the same input parameters as in previous stages, the one day consolidation was computed. These two steps were repeated once again for the static load 400 kN/m^2 and different stiffness parameters, corresponded to the load step σ_y' = 400 kPa according to the laboratory investigation. Deformation was observed in the several points located on the top of the modelling sample. Several models were performed for the best fitting of the final t-ε curves based on the laboratory investigation and observed points in the mathematical model. Final results for the modelled loading steps together with used input data of the stiffness parameters can be found in Figure 3–9. In the case of the both modelled load steps, the λ^* value had to be slightly increased in comparison with the measured one. The rest of the parameters are in complete accordance with the laboratory measurement.

One can see that the Soft-soil-creep model is suitable for the modelling of the volumetric creep behaviour. However, there is one disadvantage with this model, which consists of the usage constant value of the modified compression index λ^* for the all levels of the volumetric effective stress. Based on the Figure 3–9 it is possible to find decreasing of the λ^* value with the increasing vertical effective stress σ_y', or more generally increasing of the volumetric effective stress σ_v'. This behaviour is probably connected with the change of the soil's structure during loading and was observed also in the case of the other oedometer tests performed by the author (although it was not so significant like in the case of the Norwegian quick clay). In practical use of the Soft-soil-creep model it is of course inconvenient to change

parameter λ* manually and the average value based on the oedometer tests has to be used. As will be shown in the following parametric study the general inaccuracy in the case of the small change of the stiffness parameters is not so dramatic and for the practical reason is not so dangerous. During the modelling one should also think about possibility of this kind of behaviour by clayey soils.

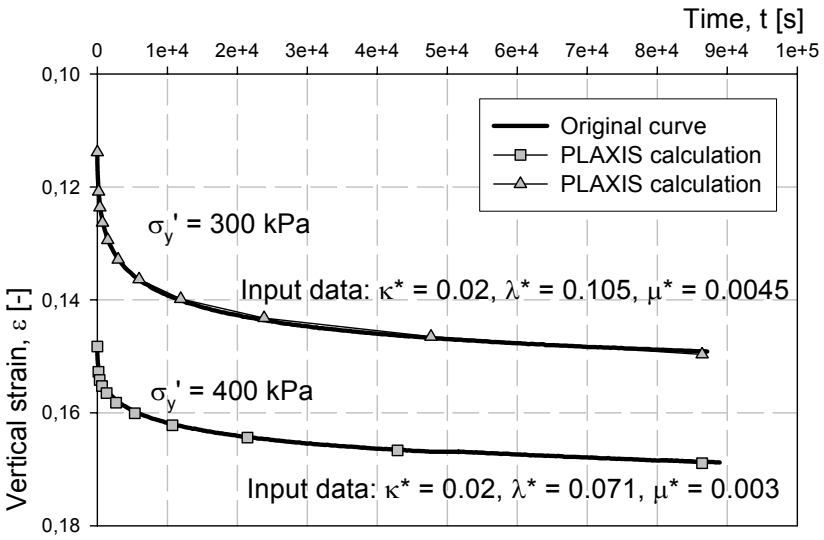

Figure 3–9: Comparison of the laboratory t-ε curves with results of the mathematical modelling, for the incremental oedometer test with the vertical effective stress σ_y' = 300 and 400 kPa.

In order to understanding the Soft-soil-creep model behaviour better the parametric study of the influence of the stiffness parameters was performed. The load step ending with the effective vertical pressure σ_y' = 400 kPa was chosen for this study. Several mathematical models with different values of the parameters κ*, λ* and μ* were performed for this particular load step. The global modelling procedure was identical with previous one explained above. The results of this parametric study with detailed information about used stiffness parameters are presented in Figure 3–10 a), b), c). Based on these diagrams it is possible to say, that variation of the modified swelling index κ* mainly influences the value of the primary consolidation. This is in contradiction to the modified compression index λ*, which influences the magnitude of the secondary consolidation. The influence of the modified creep index μ* seems to be more complex. Generally, combination of all these three parameters is used in the differential creep equation and besides individual influence of the stiffness parameters to the model's results, the influence based on the different combinations of these parameters has to be considered.

a) Influence of the modified swelling index κ*.

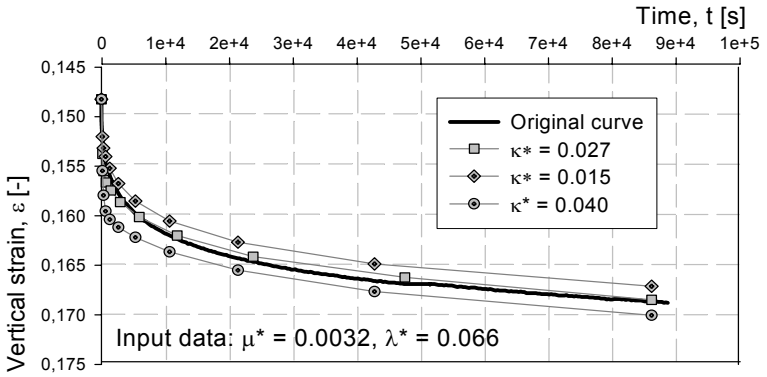

b) Influence of the modified compression index λ*.

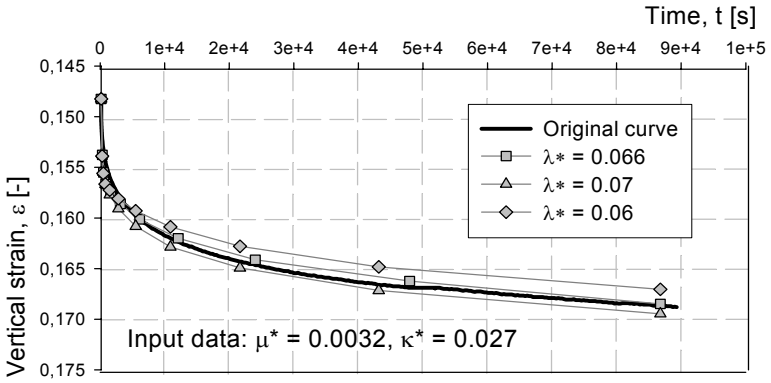

c) Influence of the modified creep index μ*.

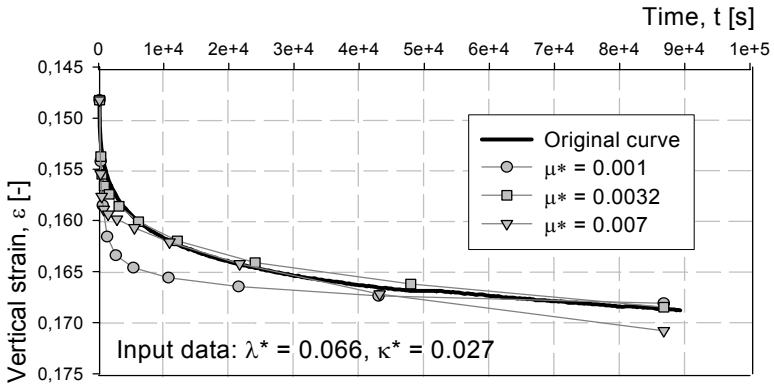

Figure 3–10: Results from the parametric study of the influence of stiffness parameters to the behaviour of the Soft-soil-creep model.

3.3.2 Glava clay

The Glava clay deposit is located in Stjørdal, which is a place approximately 35 km east of Trondheim. The deposit consists of a homogeneous marine clay, which is covered with 0.5 m thick top sand layer. The groundwater table is located on the top of the marine clay, and the initial pore pressure distribution at the site is hydrostatic. The Glava clay can be classified as a medium stiff clay, overconsolidated and low sensitive, with low plasticity. The natural water content is generally about 25-30%. The content of the clay particles, i.e. particles with a diameter smaller then 2 μm, lies in the range 35-48%, which indicates a relatively fat clay. The Glava clay can contain some small silt lenses, and occasional shell fragments and grains of coarser material. The unit weight of the Glava clay is approximately 19 kN/m^3. More information about this material can be found in Section 5.1, Table 5–1.

As part of the investigation of the Glava clay viscous behaviour with compact rheometer introduced in Chapter 5, three incremental oedometer tests of this clay were performed by the author, for the better characterisation of this material. Detailed information about these tests is given in Table 3–4.

Test	Depth	Type of the sample		Load step duration		Applied load steps
no.	[m]	Undisturbed	Remolded	1 h	24 h	[kPa]
1.	9.2	X		X		12.5-25-50-100-200 400-800-400-800-1600
2.	9.5	X		X		12.5-25-50-100-200 400-700-1200-1700
3.	9.5	X			X	12.5-25-50-100-200 400-800-1600-800

Table 3–4: Characterisation of the performed oedometer tests with Norwegian Glava clay.

Evaluation of the stress-strain behaviour of tests nos. 2 and 3 is shown in Figure 3–11. One can compare two oedometer tests of the same material, from the same depth, but with the different load step duration. Based on the σ′-M curves, the modulus number m was computed for the all tests. The average value of the m parameter was found to be around 19, with slightly increasing tendency with increasing vertical effective stress σ_y'. Evaluation of the coefficient of consolidation C_v and permeability k showed average values of these parameters for the normally consolidated range around 20 m^2/year and 5e-5 m/day. In the case of the test no. 2 the permeability was little bit smaller. The difference was found during the evaluation of the preconsolidation pressure σ_c', where tests nos. 1 and 2 showed preconsolida-

tion pressure around 300 kPa in contradiction with test no. 3, which had a preconsolidation pressure in the range from 400 to 500 kPa.

a) Test no. 2 with 1 h load step duration. b) Test no. 3 with 24 h load step duration.

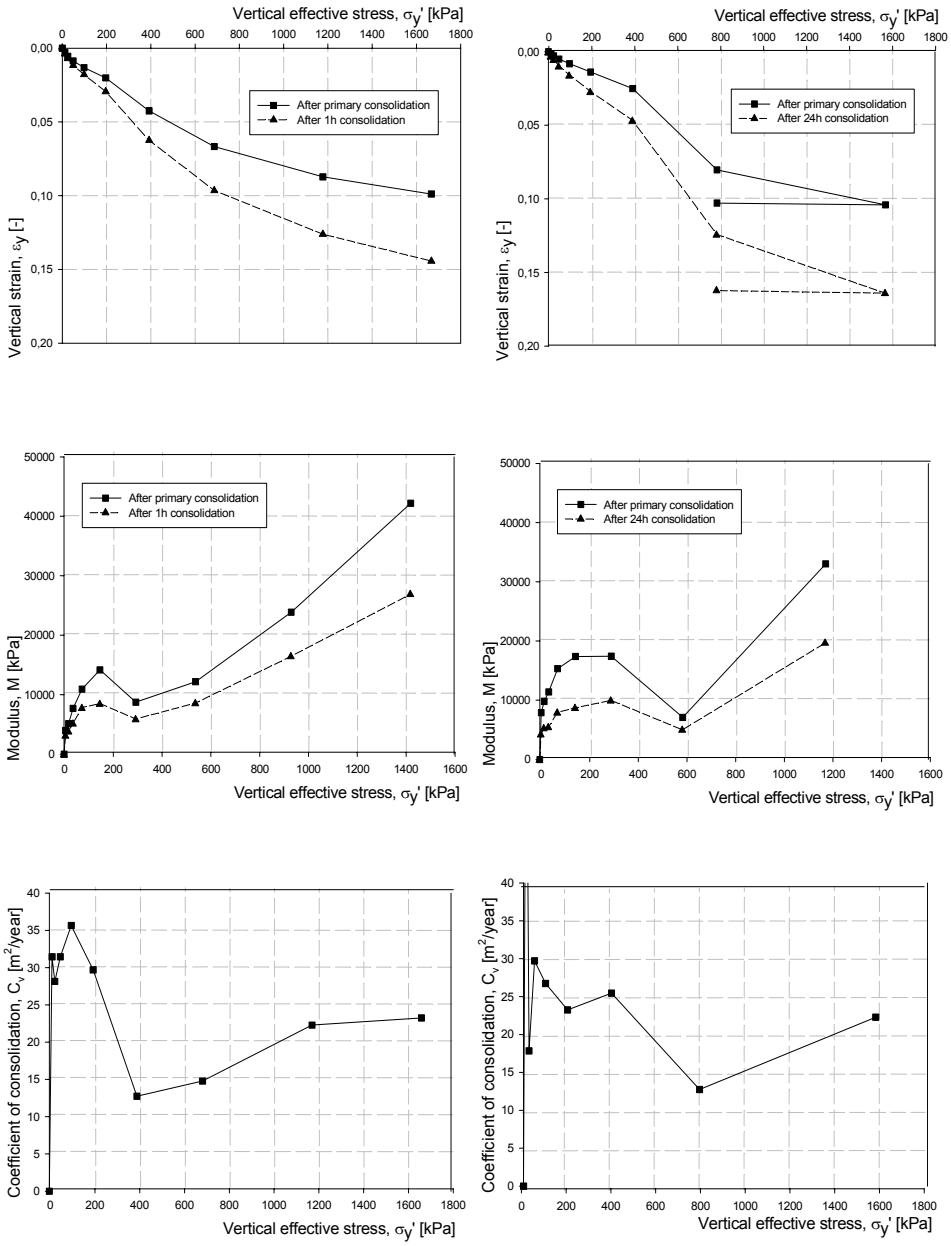

Figure 3–11: Evaluation of the Glava clay oedometer tests nos. 2 and 3 with the emphasis to the stress-strain behaviour. Comparison of Glava clay tests with the load step duration 1 h and 24 h.

Evaluation of the stress-strain-time behaviour was performed based on the approximation approach explained above. The creep resistance number r_s was computed for all three oedometer tests. Development of the creep resistance number with the vertical effective stress σ_y' for tests nos. 2 and 3 can be found in Figure 3–12. The average value of the r_s parameter for the normally consolidated Glava clay was found in the range from 400 to 500. Tests nos. 1 and 2 again show smaller preconsolidation pressure in comparison with the test no. 3.

a) Test no. 2 with 1 h load step duration. b) Test no. 3 with 24 h load step duration.

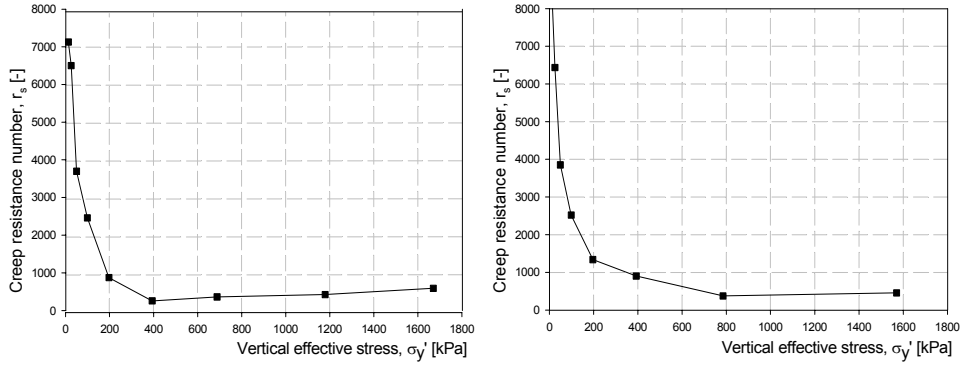

Figure 3–12: Development of the creep resistance number r_s with the vertical effective stress σ_y' for tests nos. 2 and 3 - Glava clay.

The recapitulative list of the parameters evaluated from all oedometer tests performed with Glava clay can be found in Table 3–5. Amazingly corresponding results based on the evaluation of the stress-strain-time behaviour from incremental oedometer tests with 1 h and 24 h load step duration reflect that the time resistance concept used fits well with the measured values. The difference between modulus numbers m, evaluated for the end of the "short" term and "long" term tests can be expected. In comparison with previously described quick clay one can see, that Glava clay is stiffer with shorter time of primary consolidation and has less pronounced creep behaviour.

Test no.	Average C_v [m^2/year]	Average k [m/day]	Average r_s [-]	Average m [-]	Preconsolidation pressure σ_c' [kPa]
1.	23	6.10E-05	407	18	300 - 400
2.	18	2.90E-05	406	16	300 - 400
3.	18	3.30E-05	411	24	400 - 500

Table 3–5: Evaluation of the Glava clay oedometer tests - recapitulative list of the characteristic parameters.

3.3.3 Onsøy clay

Onsøy is located about 100 km from Oslo, north of the Fredrikstad. The soils in this area are mainly marine clays, which were deposited during deglaciation at times with higher relative sea levels. Deposition occurred during a single period of submergence. The thickness of the deposition is around 40 m. Due to the great thickness and its highly uniform nature, the Onsøy site has been used for the research purposes by the Norwegian Geotechnical Institute (NGI), for many years. The summarisation of the work done on the Onsøy site, with particular references to the characterisation and engineering properties of the deposit is possible to find in [61]. Detailed information about stiffness and stress-strain behaviour can be found in [59, 60]. The basic parameters of the Onsøy clay material according to [59] are described in Table 3–6.

Parameters	Units	Typical value
Natural moisture content, w	%	65
Bulk density	g/cm^3	1.635
Clay content	%	50 - 60
Liquid limit / Plasticity index	%	≈ w / 35
Salt content	g/l	30 (no leaching)
Field vane sensitivity	-	6 - 8

Table 3–6:Description of the Onsøy clay, [59].

Four incremental oedometer tests with Onsøy clay were performed by the author as a part of the Long's work at NTNU. All of these tests were done with twenty-four hours load step duration. The "classical" oedometer ring, described above, was used. The oedometer samples were trimmed from the high quality block sample, lifted from the depth 11.4 m. The in-situ effective stress in this depth was approximately 71 kPa. First two oedometer tests were performed with the undisturbed Onsøy clay material, whereas the remolded material, with the same water content as the original one, was used for the other two tests. Detailed specification of these tests is given in Table 3–7.

The same techniques described in the previous sections were used by the author for the evaluation of the stress-strain and stress-strain-time oedometer behaviour of the Onsøy clay. First, evaluation of the undisturbed clay was performed. Based on the oedometer behaviour it is possible to say that the Onsøy clay is very soft with long primary consolidation and significant creep deformation. The average value of the modulus number m was found to be approximately 9.5 for the normally consolidated range and 24 h deformation. During the test no. 1, a slight increase of this parameter with increasing vertical effective stress was observed, whereas the con-

stant modulus number was found in test no. 2. Very low average value of the coefficient of consolidation C_v - 4 m^2/year, and low permeability k - 2.5e-5 m/day, indicates long duration of the primary consolidation. The average value of the creep resistance number r_s was found to be around 190, which indicates the significant creep behaviour. During both tests with the undisturbed clay, approximately 50% of the total deformation was creep. Preconsolidation pressure σ_c' was found in the range 100 - 150 kPa.

Test no.	Depth [m]	Type of the sample		Load step duration		Applied load steps [kPa]
		Undisturbed	Remolded	1 h	24 h	
1.	11.4	X			X	17.5-35-70-100-200 300-400-300-400-600
2.	11.4	X			X	17.5-35-70-100-200 300-400-300-400-600
3.	11.45		X		X	12.5-25-50-100-200 400-800-1600
4.	11.45		X		X	12.5-25-50-100-200 400-800-1600

Table 3–7:Characterisation of the performed oedometer tests with the Norwegian Onsøy clay.

After evaluation of the undisturbed clay tests the main emphasis was placed on the comparison with the oedometer behaviour of the remolded Onsøy clay, i.e. evaluation of the influence of structure of the clay to the results of oedometer test. Graphical comparison of the stress-strain behaviour of the test no. 2 (undisturbed clay) and test no. 4 (remolded clay) can be found in Figure 3–13. The stress-strain behaviour of the remolded clay indicated stiffer material in comparison with the undisturbed one. The average value of the modulus number m after 24 h consolidation was found to be 16.5. During the tests this parameter was almost constant with increasing vertical effective stress. This value of the modulus number m is almost two times larger in comparison with normally consolidated undisturbed material, which indicates smaller deformation after remolding. A significant difference between undisturbed and remolded Onsøy clay was also observed in duration of the primary consolidation. Two times lower average value of the coefficient of consolidation C_v was evaluated from the tests with remolded material, which indicates two times longer duration of the primary consolidation. Generally the systematic increase of the coefficient of consolidation with increasing vertical effective stress was observed during the both tests with remolded clay. Extremely small values of the C_v were observed for the low values of the acting stress, e.g. C_v=0.4 m^2/year for the σ_y'=24.5 kPa. The average value of the permeability k was found to be 3.1e-5m/

day. Conversely to the C_v behaviour, a systematic decrease in permeability was observed. Zero preconsolidation pressure was found for the remolded material.

a) Undisturbed Onsøy clay, test no. 2. b) Remolded Onsøy clay, test no. 4.

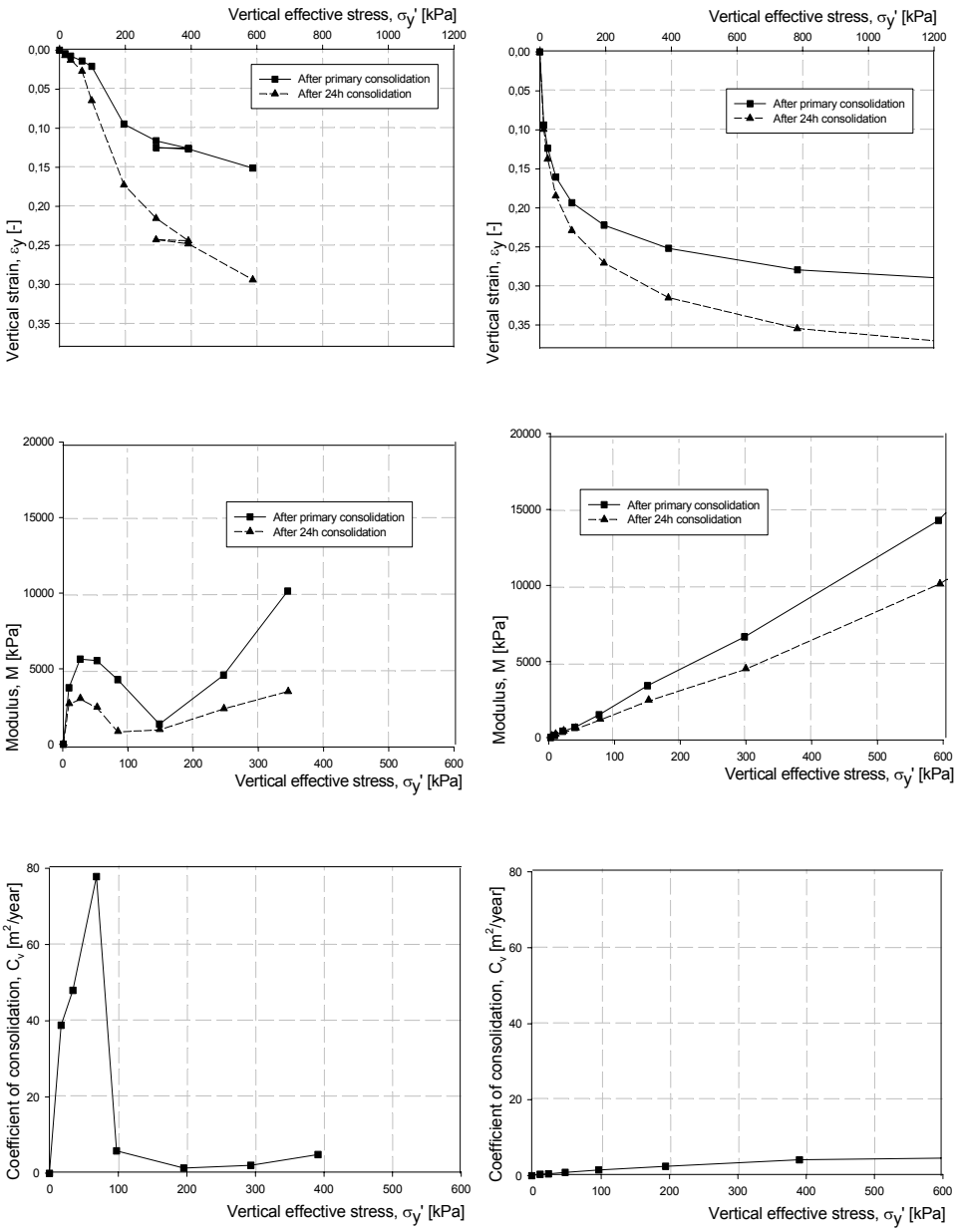

Figure 3–13: Evaluation of the Onsøy clay oedometer tests nos. 2 and 4 with the emphasis to the stress-strain behaviour. Comparison of tests with undisturbed and remolded Onsøy clay material.

Evaluation of the stress-strain-time behaviour showed more then two times higher value of the time resistance number r_s for the remolded Onsøy clay. One can see that the creep behaviour after remolding is not so significant. During both the tests with remolded material only 20% of the total deformation was made by creep. Comparison of the undisturbed and remolded Onsøy clay's creep behaviour is shown in Figure 3–14.

a) Undisturbed Onsøy clay, test no. 2. b) Remolded Onsøy clay, test no. 4.

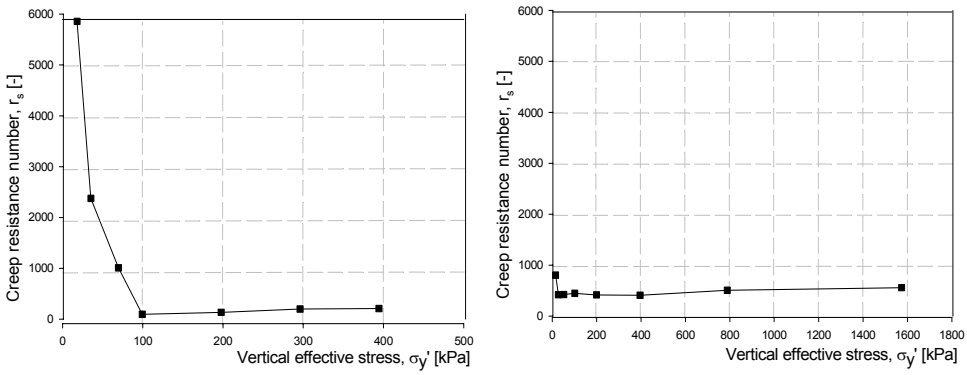

Figure 3–14: Comparison of the undisturbed and remolded Onsøy clay's creep behaviour, based on the development of the creep resistance number r_s with the vertical effective stress σ_y'.

The overview of all the parameters based on the evaluation of the oedometer tests is given in Table 3–8. Comparison of the undisturbed (normally consolidated) and remolded Onsøy clay oedometer behaviour showed smaller deformation after remolding. Incremental strain after 24 h consolidation was almost two times larger for the normally consolidated undisturbed clay in comparison with remolded one. Generally speaking, remolded clay exhibits longer primary consolidation and smaller ability of the creep deformation.

Test no.	Average C_v [m^2/year]	Average k [m/day]	Average r_s [-]	Average m [-]	Preconsolidation pressure σ_c' [kPa]
1.	4	2.80E-05	221	8	100 - 150
2.	4	2.30E-05	160	11	100 - 150
3.	2	3.50E-05	560	16	0
4.	2	2.60E-05	457	17	0

Table 3–8: Evaluation of the Onsøy clay oedometer tests - list of the characteristic parameters.

3.3.4 Terlicko clayey shale

Based on the cooperation with Povodi Odry a.s., the analysis of the Terlicko dam behaviour with emphasis to the creep was made by the author as a part of this PhD study. Performed analysis consisted of laboratory investigations of the Terlicko clayey shale material, study of the case record, 2-D mathematical modelling of the right hand slope and prediction of the future behaviour. A detailed description of the Terlicko dam from the geological and geotechnical point of view together with a summary of the whole study can be found in Chapter 6. Evaluation of the triaxial tests performed with the Terlicko clayey shale material is presented in Section 4.2.2.

Terlicko clayey shale can be described as a marly, soft or not very solid, dark-grey to black-grey material, which crumbles into small parts in dry condition and gradually softens in the contact with water. The average value of the unit weight was found to be around 20 kN/m^3. Moisture content of the testing material was approximately 11%. Material was only partly saturated with degree of saturation S=62%.

Five incremental loading oedometer tests were performed for the determination of the material's consolidation behaviour. Material from the core box no. 8 (described in Table 6–1) with diameter D=80 mm was used for all the tests. Samples were taken from the depth 7 - 8 m. As will be mentioned in Chapter 6, the rotary drilling sampling method with three walls tube sampler was used, with location of the borehole in the middle of the dam. The original depth of the sample before genesis of the valley was probably around 40 m. The characterisation of the tests with type of the sample, localisation, load step duration and sequence of the load steps can be found in Table 3–9.

Test	Depth	Type of the sample		Load step duration		Applied load steps
no.	[m]	Undisturbed	Remolded	1 h	24 h	[kPa]
1.	7.48	X		X		12.5-25-50-100-200 400-800-400-800-1600
2.	7.60	X		X		12.5-25-50-100-200-400 800-400-800-1600-3200
3.	7.63		X	X		12.5-25-50-100-200-400 800-400-800-1600-2100
4.	7.22	X			X	12.5-25-50-100-200-400 700-1200-1700-2200
5.	7.18	X			X	12.5-25-50-100-200 400-800-1600-2700

Table 3–9: Characterisation of the performed oedometer tests with the Terlicko clayey shale material.

In spite of the sophisticated sampling method, the test material was not in a good condition. Besides this problem the work was complicated due to the crumbling nature of the shale materials. Regardless of these problems four more or less undisturbed samples were trimmed from the in-situ specimen. As a first part of the laboratory study, three tests with the "classical" oedometer ring and one hour load step duration were performed. In Table 3–9 these are denoted as a tests nos. 1, 2 and 3, where test no. 3 was done with the remolded material. Loading, unloading and reloading behaviour was studied in all these three cases. One day load step duration was applied in test nos. 4 and 5. In these tests the special floating ring was used and only loading behaviour of the sample was observed. A larger oedometer ring was chosen due to the big particles contained in the Terlicko clayey shale material. Additionally the diameter of the floating ring corresponded to the core diameter, thus no trimming was required, i.e. no disturbance occurred due to the trimming and a higher quality of the mounted sample was expected.

Evaluation of the stress-strain behaviour showed the extremely difficult nature of the test material. The preconsolidation pressure σ_c' was found only in the test no. 2 in the range from 800 kPa to 1 MPa. If one would take into account the original depth of the specimen before geological erosion this value seems to be reasonable. In contradiction to this result the rest of the tests with undisturbed Terlicko clayey shale did not show any preconsolidation based on the stress-strain evaluation. A comparison of test no. 2 with undisturbed material and test no. 3 with remolded material (both with 1 h load step duration) is given in Figure 3–15. The main difference between these tests is of course the presence of the preconsolidation stress. Parameters evaluated from the stress-strain behaviour were very similar for both tests. The average value of the modulus number m for the end of the consolidation was found to be around 30 for test no. 2 (normally consolidated range), and 26 for test no. 3. The unloading-reloading value of the modulus number was very high, around 700-800 for both the tests. The same coherence is found for the average coefficient of consolidation C_v - 380 and 490 m^2/year, and the permeability k - 1.4e-4 and 2e-4 m/day. Test no. 3 exhibited continued decrease of the coefficient of consolidation with increasing effective vertical stress. Evaluation of the oedometer test no. 4 with the floating ring and 24 h load step duration, compared with the test no. 1 with the "classical" oedometer ring and 1 h load step duration can be found in Figure 3–16. Generally the smaller deformation was observed in the case of the tests with floating ring in comparison with the "classical". The average value of the modulus number m for the end of the consolidation evaluated for tests nos. 4 and 5 was found to be in the range from 55 to 60. The rest of the parameters were similar to test no. 2. Test no.1 has a smaller value of the coefficient of consolidation C_v - 150 m^2/year. Generally speaking, the stress-strain behaviour of tests nos. 1, 4, and 5 was more typical for the remolded material than for the undisturbed one.

a) Undisturbed clayey shale, test no. 2. b) Remolded clayey shale, test no. 3.

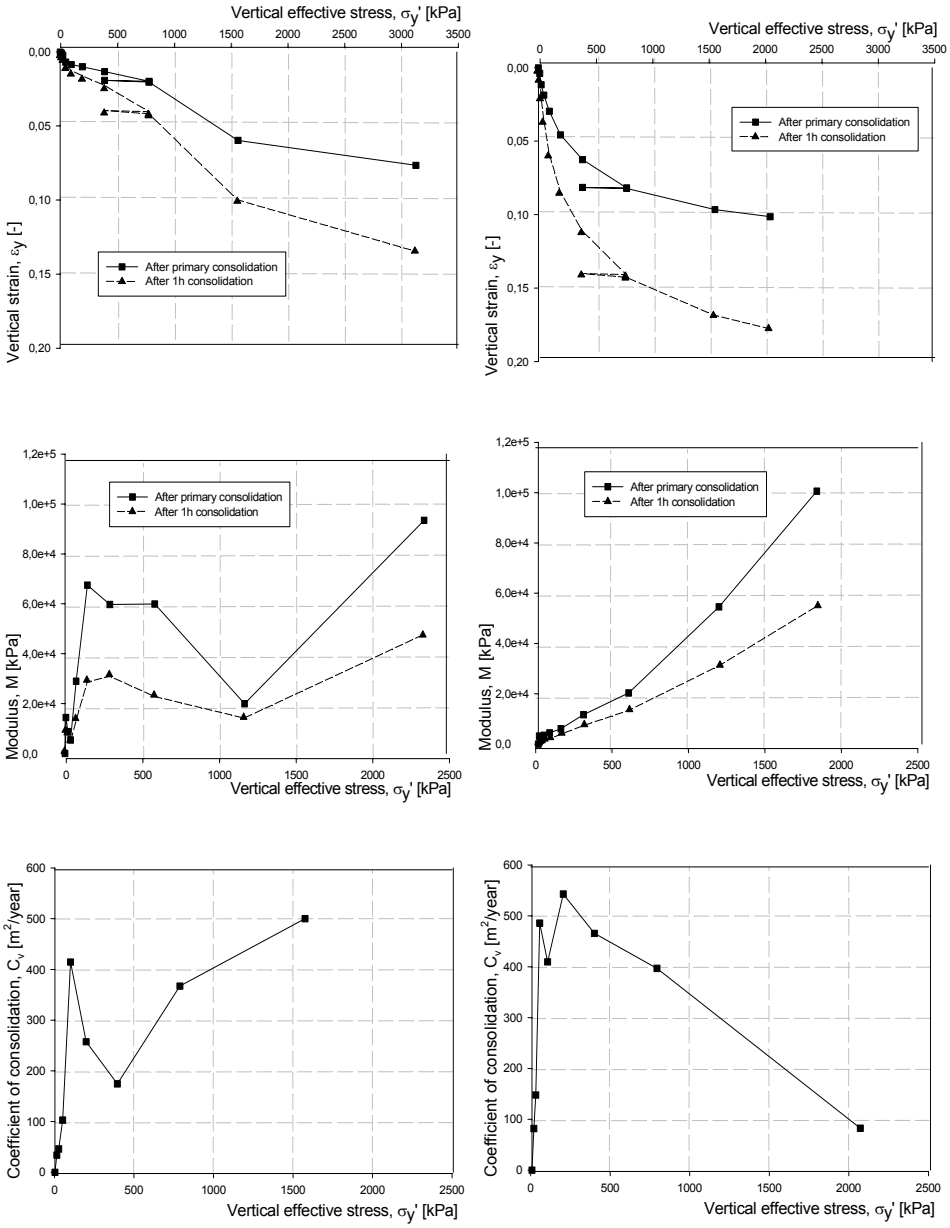

Figure 3–15: Evaluation of the Terlicko clayey shale oedometer tests nos. 2 and 3 with the emphasis to the stress-strain behaviour. Comparison of tests with undisturbed and remolded clayey shale material.

a) "Classical" oedometer ring, test no. 1. b) Floating oedometer ring, test no. 4.

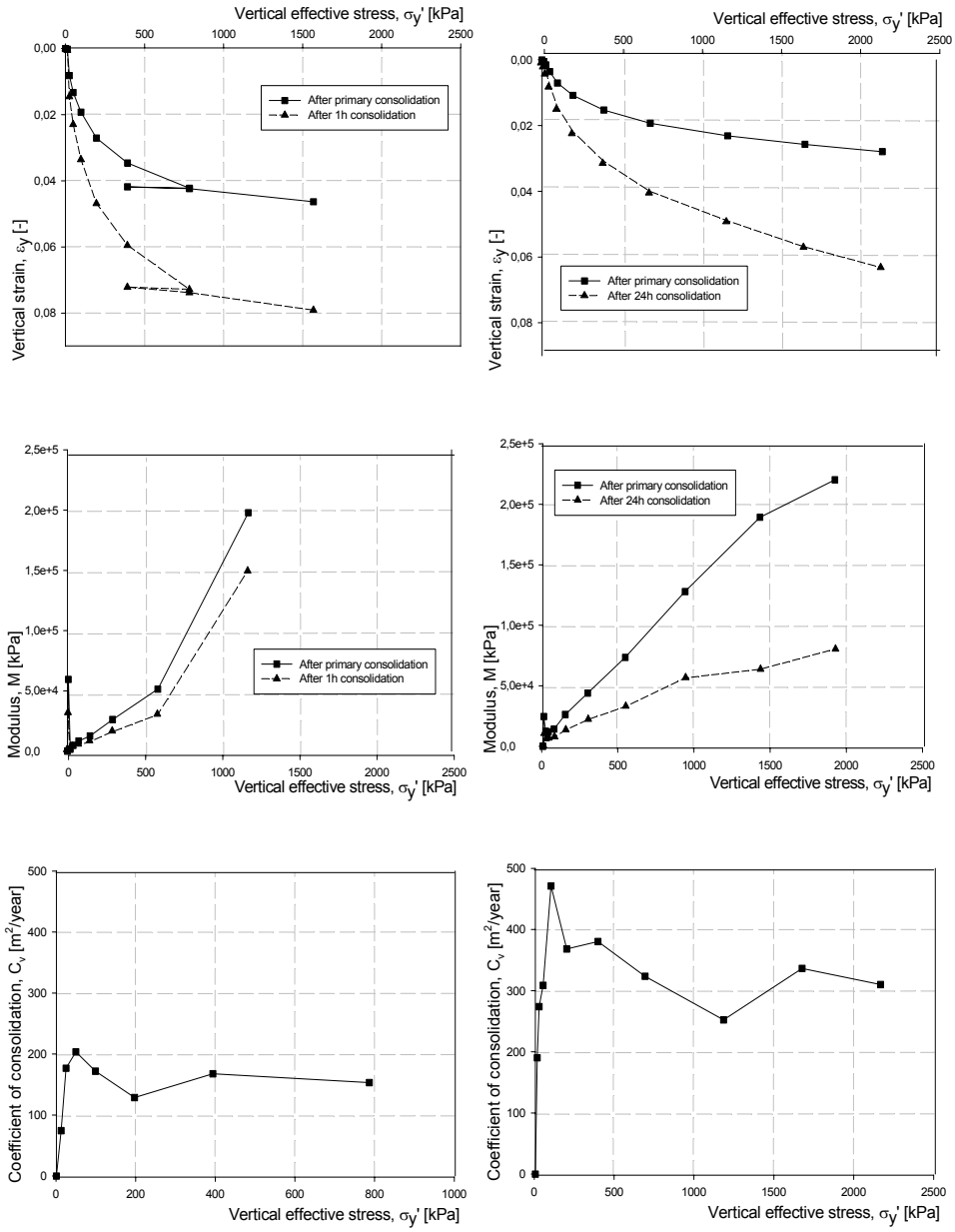

Figure 3–16: Evaluation of the stress-strain behaviour of the Terlicko clayey shale oedometer tests nos. 1 and 4. Comparison of tests with "classical" and floating oedometer ring and different duration of the consolidation.

The stress-strain-time behaviour based on the development of the creep resistance number r_s for tests nos. 2, 3 and 4 is given in Figure 3–17. The average value of the r_s parameter was found to be 1500 for test no. 2, 1200 for tests nos. 1 and 3, and 1835 for tests nos. 4 and 5. In the case of the tests with the undisturbed Terlicko clayey shale material, all these values were evaluated for the normally consolidated range. Generally the largest value of the creep resistance number was observed during the tests with the floating ring and 24 h load step duration. In contradiction to the absence of the preconsolidation stress σ_c' based on the stress-strain behaviour of test no. 4, according to the r_s-t curve the preconsolidation stress can be found to be around 400 kPa (see Figure 3–17 c)).

a) Undisturbed test no. 2 with the "classical" oedometer ring and 1 h consolidation.

b) Remolded test no. 3 with the "classical" oedometer ring and 1 h consolidation.

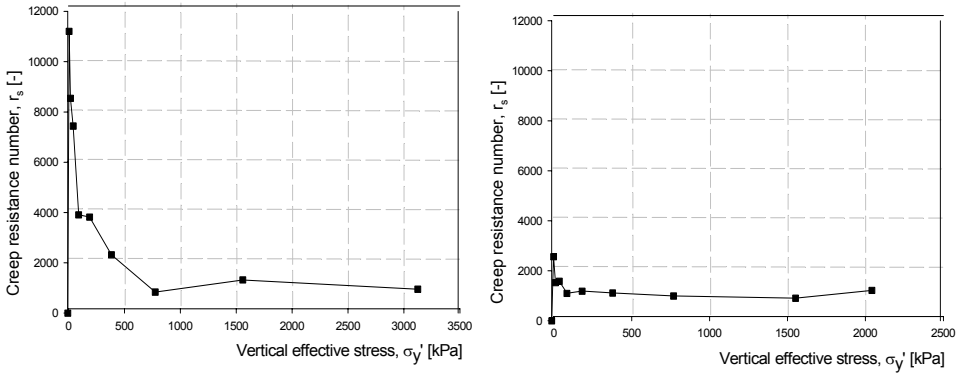

c) Undisturbed test no. 4 with floating oedometer ring and 24 h consolidation.

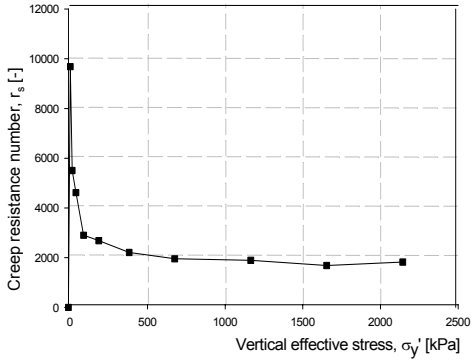

Figure 3–17: Evaluation of the stress-strain-time behaviour of the Terlicko clayey shale. Development of the creep resistance number r_s with the vertical effective stress σ_y'.

The overview of the parameters evaluated from the oedometer behaviour of the Terlicko clayey shale material is presented in Table 3–10. All tests performed with the floating oedometer ring and 24 h load step duration exhibited smaller deformation in comparison with the "classical" oedometer ring and 1 h load step duration. The in-situ remolding of the Terlicko clayey shale during the past tectonic processes can be supposed based on the problematic evaluation of the preconsolidation stress even from the test using the floating oedometer ring with larger proportions. Based on the results of the oedometer tests, the Terlicko clayey shale can be defined as a stiff material with low tendency to the volumetric creep behaviour and short duration of the primary consolidation. Based on the comparison of the average creep resistance number with previously tested materials the low ability of the volumetric creep behaviour can be found in the case of the Terlicko clayey shale, e.g. the Onsøy clay exhibited eight times smaller value of the average r_s parameter.

Test no.	Average C_v [m^2/year]	Average k [m/day]	Average r_s [-]	Average m [-]	Preconsolidation pressure σ_c' [kPa]
1.	150	1.45E-04	1200	46	25
2.	380	1.40E-04	1500	30	800 - 1000
3.	490	2.00E-04	1245	26	0
4.	320	1.10E-04	1830	60	400
5.	348	1.80E-04	1840	58	200

Table 3–10:Evaluation of the Terlicko clayey shale oedometer tests - list of characteristic quantities.

Chapter 4 Deviatoric creep behaviour

As mentioned in Chapter 2, deviatoric creep is a time dependent shear deformation caused by constant deviatoric stress. Deviatoric creep can be generally described as a mutual rearrangement of the particles of the soil, i.e. serial changes of the soil structure characterised by a mutual rearrangement of contacts and by the forces acting at the contacts. Transition from one structure to the other is not smooth, but proceeds in a jump-like way [106]. In comparison with the volumetric creep behaviour, which is unique for the soil material (due to the coupled process of the rearrangement of the particles of the soil and squeezing out water), the nature of the deviatoric creep behaviour of the soil is more or less similar to the other materials. Nevertheless, in nature, deviatoric creep usually occurs simultaneously with the volumetric deformation.

In contradiction to volumetric creep, deviatoric creep can lead to failure under certain conditions introduced in the next section. The most susceptible materials to this behaviour are saturated sensitive soft clays under undrained conditions and heavily over-consolidated clays under drained conditions. Other effects of the deviatoric creep can be changes in the strength, which are caused by the changes in effective stress due to the changes in pore pressure during undrained creep, or changes in porosity as a result of volume changes during drained creep. An illustration of this process with the stress paths can be found in Figure 4–1. Based on these facts, one can see that deviatoric creep is extremely important in order to analyse soil stability problems, e.g. bearing capacity or slope stability.

Laboratory study of the deviatoric creep behaviour was made by the author with two different triaxial apparatuses and two different materials. Deviatoric drained and undrained creep tests under different tests conditions were performed with the Norwegian Glava clay material. Triaxial apparatus made by Wille Geotechnik Gmbh and a unique Creep Triaxial apparatus made at NTNU, Department of Civil and Transport Engineering, Geotechnical Division, were used for these tests. The tests were performed with various sizes of the cylindrical specimens together with different initial conditions. Evaluation and comparison of the results will be presented in Section 4.2.

As a part of the analysis of the Terlicko dam, detailed investigation of the shear strength and deviatoric creep behaviour of the Terlicko clayey shale was done. Isotropically consolidated drained and undrained triaxial tests together with the several deviatoric undrained creep tests were performed on a triaxial apparatus made by Wille Geotechnik Gmbh. In this study only one type of the initial condition and one size of the cylindrical specimen was used.

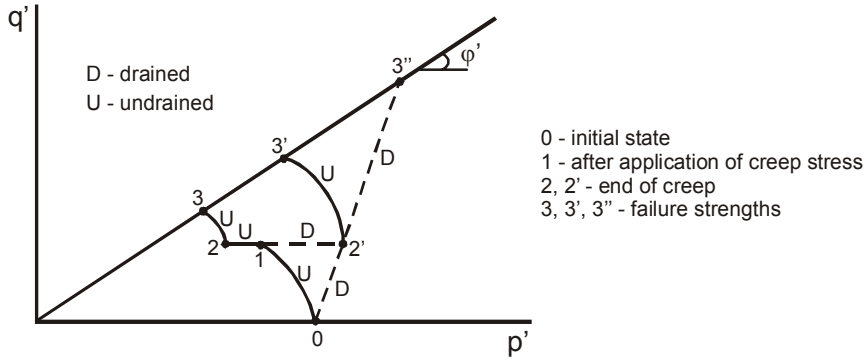

Figure 4–1: The effect of undrained creep on the strength on normally consolidated clay, [79].

Before a detailed description of the used triaxial apparatus together with evaluation and investigation of the tests results performed by the author, the theoretical background will be presented in the following section. The description of the deviatoric creep behaviour under different laboratory conditions together with explanation of the different shear apparatus will be introduced.

4.1 Theoretical background

As was mentioned in Section 2.2.2, the main difference between volumetric and deviatoric creep behaviour is the occurrence of the secondary and tertiary creep phases, which depend on the current value of the shear mobilisation, type of the soil and boundary conditions. Evaluation and approximation of the primary creep phase was introduced in Chapter 3. The approximation of the creep flow curve, i.e. secondary creep phase, is quite easy to determine because of the linear relation between creep deformation and time. The occurrence of tertiary creep leads to failure every time, provided that the deviatoric stress will not be decreased. So one of the main problems in the case of the deviatoric creep behaviour is to find the values of the shear mobilisation, which are limiting occurrence of the primary, secondary and tertiary creep phases, i.e. such values of deviatoric stress which describe the beginning of the secondary and tertiary creep phases. Simply speaking it is neces-

sary to determine the boundaries at which primary creep changes to secondary creep and subsequently to tertiary creep, culminating in the loss of the material strength. For an answer to this problem it is necessary to study deviatoric creep behaviour of the original material, in this case clayey soil, under different magnitude of the constant deviatoric stress (different shear mobilisation).

A lot of deviatoric creep tests have been performed by different authors. According to the apparatus used it is possible to divide these tests in two main groups - deviatoric creep tests performed with the direct shear apparatus and deviatoric creep tests performed with the triaxial apparatus. A description of these two approaches containing an introduction of the nature of the tests, a detailed description of the equipment, examples of the deviatoric creep behaviour under given conditions together with evaluation is presented in the next two sections.

4.1.1 Direct shear test

The simplest deformation involving change of the shape without a change in volume due to the application of the shear stress is generally called pure shear. In the case of the soil material, pure shear usually does not occur in nature and the simplest mode of the shear deformation is simple shear. Visualisation of the soil element under simple shear can be found in Figure 4–2. One can see that in the case of the simple shear normal stresses σ_x, σ_y and σ_z together with two pairs of the shear stresses τ_{xz} and τ_{zx} are applied, and the rest of the shear components are equal to zero. So in this case the soil element exhibits not only deformation of shape (shear strain) but also volumetric strain due to the normal stresses.

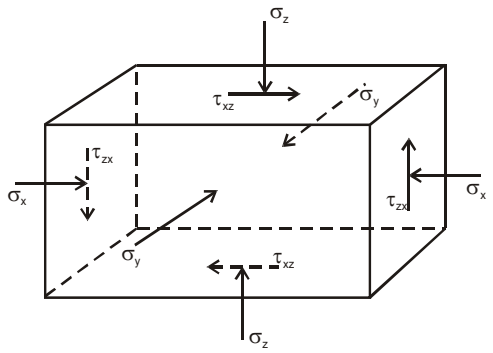

Figure 4–2: Diagram of the state of stress in a soil element under simple shear.

Tests under simple shear are widely used in geotechnical laboratories all over the world for the evaluation of the shear strength and investigation of the post-peak behaviour. Generally the simple shear test is called direct shear test and used laboratory equipment is denoted as a direct shear apparatus. A sketch of the simplest direct shear test apparatus is given in Figure 4–3. General procedure of this test in the case of the soil material can be divided into the two parts. The first part is the application of the normal stress for the consolidation of the tested material. After consolidation (in the case of the direct shear test this means mainly primary consolidation, i.e. dissipation of the pore water pressure) the shearing is gradually applied. Depending on the equipment, the direct shear test can be either strain-controlled or stress-controlled. The main advantage of the direct shear test is its extreme simplicity. It was noted by Maslov [64], quote: "Tests under simple shear best reflect the actual conditions of the possible shear of the soils structure, as they provide visible and convincing evidence of shear failure. If the drainage conditions are properly maintained, their results coincide with those obtained from compressive tests on triaxial apparatus". Nevertheless, there are several disadvantages with the direct shear test, where the main ones, according to [27], are that drainage conditions cannot be controlled and shear stress on the failure plane is not uniform. A detailed description of the direct shear test together with example of the soil behaviour under this test can be found in [27, 30].

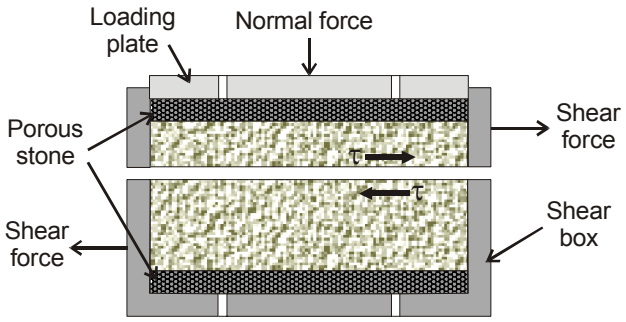

Figure 4–3: Sketch of direct shear apparatus [30].

One can find many kinds of laboratory apparatuses which have been developed for the testing of clayey soils under simple shear. Besides the classical direct shear apparatus introduced in Figure 4–3, one can find a double shear apparatus, cylindrical shear apparatus, ring shear apparatus, torsion apparatus for the testing of hollow or solid cylindrical specimens, apparatus for forced shear, free shear or cylindrical shear etc. A specification of the several of the direct shear apparatuses is given in [69].

In 1961, a special direct shear apparatus was developed at the Norwegian Geotechnical Institute, Oslo, for the study of the stress-strain and shear strength properties of highly sensitive Norwegian quick clay. The cylindrical sample of the clay with diameter D=8 cm and height H=1 cm was placed into the reinforced rubber membrane allowing vertical deformation and horizontal displacement with no change in diameter. Several constant-volume shear tests and drained shear tests were performed with this apparatus by Bjerrum and Landva. A description of these tests together with comparison of results with triaxial tests and in-situ vane tests is presented in [16].

As was mentioned above, the main problem in the case of the deviatoric creep behaviour is the evaluation of the so-called limiting shear stresses, i.e. values of shear stresses limiting occurrence of the primary, secondary and tertiary creep phases. For an answer to this question it is necessary to evaluate behaviour of the original clayey material during deviatoric creep test. The set of experimental creep curves of clayey soil obtained by testing identical specimens under constant shear stress τ of different magnitude can be found in Figure 4–4 b). Primary, secondary and tertiary parts of the deviatoric creep are illustrated in the picture as OA, AB and BC segments of the creep curve.

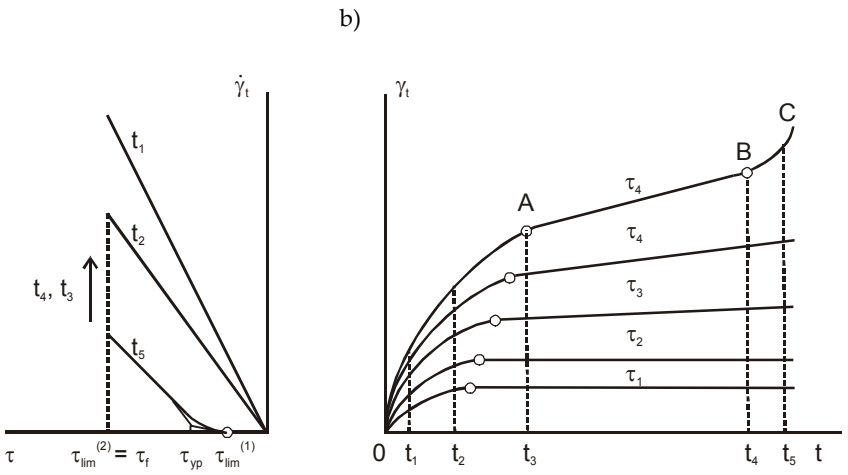

Figure 4–4: Set of the creep curves and $\tau - \dot{\gamma}_t$ curves, for various values of the shear stress τ and time t, respectively, based on the simple shear tests [69].

Based on the flow rate $\dot{\gamma}_t$ vs. shear stress τ curve illustrated in Figure 4–4 a), the following two limiting shear stress values can be identified for description of the creep deformation and strength of clayey soil:

- First limiting shear stress $\tau_{lim}^{(1)}$, which describes the beginning of the secondary creep phase, i.e. at $\tau<\tau_{lim}^{(1)}$ only primary (fading) creep phase can occur.
- Second limiting shear stress $\tau_{lim}^{(2)}$, which describes the beginning of the tertiary creep phase, i.e. at $\tau>\tau_{lim}^{(2)}$ the accumulated creep deformation results in loss of strength of the clayey soil. Consequently, the second limiting shear stress can be also called shear strength limit.

τ_{yp} in Figure 4–4 a) is a yield limit of the shear stress and usually there is very small discrepancy between $\tau_{lim}^{(1)}$ and τ_{yp}, i.e. $\tau_{yp} \cong \tau_{lim}^{(1)}$. If one assumes this condition and additionally anticipates small creep rates at $\tau<\tau_{yp}$ then the relation between flow rate and shear stress τ which is lying between first and second limiting shear stress, i.e. $\tau_{lim}^{(1)}<\tau<\tau_{lim}^{(2)}$, can be approximated by the Shvedov-Bingham equation,

$$\begin{aligned} \tau &= \tau_{yp} + \eta_v \cdot \frac{d\gamma_{vt}}{dt} = \tau_{yp} + \eta_v \cdot V_{\gamma t}; \\ \frac{d\gamma_{vt}}{dt} &= V_{\gamma t} = \frac{\tau - \tau_{yp}}{\eta_v} \end{aligned} \tag{4.1}$$

where γ_{vt} is a non-fading component of the deviatoric creep strain (secondary creep strain), and η_v is a coefficient of viscosity (also coefficient of proportionality). This relation is the simplest rheological equation of the state that describes deviatoric creep deformation of clayey soils under simple shear without taking into consideration instantaneous strain γ_0 and fading strain (primary creep) γ_{dt} [69].

A detailed study of the deviatoric creep behaviour by testing a set of ring-shaped identical specimens of clay on the torsion apparatus was made by Meschyan [69]. The set of creep curves obtained from one of his studies can be found in Figure 4–5. In these tests the clay material was first precompacted at a pressure of σ_z=0.3 MPa, which was later reduced to 0.2 MPa and left at this level until complete stabilisation (about one month). Then the shear stress τ was applied at values corresponding to the different levels of shear mobilisation τ/τ_f (where τ_f is the shear strength of the tested material). Specification of the tested material together with more information about performed tests can be found in [69].

Results of the tests show that at small levels of shear mobilisation, 0.1 - 0.4, only primary creep phase was observed. The occurrence of the secondary creep phase was recorded for the shear stress τ corresponding to the shear mobilisation 0.5 - 0.9. Nevertheless the value of the shear deformation proceeds within the primary creep phase was, according to Meschyan, significant even at these levels of the shear mobilisation. Based on this result it is possible to say that the primary creep (fading

creep) during deviatoric creep test of the clayey soil under the simple shear makes more than 60% of the total creep deformation and may not be ignored (except in very weak soils). It means that Shvedov-Bingham equation (see Eq. (4.1)) is not suitable for the general description of the deviatoric creep behaviour.

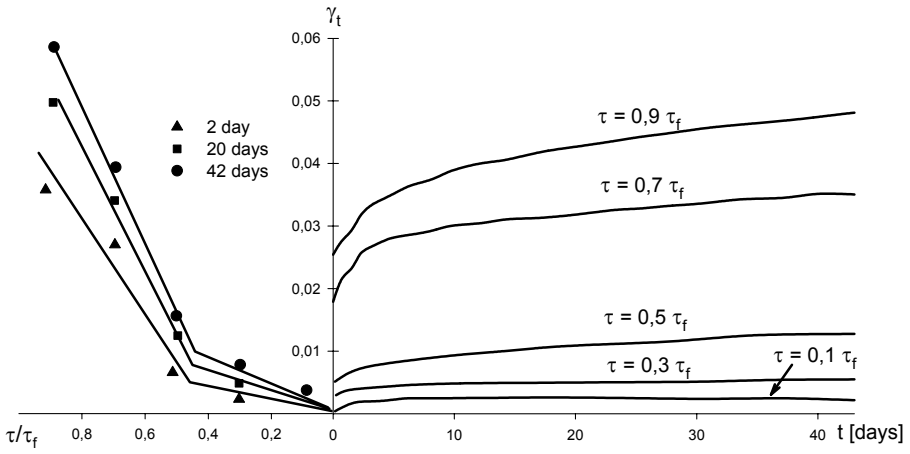

Figure 4–5: Set of the creep curves under simple shear test performed with torsion apparatus by S.R. Meschyan, [69].

According to Figure 4–5 one can see that the τ/τ_f - γ_t curves can be approximated by a bilinear diagram, first time suggested by Geuse and Tjong-Kie for the τ_f - γ_t relation in 1953 [36]. The points of inflection in these curves correspond to the structural strength of soil under shear τ_{str}. It was confirmed by experimental studies that this value of the shear stress is approximately equal to the first shear stress limit, i.e. $\tau_{str} \cong \tau_{lim}^{(1)}$. Based on experimental investigation, Meschyan has shown that for the clayey soils, except the very weak soils with liquidity index LI>1 and void ratio e>1.5, the structural strength limit under shear is almost independent of the test duration and varies in the range $0.4 \le \tau_{str} / \tau_f \le 0.55$ [69, 70].

One can find different studies of the deviatoric creep behaviour of the clayey soils in the direct shear apparatus. Besides the impressive work by Meschyan and his co-workers mention can be made of the study of the deviatoric creep behaviour in cylindrical specimens of potter's clay with torsion apparatus made by Geza and Tjong-Kie, investigation of the of the creep of the clayey soil with ring shear apparatus performed by Haefeli in 1953, study of the creep behaviour of normally consolidated clay in thick hollow cylinder tests by Anderson, Pyrah, Pang and Haji-Ali [6], or study of sensitive natural clay in triaxial and torsional hollow cylinder performed by Adachi and co-workers [3].

4.1.2 Triaxial test

Triaxial shear test is the most widely used method for the determination of the shear strength parameters, suitable for all types of soil. According to [27, 30] triaxial shear test has the following advantages in comparison with the direct shear method. It provides more uniform stress conditions, allows more flexibility in terms of loading paths, the drainage conditions can be controlled and pore water pressure measurements can be made. A sketch of the triaxial apparatus can be found in Figure 4–6. Generally a cylindrical specimen with length/diameter ratio of 2 is used in the test. The specimen is placed on either a porous or solid disc on the pedestal of the apparatus and encased by a thin rubber membrane. A top cap a with porous or solid disc is superposed on the specimen and rubber membrane is sealed to the pedestal and top cap by O-rings under tension. The cylindrical chamber and the circular cell top are installed and filled either with water or glycerine. The soil specimen is subjected to an all-around pressure by compression of the fluid in the triaxial cell. After eventual consolidation the axial load is applied through a vertical loading ram and usually transmitted to the top cap through a steel ball. Depending on the means of application of axial load, the triaxial shear test can be either stress or strain controlled. More information about triaxial test can be found in [30] or [42, 43]. Triaxial tests together with their evaluation will be described in more detail in Section 4.2.

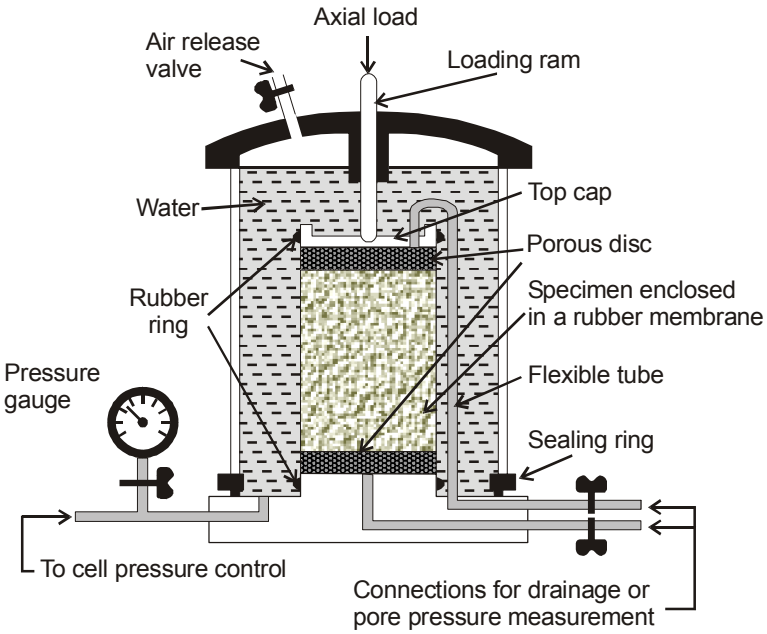

Figure 4–6: Sketch of triaxial test equipment [30, 14].

Deviatoric creep behaviour of clayey soils under triaxial compression of specimens has been investigated by many researchers. A detailed study of the prolonged deformation of clay under undrained triaxial test was made for instance by Murayama and Shibata [80, 81]. They tested clay specimens with diameter 3.5 cm and height 8 cm at five to eight different values of the deviatoric stress. Results were presented in the form of a set of ε (Δh) versus logarithm of time, log t, creep curves, and logarithm of strain rate, log(dε/dt) (log(dΔh/dt)), versus log t curves. Murayama and Shibata established that up to a certain limit of the deviatoric stress, the creep of soil follows the logarithmic law similar to Eq. (2.33). Based on their investigation they proposed the rheological model of clayey soil presented in [81].

Generally the relation between deviatoric creep strain and the logarithm of time can be linear, concave upward or downward. Series of deviatoric creep strain vs. log t curves obtained from deviatoric creep tests under triaxial compression of different clayey material with different boundary conditions can be found in Figure 4–7.

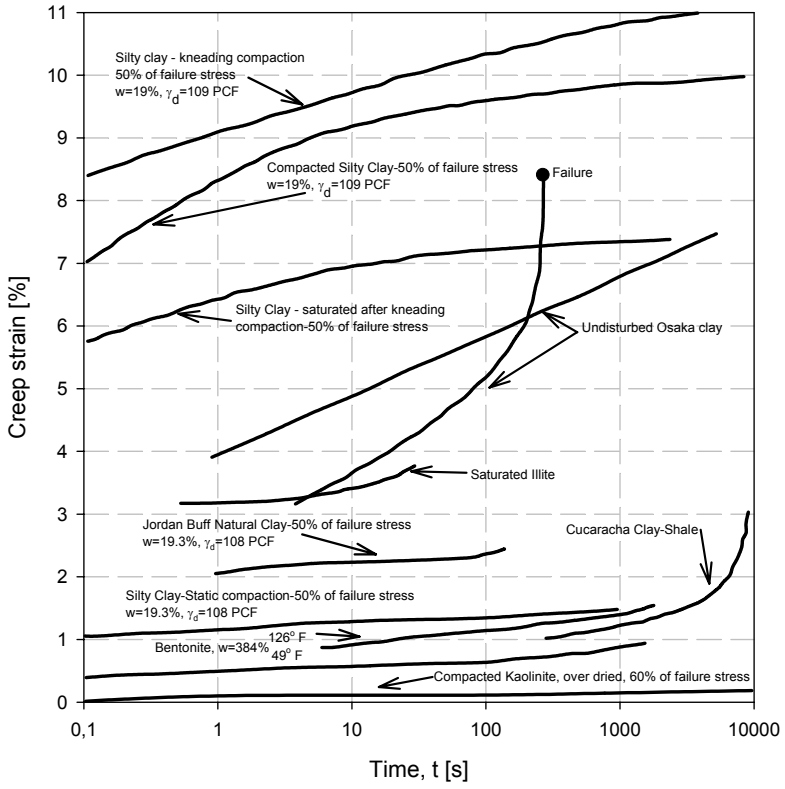

Figure 4–7: Illustration of the different forms of strain vs. logarithm of time behaviour during deviatoric creep under triaxial test [79].

One of the main contributions to the research on the deviatoric creep behaviour of soil under triaxial conditions was made by Singh and Mitchell [95]. By analysing the results of their own laboratory investigation as well as those of Murayama and Shibata [81], and Campanella [21], they introduced a new law of long-term deformation in the $\ln\dot{\varepsilon}$ - lnt co-ordinate system. Their general stress-strain-time function together with evaluation of the creep rupture can be found in Section 2.2.2. According to Singh and Mitchell a plot of the logarithm of the strain rate as a function of the logarithm of time is linear, in the absence of creep rupture [96]. This is shown in Figure 4–8 for the undrained deviatoric creep of Osaka alluvial clay, where D is deviatoric stress (σ_1-σ_3). Reversal in the slope of D=0.676 kg/m^2 signalled the occurrence of the tertiary creep phase and creep rupture. The same general behaviour can be observed for undisturbed and remolded clay, wet clay and dry clay, normally consolidated and over-consolidated soil, and sand [79, 95].

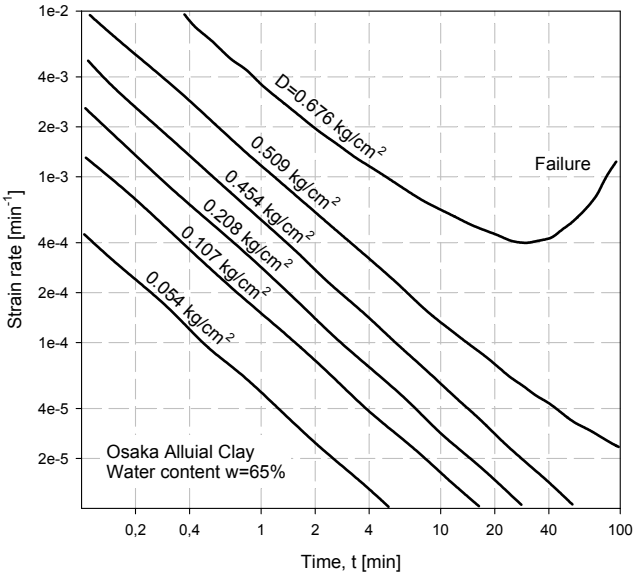

Figure 4–8: Triaxial undrained deviatoric creep behaviour of Osaka alluvial clay according to Murayama and Shibata, [79]. A plot of the logarithm of strain rate vs. logarithm of time.

A detailed study of the behaviour of the Norwegian Eberg clay and Troll clay under triaxial conditions with emphasis to the deviatoric creep was made by Christensen at SINTEF, Trondheim, as a part of the research programme "Study of soft clay deformation". In the case of the Eberg clay the following laboratory tests were per-

formed - 21 anisotropically consolidated undrained triaxial creep tests (ACU-C), 3 undrained triaxial static tests (ACU), 3 drained triaxial creep tests (ACD-C) and 3 oedotriaxial tests (OACU). In addition 6 isotropically consolidated undrained triaxial creep test (ICU-C) performed with the Eberg clay as a part of master's thesis were used for the study. 8 ACU-C, 1 ACU and 2 ACU-CY (undrained cyclic triaxial test) were done by Christensen with the Norwegian Troll clay material. The special creep triaxial equipment developed within this project was used for the testing. The interpretation of the deviatoric creep behaviour was based on modified Janbu's resistance concept, introduced in Section 2.2.3., see Eq. (2.85)-Eq. (2.87). The first limiting shear stress $\tau_{lim}^{(1)}$ was found to be corresponding to the value of the shear mobilisation of 0.5 - 0.6 for all undrained triaxial creep tests. This value is comparable to the value obtained by Meschyan from direct shear tests. When the tests passed the first limiting shear stress, they went through both, secondary and tertiary creep, until creep rupture finally occurred. The creep resistance number r_s was found to be in the range 300-600 for the primary creep phases. In the case of the high level of the shear mobilisation there was no great difference in creep resistance number r_s between undrained and drained creep, i.e. they where almost identical. On the contrary, the r_s value for undrained creep was about two times larger at low shear mobilisation (0.3-0.4). A comparison of ICU and ACU tests of Eberg clay showed that ICU tests displayed higher strain and higher strain rate than corresponding ACU tests when loading to the same degree of shear mobilisation. Detailed description of the studies together with material properties and tests evaluation can be found in [23, 24].

As mentioned above, many different studies of deviatoric creep behaviour under triaxial tests can be found in the literature. Briefly one can mention several authors and their studies. Investigation of the stress-strain-time behaviour of reconstituted English kaolin NF and Cucaracha shale obtained in Panama Canal was made by Mesri and co-workers [75]. Time effects on the undrained stress-strain behaviour of lightly over-consolidated natural clay was studied by Graham and co-workers [39]. A large number of undrained creep tests with triaxial apparatus were performed with normally-consolidated and lightly over-consolidated silty clay by O'Reilly, Brown and Austin [86]. A visco-plastic behaviour of a natural soft clay obtained from foundation of Le Flumet Dam, France was investigated by Fodil, Aloulou and Hicher [35]. Series of triaxial creep tests on undisturbed and remolded Haney clay under a variety of time loading histories were performed by Vaid [109]. Walker investigated undrained creep behaviour of sensitive Leda clay [115]. Undrained triaxial creep behaviour of anisotropic Finnish clays were studied by Korhonen, Järvenmäki and Lojander [55].

4.2 Evaluation of creep Triaxial tests performed by the author

The laboratory behaviour of the undisturbed Norwegian Glava clay and Czech Terlicko clayey shale under triaxial compression was studied by the author. Several drained and undrained long term triaxial tests with constant deviatoric stress were performed with the Norwegian Glava clay. A detailed investigation of the Terlicko clayey shale with emphasis on the drained and undrained shear strength and undrained deviatoric creep behaviour was done. All tests were carried out in the geotechnical laboratory at NTNU, Department of Civil and Transport Engineering, Geotechnical Division.

Two different triaxial apparatuses with "standard" triaxial cells were used for this study. Isotropically consolidated drained (ICD) and undrained (ICU) tests together with deviatoric drained (ICD-C) and undrained (ICU-C) creep tests were done on a triaxial apparatus made by Wille Geotechnik Gmbh, see Figure 4–10 a). Almost all measurements were carried out on 50x50 mm (1:1) cylindrical specimens, which were trimmed from the 80 mm diameter samples in the case of the Terlicko clayey shale. Because of the used 1:1 specimens so called lubricated ends in triaxial tests had to be used for the elimination of the "dead zones" at the ends of the samples, and prevention of any spurious increase in measured strength caused by end restraint. Principle of the used lubricated end can be found in Figure 4–9. Detailed information about triaxial test with 1:1 sample is given in [42].

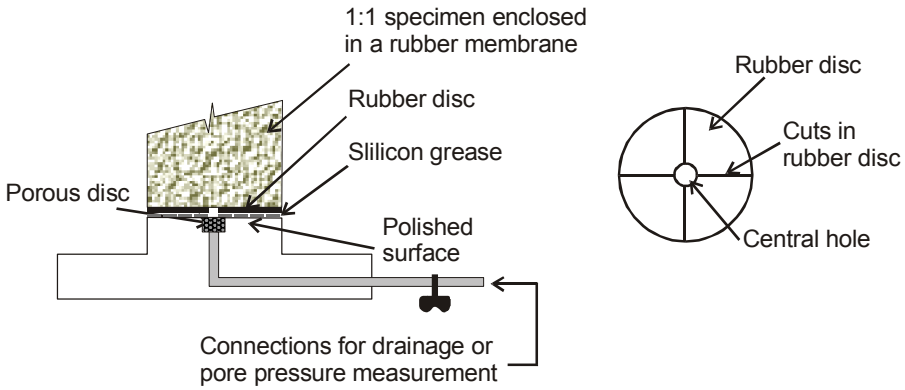

Figure 4–9: Visualisation of the used lubricated end for 1:1 triaxial test with pore pressure measurement.

As a first stage of the tests all specimens were isotropically consolidated under a given consolidation pressure. Duration of the consolidation varied from 1 to 4

hours depending on the tested material. After consolidation the axial stress was applied by giving an axial deformation at a constant rate by a geared loading press, i.e. the strain-controlled tests were performed. In the case of the ICD-C and ICU-C tests the axial force was kept constant for a certain reach level of the deviatoric stress, and the vertical and, for the evaluation of the ICD-C tests, volumetric deformation was recorded with time, i.e. deviatoric creep behaviour was observed. All measured data was recorded by the computer program developed by Wille Geotechnik Gmbh.

The unique Creep Triaxial apparatus made at NTNU, Department of Civil and Transport Engineering, Geotechnical Division was used for performing the ICD-C tests. In contradiction to the Wille apparatus the axial loading system in the case of the Creep Triaxial apparatus was mounted on the top of the cell and controlled by air pressure, i.e. only stress-controlled tests were performed with this apparatus. The load transducer connected to the loading ram was used for the measurement of the axial load values. Cell pressure was also primary controlled by air through an air-water pressure box. There was no possibility to apply back pressure. The Creep Triaxial apparatus was connected to the computer and measured data was recorded by a computer program developed at NTNU. Measurements were carried out on 100x50 mm (1:2) cylindrical specimens. As mentioned above, only drained tests were performed with this apparatus, and the filter paper was fitted around a triaxial sample to accelerate the rate of drainage. The way of testing was similar to the way described above for the Wille apparatus, except for the application of the axial force, which was increasing manually through to the air valve connected to the air loading system. A photograph of the Creep Triaxial apparatus can be found in Figure 4–10 b).

The maximum rate of axial displacement $\dot{\delta}_{max}$ in the case of the ICD tests and shearing part of the ICD-C tests was established based on the investigations by Bishop and Henkel, and Gilbert and Henkel, as

$$\dot{\delta}_{max} = \frac{\varepsilon_f \cdot L}{t_f} \quad [\text{mm/min}] \tag{4.2}$$

where ε_f [%] is the strain at failure, L is the length of the consolidated specimen [mm] and t_f is the time to failure [min] calculated from

$$t_f = \left[\frac{5 \cdot r^2}{\pi} \cdot \frac{\lambda}{\eta_1}\right] \cdot t_{100} \tag{4.3}$$

t_{100} is the time representing theoretical “100%” consolidation, η_1 is a factor depending upon drainage conditions at the sample boundaries, λ is dependent on r and

drainage boundary conditions and r is length/diameter ratio (L/D). Values of parameters λ and η_1 can be found in [42, 43].

a) Triaxial apparatus made by Wille Geotechnik Gmbh.

b) Creep Triaxial apparatus made at NTNU.

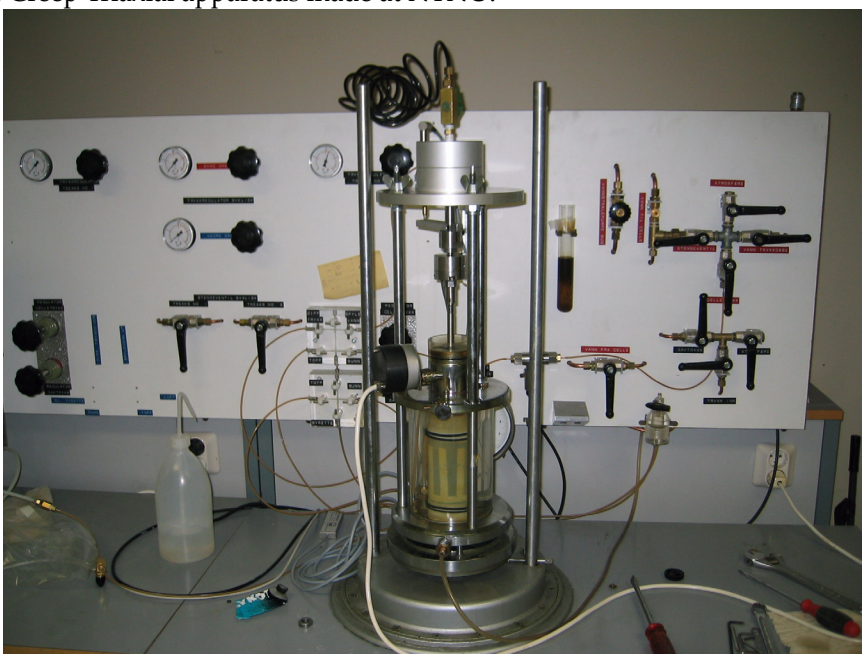

Figure 4–10: Photographs of Triaxial equipment used for the creep tests.

The evaluation of the all triaxial tests performed by the author was done according to the standard procedure contained area correction after consolidation, area correction during shearing, correction of the influence of weight of top cap and loading ram (piston correction) and membrane correction. Detailed description of the tests evaluations together with used area corrections can be found in Appendix 1. The following curves were constructed for all the performed tests,

- Volumetric stress p′ vs. deviatoric stress q, p′-q, for the drained and undrained tests together with the failure envelope.
- Vertical (axial) strain ε_1 vs. deviatoric stress q, ε_1-q.
- Pore pressure u vs. vertical (axial) strain ε_1, u-ε_1, for the undrained shear tests.
- Volumetric strain ε_v vs. vertical (axial) strain ε_1, ε_v-ε_1, for the drained tests.

Microsoft Excel and SigmaPlot 8.0 were used for the construction and interpretation of these curves.

The interpretation of the deviatoric creep behaviour was based on Janbu's time resistance concept introduced in Section 2.2.3. Generally the way of the evaluation of time resistance parameters was built on the evaluation of the volumetric creep behaviour described for several oedometer tests performed by the author in Section 3.3. For the evaluation of the deviatoric creep the following plots were made for all tests,

- Time t vs. vertical (axial) strain ε_1, t-ε_1.
- Time t vs. volumetric strain ε_v, t-ε_v, for the drained tests.
- Time t vs. shear strain γ, t-γ, for the drained tests.
- Time t vs. pore pressure u, t-u, for the undrained tests.
- Time t vs. time resistance R, t-R.
- Degree of the shear mobilisation in the start of the deviatoric creep f_c vs. creep resistance number r_s, f-r_s.

Different ways were used for the evaluation of the drained and undrained deviatoric creep behaviour. In the case of the undrained tests the creep resistance number was evaluated only for primary creep phases from the t-ε_1 curves. Secondary creep phases (if they occurred) were evaluated based on the dynamic viscosity η computed from the equation,

$$\eta = \frac{\tau}{\dot{\gamma}} \tag{4.4}$$

where τ is the shear stress and $\dot{\gamma}$ is rate of the shear strain. Total values of the fading component of the strain ε_{pc} (primary creep phase) and non-fading component of the

strain ε_{sc} (secondary creep phase) in the end of the creep were recorded. Additionally, development of the pore pressure during deviatoric creep was observed.

Drained creep behaviour under triaxial compression contains a coupling process of the volumetric and deviatoric creep. Because of this situation the volumetric and vertical strains were used separately for the evaluation of the value of the creep resistance number, i.e. two creep resistance numbers were computed from the t-ε_1 and t-ε_v curves. Similarly as for the undrained deviatoric creep the total value of the volumetric strain ε_v and vertical strain ε_1 at the end of the creep were recorded.

Evaluation of the creep resistance number for all deviatoric creep tests was based on the regression introduced in Section 3.3,

$$\varepsilon(t) = y_{s0} + a_p \cdot \ln(t - x_{s0}) \tag{4.5}$$

where a_p, y_{s0} and x_{s0} are constants.

4.2.1 Glava clay

Detailed study of the deviatoric creep behaviour of the Norwegian Glava clay was done by the author as a part of the investigation of the viscosity of the Glava clay with compact rheometer, described in Chapter 5. As mentioned in Section 3.3.2 the Glava clay is a low sensitive, medium stiff marine clay from the deposit located in Stjørdal, Norway. The behaviour of this clay has been thoroughly investigated in several contexts in geotechnical laboratory at NTNU mainly by Sandven [92]. A detailed description of the Glava clay can be found in Chapter 5, see Table 5–1. Evaluation of the several oedometer tests performed by the author with emphasis to the volumetric creep behaviour is presented in Section 3.3.2.

Two 80 cm long specimens placed in the metal tube sampler were used for the testing with triaxial apparatus. Specimens were taken from the depth 9-9.8 m by the staff from the geotechnical laboratory at NTNU, Department of Civil and Transport Engineering, Geotechnical Division. The following geotechnical parameters of the Glava clay were evaluated according to the general index tests performed by the author. The average moisture content $w \approx 25\%$, unit weight $\gamma \approx 19\text{kN/m}^3$, liquid limit w_L=32%, plastic limit w_p=23% and porosity n=46%. The degree of saturation was found to be around 100%, i.e. specimens were fully saturated. Based on the triaxial tests performed by Sandven and co-workers the effective values of the cohesion c′ and friction angle φ′ were evaluated as c′=18kPa and $\varphi'=29^o$. From the in-situ investigation the Glava clay was found to be over-consolidated with the preconsolidation pressure σ_c'=400 kPa [92].

Thirteen isotropically consolidated drained triaxial creep tests (ICD-C) and four isotropically consolidated undrained triaxial creep tests (ICU-C) were performed by the author in the triaxial apparatus made by Wille Geotechnik Gmbh and the Creep Triaxial apparatus made at NTNU, Department of Civil and Transport Engineering, Geotechnical Division, described in Section 4.2. In the first stage, all specimens were isotropically consolidated for about 24 h. Two values of the consolidation pressure were chosen - 100 and 200 kPa. Two tests were performed with artificially over-consolidated samples, i.e. samples were consolidated to a higher level of the consolidation pressure (700 and 800 kPa) which was later decreased. One sample was consolidated under preconsolidation pressure 400 kPa (the in-situ preconsolidation pressure) which was later reduced to 100 kPa. After consolidation the shearing was applied to a certain limit of a degree of shear mobilisation and then the value of the vertical pressure was kept constant and creep occurred. Duration of the observed deviatoric creep was varied from 2 to 12.5 days. In the case of drained tests the creep behaviour of the specimen was tested under so called "step-wise" incremental shear stress, i.e. under two or three different values of the shear mobilisation. Undrained deviatoric creep behaviour was observed only at one level of the shear mobilisation. All tests were performed without application of the back pressure. Overview of the performed triaxial creep tests can be found in Table 4–1.

Test no.	Depth [m]	Type of the sample	Type of the test	Consolidation pressure p_c'
1. (a, b, c)	9.48	1:1	ICD-C	100 kPa
2.	9.25	1:2	ICU-C	200 kPa
3.	9.1	1:1	ICU-C	200 kPa
4.	9.2	1:1	ICU-C	200 kPa
5.	9.6	1:1	ICU-C	Overconsolidated sample 200-400-800-600-400-200 kPa
6. (a, b, c)	9.42	1:2	ICD-C	100 kPa
7. (a, b)	9.35	1:2	ICD-C	200 kPa
8. (a, b)	9.58	1:2	ICD-C	Overconsolidated sample 100-200-400-700-400-200 kPa
9. (a, b, c)	9.1	1:2	ICD-C	Overconsolidated sample 100-200-400-200-100 kPa

Table 4–1:Basic characterisation of triaxial tests with the Norwegian Glava clay performed by the author.

Both triaxial apparatuses were used for the drained deviatoric creep testing. Nevertheless only test no. 1 was performed with Geotechnik Gmbh apparatus and 1:1 specimen. After evaluation of this test the 1:1 specimen was found to be problematic for the drained tests mainly because of the small filters used due to the lubri-

cated ends described in Figure 4–9. Even with a very small constant rate of the axial deformation applied during shearing (0.001 mm/minute) it seems that the pore pressure was not dissipated enough and effective values of the horizontal and vertical stresses were not measured. This behaviour can be indicated from the p'-q and ε_v-ε_1 curves shown in Appendix 2. So finally only the special Creep Triaxial apparatus was used for the rest of drained tests. Problems with the 1:1 specimens will be discussed later for the undrained triaxial creep tests.

As mentioned, the drained deviatoric creep behaviour was investigated by so-called "step-wise" incremental shear stress, i.e. one specimen was used for two or three deviatoric creep tests under different degrees of shear mobilisation. In contradiction to the undrained deviatoric creep test, the drained deviatoric creep test performed in the so-called "wet" side of the p'-q diagram usually does not lead to failure. On the contrary it produces increased stiffness in the tested material. During the creep the pore pressure dissipates and volume change occurs. It means that two coupled processes can be observed during the drained deviatoric creep test - volumetric creep and deviatoric creep. In the case of the test the volumetric creep strain and vertical creep strain were evaluated. Development of these two quantities with time for tests nos. 6a, b, c is illustrated in Figure 4–11. One can see that the rate of the volumetric creep strain decreases with increasing degree of the shear mobilisation, where for the low values of the shear mobilisation the volumetric creep can be denoted as a creep flow or secondary creep phase. After evaluation of the volumetric creep resistance number for the primary phase of the volumetric creep r_{vs} the increasing tendency was observed. This behaviour was found during all tests except for tests performed with heavily over-consolidated material (test nos. 8a, b). In this case the volume changes during the creep were almost negligible for all values of the shear mobilisation in the start of the creep tests. Vertical creep strain shown in Figure 4–11 indicates increasing rate tendency with increasing degree of the shear mobilisation. Nevertheless only primary creep phases were observed during testing. The creep resistance numbers r_{1s} evaluated for the vertical creep strain (deformation creep resistance number) was found to be in the range from 470 to 150, decreasing with increasing shear mobilisation. A several times larger value of the r_{1s} was found for tests nos. 8a, b and 9a, b, c performed with the artificially over-consolidated Glava clay. A detailed graphical description of all test containing visualisation of the general triaxial behaviour and drained deviatoric creep behaviour for the original Glava clay material and artificially over-consolidated Glava clay can be found in Section A2.3.

a) Development of the vertical creep strain with time.

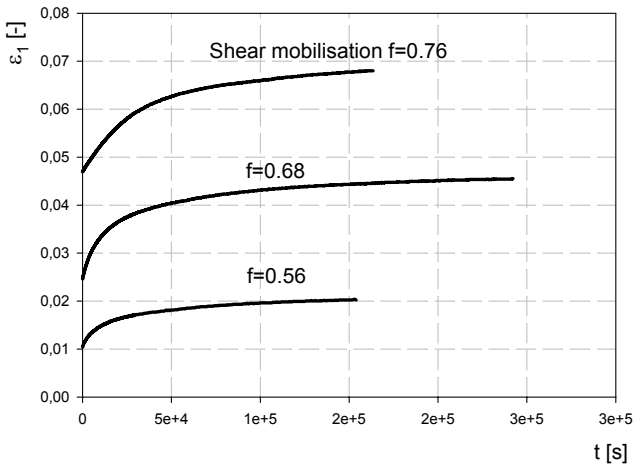

b) Development of the volumetric creep strain with time.

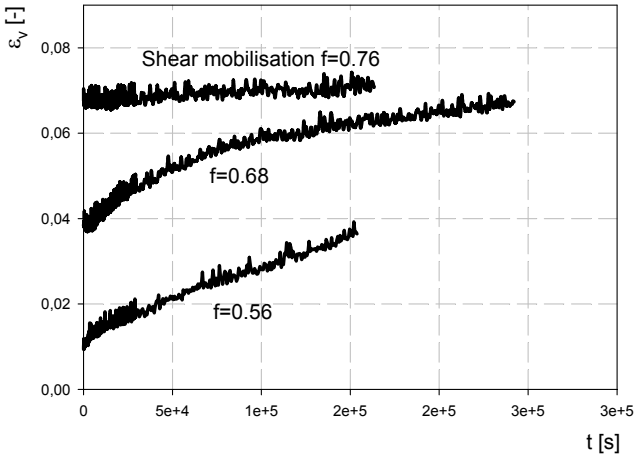

Figure 4–11: Drained deviatoric creep behaviour of tests nos. 6a, b, c.

Based on the evaluation of the creep resistance number the connection can be found between deviatoric deformation and simultaneously running volumetric deformation. At the start of the deviatoric creep test, the development of the creep resistance numbers evaluated from the vertical and volumetric creep strains show an increasing amount of the deviatoric creep deformation and a decreasing amount of the volumetric creep deformation with increasing value of shear mobilisation. This behaviour seems to be typical for the normally consolidated and lightly over-consolidated clay material. In the case of the heavily over-consolidated clays the situa-

tion is more complex and in theory this can easily leads to the creep rupture. Development of the volumetric and deformation creep resistance numbers r_{vs} and r_{1s} with the degree of shear mobilisation at the start of the creep is presented in Figure 4–12 a) and b) for the normally and over-consolidated Glava clay.

a) Normally consolidated Glava clay.

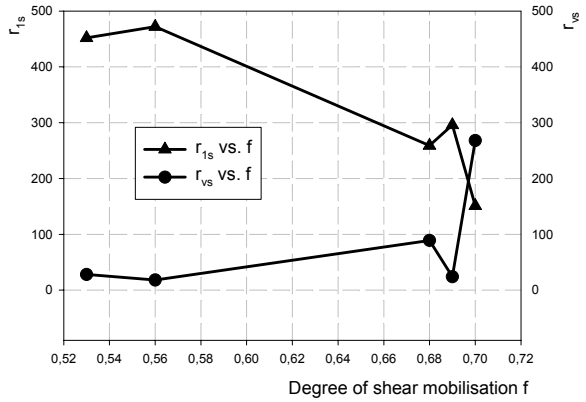

b) Over-consolidated Glava clay.

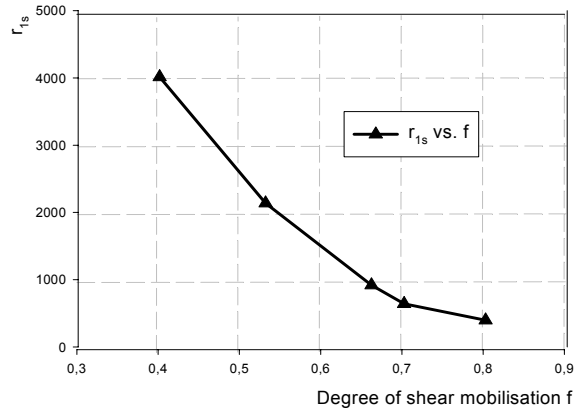

Figure 4–12: Development of the volumetric and deformation creep resistance number with degree of the shear mobilisation at the start of the creep.

The overview of all parameters evaluated from the drained deviatoric creep behaviour of the Norwegian Glava clay can be found in Table 4–2. Evaluation of tests nos. 1a, b, c is shown in the table only for the illustration and should not be considered, due to the problems described above, for the general description of the drained deviatoric creep behaviour of the Glava clay. Because of the different duration of the performed creep tests it is also impossible to compare absolute values of the

recorded creep strains ε_{vc} and ε_{1c} under different degree of the shear mobilisation at the start of the creep.

Test no.	Degree of shear mobilisation at the start of the creep, f	Volumetric creep		Deformation creep		Duration of the creep [days]
		ε_{vc} [-]	r_{vs} [-]	ε_{1c} [-]	r_{1s} [-]	
1a.	0.31	0.01	305.3	0.004	1029.2	1.5
1b.	0.64	0.015	185.6	0.0054	799	2
1c.	1.1	0.017	28.33	0.0084	486.9	3.5
6a.	0.56	0.027	18.2	0.01	472.6	2
6b.	0.68	0.03	89.7	0.02	259.3	3
6c.	0.76	0.003	268	0.02	151.2	2
7a.	0.53	0.028	28.2	0.017	452.2	6
7b.	0.69	0.036	23.6	0.025	296.8	9
8a.	0.53	0	-	0.0031	2139	1.5
8b.	0.7	0.005	572	0.01	641	3
9a.	0.4	0.0129	11	0.0021	4014	5
9b.	0.66	0.0045	779	0.0064	918.9	2
9c.	0.8	0	-	0.02	397.4	12.5

Table 4–2:Evaluation of the drained deviatoric creep tests under triaxial compression with the Norwegian Glava clay performed by the author.

All undrained deviatoric creep tests were done in the triaxial apparatus made by Wille Geotechnik Gmbh. The first undrained test (test no. 2) was done with 1:2 specimen, i.e. with 100x50 mm cylindrical specimen. Visualisation of the stress path of effective stresses in p'-q diagram for this test together with representation of the failure envelope can be found in Figure 4–13. The failure envelope was constructed based on the previous laboratory investigation of Glava clay made by R. Sandven and co-workers [92], mentioned above. After investigation of the general undrained triaxial behaviour one can see that the effective cohesion c' evaluated from the test performed by the author seems to be smaller then the previously measured one. As for the effective friction angle φ', the measured value is close to the 29^o evaluated earlier. The shearing part of the undrained triaxial test no. 2 before creep shows the typical undrained behaviour of the over-consolidated clay material. At the point of the shear mobilisation equal to 0.61 the shearing part was stopped and the creep occurred. A typical stress path for the undrained creep triaxial behaviour with the constant value of the deviatoric stress q and decreasing value of the volumetric stress p' due to the pore pressure increase can be observed in Figure 4–13. The duration of the creep part was 9 days. The undrained creep behaviour will be discussed in more details later in this section. After deviatoric creep the shearing was renewed

and the "after-creep" shearing behaviour was investigated. Here, one can see the stiffer response of the tested material following the undrained deviatoric creep, see Figure 4–13. After reaching failure, the Glava clay material showed dilatant behaviour.

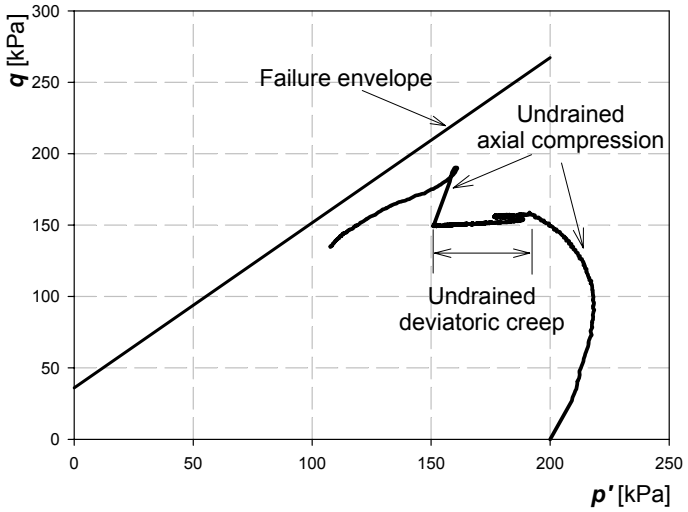

Figure 4–13: Stress path of effective stresses for undrained deviatoric creep test on 1:2 specimen of the Norwegian Glava clay with representation of the failure envelope.

Development of the axial strain ε_1 and the pore pressure u with time t during the undrained triaxial creep test no. 2 is shown in Figure 4–14 a) and b). One can see that only primary creep occurred during testing. The creep resistance number r_{1s} evaluated for the axial, or vertical creep strain ε_1 was found to be 168.5. Final vertical creep strain after 9 days was observed to be 4%. As for the evaluation of the pore pressure the value of the measured pore pressure increased with the logarithmic tendency. The final value of the pore pressure after 9 days creep was found to be around 100 kPa.

Three other undrained triaxial deviatoric creep tests were performed by the author with the special 1:1 samples (tests nos. 3, 4 and 5). As mentioned earlier in this section, there was a problematic response of the 1:1 sample during the drained triaxial testing, probably connected with the "non-standard" pore pressure development, and it was impossible to use these test results for the evaluation of the investigated

drained triaxial deviatoric creep behaviour. A similar problem was also found during the undrained triaxial deviatoric creep test.

a) Development of the axial strain ε_1.

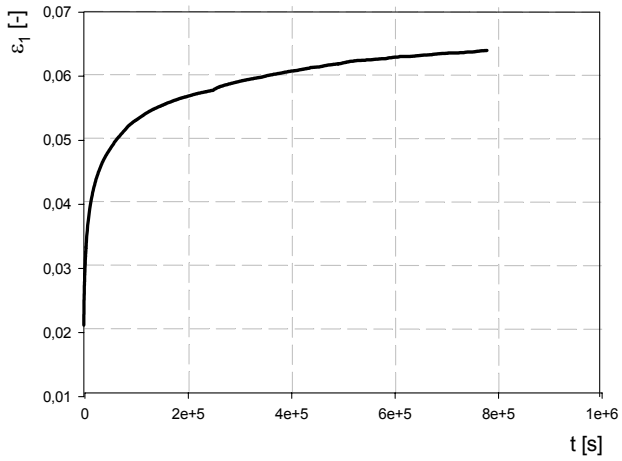

b) Development of the pore pressure u.

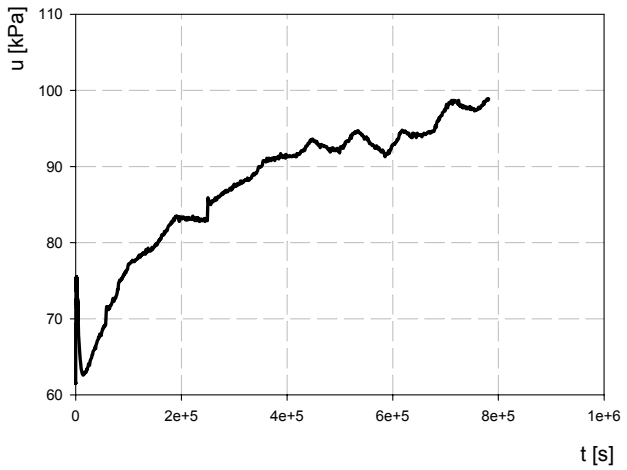

Figure 4–14: Undrained deviatoric creep behaviour of the test no. 2.

Comparison of the undrained triaxial behaviour of test no. 2 (1:2 sample) and test no. 3 (1:1 sample) with emphasis on the undrained deviatoric creep behaviour is shown in Figure 4–15 a), b), c). Figure 4–15 a) shows the general undrained triaxial behaviour illustrated in p'-q diagram, i.e. the stress paths of effective stresses during the testing, together with the failure envelope. The first shearing part of both tests shows the standard undrained behaviour of the clay material during the triax-

ial shearing test. The shearing started at the same stress point and stopped after the same certain value of the vertical force was reached in both tests. Figure 4–15 shows the stiffer response of the 1:1 sample and lower value of the degree of shear mobilisation at the end of the shearing and start of the undrained triaxial deviatoric creep phase (f=0.52 for the test no. 3 and 1:1 sample, and 0.61 for the test no. 2 and 1:2 sample). In the case of the 1:1 sample, the measured excess pore pressure during the initial triaxial shearing was significantly smaller.

a) General undrained triaxial behaviour - p'-q diagram.

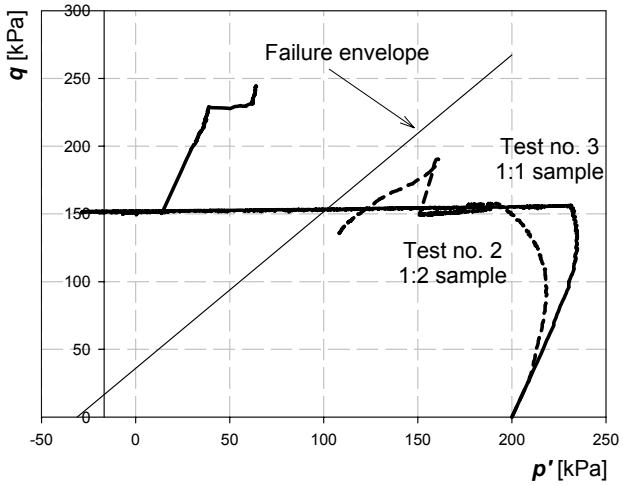

b) Development of the creep vertical strain with time for the creep phase.

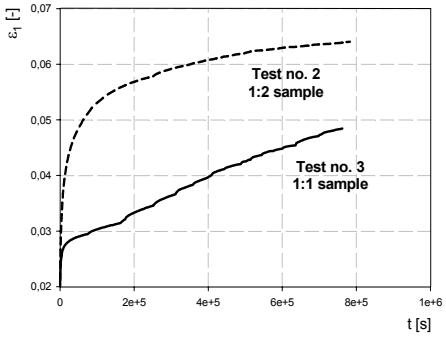

c) Development of the pore pressure with time for the creep phase.

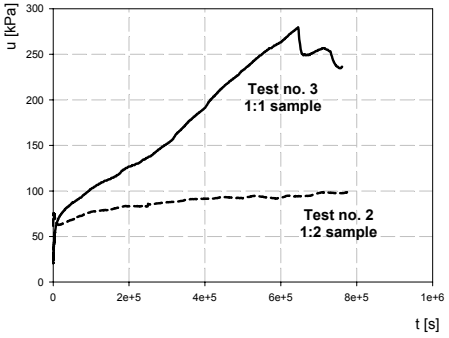

Figure 4–15: Comparison of the undrained triaxial behaviour of the 1:2 and 1:1 sample with emphasis on the undrained deviatoric creep behaviour.

Typical stress paths with the constant value of the deviatoric stress q and decreasing value of the volumetric stress p' due to the pore pressure increase can be observed for the undrained deviatoric creep behaviour, see Figure 4–15. One can also see that during the creep test with 1:1 sample the stress path crosses the failure envelope and continues to the so-called "dry" or "low stress" side. The volumetric stress during the deviatoric creep phase even advances to negative values. This behaviour is at least "non-standard" and one possible explanation of this response introduced by the author will be described later in this section.

A detailed comparison of the vertical creep strain and pore pressure development with time during triaxial deviatoric creep tests on 1:1 and 1:2 specimen (tests nos. 3 and 2) can be seen in Figure 4–15 b) and c). As for the vertical creep strain one can observe the higher value obtained in the case of the test no. 2 and 1:2 sample. As mentioned above, only a primary creep phase was indicated in this test. In contradiction to this result the primary creep phase was followed by the secondary one in test no. 3 (1:1 sample). However, no occurrence of the tertiary creep phase and creep rupture was observed. Creep resistance number r_{1s} evaluated for the primary creep phase of test no. 3 was found to be 543, what is more than three times higher than in test no. 2. Evaluation of the pore pressure development with time showed the significant difference between test with the 1:1 and 1:2 sample. Test no. 3 exhibited 2.5 times higher value in the excess pore pressure developed during the nine days undrained deviatoric creep phase.

Because of the "unusual" behaviour of the 1:1 sample during the undrained triaxial deviatoric creep test no. 3, two other tests (test nos. 4 and 5) with the same shape of the sample were done by the author. Almost identical behaviour as observed during the previous test with the 1:1 specimen was recorded for test no. 4. The shearing part was practically equal with test no. 3 and during the undrained deviatoric creep phase the failure envelope was crossed by the stress path. Test no. 5 was performed with heavily over-consolidated Glava clay and the general behaviour of this specimen was stiffer in comparison with previous tests with 1:1 specimen. Even in the case of this heavily over-consolidated material the failure surface was slightly crossed and the linear increase of the excess pore pressure with time was observed. Based on this behaviour one can expect that the following increase of the excess pore pressure with the continuing deviatoric creep, i.e. the deviatoric creep stress path, will probably continue to move to the left.

After investigating the undrained deviatoric creep behaviour of all triaxial tests with the 1:1 sample it was possible to see that in the case of all these tests the secondary creep phase occurred. Again the tertiary creep phase or creep rupture was not observed. The significant linear increase of the pore pressure with time was typ-

ical for all tests with the 1:1 Glava clay specimen. The value of the creep resistance number evaluated for the primary creep phase had decreasing tendency with increasing degree of the shear mobilisation at the start of the undrained deviatoric creep phase. Detailed description of all tests contained several plots illustrating the general and deviatoric creep behaviour is presented in Section A2.2. A summary of all undrained deviatoric creep tests is given in Table 4–3.

Test no.	Type of the sample	Degree of shear mobilisation at the start of the creep, f	Primary creep		Secondary creep	Duration of the creep [days]
			ε_{cp} [-]	r_{1s} [-]	ε_{cs} [-]	
2.	1:2	0.61	0.0400	168.5	-	9
3.	1:1	0.52	0.0074	543.4	0.02	9
4.	1:1	0.63	0.0100	294.5	0.03	4
5.	1:1	0.9	0.0127	163.7	0.01	3

Table 4–3: Evaluation of the undrained deviatoric creep tests under triaxial compression with the Norwegian Glava clay performed by the author.

As a first step for understanding of the "non-standard" behaviour of the 1:1 specimen during the undrained deviatoric creep test the author tried to find some more information about triaxial tests performed with 1:1 clayey samples. Fortunately the general comparison of the undrained triaxial behaviour of 1:1 and 1:2 samples was completed at NTNU by Braaten [20]. Several tests were done with the Norwegian Glava clay material taken from the depth 9-11.8 m. Comparison of two undrained triaxial tests performed with the Glava clay material taken from 9 m depth can be found in Figure 4–16. Two stress paths of effective stresses in p'-q diagram evaluated from undrained triaxial behaviour of 1:1 and 1:2 specimens are illustrated in this figure. One can see the same shear behaviour as described above by the author and illustrated in Figure 4–15 a), i.e. the stiffer response of the 1:1 sample. After crossing the peak value of the deviatoric stress the stress path of the 1:1 sample has a flat character, in contradiction to the clear stress reduction after failure in the case of the 1:2 specimen.

The stiffer behaviour of 1:1 sample during the shear part of the undrained triaxial test in comparison with 1:2 sample was found in all tests performed by Braaten. In other words the smaller samples demonstrated the lower values of the pore pressure developed during the triaxial shearing in comparison with the higher one. Braaten explained - "The constant rate of the axial deformation applied during the shearing was chosen to be 1% and 3%. However, the rate of the axial deformation did not have a large influence on the excess pore pressure development". Based on this information it is possible to consider this behaviour as a characteristic feature of the 1:1 clayey specimens in comparison with the 1:2 ones.

Although the flat stress path of 1:1 sample after failure, described above, was not found in all tests, at least 60% of all undrained triaxial tests performed by Braaten with the 1:1 specimens exhibited this behaviour. According to Braaten this response is connected with the more homogeneous stress situation in the 1:1 sample. He assumes that close to failure the whole 1:1 sample is mobilised and, due to the homogeneous stress situation, a lot of shear planes are generated inside the sample, in contradiction to the few long shear planes in the case of the 1:2 specimen.

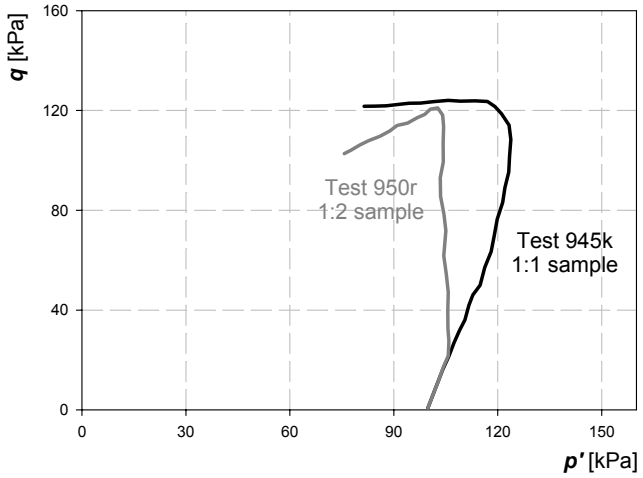

Figure 4–16: Example of the stress path of effective stresses of undrained triaxial tests performed at NTNU by T. Braaten on 1:1 and 1:2 specimens of Norwegian Glava clay [20].

As mentioned above, the behaviour of the 1:1 Glava clay specimen during the undrained triaxial deviatoric creep tests (mainly the measured pore pressure development during the creep phase) performed by the author is of course unrealistic and probably reflects the problem with the measuring of the real global excess pore pressure development in the sample. As was described in Section 4.2 and illustrated in Figure 4–9, the main difference in comparison with the 1:2 specimen (besides the difference in the shape of the sample) is the use of so-called lubricated ends and, consequently, the smaller filter with a diameter of only 6 mm. In the case of the triaxial apparatus made by Wille Geotechnik Gmbh the pore pressure transducer is connected to the bottom filter, which means that only pore pressure development in the centre of the bottom part of the 1:1 sample is measured (in contradiction to the 1:2 specimen where the whole bottom area is monitored). Due to the smaller filter a higher hydraulic gradient and longer drainage path are occurs inside the 1:1 sample

which has a significant influence on the general behaviour of the sample during the triaxial test. The other main problem is the friction between the sample and the bottom pedestal or top cap respectively. Even with lubrication the friction is only reduced to a smaller value and still there is high friction between the sample and the small filter without lubrication.

In order to prove these suggestions, several 2D numerical models were done by the author with the geotechnical finite element program PLAXIS 8.1. Finally four numerical models of the 1:1 specimen with slightly different boundary conditions, and, for comparison, two models of the conventional 1:2 specimen were studied more thoroughly. The finite element meshes used together with loads and general boundary conditions are illustrated in Figure 4–17 a) and b). Because of the simplification and better recognition, the numerical models of the 1:1 specimen were generally denoted as models A (precisely models A1, A2, A3 and A4), and models of the 1:2 specimen as models B (B1 and B2).

a) 1:1 specimen - models A.

b) 1:2 specimen - models B.

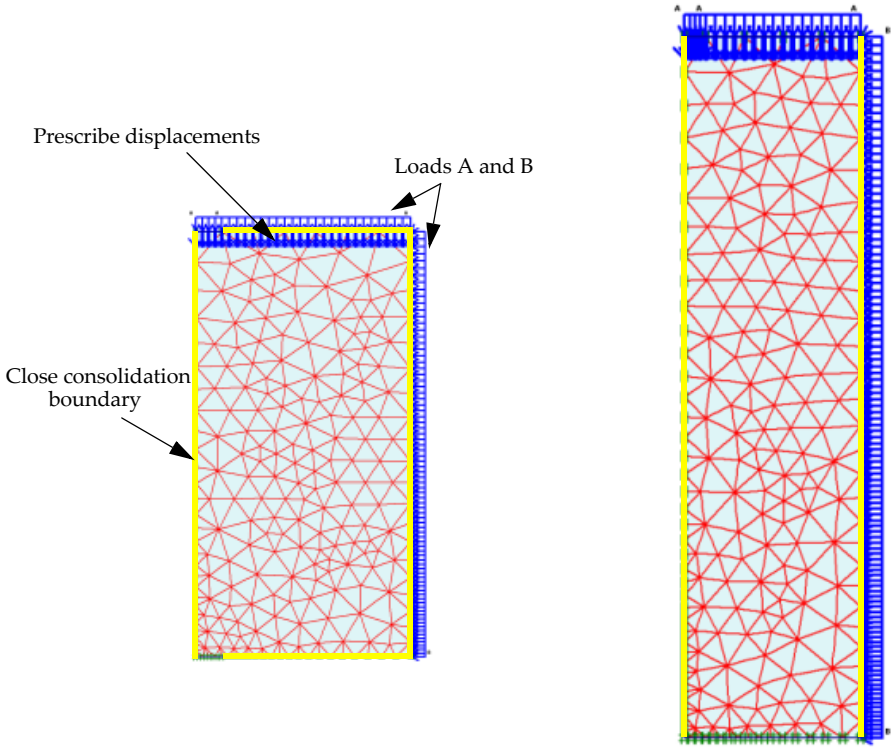

Figure 4–17: Plots of the geometry of the PLAXIS models together with loads and the general boundary conditions.

Considering the cylindrical shape of the real triaxial samples the axisymmetry model with six-node triangular elements was used in the case of both specimens, i.e. only half of the specimen was modelled. The geometry of the used finite element meshes was chosen according to the real samples. It means that the height of the modelled sample was equal to 50 mm in the case of the models A and 100 mm in the case of the models B. The width of both used finite element meshes was only 25 mm because of the applied symmetry. Mesh was generated in the way to be denser around the bottom filter, i.e. in the left bottom corner, for the better investigation of this area. More detailed information about the used finite element meshes can be found in Table 4–4.

Model	Size of the mesh (H/W)	Number of elements	Number of nodes	Number of stress points	Average element size
A (1, 2, 3, 4)	50/25 mm	382	3213	4584	1.81E-3 m
B (1, 2)	100/25 mm	351	2987	4212	2.67E-3 m

Table 4–4:General information about finite element meshes used.

Because of the creep investigation the Soft-soil-creep constitutive model was used for all tests. From the point of the deeper understanding of the all processes running in the sample during the undrained triaxial tests, two soil data-set parameters based on the laboratory tests done with the Norwegian Glava clay and the Czech Terlicko clayey shale were chosen for numerical models. The overview of the parameters used is presented in Table 4–5.

Material model	Material set	
Soft soil creep	Glava clay	Terlicko clayey shale
Type	Undrained	Undrained
γ_{unsat} [kN/m^3]	19	18
γ_{sat} [kN/m^3]	19	20
k_x [m/day]	3E-5	2E-4
k_y [m/day]	3E-5	2E-4
λ^*	0.04	0.01
κ^*	0.018	0.003
μ^*	0.0024	8E-5
c [kN/m^2]	18	2
φ [^{o}]	29	29
ψ [^{o}]	0	1.2
Performed models	A1, A2, A3, B1	A4, B2

Table 4–5:Presentation of the used soil data-set parameters.

As a first step a numerical investigation was done of the behaviour of the Glava clay during an undrained triaxial deviatoric creep test. Three models of the 1:1 specimen, i.e. models A1, A2 and A3, and the one model of the 1:2 specimen B1 were used. As for the boundary conditions, the left lateral boundary was horizontally restrained because of the applied axisymmetry in the case of the all models. As illustrated in Figure 4–17 a) and b) the close consolidation boundary was applied to both lateral boundaries in the case of the models B and, except for the 3 mm long area represented the small filter, also to the bottom and top boundaries in the case of models A. This kind of boundary condition was used to avoid the occurrence of the zero excess pore pressure at the chosen boundaries during consolidation analysis, i.e. the flow across the boundary was allowed only in the filter areas. To simulate the cell pressure two static load systems "a" and "b" were applied to the top horizontal and right vertical boundaries. Different load systems were used because of the later application of the vertical stress which was of course higher than the cell pressure σ_{cell}. The prescribed displacement was applied to the top boundary for the modelling of the strain controlled triaxial shearing part.

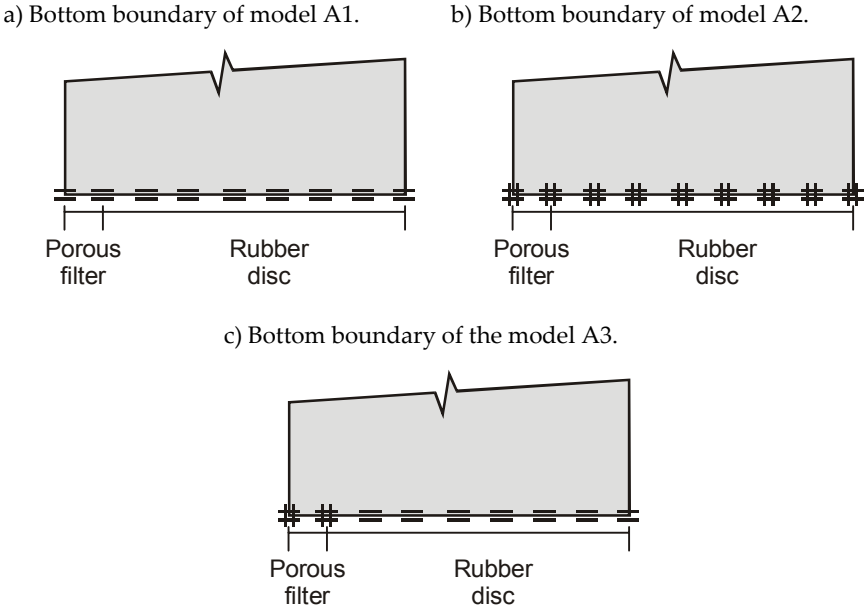

Figure 4–18: Illustration of the applied fixities to the bottom boundary in the case of the performed numerical models A1, A2 and A3 of undrained triaxial creep test on the 1:1 Glava clay sample.

As mentioned, the "non-standard" behaviour of the 1:1 Glava clay specimen during the undrained triaxial deviatoric creep test is thought to be partly connected with the friction between the sample and the bottom pedestal (from the point of the pore

pressure transducer connected to the bottom filter) or the top cap respectively. Because of this assumption the main emphasis was placed on the bottom and top boundaries in the case of models A. Three different boundary conditions from the fixities point of view were applied to the horizontal boundaries for the closer study of this problem. An illustration of the applied fixities to the bottom boundary in the case of models A1, A2 and A3 can be found in Figure 4–18 a), b), c). The same boundary conditions, except for the vertical fixities, were applied also to the top boundary. It means that in the case of model A1 the whole bottom boundary was vertically restrained and the top boundary was not fixed at all, i.e. the situation without any friction between the sample and bottom pedestal or top cap respectively was studied numerically. The opposite conditions were applied to model A2 where the whole bottom boundary was fixed in the both directions and the top boundary was horizontally restrained. One can see that both extreme situations with full connection and without any friction between the triaxial sample and the whole bottom pedestal or top cap respectively were contained in models A1 and A2. These two models were used for comparison with the more realistic situation applied in the case of model A3 where the full connection between the sample and the filter areas and no friction between the sample and the rest of the bottom and the top part is suggested. It means that the horizontal fixities were applied only to the part of the bottom and top boundaries represented the filter areas. The whole bottom boundary was also vertically restrained. This situation is of course also not real but represents the extreme state in the case of the so-called lubricated ends and, from this point of view, can be efficiently used to obtain a better understanding of the processes inside the 1:1 sample during the undrained triaxial testing.

In the case of the numerical models B, the boundary conditions applied to horizontal boundaries from the fixities point of view corresponded to model A2 (see Figure 4–18 b)). Thus the full connection between the sample and the bottom or top filter respectively was studied. This state is close to the real situation and can be used for the numerical simulation.

After the full basic construction of models A1, A2, A3 and B1 the initial conditions were applied. The general water pressure was generated by the phreatic level placed on the top boundary in the case of all models. The K_0-procedure was used for the generation of the initial stress situation, where the K_0 value was computed from the effective friction angle according to the Jaky's formula,

$$K_0 = 1 - \sin\phi' \tag{4.6}$$

Based on the laboratory tests performed by the author on the Norwegian Glava clay material the pre-overburden pressure POP was chosen to be 400 kPa for the generation of the pre-consolidation pressure for the Soft-soil-creep model.

Seven calculation phases were computed in the case of the all-numerical models A and B. The overview of these phases can be found in Table 4–6. One can see that as the first distributed load systems "a" and "b" were activated where applied external stresses were chosen to be 100 kN/m^2 for both load systems. Following the real laboratory schedule the consolidation with duration 2.5 hours was computed as the next phase. In the third phase the external stresses were increased to 200 kN/m^2 and a second consolidation with a duration of half a day was calculated. In other words, the application of the 100 kPa cell pressure, "short" consolidation, increasing of the cell pressure to the value 200 kPa and half a day consolidation were modelled.

Phase no.	Start phase	Calculation type	Load input	Calculated process
0	0	-	-	Initial conditions
1	0	Plastic	Stage construction	External Stress application
2	1	Consolidation	Ultimate time	2.5h consolidation
3	2	Plastic	Total multipliers	External stress increasing
4	3	Consolidation	Ultimate time	12h consolidation
5	4	Plastic	Stage construction	Application of the shearing phase
6	5	Plastic	Stage construction	End of the shearing phase
7	6	Plastic	Stage construction	Creep phase

Table 4–6:List of the applied calculation phases in the case of the all-numerical models A and B, tests by the author.

As next stage the strain controlled shear triaxial phase was modelled. All displacements were reset to the zero and the prescribed vertical displacement (0.25-0.5 mm) applied on the top boundary. The duration of the shearing phase was chosen to be approximately half an hour. After shearing the prescribed displacement was deactivated and the external stress applied on the top boundary was increased to the value corresponding to the stage in the end of the shearing. The size of the applied prescribed displacement was not the same for all models but was deliberately chosen to reach the same value of the external stress applied on the top boundary in the case of all the numerical models A and B. As a last stage the nine-day creep phase was applied and studied. After computing all these phases in the case of

numerical simulations A1, A2, A3 and B1 the comparison of results led to the following conclusions.

At first the state in the ***end of consolidation*** was investigated. Plots of the mean effective stresses for models A3 and B1 can be found in Figure 4–19. In the case of model A3 the minimum and maximum concentrations of the mean effective stresses were found in the right end of the filter areas in contradiction to model B1

a) Numerical model A3 - bottom part of the modelled sample.

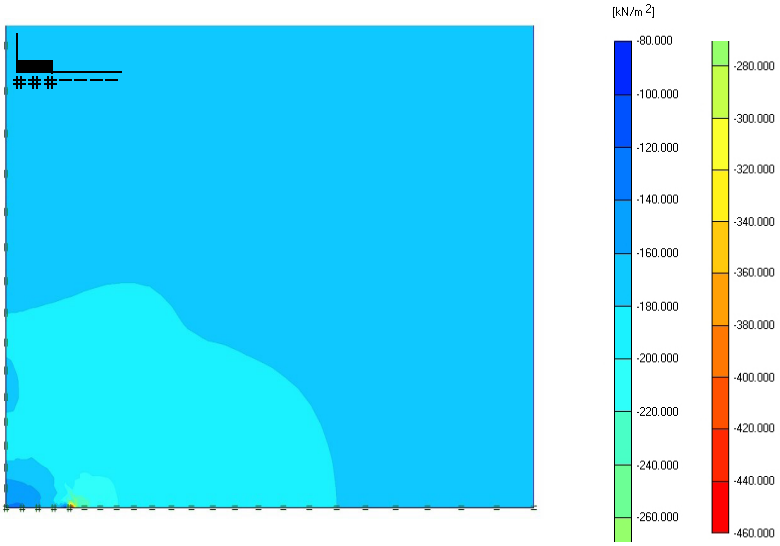

b) Numerical model B1 - bottom part of the modelled sample.

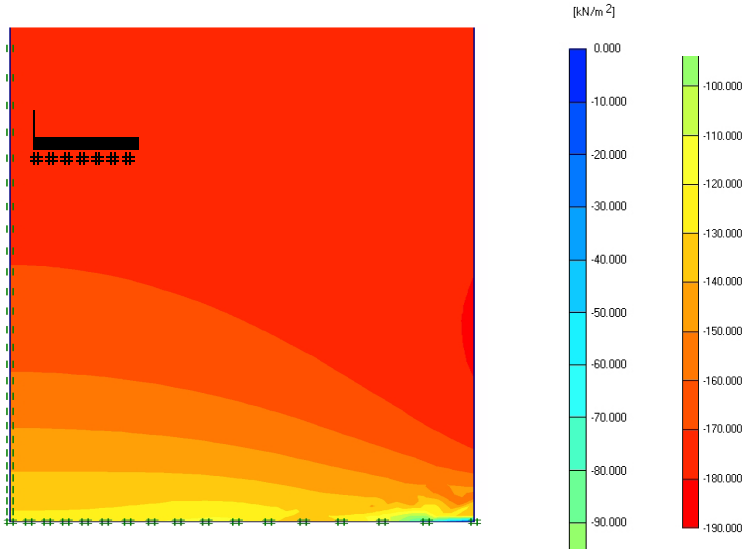

Figure 4–19: Plot of effective mean stresses in the case of models A3 and B1.

with the maximum concentration close the right vertical boundary. The smaller values of the mean effective stresses can be found around filter areas in both models. The stress behaviour of model A3 (location of the effective stress concentration) is probably connected with the sharp change in boundary conditions applied to the horizontal boundaries, and is close to the real behaviour. One can also mention more homogeneous stress state in the case of the 1:1 sample, i.e. model A3, in comparison with the 1:2 one. As for models A1 and A2, model A2 with the full fixed bottom boundary shows the similar main effective stress distribution as the model of the longer, 1:2 sample B1. In the case of model A1, which represented the situation without any friction between samples and the bottom or top area respectively, the maximal concentration of the mean effective stresses was observed around the filter areas.

The greatest difference between all A models and model B1 was found as for the distribution of the active pore pressure inside the investigated samples. Zero active pore pressure around the filter area and the highest hydraulic gradients were observed inside all A models, i.e. inside the 1:1 sample. Comparison of the active pore pressure distribution inside model B1 and A3 can be found in Figure 4–20.

a) Model B1. b) Model A3.

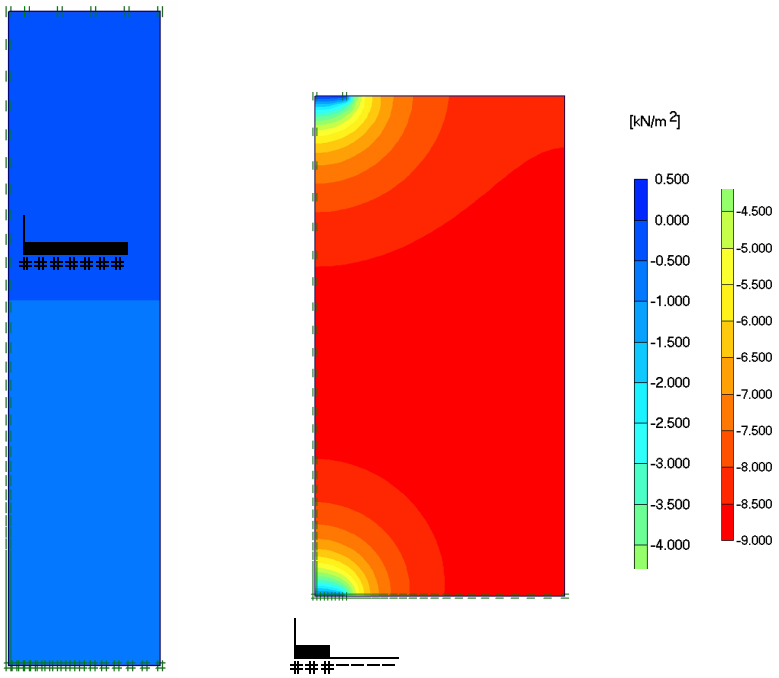

Figure 4–20: Distribution of the active pore pressure in the case of models A3 and B1 at the end of the consolidation phase.

Close attention was paid by the author to the ***shearing*** and the following ***creep phase***. At first a detailed study of the numerical model A3 was performed. Three stages were compared for a better understanding of the behaviour of the modelled sample - at the end of the consolidation, end of the shearing and the end of the applied nine-day creep. Additionally all processes running in the sample during the shearing and creep phases were investigated. After comparison and evaluation of all these stages it was possible to established the following conclusions. In the case of the situation of the mean effective stresses a certain homogenisation of the principal directions was observed with increasing external vertical pressure. Simultaneously relative shear stresses increased and during the nine-day creep phase the sample became fully shear mobilised except for the small areas close to the filters. There was not any observed global shearing plane like in the case of the 1:2 specimen. On the contrary a lot of local shearing planes developed. The distribution of the effective mean stresses had the same pattern during all observed phases (compare Figure 4–19 a) and Figure 4–22 c)), i.e. the stress concentration was recorded in the right end of filter areas and the minimum values were found close to the filters in the case of all discussed phases. A general decrease of the effective mean stresses during the creep phase was observed. As for the active pore pressure development dramatic changes were recorded during calculation. One could see in Figure 4–20 b) that at the end of the consolidation the zero active pore pressure was found around filter areas. During the shearing phase a slowly increasing negative concentration (pressure) of the active pore pressure followed by the positive one (tension) which was almost two time smaller was observed in the right end of the filter area. Generally higher active pore pressure (around 200 kPa) was found around the filter areas in comparison with the rest of the sample at the end of the creep phase. This kind of behaviour was observed only in the case of model A3. The observed concentration was considered to be fully related to the modelled connection between the sample and the bottom pedestal or top cap respectively. The concentration also slowly increased during the creep phases to a certain point where the sudden drop and the following increase was recorded. Similar behaviour was found during the real laboratory test performed by the author and can be found in Figure 4–15 c).

After the evaluation of the numerical model A3, a comparison with the model of the 1:2 sample, i.e. model B1, was done. The stress situation of the B1 model was not as homogeneous as in the case of model A3. The effective stresses inside model B1 tilted to the left in the areas close to the bottom and upper horizontal boundaries. Even after the nine-day creep the B1 sample was not fully shear mobilised in the big areas around modelled filters. As was indicated above, the one global shear plane was observed in the model of the 1:2 specimen after the creep phase. Distribution of the active pore pressure at the end of the creep phase showed a high negative (com-

pression) and positive (tension) concentrations in the area around the global shearing plane, where both extreme values were almost identical.

a) Numerical model A3. b) Numerical model B1.
Development of the deviatoric stress q.

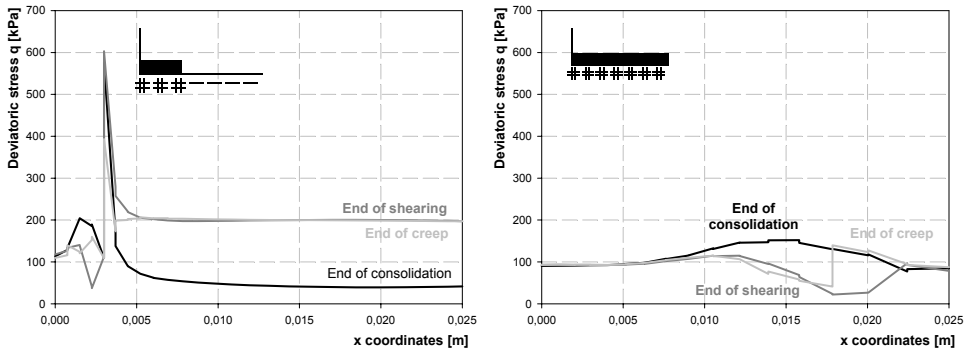

Development of the volumetric stresses p′.

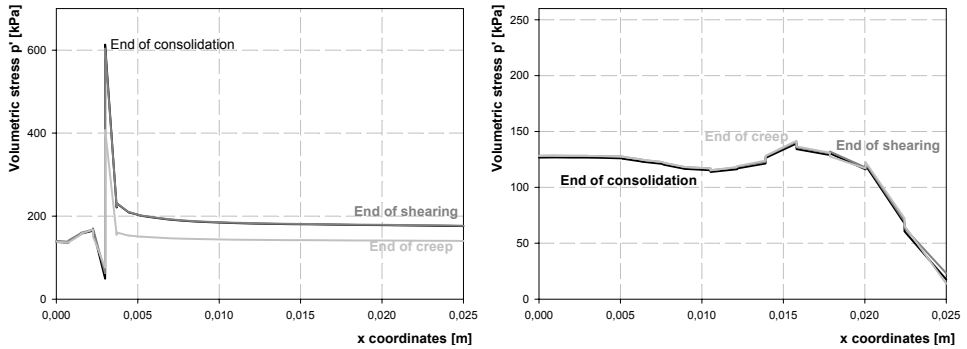

Development of the active pore pressure.

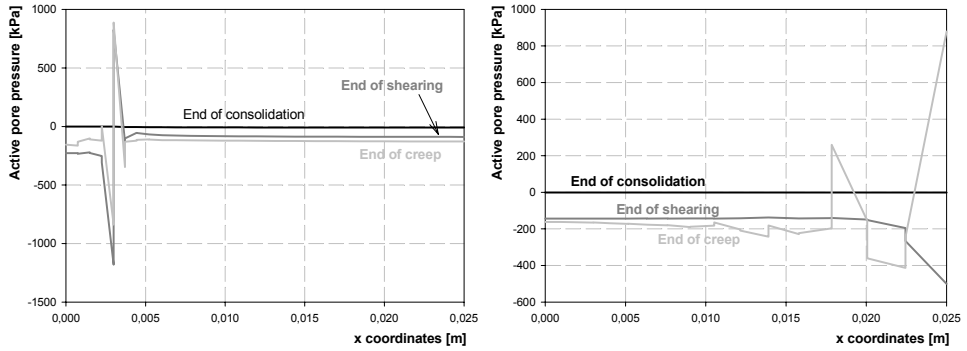

Figure 4–21: Development of p′ and q′ stresses and the active pore pressure along the bottom horizontal boundary in the case of numerical models A3 and B1.

Individual attention was paid to distribution of the effective volumetric stress, deviatoric stress and the active pore pressure along the cross-section that led through to the bottom horizontal boundary. Investigated situations for numerical models A3 and B1 at the end of the consolidation, end of the shearing and end of the creep phases can be found in Figure 4–21 a) and b). As for model A3 one can see the "problematic" behaviour in the right end of the filter area in comparison to the rest of the bottom boundary. All observed quantities exhibit several times higher or lower values in this location. The behaviour of the active pore pressure seems to be very interesting. The high negative value (pressure) followed by the positive one (tension) were recorded in the right end of the modelled filter area at the end of the shearing and creep phases.

In the case of model B1, i.e. 1:2 specimen, the bottom boundary can be divided to the left and right side with different behaviour, where left side seems to be more homogeneous in comparison with the right one. The biggest differences can be found for the development of the volumetric stress p' and active pore pressure. One can observe a significant decrease of the volumetric stress in the right side of the bottom boundary. In the case of the active pore pressure a dramatic increase in the right end of the boundary was recorded.

The general distribution of mean effective stresses and active pore pressures after nine-day creep duration for the all numerical models with the Norwegian Glava clay material, i.e. models A1, A2, A3 and B1, can be found in Figure 4–22 a), b), c), d) and Figure 4–23 a), b), c), d). From these plots one may say that the stress situation is more associated with the connection between the sample and the bottom pedestal or the top cap respectively, than with the height of the sample or, more precisely, the ratio between the height and diameter of the sample. After comparison of model A2 and B1 with the same applied fixities on the top and bottom boundaries one can see almost identical stress and strain behaviour (including the not full shear mobilised sample after nine days duration of creep and the existence of the global shearing plane even in the case of the 1:1 specimen). A certain difference can be found only for the active pore pressure distribution regarding the clear concentration around the global shear plane described above for model B1. Completely different behaviour can be found in the case of model A1 with smooth pedestal and top cap. From the general point of view the mean effective stress situation at the end of the creep phase is fully comparable with the end of the consolidation phase. It means that the main concentration of the mean effective stresses can be found around the modelled filter areas in both cases. As for the active pore pressure the smallest values can be again found around modelled filters. In contradiction to model A2, model A1 became fully shear mobilised during the nine-day creep phase and no global shearing plane was observed.

a) Numerical model A1 of the 1:1 sample.

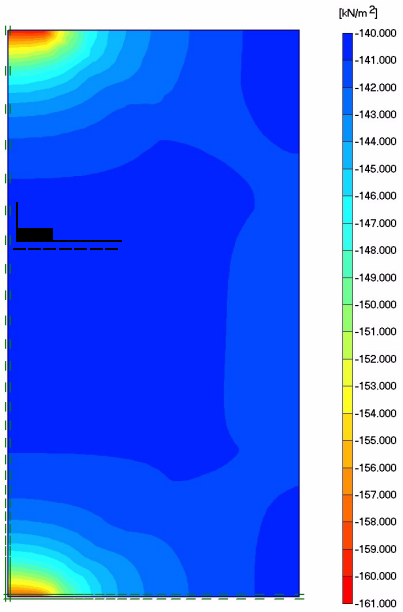

b) Numerical model A2 of the 1:1 sample.

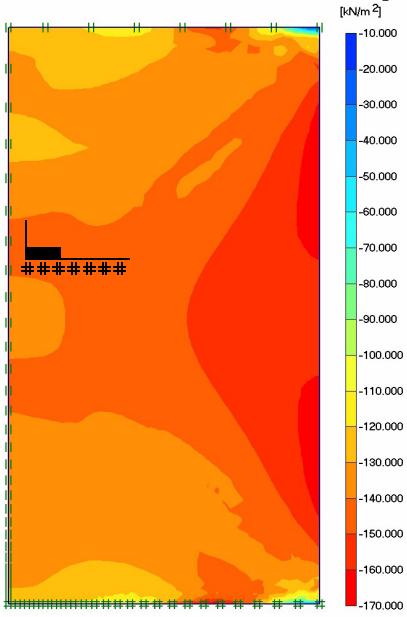

c) Numerical model A3 of the 1:1 sample.

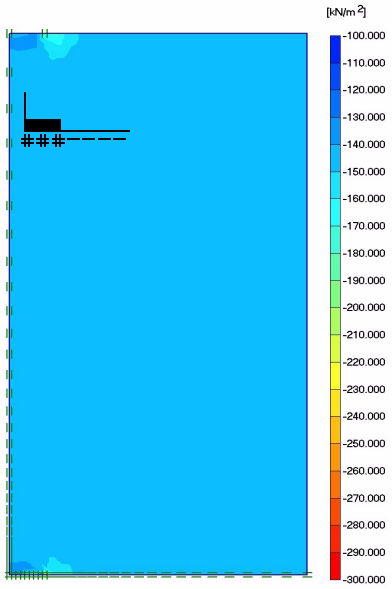

d) Numerical model B1 of the 1:2 sample.

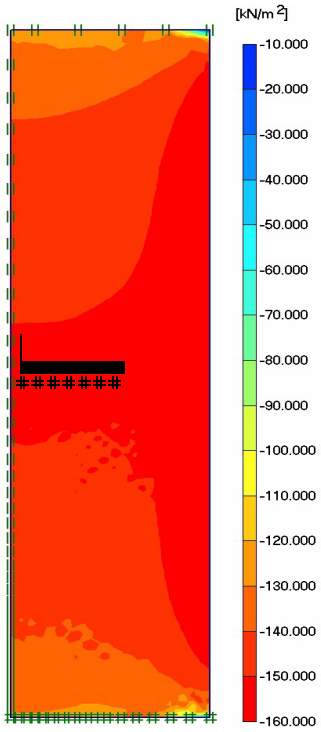

Figure 4–22: Plot of the mean effective stresses after nine-day creep duration for numerical models A1, A2, A3 and B1.

a) Numerical model A1 of the 1:1 sample.

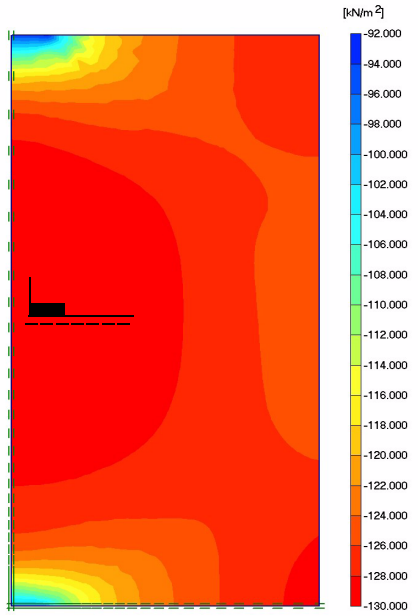

b) Numerical model A2 of the 1:1 sample.

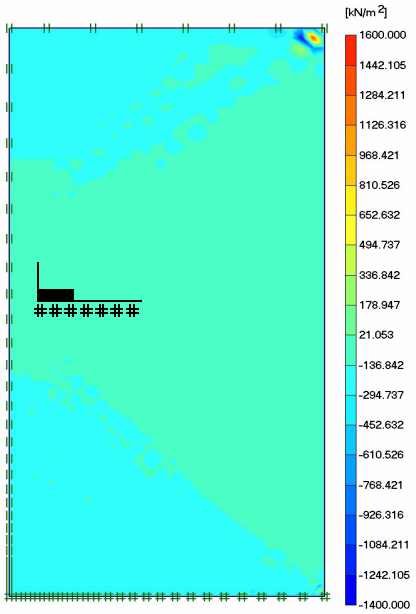

c) Numerical model A3 of the 1:1 sample.

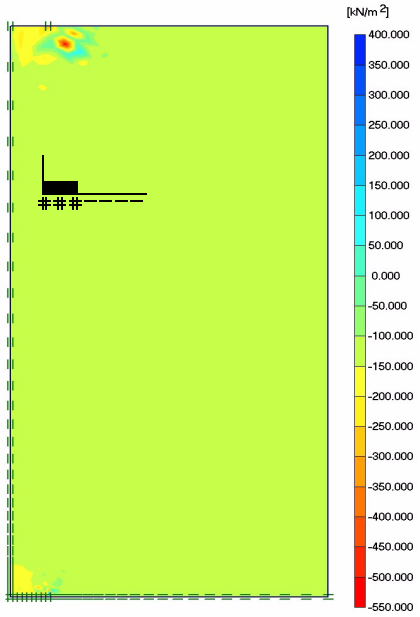

d) Numerical model B1 of the 1:2 sample.

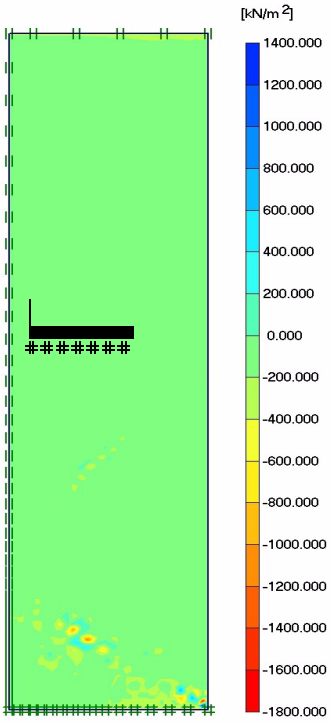

Figure 4–23: Plot of the active pore pressures after nine-day creep duration for numerical models A1, A2, A3 and B1.

The undrained triaxial deviatoric creep tests on 1:1 specimens of the Czech Terlicko clayey shale performed by the author will be introduced in Section 4.2.2. After evaluation of these tests it was possible to say that the observed behaviour of the 1:1 clayey shale specimens could be denote as "standard", i.e. there was no record of any of the problems discussed above. Because of this situation two numerical models A4 and B2 were analysed with the soil parameters based on the Czech Terlicko clayey shale (see Table 4–5) and the final results of these tests were compared with previously described numerical models A3 and B1 with the soil parameters based on the Norwegian Glava clay. As for the boundary conditions, generation of the initial conditions and calculation phases, model A4 was identical with model A3, and model B2 was identical with model B1.

After evaluation of the numerical models performed with the clayey shale it was possible to see stiffer behaviour of this material in comparison with the Glava clay, i.e. lower deformation and higher effective stresses. As for model B2, the general stress and strain distributions were comparable with model B1. One difference was found only in the stage after the nine-day creep duration where the concentration of the main effective stress was found around the left vertical boundary, i.e. in the middle of the sample, in contradiction to model B1 where the observed concentration was placed in the opposite side. In the case of the 1:1 sample, models A4 and A3, the main emphasis was placed on the comparison of the active pore pressure development during the shearing and creep phases. Distributions of the active pore pressures for the Terlicko clayey shale in the stage after consolidation (i.e. at the start of the shearing phase) and after the creep phase can be found in Figure 4–24 a) and b). One can see completely different active pore pressure behaviour at the end of the consolidation in comparison with model A3 (see Figure 4–20 b)). This kind of the pore pressure distribution is, in fact, almost identical with the 1:2 modelled specimens, i.e. with models B1 and B2. Similar concentrations of the active pore pressure described above for model A3 at the end of the shearing and creep phases were found also inside the numerical model of the 1:1 Terlicko clayey shale sample. Observed concentrations were placed behind the right end of the modelled filter area in the different order in comparison with model A3, i.e. as a first was found positive one (tension) followed by the negative (pressure). After nine-day creep phase the recorded active pore pressure concentrations for the Terlicko clayey shale were raised slightly and were several times larger than in the case of the modelled Norwegian Glava clay material. However, the lower values of the active pore pressure corresponded to the rest of the modelled sample were observed around the bottom filter area, what can indicate the "standard" values of the pore pressure measured during the real laboratory triaxial tests.

a) Situation after consolidation phase.

b) Situation after creep phase - bottom part of the sample.

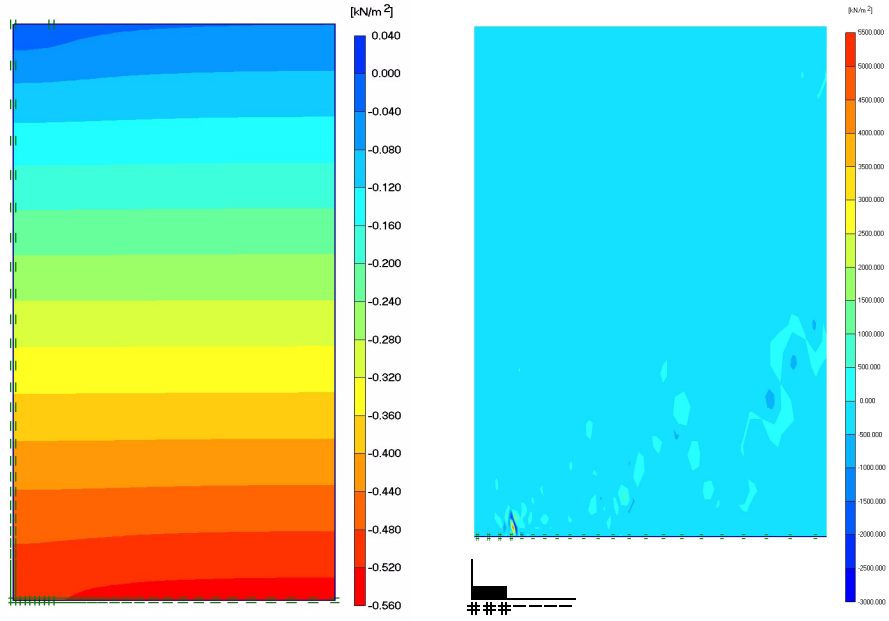

Figure 4–24: Plot of the active pore pressures after consolidation and nine-day creep duration for the numerical model A4 with the Czech Terlicko clayey shale material.

Based on the performed laboratory and numerical models it is possible to say that the main problem of triaxial tests with 1:1 clay samples is the location of the pore pressure transducer, i.e. connection of the pore pressure transducer to the bottom small filter. It was possible to see that the behaviour of the material close to the small filters is completely different than the general response of the sample. This problem is particularly connected with the clay materials because of their low permeability and probably also because of their high effective cohesion. Due to the low permeability and small filters the specific pore pressure distribution with the zero values around the filter areas and relatively high hydraulic gradient inside the sample come at the end of the consolidation in the case of the Glava clay material. One can avoid this by using a longer consolidation time which has to be, according to the performed numerical models, at least four days. However, even after longer consolidation and a more standard "after-consolidation" situation the observed increase of the pore pressure during the applied undrained triaxial shearing was slower in the area close to the filter. Performed numerical models with the clayey shale material did not show this behaviour as significantly which can indicates connection of this behaviour with the low permeability of the clay. As was proved above the other main problem during triaxial test with 1:1 specimen is friction

between the sample and the bottom pedestal or the top cap respectively. With increasing shear mobilisation the shearing between the sample and these two contact plates is also increasing. Due to the sharp friction change in the boundary between the small filter and the rest of the bottom pedestal (or the top cap) there is a concentration of the active pore pressure in the sample around this boundary. This has, of course, an influence on the pore pressure values measured by the pore pressure transducer. This behaviour can also explain the enormous measured values of the pore pressure during the undrained triaxial deviatoric creep. Based on the laboratory and numerical tests it is possible to say that this response is connected with the low permeability of the clay and probably also with the high effective cohesion.

One can see that the presented behaviour of the 1:1 specimen during the undrained (and apparently also during the drained) triaxial deviatoric creep tests, or more generally during triaxial tests, is very complicated. For a better understanding of this problem it will be necessary to perform other laboratory and numerical tests.

4.2.2 Terlicko clayey shale

An investigation of the shear strength parameters together with a study of the undrained deviatoric creep behaviour of the Czech Terlicko clayey shale material was performed by the author as a part of analysis of Terlicko dam described in Chapter 6. As mentioned earlier the Terlicko clayey shale can be basically characterised as a marly, soft or not very solid, dark-grey to black-grey material, which crumbles to small parts in dry conditions and gradually softens in contact with water. Additionally the strong non-homogeneity of the used material was observed. Because of the crumbling, the Terlicko clayey shale was generally quite a problem to handle for sample preparation.

Probably during the sampling process the moisture inside the Terlicko clayey shale samples was partly lost and almost all laboratory investigations had to be performed with not fully saturated material (degree of saturation S was found to be in range from 62 to 99% and the moisture content w varied from 8 to 17%). The best material from this point of view was clayey shale material lifted from 9 - 10 m depth and placed into the core box no. 10 (see Table 6–1). Based on the performed index tests the void ratio and porosity of the tested material was evaluated to be e=0.47 and n=31.7%. The average value of the unit weight was found to be around 20 kN/m^3. Detailed information about Terlicko clayey shale containing determination of the soil composition and results of general index tests can be found in Chapter 6. Investigation of the behaviour of the clayey material under oedometer test conditions with emphasis placed on the volumetric creep behaviour was described in Section 3.3.4.

Fifteen laboratory tests were performed with triaxial apparatus made by Wille Geotechnik Gmbh, where all measurements were carried out on 50x50 mm (1:1) cylindrical specimens trimmed from the 80 mm diameter samples. Two isotropically consolidated drained triaxial tests (ICD) and seven isotropically consolidated undrained triaxial tests (ICU) were done for the investigation of the shear strength parameters, i.e. effective friction angle φ' and effective cohesion c'. For the evaluation of the undrained deviatoric creep behaviour of the Terlicko clayey shale material six isotropically consolidated undrained triaxial deviatoric creep tests (ICU-C) were made. An overview of all performed triaxial tests can be found in Table 4–7.

Test no.	Depth [m]	Core box no.	Type of the test	Consolidation pressure p_c'
1.	7.4	8.	ICU	100 kPa
2.	7.3	8.	ICU	150 kPa
3.	4.9	4.	ICU	50 kPa
4.	4.15	4.	ICU	100 kPa
5.	4.35	4.	ICU	150 kPa
6.	4.2	4.	ICU	150 kPa
7.	4.47	4.	ICD	100 kPa
8.	4.70	4.	ICD	150 kPa
9.	4.80	4.	ICU-C	100 kPa
10.	9.37	10.	ICU-C	100 kPa
11.	9.27	10.	ICU-C	100 kPa
12.	9.03	10.	ICU	100 kPa
13.	9.07	10.	ICU-C	100 kPa
14.	9.80	10.	ICU-C	100 kPa
15.	9.90	10.	ICU-C	100 kPa

Table 4–7:Basic characterisation of triaxial tests with Czech Terlicko clayey shale performed by the author.

The same procedure for the sample preparation was applied for all tests. As a first stage (after saturation of the used filters) the sample was saturated by simply using of the water head in the burette volume change gauge, i.e. by opening the valve connecting the burette with the bottom part of the sample, and allowing drainage in the upper part of the sample. The duration of this stage was approximately half an hour. Then the small values of the cell and back pressures were applied for checking of the eventual membrane leakage and the previous stage was repeated. After basic saturation of the sample the consolidation under the small value of consolidation pressure was performed. Duration of the consolidation was controlled according to the ΔV-$\sqrt{t}$ diagram observed with the computer and usually it was

approximately one hour. Because of the partly saturated character of the specimens used the so-called "automatic saturation" was applied in the line of incremental steps. It means that the cell and back pressures were continuously increased in parallel to a certain value corresponding to the constant increment 10 kPa and then kept constant for a duration of ten minutes. The general duration of this stage was approximately 15 hours. The final degree of saturation was checked based on the incremental increase of the cell pressure under undrained conditions and evaluation of the pore pressure coefficient B from the equation,

$$B = \frac{\Delta u}{\Delta \sigma_3} \tag{4.7}$$

where Δu is the measured excess pore pressure and $\Delta\sigma_3$ is change of the cell pressure. The value of the coefficient B after automatic saturation was found to be in the range from 0.98 to 0.99 for all tests, what corresponds, according to Black and Lee [18], to the degree of saturation $S \approx 100\%$. The fully saturated sample was then isotropically consolidated to the final value of the consolidation pressure, i.e. 50, 100 or 150 kPa (see Table 4–7).

As a first part of the Terlicko clayey shale investigation under triaxial compression, the ICD and ICU tests were performed and shear strength parameters were evaluated. Based on these tests one can define the Terlicko clayey shale like a shale material with dilatant behaviour, small cohesion c′ varying between 2.9 and 5 kPa and effective friction angle φ' which is increasing with depth from 21^o for the specimen from 4-5 m to the 34^o for the specimen from 9-10 m. Increase of the friction angle will probably be caused by the change in the composition of the tested material from clayey to more sandy. ICD tests were additionally used for the evaluation of the dilatancy angle which was found to be 1.2^o for the specimen from 4-5 m depth.

As mentioned above, the six ICU-C triaxial tests were performed for the evaluation of the undrained deviatoric creep behavior of the Terlicko clayey shale. The creep tests were performed in the same way as described in the previous section for Norwegian Glava clay, i.e. after consolidation the shearing was applied and at a certain level of the degree of shear mobilisation the axial force was kept constant and the undrained creep behaviour was observed. Duration of the creep was varied from one to five days. Finally the shearing was applied again and the "post-creep" behaviour was recorded. The overview of the general behaviour of the tested material during the performed ICU-C tests is given in Figure 4–25 a), b) and c). Because of the different material used in the case of the test no. 9, the stress path of this test was plotted with a dash lines together with additional failure envelope corresponding to this material in Figure 4–25 a).

a) Stress paths of effective stresses.

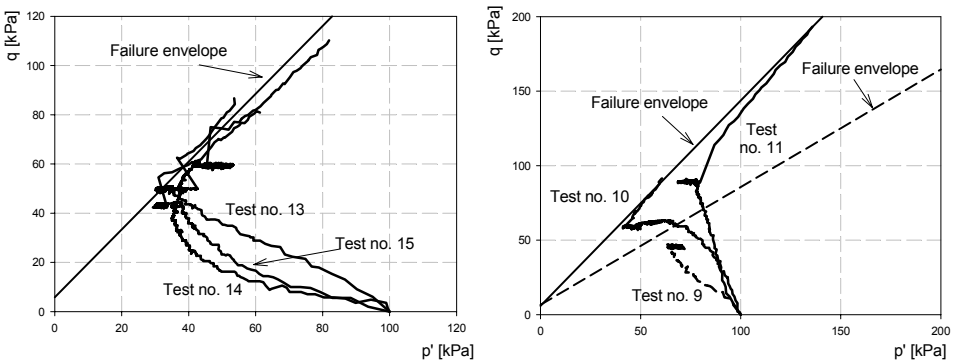

b) Deviatoric stress q vs. axial strain ε_1.

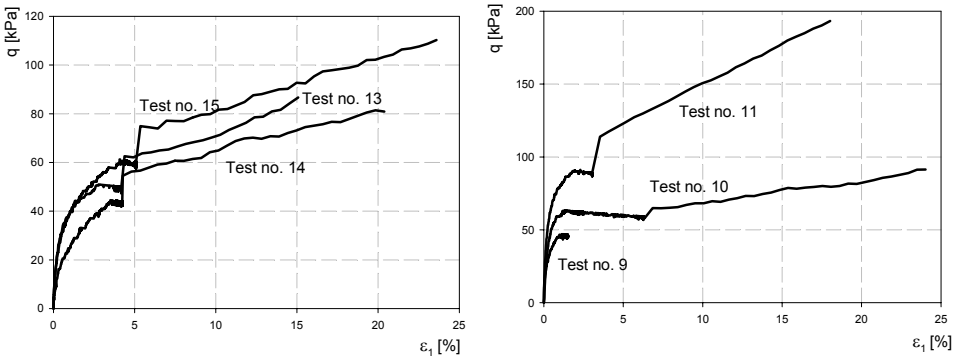

c) Pore pressure u vs. axial strain ε_1.

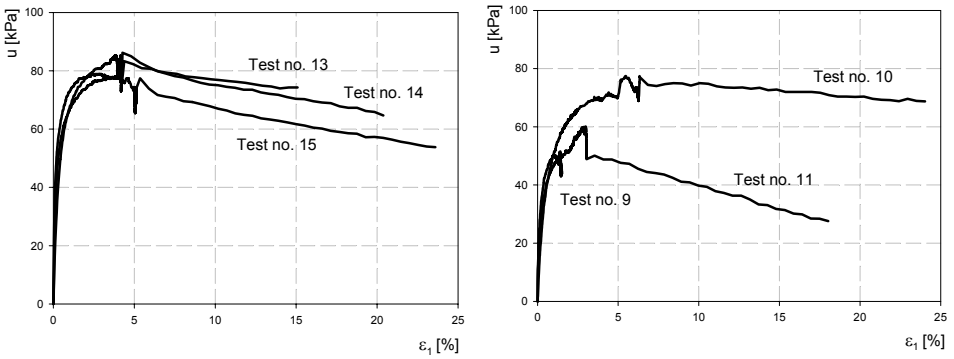

Figure 4–25: General behaviour of the performed undrained deviatoric creep tests with the Czech Terlicko clayey shale material.

Detailed graphical description of the undrained triaxial deviatoric creep behaviour of the Terlicko clayey shale with emphasis on the development of the axial strain ε_1 and pore pressure u with time can be found in Figure 4–26 a) and b). One can see disturbances during the creep tests that are obvious mainly from the presented ε_t-t curves. This behaviour is clearly visible in the case of test no. 11 (seems like a new loading) and was probably connected with the problem to keep a constant axial force.

a) Development of the axial strain ε_1.

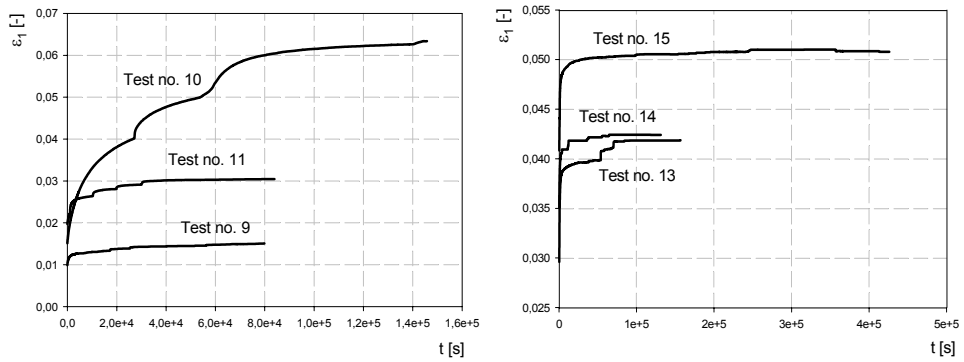

b) Development of the pore pressure u.

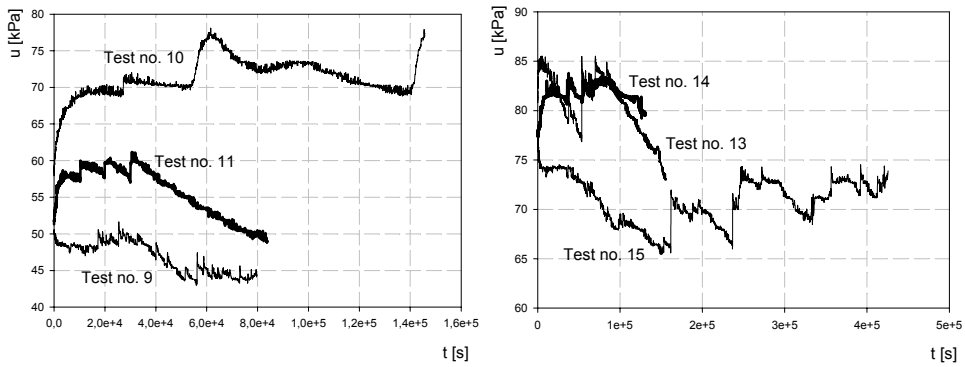

Figure 4–26: Undrained deviatoric creep behaviour of tests performed by the author with the Czech Terlicko clayey shale material.

Based on the Figure 4–26 a) only primary creep phase occurred in the case of all the triaxial deviatoric creep tests on Terlicko clayey shale. Generally it is possible to say that material has no tendency towards secondary creep or creep rupture in undrained conditions at tested levels of the shear mobilisation. As for the excess pore pressure development the continuing decrease with time was recorded almost for all the tests. The creep resistance number r_s evaluated for the vertical (or axial) creep strain was found to be in a range from 1400 to 2500. However, these values

are influenced by the discussed disturbances during the creep tests and, according to the author, will be even larger. The greatest problem with the evaluation of the creep resistance number was found in the case of test no. 10 and value r_s=216 cannot be taken into account.

In comparison with the creep resistance number found from deviatoric creep triaxial tests performed on the Norwegian Glava clay (r_s=168 for the shear mobilisation 0.61) or Norwegian Eberg clay (r_s is varying from 1000 to 200 for shear mobilization 0.25 to 0.6), the Terlicko clayey shale shows high resistance in deviatoric creep behaviour and low risk of the deviatoric creep rupture. Overview of all evaluated parameters based on all performed deviatoric creep tests under triaxial compression with the Terlicko clayey shale material is presented in Table 4–8.

Test no.	Degree of shear mobilisation at the start of the creep, f	Primary creep		Secondary creep ε_{cs} [-]	Duration of the creep [days]
		ε_{cp} [-]	r_s [-]		
9.	0.81	0.0051	1400	-	1
10.	0.69	0.048	216	-	2
11.	0.80	0.01	1500	-	1
13.	0.8	0.012	1900	-	2
14.	0.79	0.0074	2500	-	1.5
15.	0.96	0.01	2300	-	5

Table 4–8:Evaluation of the undrained deviatoric creep tests under triaxial compression with the Terlicko clayey shale performed by the author.

Chapter 5 Investigation of the natural clay's viscosity with compact rheometer

During the deformation of the soil there are frictional forces between molecules and, therefore, this material displays a certain resistance which can be measured as viscosity. According this definition the natural viscosity of the clayey soil seems to be one of the main characteristics influencing the creep, or more generally the rheological behaviour of this material. This idea can be found in many rheological models as indicated in Section 2.1 (Maxwell, Kelvin and Voight, and Bingham models - Eq. (2.5)-Eq. (2.18)) and Section 4.1.1 (Shvedov-Bingham equation - Eq. (4.1)). Viscous behaviour in all these models is controlled by the Newton's viscous element introduced in Section 2.1. The first application of the Newtonian viscous fluid equation (Eq. (2.2)) to clayey soil was done by Hvoroslev in 1937-1939 to describe the creep of clay under shear produced in ring-shaped specimens subjected to torsion on a ring shear apparatus [69]. Haefeli and Sherman applied the same equation to evaluate creep in specimens tested under uniaxial and triaxial compression in 1946. In 1952, N.N. Maslov solved a problem of the rate of deformation of a clayey soil layer on an inclined plane. Based on this observation he found, using the Shvedov-Bingham equation (Eq. (4.1)) and his own condition of plasticity of clayey soils [67,70], that variation of the coefficient of viscosity of soils occurred between 1E3 to 4.4E6 MPa.s [66]. In 1953, Geza and Tan Tjong-Kie studied creep deformation in cylindrical specimens of Potter's clay subjected to torsion for periods up to 118 hours. In the flow stage the coefficient of viscosity according to Bingham was found to be 2.63E6 MPa.s. In 1953, Haefeli conducted tests on clayey soil specimens for a period of two months. The ring shear apparatus with open drainage system and cylindrical specimens under vertical compression in the chamber of triaxial tests apparatus were used for the tests. Evaluation of the stress-flow rate relation was done according to Bingham's rheological equation and the coefficient of viscosity according to Bingham was found to be approximately equal to 5E7 MPa.s in both cases.

As mentioned, the viscosity of the natural clay can be an extremely important parameter for the evaluation of rheological behaviour in general, or creep behaviour in particular. However, the problem with the real physical meaning of the evaluated viscosity by different authors can be found, as for example mentioned in Section 2.1 that so-called "Bingham viscosity" is not a physical viscosity value. Gen-

erally it can be said that the possibilities of the direct measurement of the natural clayey soils viscosity are limited. In these days modern rheometers are opening new doors to the investigation of the viscous behaviour of a natural soil material.

The MCR 300 rheometer was used by the author for the investigation of the Norwegian Glava clay. Oscillatory, rotational and creep tests were performed. All rheometer tests were done in SINTEF, Cement and Concrete laboratory. Description of the MCR 300 rheometer together with description and evaluation of all performed tests will be presented in the following sections. Additionally a basic comparison of the rheometer creep tests with triaxial deviatoric creep tests on the Norwegian Glava clay (described in Section 4.2.1) will be introduced based on the reached values of the dynamic viscosity.

5.1 Characterisation of the test material

Norwegian Glava clay from the 9.0-9.8 m depth was chosen for the viscosity testing. As was presented in Section 3.3.2 the Norwegian Glava clay is a medium stiff clay material from the Trondheim area. Behaviour of this clay was thoroughly investigated in several contexts in the NTNU geotechnical laboratory [92]. Results from the index, consolidation and strength test are shown in Table 5–1 where cohesion and friction angle are effective values. More information about investigation of the oedometric and triaxial creep behaviour of the Glava clay are presented in Section 3.3.2 and Section 4.2.1.

General index tests		Consolidation and strength tests	
Moisture content, w [%]	25	Coef. of cons., C_v [m^2/year]	25
Unit weight of solid particles, γ_S [kN/m^3]	26.95	Permeability, k [m/day]	4.00E-05
Unit weight, γ [kN/m^3]	19.3	Modulus number, m [-]	20
Dry unit weight, γ_d [kN/m^3]	19.8	Pre-consolidation, σ_c [kN/m^3]	400
Liquid limit, w_L [%]	31.80		
Plastic limit, w_p [%]	22.60	Uniaxial strength, s_u [kPa]	37.5
Void ratio, e [-]	0.86		
Porosity, n [%]	46.10	Cohesion, c′ [kPa]	18
Degree of saturation, S [%]	99	Friction angle, φ′ [°]	29

Table 5–1:Description of the Glava clay based on the index, consolidation and strength tests results.

5.2 Modular compact rheometer tests

All apparatuses used for the measurement of viscosity can be divided into the two groups - viscosimeters and rheometers. Viscosimeters are defined as simple devices measuring viscosity function via speed, or shear rate controlled rotational tests. Rheometers are more “sophisticated” apparatuses which enable further rheological tests, such as torque controlled rotational test, creep test, relaxation test or oscillatory test. The first rotational viscosimeter was quite a simple apparatus with a cylinder measuring system, constructed by Maurice Couette in 1888. Due to the more complex approach the first rheometer was constructed more than 70 years later in 1951 by Karl Weissenberg. One can see that rheometers are a relatively young apparatuses. After the first rheometer, the technology of the rheometers has advanced rapidly and since 1980 digital instruments using microprocessors, computers and special software for the measuring and analysing of tests data are available.

The **M**odular **C**ompact **R**heometer MCR 300, see Figure 5–1, was used by the author for the measuring of the natural clay viscosity. The rheometer MCR 300 is a unique piece of equipment which can be used in a wide range of applications - from fluids and colloidal suspensions to adhesives, food, coatings, melts, thermosets, and composites. After the investigations no application to the natural clay materials was apparent. More information about rheometer MCR 300 is presented in [45]. Description of the special software US200 used for the measuring and analysing together with the rheometer can be found in [88].

Figure 5–1: Illustration of the Modular compact rheometer MCR 300 [45].

Three main groups of tests were performed for the investigation of the viscous behaviour of the Glava clay:

- Amplitude sweep test with controlled shear strain (Oscillatory test)
- Controlled shear stress test (Rotation test)
- Creep test

For all tests 3 mm height sample with cross-section area 22.9 cm^2 was used. Tests were done in temperature 20^oC. Concentric cylinder cone/plate with angle α_c=1 degree was used for the testing. A sketch of this cylinder is presented in Figure 5–2.

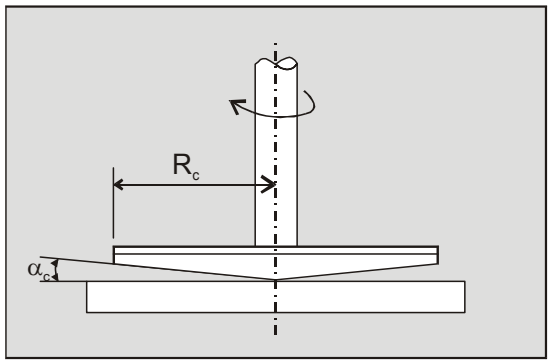

Figure 5–2: The cone/plate measuring system [77].

5.2.1 Amplitude sweep test with controlled shear strain

An amplitude sweep test is a special kind of oscillatory test. Because of this, the first basic principles of a general oscillatory test will be explained using a two-plate-model with immovable bottom plate, illustrated in Figure 5–3 a). One can see that upper plate is oscillating where the oscillation is produced by a turning wheel with eccentrically connected rod. Fixed bottom and oscillating upper plates cause shearing of the sample placed between these plates. The following conditions have to be accomplished for the successful measurement:

- Connection between the sample and plates has to be fixed, i.e. slide or slip must not occur.
- Deformation of the sample has to be homogeneous over the whole shear gap (in this case the distance h between the plates).

Shear force $\pm F$ applied on the top of the sample together with deflection $\pm s$ and deflection angle $\pm\varphi_s$ are presented in Figure 5–3 b). The shear stress which occurs due to the shear force $\pm F$ is then,

$$\pm\tau = \frac{\pm F}{A} \tag{5.1}$$

where A is a top area of the sample. Based on Figure 5–3 b) the shear deformation is,

$$\pm\gamma = \frac{\pm s}{h} = \pm\tan\varphi_s \tag{5.2}$$

a) Two-plate-model for oscillatory test. b) Shear force and deformations.

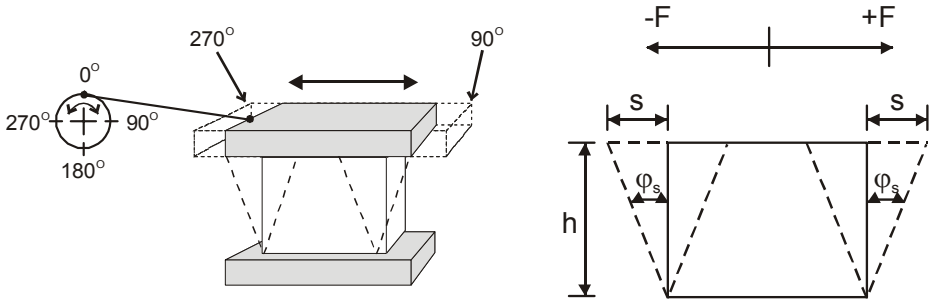

Figure 5–3: Visualisation of the oscillatory test through the two-plate-model together with illustration of shear force and deformations [77].

Based on Hook's law the relation between shear stress and shear strain can be written as,

$$\tau(t) = G^* \cdot \gamma(t) \tag{5.3}$$

where G* is the complex shear modulus (also complex modulus measured in shear) representing resistance to deformation. If one assumes viscoelastic behaviour of the tested material, then G* has to contain a viscous and elastic portion and can be divided as,

$$G^* = \sqrt{(G')^2 + (G'')^2} \tag{5.4}$$

G′ is called storage modulus and represents the elastic behaviour of the tested material. A loss modulus G″ represents irreversible deformation behaviour, i.e. viscous behaviour.

After application of Newton's law described in Section 2.1 (see Eq. (2.2)) one can evaluated the so-called complex viscosity η* in the form

$$\eta^* = \frac{\tau(t)}{\dot{\gamma}(t)} \tag{5.5}$$

Similarly like G* also η* can be divided into the so-called real part of the complex viscosity η′ that represents the viscous behaviour and the imaginary part of the complex viscosity η″ that represents the elastic behaviour as,

$$\eta^* = \sqrt{(\eta')^2 + (\eta'')^2} \tag{5.6}$$

As mentioned above in this section, amplitude sweep test with controlled shear strain was used by the author for the evaluation of the Norwegian Glava clay. The amplitude sweep test is an oscillatory test with variable amplitude and constant frequency values of shear strain or shear stress respectively. In the case of the controlled shear strain the amplitude of the shear strain is controlled and increases with the logarithm of time as shown in Figure 5–4. The shear strain in time t can be computed based on the following equation,

$$\gamma(t) = \gamma_A \cdot \sin(\omega \cdot t) \tag{5.7}$$

where ω is the angular frequency in [1/s] (in this case it is constant), and γ_A is the variable strain amplitude.

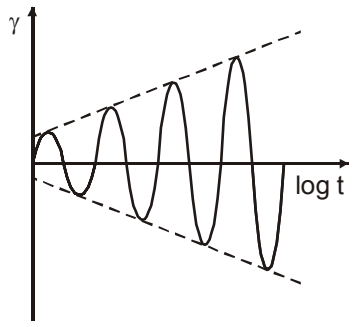

Figure 5–4: Illustration of the amplitude sweep test with controlled shear strain - variable strain amplitude [77].

The following values of the angular frequency and strain amplitude were chosen for the test with the Norwegian Glava clay - ω = 10 1/s and γ_A was increased from 0.1 to 10%. As a first value of the complex viscosity η* was evaluated from the test. After the first drop from the maximum value 55 kPa.s the complex viscosity levelled off around the value 2 kPa.s. Based on the theoretical evaluation of the amplitude sweep test, development of the logarithm of storage and loss modulus (G′, G″) with logarithm of time was observed. Theoretical and practical behaviour can be compared in Figure 5–5 a) and b), where γ_L is limit of the linear viscosity range. In the case of the test on the Norwegian Glava clay γ_L was found around 0.12%. The

character of the presented curves corresponding to the so-called “paste type” materials, i.e. the structure shows a certain rigidity and elastic behaviour that dominated over the viscous one.

a) Theoretical curve [77]. b) Evaluation of the Norwegian Glava clay.

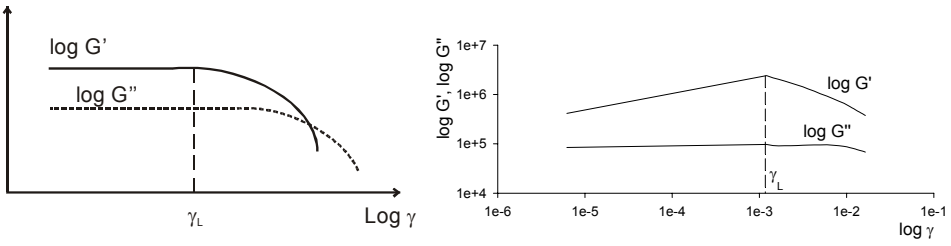

Figure 5–5: Amplitude sweep test with controlled shear strain - development of logarithm of the storage and loss modulus with logarithm of strain.

More information about oscillatory tests in general and amplitude sweep tests in particular are presented in [77].

5.2.2 Rotational controlled shear stress test

In comparison with oscillatory tests described in the previous section, the rotational tests are relatively simple tests where the top cone is rotating and upper plate is immovable. The performance of rotational test produces flow ($\dot{\gamma}(\tau)$) and viscosity ($\eta(\tau)$) curves. Viscosity evaluated based on rotational test is called shear or dynamic viscosity η, and can be computed according to the following equation,

$$\eta = \frac{\tau}{\dot{\gamma}} \tag{5.8}$$

Rotational tests can be divided into controlled shear rate tests (CRS) and controlled shear stress tests (CSS), where in the case of the CRS test the speed n or the shear rate $\dot{\gamma}$ is controlled. In CSS test the shear stress τ or the torque M is set and controlled. The CRS test is usually selected when specific flow velocities of technical processes have to be simulated, e.g. coating, flow in pipes or particle sedimentation [77]. The CSS test is used in the case of simulation of processes such as flowing or creeping which are always a reaction to an acting force, e.g. rivers, avalanches, glaciers, landslides, waves in the ocean or blood circulation [77]. Based on these considerations the CSS test was chosen by the author for testing of the Norwegian Glava clay material. Finally three CSS tests were performed with linear and logarithmic increase of the shear stress τ with time t. An overview of these tests is presented in Table 5–2.

Test no.	Shear stress τ [Pa]	Type of the shear stress increase
1.	100 - 1000	Linear
2.	500 - 5000	Logarithmic
3.	500 - 30000	Logarithmic

Table 5–2:Characterisation of the CSS tests done with the Norwegian Glava clay material.

Flow curves with logarithm of the shear rate $\dot{\gamma}$ on the x axis and logarithm of the shear stress τ on the y axis (so-called double logarithmic flow curve) were established for all tests and can be found in Figure 5–6 a), b) and c). Based on these curves one can evaluate the yield point or yield stress τ_L as the limit of the elastic deformation range. Theoretical evaluation of τ_L is presented in Figure 5–6 b). One

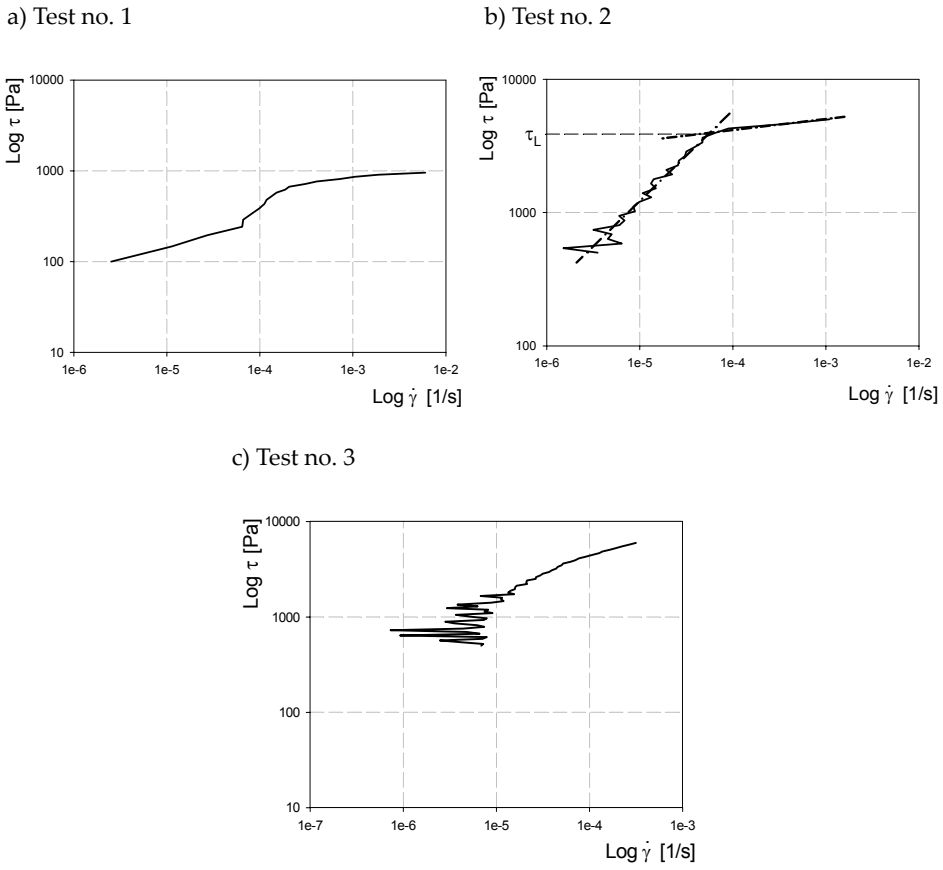

Figure 5–6: Controlled shear stress tests on the Norwegian Glava clay - flow curves in logarithmic scale.

can find value of the τ_L equal to the 0.6 kPa in the case of the test no. 1, i.e. linear increase of the shear stress, and 4 kPa in tests nos. 2 and 3, i.e. logarithmic increase of the shear stress.

Viscosity curves of all CSS tests on the Norwegian Glava clay are presented in Figure 5–7 a), b) and c). Curves are plotted with the shear rate $\dot{\gamma}$ on the x axis and dynamic viscosity η on the y axis. In the case of the test no. 1 the starting value of dynamic viscosity was recorded around 4E+7 Pa.s. After an initial drop the η levelled off in the range 1E+5 Pa.s. In comparison with the test no. 1, tests nos. 3 and 4 showed a higher value in the dynamic viscosity. After the initial drop the value of η stabilised around 1E+7 Pa.s in both cases. The shape of viscosity curves presented in Figure 5–7, i.e. decreasing curves slope (η decreases with increasing shear stress), corresponds to the so-called "shear-thinning" flow behaviour typical for polymer solutions, paints, glues etc. More information about this behaviour with practical examples is presented in [77].

a) Test no. 1

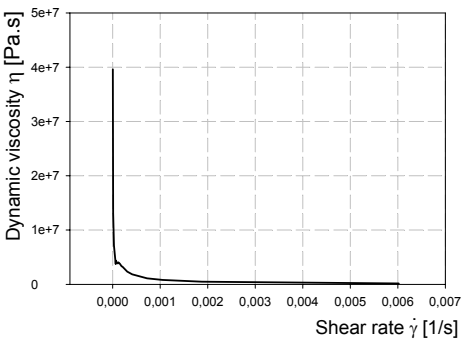

b) Test no. 2

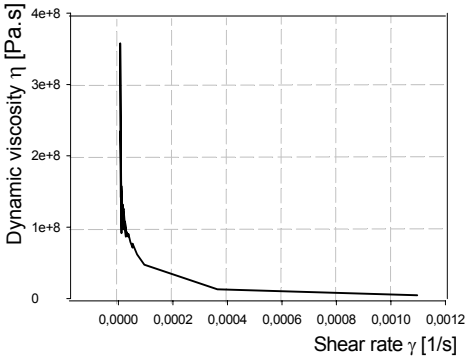

c) Test no. 3

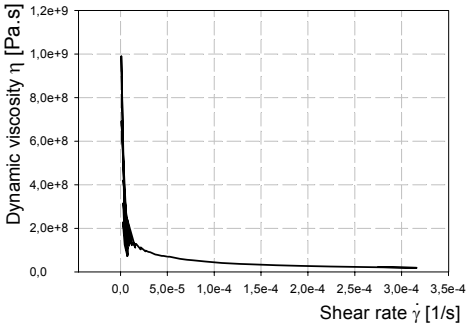

Figure 5–7: Controlled shear stress tests on the Norwegian Glava clay - viscosity curves.

5.2.3 Creep test

Finally several creep tests on Norwegian Glava clay were performed with the MCR 300 rheometer. As these tests can be denoted deviatoric creep tests, the shear stress τ was kept constant and the shear deformation γ was recorded. Deviatoric creep behaviour was investigated under the so-called "step-wise" incremental shear stresses where the torque M or the shear stress τ was incrementally increased and kept constant in time duration equal to one hour. Five tests were performed with shear stress equal to 1, 1.5, 2, 3 and 5 kPa. A basic overview of these tests is presented in Figure 5–8 a) and b).

a) Preset of the shear stress τ.

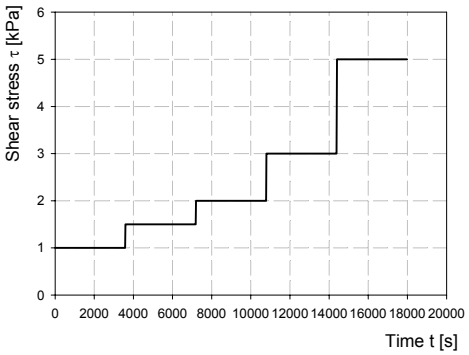

b) Overview of the creep curves.

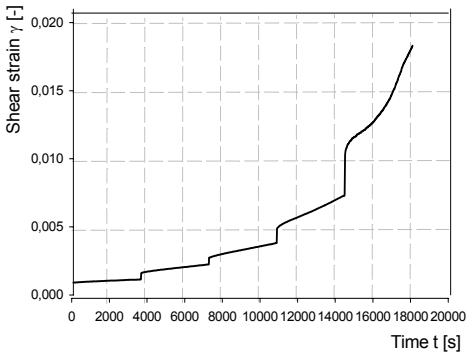

Figure 5–8: Creep tests performed by the author with the MCR 300 rheometer on the Norwegian Glava clay.

All deviatoric creep tests with the MCR 300 rheometer were evaluated according to the Janbu's resistance concept described in Section 2.2.3. Time resistance R_γ and creep resistance number $r_{s\gamma}$ were computed for all tests based on the shear stress γ using the following equations,

$$R_\gamma = \frac{dt}{d\gamma} = \frac{1}{\dot{\gamma}} \tag{5.9}$$

$$r_{s\gamma} = \frac{dR}{dt} \tag{5.10}$$

When combining these equations with Eq. (5.8) the following relationship between the creep resistance number $r_{s\gamma}$ and the dynamic viscosity η can be found,

$$\eta = \frac{\tau}{\dot{\gamma}} = \tau \cdot R_\gamma \Rightarrow R_\gamma = \frac{\eta}{\tau} \tag{5.11}$$

$$r_{s\gamma} = \frac{d\left(\frac{\eta(t)}{\tau(t)}\right)}{dt} \tag{5.12}$$

In the case of the deviatoric creep test (where the shear stress τ is a constant),

$$r_{s\gamma} = \frac{1}{\tau} \cdot \dot{\eta} \tag{5.13}$$

Eq. (5.12) and Eq. (5.13) demonstrates the physical meaning of the creep resistance number.

A Summary of the results of all creep tests performed with the MCR300 rheometer, together with presentation of the evaluated parameters according to resistance concept can be found in Table 5–3.

Test no.	Applied constant shear stress τ [kPa]	Primary creep		Secondary creep
		γ_{cp} [-]	$r_{s\gamma}$ [-]	γ_{cs} [-]
1.	1	0.00024	2430	-
2.	1.5	0.00064	780	-
3.	2	0.00079	300	0.0003
4.	3	0.001	75	0.0014
5.	5	0.0014	14	0.0065

Table 5–3:Evaluation of the deviatoric creep tests performed by the author with the MCR 300 rheometer on the Norwegian Glava clay.

One can see decrease of the creep resistance number $r_{s\gamma}$ (evaluated for the shear strain γ) with increasing value of the shear stress. In the case of the applied constant shear stress τ equal to 5 kPa the value of $r_{s\gamma}$ was even found to be only 14 (compare with Section 4.2.1). Average dynamic viscosity evaluated for all creep steps and presented in Table 5–4 displayed similar behaviour, i.e. decreasing tendency with increasing shear stress.

Constant shear stress τ [kPa]	1	1.5	2	3	5
Average dynamic viscosity η [Pa.s]	1.62E+10	6.14E+09	3.49E+09	1.58E+09	4.96E+08

Table 5–4:Average values of the dynamic viscosity based on the deviatoric creep tests performed by the author with the MCR300 rheometer.

Because of problems, which will be describe in the end of this section, comparison of the results based on the creep tests with MCR 300 rheometer with the Triaxial deviatoric creep tests reported in Section 4.2.1 is almost impossible. Due to the unknown degree of the shear mobilisation at the start of the deviatoric creep in the case of the MCR 300 rheometer, it is hard to compare values of the creep resistance numbers. However, reached values of the dynamic viscosity can be a certain guideline. After evaluation of the drained triaxial deviatoric creep tests nos. 6 a), b) and c) (see Section 4.2.1) the value of the dynamic viscosity η was found in the range from 1E+11 to 1E+12 Pa.s. In the case of the undrained triaxial deviatoric creep test no. 2 the value of the dynamic viscosity was found to be around 1E+9 Pa.s at the start of the creep and around 1E+11 Pa.s at the end. After comparison with Table 5–4, these results can indicate the undrained character of the creep tests with the MCR 300 rheometer.

Based on experience the introduced deviatoric creep behaviour of the clayey material seems to be perfectly reasonable. However, several problems with the performance and evaluation of the creep test with the MCR300 rheometer on the natural clayey material were found. Basically it is possible to say that all these problems are connected with measuring conditions, precisely uncontrolled drainage conditions and, consequently, uncontrolled volume changes of the clayey sample. The observed normal force applied on the sample (10 kPa) was continuously decreasing during all creep steps and in the case of the last creep step was find to be negative (-1 kPa). Due to these problems it was impossible to identify the exact stress situation applied to the clayey sample. Additionally, changes in the normal stress during the creep had a significant influence on the final results. In spite of this situation the tests show a basic overview of the creep test with MCR300 rheometer and approximate values of the dynamic viscosity of the undisturbed Norwegian Glava clay in the case of deviatoric creep conditions.

Chapter 6 Analysis of the Czech Terlicko dam

In-situ creep behaviour of geotechnical structures starting to be more and more significant in theoretical and practical geotechnical engineering. Several cases of prolonged deformations of hydrotechnical, transport, industrial, civil and other structures due to the creep of clayey soils can be found for example in [33, 50, 51, 69]. Because of the importance of the in-situ creep behaviour, a practical application of the knowledge and experience obtained during this PhD work (and described in previous chapters) will be presented.

A Terlicko Dam located in the Czech Republic has been investigated with the emphasis to the creep behaviour in cooperation with the owner of the Terlicko dam, Povodi Odry a.s., and AQUATIS a.s., leader of the project "Modernisation of the Terlicko dam instrumentation". The main problem of the Terlicko dam in-situ behaviour and, consequently, reason of the performed investigation has been a continuous uplift of the right-hand slope hillside together with the dam observed during last twelve years. From 1982 to 1995, the value of the uplift varied from 0.54 to 0.26 mm/year with decreasing trend. From 1995, the uplift increased to 0.82 mm/year. By virtue of this fact, extra measuring with three extensometers and one inclinometer together with piezometric measurement (where all instruments have been installed in one borehole) have been performed from the middle of the 1990's. Observed uplift has been connected with the creep deformation of the right-hand slope which was recorded before construction of the Terlicko dam or with the presence of the swelling minerals influenced by the ground-water, where the first possibility was preferred [7]. Based on the preferred anticipation of the creep movement of the right-hand slope, laboratory investigation of the clayey shale material from the Terlicko dam substratum has been performed at NTNU geotechnical laboratory with the emphasis placed on the creep behaviour. In addition to these tests an X-ray diffraction test and Differential Thermal Analysis test have been done for the determination of the minerals of the Terlicko clayey shale in geological laboratory, Department of Geology and Mineral Resource Engineering. Obtained laboratory results have been used as an input parameters for the 2D numerical model of the Terlicko dam behaviour with the finite element geotechnical program PLAXIS 8.1. Finally numerical model of the right-hand slope has been performed and results have been compared with the observed in-situ behaviour.

6.1 Basic characterisation of the Terlicko dam

The Terlicko dam is located in the River Stonavka by Terlicko in the northeast part of the Czech Republic. The dam was built in the time period from 1955 to 1964, and the purpose of the dam is for one thing industrial and for another protection against flooding. Additionally the recreation use of the dam is significant.

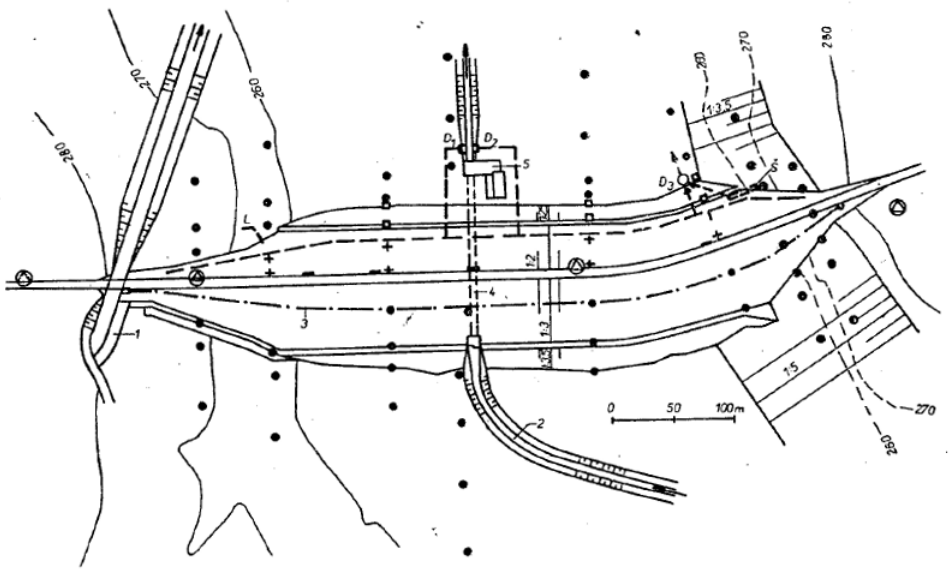

Site plan: ● — Levelling points, ◎ — Aiming line point, + — Telescopic crossarms, □ — Observation pipes, D1, D2, D3 — Drains, L — Spring, Š — Investigation gallery, 1 — Spillweir and chute, 2 — Approach channel, 3 — Grouting gallery axis, 4 — Outlet conduit, 5 — Pumping station.

Figure 6–1: Site plan of the Terlicko dam with illustrated measuring points before modernisation [12].

The dam is an earth-fill type with 25 m height and 617 m length at the crown. The impervious core from the loess loam is bonded into the rock substratum by means of a reinforced concrete grouting gallery that is 180/200 cm. There is a sand filter on both sides of the core. Stabilization parts consist of proluvial gravel, gravel sand and, partly, burnt-out pit heap material from the old heaps. The rock substratum was made impervious by the one line injection, partly reaching as far as 33 m depth. Chemical injection with sodium silicate was used in the middle of the valley whereas the cement mixture was chosen for the right-hand bank. Left-hand bank was found to be sufficiently impermeable. Site plan of the Terlicko dam is presented in Figure 6–1.

The rock substratum in the surrounding of the dam is formed of Lower Cretaceous Hradiste-Tesin layers consisting of the calcareous shales, sandstones and clay-stones, where the shale forms the main component below the dam. The calcareous shales and clay stones are, for the most part, marly, soft or not very solid, dark-grey to black-grey. They crumble to small parts in dry conditions and gradually soften in the contact with water. The clay stones are more solid than the shales. Deposition conditions of the rock substratum layers are rather variegated. Generally the layers run in the west-east direction, i.e. parallel to the valley axis, inclined between 10^o and 35^o towards the south. The rock substratum is disturbed, on the one hand tectonically and on the other hand through weathering. Larger tectonic faults have not been found. Some of the cracks are healed with secondary calcite, while in the surface layers the calcite fill is leached. Besides Lower Cretaceous layers, eruptive rocks, i.e. teschenites and tuffites, are developed. These eruptive rocks form more or less isolated elements, which are jointed and weathered. The most upper, quaternary layers of the soil are formed of proluvial gravel sand, loess loams, eluvial loams and alluvial deposits of the River Stonavka, where lower stage is for the most part gravely, while the upper one is loamy.

The rock substratum in the slopes is more disturbed in depth in comparison with the valley. Material disturbance is observed to great depths than 30 m in the right-hand downstream slope. This is caused through under-washing of the toe of the slope by River Stonavka and the creep of the entire massif into the valley. The slope movement was partly renewed during the building works.

The ground-water level in the valley is 1.5 to 2 m below the ground. Ground-water seeps through the weathered rock substratum to hidden springs or joint springs in the valley's slopes.

The mechanical properties of the shales were established by load tests at quiescent pressure, shear tests and seismic tests, performed during the building period of the dam. Additionally investigation by cone penetration tests was done. The shear tests performed in the exploratory gallery in the right-hand slope showed value of the effective cohesion c=35 kPa and friction angle $\varphi=18^o$. The modulus of elasticity was found to be E=95 MPa for the weathered shales and 265-585 MPa for the solid shales. As for the eruptive rocks, the teschenite had a modulus of elasticity equal to 4000 MPa.

More information about Terlicko dam is presented in [7, 12].

6.2 Laboratory investigation of the Terlicko shale

6.2.1 Description of the specimens

Three specimens of the undisturbed soil were brought from the Czech Republic. Because of the difficult material conditions the rotary drilling sampling method with three walls tube sampler was used. After exploration, the soil samples were carried in closed plastic tubes placed in wooden boxes. Location of the sampling boreholes has been situated in the middle of the dam in the grouting gallery illustrated in Figure 6–1. More information about investigated specimens can be found in Table 6–1. Drilling core depth presented in the table was measured from floor of the grouting gallery and approximately corresponds with the original one, i.e. before construction of the dam.

Sample no.	Borehole no.	Core box no.	Drilling core depth	Diameter
1	HT - 51 - 01	8	7.0 - 8.0 m	8 cm
2	HT - 51 - 01	4	4.0 - 5.0 m	8 cm
3	HT - 53 - 01	10	9.0 - 10.0 m	8 cm

Table 6–1:Characterisation of the clayey shale specimens.

6.2.2 Laboratory test programme

Knowledge of the foundation soil parameters is the basic aspect for comprehension of the in situ behaviour for all geotechnical constructions. Detailed laboratory investigation of the Terlicko clayey shale material from the dam substratum was performed in Geotechnical and Geological laboratories. The laboratory test programme included the following parts:

- Determination of the soil composition (mineralogy tests, soil-particle size analysis, determination of content of the organic material)
- General index tests (moisture content, unit weight, unit weight of solid particles etc.)
- Consolidation and strength tests together with investigation of the creep behaviour (oedometer test, triaxial test)

6.2.3 Determination of the soil composition

Several laboratory tests were performed for determination of the soil composition. Performed tests can divided into three main groups:

- Identification of the soil minerals
- Soil-particle size analysis
- Determination of content of the organic material

Identification of the soil minerals was done in the Department of Geology and Mineral Resources Engineering by Dr.Geert-Jan L.M. de Haas and Dr.Toril Sørløkk. Two methods were used - X-ray diffraction analysis and Differential thermal analysis (DTA).

X-ray diffraction is a non-destructive method which measures the diffraction of the X-ray electromagnetic waves on the atomic planes of the testing material. Since no two minerals have the same spacing of inter-atomic planes in three dimensions, the angles at which diffraction occurs (and the atomic spacing calculated there from) are used for identification. More information about this measuring method is given in [40]. In the case of the Terlicko clayey shale material two X-ray diffraction tests were made in diffractometer PW1710 with copper anode. Based on the analysis of the X-ray diffraction pattern, the following soil minerals presented in the Table 6–2 were found.

Soil mineral	Chemical composition	Volume [%]
Quartz	SiO_2	45
Pyrite	FeS_2	8
Calcite	$CaCO_3$	24
Albite, calcian	$(Na, Ca)\ Al\ (Si, Al)_3O_8$	13
Clinochlore - 1MIIb	$(Mg, Fe)_6\ (Si, Al)_4\ O_{10}\ (OH)_8$	3
Muscovite - 2M1	$KAl_2\ (Si_3Al)\ O_{10}\ (OH, F)_2$	1
Ankerite	$Ca\ (Fe, Mg)\ (CO_3)_2$	6

Table 6–2:X-ray diffraction analysis results.

The presence of the swelling materials was tested by adding glycol to the soil sample and performing the X-ray diffraction test. From a comparison of the clay molecular distance with and without glycol, no swelling minerals were found in the clayey specimen.

Diffraction thermal analysis (DTA) involves heating a test sample at a constant rate (usually about 10°C/min.) to a pre-determined temperature and continuously measuring any chemical emissions of heat (exothermic reaction) or absorptions of heat (endothermic reaction) from the sample in comparison with a inert material such as alumina (in this case Al_3O_3 powder) [40]. By DTA analysis two minerals were identified - Quartz and Pyrrhotite. Because of the significant amount of the Pyrrhotite (more then 2%) the sample had to be mixed with albite to prevent secondary reaction. Three tests with different ratios of soil and albite were performed - 1:5, 1:10 and 1:15. After comparison of these tests, the last ratio, i.e. 1:15, was found to be the most appropriate and was used for the evaluation of minerals. Based on the DTA

thermogram the following amount of the observed minerals can be assumed - *Quartz to be about 30%* and *Pyrrhotite to be about 11%*.

The soil-particle size distribution was measured by sieving and the hydrometer method. As a first particle size analysis by sieving was done in a standard apparatus. Twelve sieves were used for the test - set from 157 mm (6'') to 74 mm (''200). After sieving, the fraction passing 74 mm was mixed with dispersant and used for the hydrometer analysis on the ASTM hydrometer.

Two ways of the sieve analysis were used - "wet" and "dry" sieving, i.e. with the disturbed dry sample and with the sample mixed with water. Significant difference was found between results from these two methods. Based on performed tests and visual observation of the material placed into the plastic tubes the tested material from the Terlicko dam substratum can be describe as a clayey sand with increasing sand amount with the depth. Because of the shale character of this material the significant influence of water and any mechanical disturbance to increasing content of small particles was observed. Results of particle size distribution tests for the core box no. 8 are presented on the semi logarithmic distribution curves in Figure 6–2 a) and b).

6.2.4 General index tests

The general index tests included investigation of basic geotechnical parameters of the soil (such as moisture content, unit weight and unit weight of solid particles) and relative geotechnical parameters (such as void ratio, porosity and degree of saturation). Average values of these parameters are presented in Table 6–3. Based on this table one can observe low saturation in the case of the sample placed in the core box no. 8. This situation is probably caused by the poor sampling. The same result can be found according to the value of the moisture content.

Average values of parameters	Core box no. 4	8	10
Moisture content, w [%]	16.18	10.98	16.15
Unit weight of solid particles, γ_S [kN/m^3]	26.99	26.81	27.66
Unit weight, γ [kN/m^3]	20.83	19.83	20.81
Dry unit weight, γ_d [kN/m^3]	18.42	18.06	18.96
Void ratio, e [-]	0.47	0.48	0.46
Porosity, n [%]	31.77	32.64	31.47
Degree of saturation, S [%]	95.62	61.91	99.18

Table 6–3:Average index tests results.

a) “dry” sample test (dry sieving).

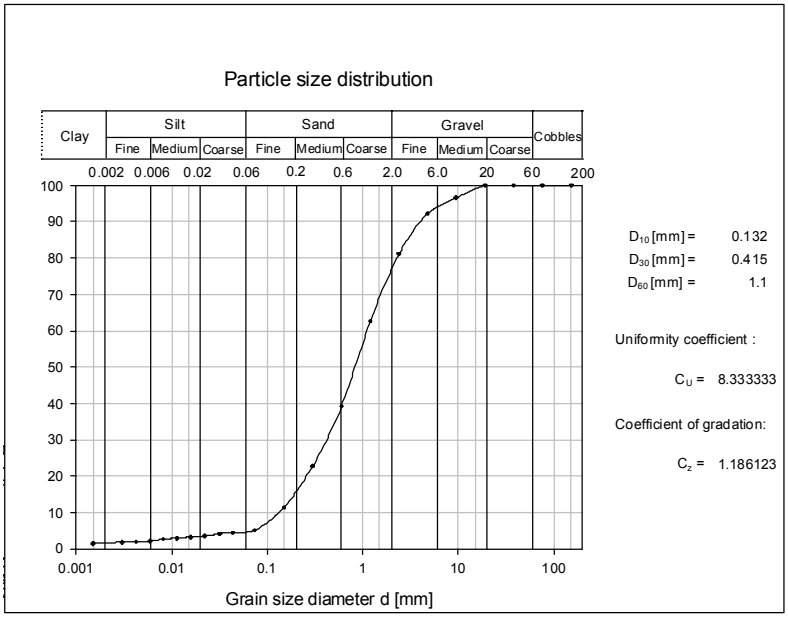

b) “wet” sample test (wet sieving).

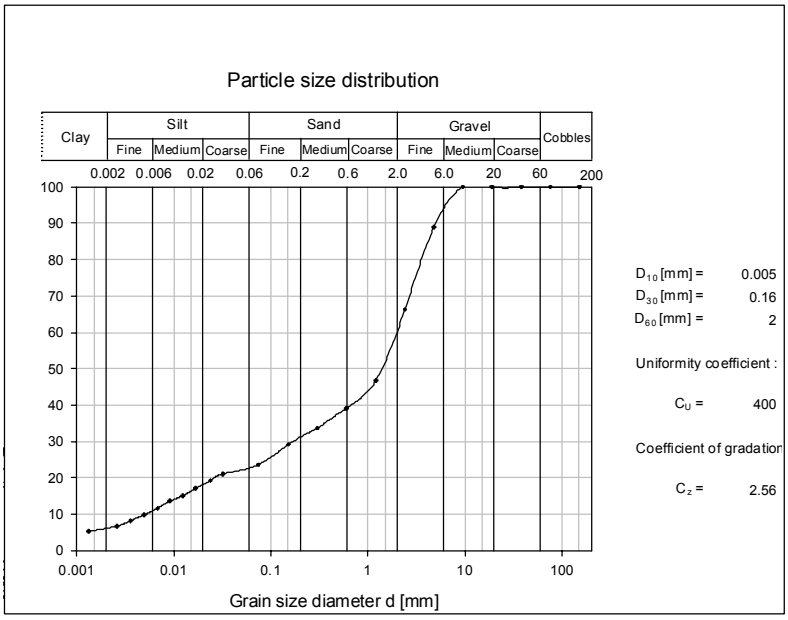

Figure 6–2: Particle size distribution for the core box no. 8 specimen.

6.2.5 Consolidation and strength tests

Investigation of the consolidation and strength parameters together with determination of the volumetric and deviatoric creep behaviour of the Terlicko clayey shale was described in Section 3.3.4 and Section 5.3. So only short summary will be presented here.

Based on the results of the oedometer tests, the Terlicko clayey shale can be defined as a stiff material with low tendency to the volumetric creep behaviour and short duration of the primary consolidation. The in-situ remolding of the Terlicko clayey shale during the past tectonic processes can be supposed based on the problematic evaluation of the pre-consolidation stress. Standard and creep parameters evaluated according to the oedometer tests are presented in Table 3–10.

Conventional drained and undrained triaxial tests show dilatant behaviour of the Terlicko clayey shale, small cohesion c′ varying between 2.9 and 5 kPa and effective friction angle φ' which is increasing with depth from 21^{o} (for the specimen from 4-5 m) to the 34^{o} (for the specimen from 9-10 m). The dilatancy angle was found to be 1.2^{o} for the specimen from 4-5 m depth. Investigation of the deviatoric creep behaviour under undrained triaxial deviatoric creep tests shows high resistance in deviatoric creep and low risk of the deviatoric creep rupture at tested levels of the shear mobilisation. Overview of all evaluated parameters based on deviatoric creep tests under triaxial compression can be found in Table 4–8.

6.3 Mathematical modelling of the Terlicko dam

After analysis of the laboratory tests results, the 2D mathematical model of the right-hand slope of the Terlicko dam was performed. Several numerical models were done with the finite element program for geotechnical applications PLAXIS 8.1. Detailed description of the geometry of the finite element mesh together with the soil data-set parameters, initial conditions and modelling phases will be presented in the following sections. Finally analysis of the numerical model results will be performed and recommendations will be introduced.

6.3.1 Geometry and material properties

The geometry of the right-hand slope was partly reconstructed by the author from the AutoCAD drawing and the old situation maps. 3D view of the right-hand slope reconstructed in the program Surfer 7.0 (Surface Mapping System) is illustrated in Figure 6–3.

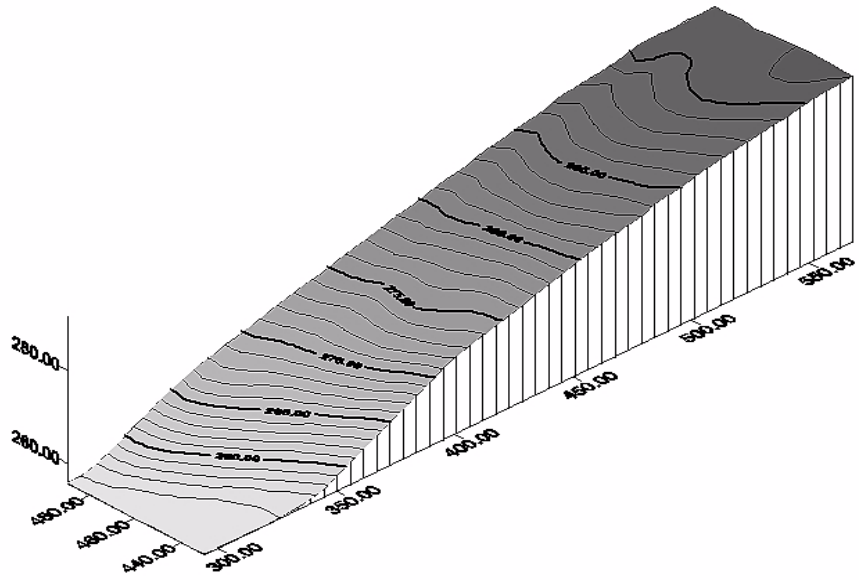

Figure 6–3: 3D view of the right-hand slope of the Terlicko dam.

The finite element mesh of the right-hand valley with the dam is shown in Figure 6–4. The mesh consists 1051 six-node triangular elements and the geometry of the mesh is 700x145 m. The plane strain finite element model was used for the analysis.

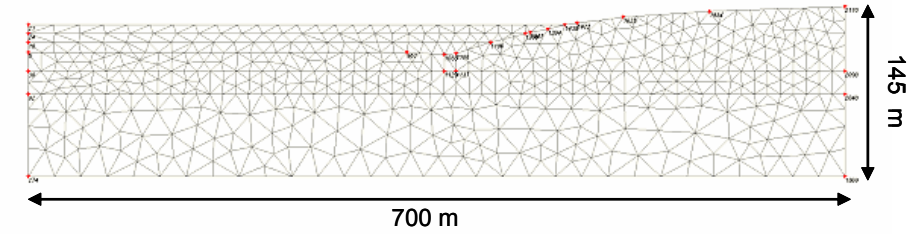

Figure 6–4: Finite element mesh for the numerical study of the Terlicko dam.

According to laboratory tests results and in-situ geology situation, three types of constitutive models were applied. The Soft-soil-creep model was used for the slope material and soil layers lying relatively close to the surface. Two types of parameter

sets were used to decrease amount of the volumetric creep deformation with depth and avoid unrealistic behaviour of the numerical model. The hardening soil model was applied to the bottom soil layer. For Tesinit and dam fill material the linear elastic model was used. Detailed information about soil data-set parameters of the constitutive models is presented in Table 6–4. The distribution of the soil constitutive models in the finite element mesh can be found in Figure 6–5.

Parameters	Material model						
	Linear elastic				Soft-soil-creep		Hardening soil
	1.	2.	3.	4.	1.	2.	
γ_{unsat} [kN/m^3]	18	20	22	26	18	18	18
γ_{sat} [kN/m^3]	20	22	25	26	19	19	20
k_x [m/day]	1E-6	1E-6	1E-6	2E-6	2E-4	2E-4	2E-4
k_y [m/day]	1E-6	1E-6	1E-6	2E-6	2E-4	2E-4	2E-4
E_{ref} [kN/m^2]	1E+5	1E+5	1E+5	4E+6	-	-	-
E^{ref}_{50} [kN/m^2]	-	-	-	-	-	-	3E+4
E^{ref}_{oedo} [kN/m^2]	-	-	-	-	-	-	4.53E+4
power (m) [-]	-	-	-	-	-	-	1
ν [-]	0.35	0.35	0.35	0.33	-	-	-
λ^*	-	-	-	-	0.01	0.01	-
κ^*	-	-	-	-	0.003	0.003	-
μ^*	-	-	-	-	2E-5	8E-5	-
c [kN/m^2]	-	-	-	-	0.1	0.1	1
φ [^{o}]	-	-	-	-	29	29	29
ψ [^{o}]	-	-	-	-	1.2	1.2	1.2

Table 6–4:Presentation of the used soil data-set parameters.

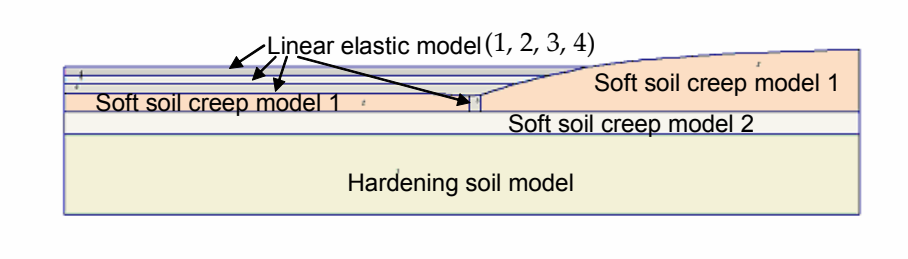

Figure 6–5: Illustration of the location of the different constitutive models inside the finite element mesh.

6.3.2 Initial conditions

First several models were chosen with different initial shapes of the mesh in an effort to involve geological processes connected with valley genesis. After evaluation of these models with respect of the in-situ situation and laboratory test results, the right-hand valley side geometry before Terlicko dam installation was chosen for the initial phase.

As for the boundary conditions, generated finite element mesh was horizontally restrained at lateral boundaries and fixed in both directions at the bottom boundary. Lateral and bottom boundaries were chosen to be close for consolidation to avoid zero excess pore pressure at the boundaries during consolidation analysis. Pore water pressure was generated according to the ground-water phreatic level. The water-table was supposed to be one metre below the surface in the valley. Plot of the principal directions of the active pore pressure together with the ground-water phreatic level and close consolidation boundaries can be found in Figure 6–6.

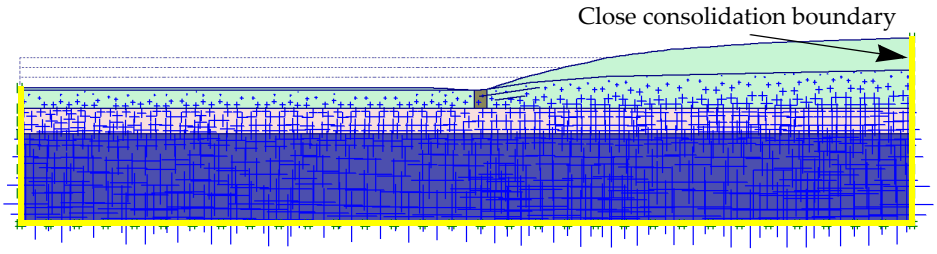

Figure 6–6: Initial phase with demonstration of the ground-water phreatic level together with close consolidation boundary.

Generation of the initial stress was based on the K_0-procedure. The K_0 value was connected with the friction angle through Jaky's formula, shown in Eq. (6.1). In our case K_0 was 0.7-0.8 for Soft-soil-creep model and 0.5 for Hardening soil model.

$$K_0 = 1 - \sin\phi' \tag{6.1}$$

6.3.3 Stability analysis

As a second phase, the stability analysis of the right-hand valley slope was performed. The Phi-c reduction was used for the computing of the slope safety factor. In the Phi-c reduction approach the strength parameters of the soil - $\tan\varphi$ and c, are successively reduced until failure of the structure occurs. The resulting safety factor F is computed according to the following equation,

$$F = \frac{\text{available strength}}{\text{strength at failure}} = \frac{c_{input}}{c_{reduced}} = \frac{\tan\varphi_{input}}{\tan\varphi_{reduced}} \tag{6.2}$$

where the strength parameters with the subscript "input" refer to the properties entered in the material sets and parameters with the subscript "reduced" refer to the reduced values used in the analysis [89].

After evaluation of the stability analyses the safety factor F was found to be around 1 for the right-hand valley slope. Based on this value of the safety factor, an indifferent situation of the right-hand valley slope can be expected, i.e. movement of the slope can be initiated at any time. Plot of the total displacement together with the relative shear stresses can be found in Figure 6–7 a) and b). In the picture one can see, that the critical shear surface is probably "relatively" shallow.

a) Plot of the total displacement.

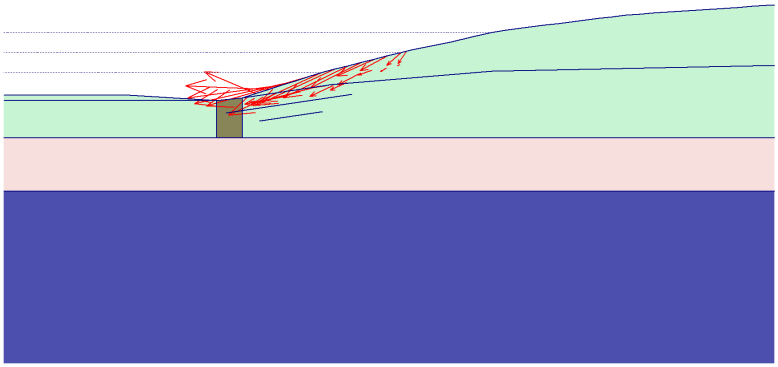

b) Plot of the relative shear stresses.

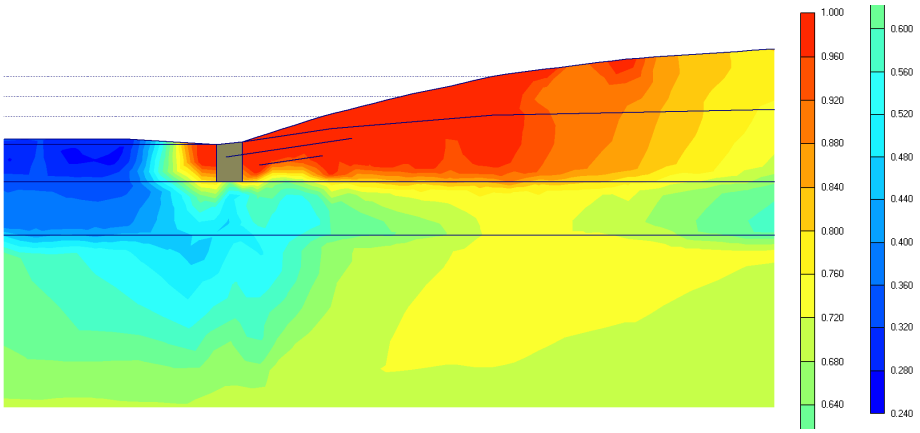

Figure 6–7: Plot of the total displacement and relative shear stresses after stability analysis.

6.3.4 Study of the slope hillside uplift

As a next stage numerical study of the right-hand slope hillside uplift was performed. The overview of all calculation phases (including the Phi/c reduction for the slope stability analysis) applied to the numerical modelling of the Terlicko dam is presented in Table 6–5 for the better orientation.

Phase no.	Start phase	Calculation type	Load input
0	0	-	-
1	0	Plastic	Stage construction
2	1	Phi/c reduction	Incremental multipliers
3	1	Plastic	1st layer imposition
4	3	Plastic	2nd layer imposition
5	4	Plastic	3rd layer imposition
6	5	Plastic	Water head elevation
7	6	Consolidation	30 years consolidation

Table 6–5:List of the applied calculation phases in the case of the numerical model of the Terlicko dam, tests by the author.

Three calculation phases (nos. 3, 4, and 5) were computed for the simulation of the installation of the Terlicko dam. It means that the model of the Terlicko dam was installed in three layers, where for every layer was assumed installation time interval 100 days. After construction of the dam, the elevation of the ground-water table due to the filling of reservoir was modelled. The time interval of the water head elevation was supposed to be 2 years. This process was performed mainly in the valley part of the model and did not result in large differences in stress and strain situation. Distribution of the relative shear stresses after construction of the Terlicko dam and elevation of the ground-water head is possible found in Figure 6–8.

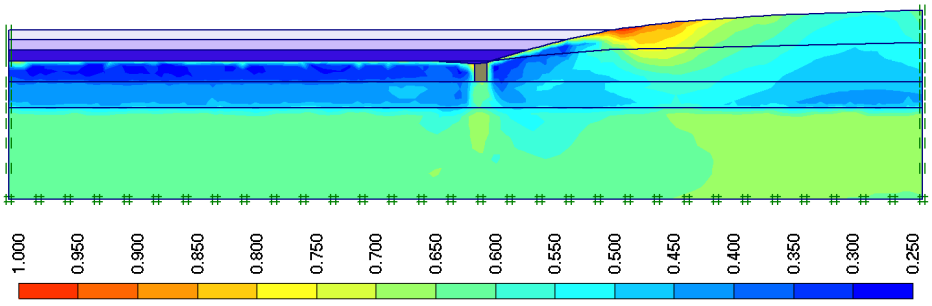

Figure 6–8: Plot of the relative shear stresses after construction of the dam and elevation of the ground-water head.

Following the real in-situ situation the consolidation with duration 30 years was computed as the next stage. This phase did not show any uplift of the right-hand slope hillside. Volumetric deformations connected with creep behaviour were dominated during all consolidation. The vertical deformation of the Terlicko dam during consolidation was approximately 2 mm in the valley. The vertical deformation in the right-hand model side was found to be in range from 4 to 6 mm and no uplift was found here. Domination of the volumetric deformations over the shear ones can be shown in the plots of the volumetric and shear strains presented in Figure 6–9. As for the stress situation there was not record of any large differences in comparison with stages after the Terlicko dam construction.

a) Plot of the volumetric strains.

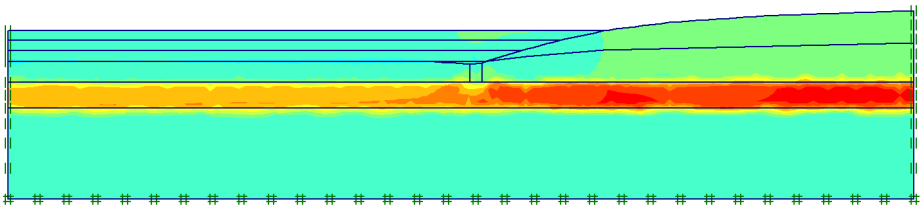

b) Plot of the shear strains.

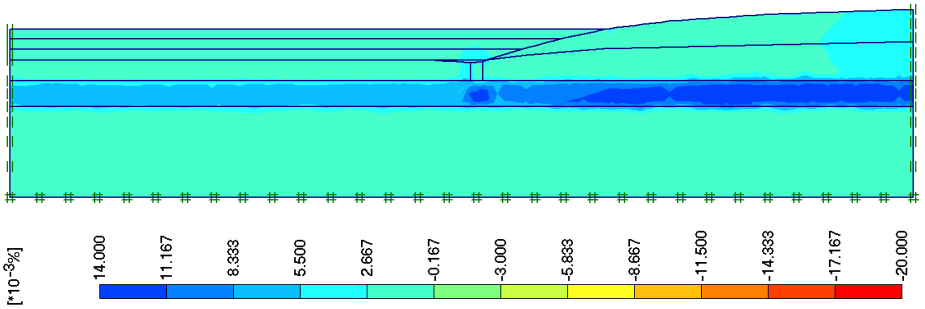

Figure 6–9: Illustration of the volumetric and shear deformations after 30 years of consolidation.

As mentioned, theories about the right-hand slope hillside uplifting are concentrating on deviatoric creep processes running in the slope or the presence of the swelling material below the Terlicko dam. According to the laboratory tests results presented in Section 6.2, the Terlicko clayey shale does not contain swelling minerals and has no significant volumetric and deviatoric creep behaviour in comparison with soft clay. Additionally, also the numerical model did not show any uplift or significant horizontal deformations. By virtue of this information it is necessary to find other possible explanation of the present in-situ Terlico dam behaviour, i.e. uplift of the right-hand slope. After studying the in-situ situation one can find prob-

lems with drainage system in the right-hand slope hillside. According to documentation prepared by Aquatis a.s. [7], a gradual deterioration of the drainage system is observed mainly in the right-hand slope. This problem can lead to gradual elevation of the ground-water head what can be connected with uplift of the right-hand slope.

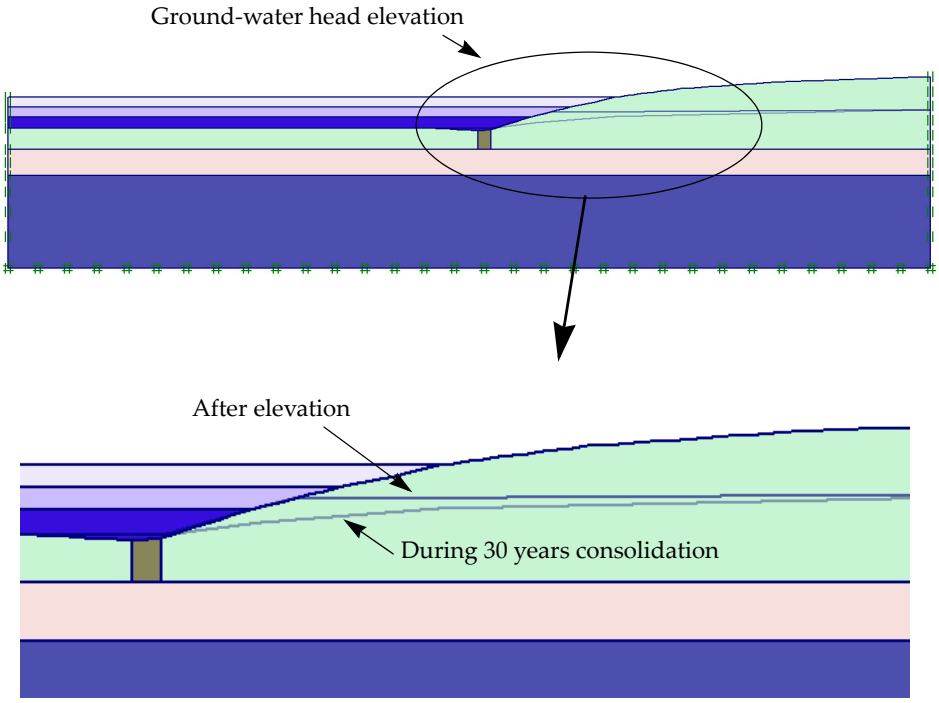

Figure 6–10: Illustration of the ground-water head elevation - global and detailed view.

Based on these facts, the elevation of the ground-water table was modelled after the phase no. 7, i.e. 30 years consolidation (see Table 6–5). Ground-water head was elevated only in the right-hand slope hillside below the Terlicko dam. The maximal rise in the ground-water level was about 5 m. Changing of position of the ground-water head was supposed to be gradual in the time interval 10 years. Illustration of level of the ground-water table during 30 years consolidation and after elevation is presented in Figure 6–10.

Influence of this calculation phase to the general behaviour of the numerical model of the Terlicko dam was significant. In contradiction to the previous phase the uplift

of the right-hand slope hillside was recorded after gradual elevation of the ground-water head. Figure 6–11 a) shows horizontal displacement with the maximal value 10 cm. Distribution of the relative shear stresses after the ground-water head elevation is presented in Figure 6–11 b).

a) Plot of the horizontal displacements.

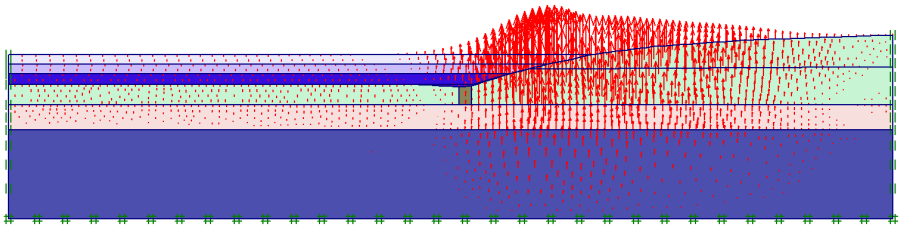

b) Plot of the relative shear stresses.

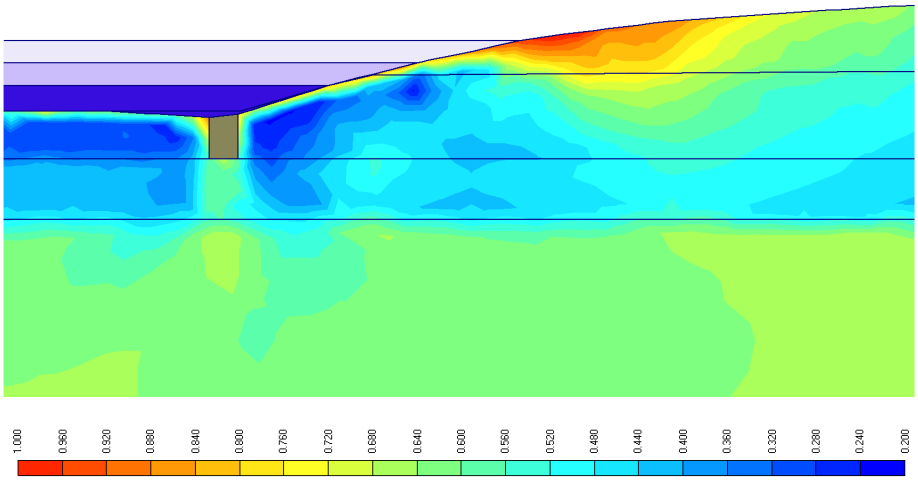

Figure 6–11: Plot of the horizontal displacements and relative shear stresses after the ground-water head elevation.

6.4 Summary

Laboratory investigation of the Terlicko dam substratum material was done including time dependency behaviour. Material is not showing significant creep either volumetric or deviatoric in comparison with soft clays. There is low risk of the secondary deviatoric creep or creep rupture for design shear mobilization level.

The study of the in-situ Terlicko dam behaviour was done using the PLAXIS 8.1 program. After construction of the Terlicko dam and 30 years consolidation there was no uplift observed. With respect of the in-situ situation study, the elevation of the ground-water head during last 10 years was modelled. Changing the ground-water head showed significant influence to the Terlicko dam model behaviour from the point of the recorded right-hand slope hillside uplift.

The theory of the ground-water head elevation seems to be in good accordance with in-situ Terlicko dam behaviour. Solution of this problem is in the reconstruction of the drainage system below the right-hand slope hillside. But of course there are still some other possibilities to explain the right-hand slope uplift. Better in-situ monitoring of the pore water pressure in the uplift zone will be necessary to determinate the correct solution.

Chapter 7 Summary, conclusions and recommendations

7.1 Summary and conclusions

Rheological behaviour of clayey soils in general and the creep behaviour of this material in particular is starting to be more and more significant in theoretical and practical geotechnical engineering. Increasing building activities on the soft clay foundations demand a better understanding of the creep phenomenon and more powerful tools for the analysis and prediction of this behaviour.

The main contribution of this thesis is the presentation of the creep behaviour of several clayey soil materials under different laboratory conditions together with the application of the obtained knowledge to the in-situ behaviour of the geotechnical structure. The main effort has been placed on the application of the Janbu's resistance concept to the evaluation and description of the observed creep behaviour. The geotechnical finite element program PLAXIS 8.1. has been used for the numerical study of the laboratory and in-situ cases. Additionally unique tests of rheological behaviour of the natural clay with the Modular Compact Rheometer MCR300 have been performed, evaluated and presented.

Janbu's resistance concept has been developed by Professor Nilmar Janbu and coworkers at NTH and NTNU since the 1960s. Many applications of this concept to the laboratory and in-situ creep behaviour have been performed and the rich theoretical and practical background can be found in many publications. Anyway the resistance concept is using mainly only in Scandinavian counties and is almost unknown in the rest of the world, although it can for instance be found as a partial background of the Soft-soil-creep constitutive model implemented in the PLAXIS.

Detailed study of the application of the Janbu's resistance concept to the oedometer and triaxial creep behaviour of the clayey soils has been performed and presented. The "step by step" application of this concept to the long-term oedometer tests on the Norwegian quick clay shows its relatively easy use and recapitulative final description of the tested clayey material. Significantly corresponding results of the "short-term" and "long-term" creep resistance numbers r_s for the Norwegian Glava clay material reflect that the resistance concept fits well even with the "short" term

oedometer tests. This finding is based on the evaluation and comparison of the stress-strain-time behaviour from incremental oedometer tests with 1 h and 24 h load step durations. All these aspects make the Janbu's resistance concept a simple and powerful tool for the practical investigation of creep behaviour of the clayey soil material.

The numerical model of the long term oedometer test with emphasis on the creep behaviour with geotechnical finite element code PLAXIS 8.1 and the Soft-soil-creep constitutive model show good agreement with the input data based on the Janbu's resistance concept. The numerical behaviour was almost identical with the laboratory behaviour. However, the constant value of the modified compression index λ^* used for the all levels of the volumetric effective stress in the case of the Soft-soil-creep model was found to be a significant disadvantage for the sensitive clays. Based on the performed laboratory tests on the natural clayey material, a decreasing value of the λ^* with the increasing vertical effective stress σ_y' has been found. This behaviour is probably due to the influence of the structure of the soil.

The influence of the clayey soils structure on the oedometric creep behaviour was investigated with the Norwegian Onsøy clay material. Evaluation and comparison of four long-term oedometer tests with the undisturbed and remolded Onsøy clay show smaller vertical deformations after remolding. Incremental strain after 24 h consolidation has been found to be almost two times larger for the normally consolidated undisturbed clay in comparison with the remolded one. Based on the these tests the remolded clay exhibits longer primary consolidation and smaller ability of the creep deformation.

The possible occurrence of the secondary and tertiary creep which leads to the failure makes deviatoric creep behaviour extremely important in the case of clayey soil stability problems. Investigation of deviatoric creep under triaxial compression can help to give better understanding of this phenomenon. Janbu's resistance concept has been used for the evaluation of the undrained and drained deviatoric creep triaxial tests with the Norwegian Glava clay and Czech Terlicko clayey shale materials. In the case of the drained deviatoric creep, the connection can be found between deviatoric deformation and simultaneously running volumetric deformation. At the start of the deviatoric creep test, the development of the creep resistance numbers evaluated from the vertical and volumetric creep strains show an increasing amount of the deviatoric creep deformation and a decreasing amount of the volumetric creep deformation with increasing value of shear mobilisation. This behaviour seems to be typical for the normally consolidated and lightly over-consolidated clay material. In the case of the heavily over-consolidated clays the situation is more complex and in theory this can easily leads to the creep rupture.

The undrained deviatoric creep tests under triaxial compressions have shown significant problems of the use of the 1:1 triaxial specimen in the case of the clay material. According to the comparison of the classical undrained triaxial tests with 1:2 and 1:1 samples of the Norwegian Glava clay the measured excess pore pressure during the initial triaxial shearing is usually significantly smaller in the case of the 1:1 sample. However, during undrained deviatoric creep triaxial tests the 1:1 sample of Glava clay exhibits a considerable increase in the excess pore pressure so that finally the stress path of effective stresses crosses the failure envelope and continues to the so-called "dry" or "low stress" side. The possible explanation of this "non-standard" behaviour can be inappropriate location of the pore pressure transducer, i.e. the connection to the bottom filter. Due to the so-called lubricated ends used in the case of the 1:1 specimen (to avoid the occurrence of the "dead zones" at the ends of the sample) the small filter with a diameter of only 6 mm has to be used. This small filter causes a higher hydraulic gradient and a longer drainage path. Also the significantly higher friction between the sample and the small filter than between the sample and the rest of the lubricated bottom pedestal has a considerable influence to the general behaviour of the 1:1 sample during the triaxial test. The effect of this behaviour is, according to the author, multiplied by low permeability and high effective cohesion of the clay. The numerical models with the PLAXIS 8.1 and Soft-soil-creep constitutive model have shown greater active pore pressure around the small filter (in comparison with the rest of the sample) and extremely large concentrations of the pore pressure in the boundary between the filter and the rest of the bottom pedestal in the case of the Norwegian Glava clay material. The same numerical tests using the Czech Terlicko clayey shale with the lower effective cohesion and higher permeability have shown lower values in the active pore pressure, which are comparable with the rest of the modelled sample. This is in accordance with the observed laboratory tests which have shown more "standard" behaviour of the 1:1 triaxial sample in the case of the Terlicko clayey shale.

A dam located in the River Stonavka by Terlicko in the Czech Republic has been chosen for the practical application of the knowledge and experience obtained during this PhD work about the creep behaviour of the clayey material. An uplift of the bottom part of the right-hand slope together with the dam crown has been observed from 1982. This behaviour has been connected with the creep deformation of the right-hand slope which was recorded before construction of the Terlicko dam or with the presence of the swelling minerals influenced by the ground-water, where the first possibility was preferred. Based on this information, an investigation of the Terlicko clayey shale material from the Terlicko dam substratum has been done with the emphasis placed on the creep behaviour. However, oedometer and triaxial creep tests have shown relatively high resistance in deviatoric and volumetric creep behaviour and low risk of the big creep deformations. Additionally the special X-

ray diffraction test did not exhibit any presence of the swelling minerals in the Terlicko clayey shale. This behaviour has been confirmed by numerical model with the PLAXIS 8.1 which has not shown any uplift or significant horizontal deformations based on the creep movement of the right-hand slope. Additional study of materials connected with the monitoring of the Terlicko dam behaviour has displayed problems with the drainage system in the right-hand slope hillside which can create elevation of the ground-water head. The numerical model which places emphasis on the gradual changing the water head level in the time interval of 10 years indicates the possible influence of this change on the observed uplift.

The natural viscosity of the clayey soil seems to be one of the main characteristics influencing the creep, or more generally the rheological behaviour of this material. Investigation of this parameter can help to obtain a better understanding and prediction of the creep deformations. Modern rheometers are opening new doors to investigation of the rheological behaviour in general and creep behaviour in particular. Several tests with the Modular compact rheometer MCR300 on the Norwegian Glava clay have shown the behaviour of this material with emphasis on the viscosity during the amplitude sweep test with controlled shear strain, controlled shear stress test and the creep test. However, the problems connected with measuring conditions, especially with uncontrolled drainage conditions and, consequently, uncontrolled volume changes of the clayey sample were mainly found in creep test. Other tests were relatively short and this behaviour was considered to have no significant influence on the tests results.

7.2 Recommendations for the further work

The following recommendations for the further work can be established based on this work in this thesis:

- More long-term oedometer tests with the natural clay material will have to be done. Emphasis should be placed on the influence of the structure of the clay on the creep behaviour and development of the (modified) compression index with increasing value of the vertical or volumetric effective stress.
- Oedometer creep behaviour of the natural clay material using the floating ring with larger diameter and height in comparison with the standard one should be investigated in more detail.
- More drained and undrained triaxial tests in general, and deviatoric creep triaxial tests in particular will have to be performed on the 1:1 sample of the natural clay material for more in-depth understanding of the observed “nonstandard” behaviour. A change of the location of the pore pressure transducer will be probably necessary. Additionally more numerical models of the triaxial test will have to be done to obtain further understanding of the stress and strain situation inside the 1:1 and 1:2 specimens during deviatoric creep.

- More detailed investigation of the natural clay viscosity with the Modular compact rheometer should be performed. Technical modification of the rheometer will have to be done with emphasis on better control of the drainage conditions and better control of the applied normal force. Detailed study of the rheological behaviour of the natural clay material with the modified Modular compact rheometer can significantly help to further the understanding of this material from the rheological point of view.
- Special attention should be paid to the investigation of the true physical viscosity of the natural clay and its influence on the creep behaviour (or more generally rheological behaviour) of this material.

References

1. Abdel-Hady, M., Herrin, M., 1966. Characteristics of soil asphalt as a rate process, Journal of the Highway division, A.S.C.E., Vol. 92, No. HW1, pp. 49-69
2. Abe, N., 1987. Elasto-viscoplastic model of clays including creep rupture criteria. Proc. 8th ARC, Vol. 1, Kyoto, pp. 1-4
3. Adachi, T., Oka, F., Hirata, T., Hashimoto, T., Pradhan, T.B.S., Nagaya, J., Mimura, M., 1991. Triaxial and torsional hollow cylinder tests of sensitive natural clay and an elastic-viscoplastic constitutive model, X ECSMFE, Deformation of soils and displacements of structures, Volume I, A.A. Balkema, Rotterdam, pp. 3-6
4. Andersland, O.B., Douglas A.G., 1970. Soil deformation rates and activation energies, Geotechnique, Vol. 20, Issue 01, pp. 1-16
5. Anderson, J.G.K., Trigg, K.F., 1981. Interesting Case Studies from the Practice of Engineering Geology, Nedra, Moskow, 224 p.
6. Anderson, W.F., Pyrah, I.C., Pang, L.S., Haji-Ali, F., 1988. The time dependent behaviour of normally consolidated clay in thick hollow cylinder test, International conference on rheology and soil mechanics, edited by Keedwell M.J., ISBN 1-85166-273-1, pp. 204-218
7. AQUATIS a.s. 2000, Modernisation of the Terlicko dam instrumentation, Czech republic (Report in Czech)
8. Aubry, D., Kodaissi, E., Meimon, Y., 1985. A viscoplastic constitutive equation for clays including a damage law, Fifth international conference on numerical methods in geomechanics, Nagoya, pp. 421-428
9. Bailkir, T., Marsh, A.D., 1974. Triaxial tests on soil: correction for effect of membrane and filter drain, TRRL Supplementary Report 90 UC, Transport and Road Research Laboratory, Crowthorne
10. Barden, L., 1968. Primary and secondary consolidation of clay and peat, Geotechnique, Vol. 18, Issue 01, pp. 1-24

11. Barnes, H.A., Hutton, J.F., Walters, K. 1989. An introduction to rheology, Rheology series, Amsterdam, Elsevier, Netherlands, 199 p.
12. Bilik, M. et al. 1969. Large Dam in the Carpathian Flysh of Moravia. Czechoslovak National Committee on Large Dams, Prague, Czechoslovakia
13. Biot, M.A., 1941. General theory of three-dimensional consolidation, Jnl. Appl. Phys., Vol. 12, pp 155-164
14. Bishop, A.W., Bjerrum, L., 1960. The Relevance of the Triaxial Test to the Solution of Stability Problems, Proceedings, Research conference on shear strength of cohesive soils, ASCE, pp. 437-501
15. Bjerrum, L. 1967. Engineering geology of Norwegian normally-consolidated marine clays as related to settlements of buildings, Seventh rankine lecture, Geotechnique, Vol. 17, pp. 83-118
16. Bjerrum, L., Landva, A., 1966. Direct simple-shear tests on a Norwegian quick clay, Geotechnique, Vol. 16, No. 01, pp. 1-20
17. Bjerrum, L., Lo, K.Y., 1963. Effect of aging on the shear-strength properties of a normally consolidated clay, Geotechnique, Vol. 13, No. 02, pp. 147-157
18. Black, D.K., Lee, K.L., 1973. Saturating laboratory samples by back pressure, J. Soil Mech. and Foundation Division ASCE. Vol. 99., No. SM1, Paper 9484, pp. 75-93
19. Borja, R.I., 1991. Generalized creep and stress relaxation model for clays, Journal of Geotechnical Engineering, Vol. 118, No. 11, pp. 1765-1786
20. Braaten, T., 2003. Treaksialforsøk på leire med bruk av glatte endeflater, Hovedoppgave, NTNU, Instittut for bygg og transport, Faggruppe for geoteknikk, Trondheim, Norway, 103 p.
21. Campanella, R.G., 1965. Effect of Temperature and Stress on the Time-Depending Behaviour of Saturated Clay, Ph.D. diss., University California, Berkley
22. Christensen, R.W., Wu, T.H., 1964. Analyses of clay deformation as a rate process, Journal of the soil mechanics and foundation division, A.S.C.E., Vol. 90, No. 6, pp. 125-157
23. Christensen, S. 1986. Triaxial creep tests, Eberg clay. SINTEF report no. STF69 F86016, Division of Geotechnical Engineering, Norway, Trondheim
24. Christensen, S. 1986. Triaxial creep tests, Troll clay, SINTEF report no. STF69 F86020, Division of Geotechnical Engineering, Norway, Trondheim

25. Christensen, S., 1985. Creep Tests in Oedometer Eberg Clay, SINTEF report no. STF69 F85005, Division of Geotechnical Engineering, Norway, Trondheim

26. Christensen, S., 1985. Creep Tests in Oedometer Troll Clay, SINTEF report no. STF69 F85045, Division of Geotechnical Engineering, Norway, Trondheim

27. Craig, R.F., 1992. Soils mechanics, fifth edition, Published by Chapman & Hall, Printed in Great Britain by T.J.Press, ISBN 0 412 39590 8, pp. 427

28. Cundall, P.A., Drescher, A., Strack, O.D.L., 1982. Numerical experiments on granular assemblies, measurement and observations, In Vermeer, P.A., Luger, H.J. (Eds.), Deformation and failure of granular materials. IUTAM Symp., Delft, A.A. Balkema, pp. 355-370

29. Cundall, P.A., Strack, O.D.L., 1983. Modeling of microscopic mechanisms in granular material, In: Jenkins J.T. and Satake M. (Eds.), Mechanics of granular materials-new models and constitutive relations. Elsevier, pp. 137-149

30. Das, Braja M. 2000. Fundamentals of Geotechnical Engineering, Brooks/Cole, Thomson Learning$_{TM}$, Printed in USA, 593 p.

31. Desai, C.S., Siriwardane, H.J., 1984. Constitutive laws for engineering materials with emphasis on geologic materials, Prentice-Hall, New Jersey, 468 p.

32. Emdal, A., Svanø, G., 1988. KRYKON Ver. 02, A FEM-program for one-dimensional consolidation analysis including creep effects, documentation and user's manual, SINTEF report no. STF69 F88009, Division of Geotechnical Engineering, Norway, Trondheim

33. Feda, J. 1992. Creep of soils and related phenomena, Development in geotechnical engineering 68, Amsterdam, Elsevier, Printed in Czechoslovakia, 422 p.

34. Feda, J., 1989. Interpretation of creep of soil by rate process theory, Geotechnique, Vol. 39, No. 4, pp. 667-677

35. Fodil, A., Aloulou, W., Hicher, P. Y., 1997. Viscoplastic behaviour of soft clay, Geotechnique, Vol. 47, No. 3, pp. 581-591

36. Geuse, E.C.W.A., Tjong-Kie, T., 1953. The mechanical behaviour of clays, Proc. Second Int. Conf. Rheology, London, pp. 247-259

37. Gibson, R.E., Lo, K.Y., 1961. Theory of consolidation of soils exhibiting secondary compression, NGI, Norway, Publication No. 41 (also Acta Polytechnice Scandinavi, 296/191, c_i 10)

38. Glasstone, S., Laidler, K., Eyring, H., 1941. The theory of rate processes, McGraw-Hill, New York

39. Graham, J., Crooks, J.H.A., Bell, A.L., 1983. Time effects on the stress-strain behaviour of natural soft clays, Geotechnique, Vol. 33, No. 03, pp. 327-340

40. Grim, Ralph E. 1953, Clay Mineralogy, McGraw-hill book company, INC., Series in Geology, 384 p.

41. Gussmann, P., 1987. Kinematical element method in soil mechanics, Proc. 1st Czech. CONMIG, Vysoke Tatry, Vol. 1, pp. 116-128

42. Head, K.H., 1986. Manual of Soil Laboratory Testing, Volume 3: Effective Stress Tests, Pentech Press, ISBN 0-7273-1306-1, 1238 p.

43. Head, K.H., 1989. Soil Technicians' Handbook, Pentech Press, ISBN 0-7273-1906-X, 158 p.

44. http://torre.duomo.pisa.it

45. http://www.physica.de

46. Janbu, N. 1967. Settlement calculations based on the tangent modulus concept, Bulletin 2, NTH, Department of soil mechanics and foundation engineering, Trondheim, Norway

47. Janbu, N. 1997. Stress-strain-time behaviour of porous media. A case record based review, Bulletin 29, NTNU, Department of Geotechnical Engineering, Trondheim, pp. 1-14

48. Janbu, N. 1998. Sediment deformations - A classical approach to stress - strain - time behaviour of granular media as developed at NTH over 50 year period, Bulletin 35, NTNU, Department of Geotechnical Engineering, Trondheim, 86 p.

49. Janbu, N., 1965. Consolidation of clay layers based on non-linear stress strain, Proc. 5. ICSMFE, Montreal 2, pp. 83-87

50. Janbu, N., 1994, In situ creep behaviour obtained from long-term settlement observations, XIII ICSMFE, New Delhi, India

51. Janbu, N., Svanø, G. & Christensen, S. 1992. Back-calculated creep rates from case records, Bulletin 25, NTNU, Department of Geotechnical Engineering, Trondheim

52. Janbu, N., Tokheim, O., Senneset, K., 1981. Consolidation tests with continuous loading, Proc. 10 ICSMFE, Stockholm, Vol. 4, pp. 645-654

53. Kavazajian, E., 1988. A creep-inclusive non-associative cam-clay plasticity model, International conference on rheology and soil mechanics, edited by Keedwell M.J., ISBN 1-85166-273-1, pp. 29-43

54. Kavli, A., 1994. Long-term processes in geomaterials. Basis for development of creep models, Project no. 690303, SINTEF, Division of Geotechnical Engineering, Trondheim, Norway, 49 p.

56. Kobayashi, S., 1985. Application of boundary integral equation method to geomechanics, Proc. 5th ICONMIG, Nagoya, Vol 1., pp. 83-92

55. Korhonen, K.H., Järvenmäki, P., Lojander, M., 1988. Undrained and drained creep in clay, International conference on rheology and soil mechanics, edited by Keedwell M.J., ISBN 1-85166-273-1, pp. 288-300

57. Leroueil, S., Kabbaj, M., Tavenas, F., Bouchard, R., 1985. Stress-strain-strain rate relation for the compressibility of sensitive natural clays, Geotechnique, Vol. 35, No. 2, pp. 159-180

58. Lo, K.Y., 1961. Secondary compression of clays, J. Soil Mech. and Found. Div., Proc. ASCE, Vol. 87, SM4, pp. 61-87

59. Long, M., 2003. Modelling the stress-strain behaviour of Onsøy clay, Proc. to Int. Workshop on Geotechnics of Soft Soil - Theory and Practice, Noordwijkerhout, The Netherlands, Published by Verlag Glückauf GmbH, pp. 461-466

60. Long., M., Lunne, T., 2003. Stiffness of Onsøy clay, Deformation characteristics of Geomaterials, Proc. IS-Lyon '03, Rotterdam, Swets and Zeiltlinger

61. Lunne, T., Long, M., Forsberg, C.F., 2003. Characterisation and engineering properties of Onsøy clay. Characterisation and Engineering Properties of Natural Soils, Balkema, Rotterdam, Vol. 1, pp. 395-428

62. Maleki, M., Cambou, B., Farsi, M., Dubujet, Ph., 1999. An elastoplastic - viscoplastic model for soils, NUMOG VII, Pande, pp. 15-20

63. Maslov, N.N. 1968, Long-term stability and displacements of retaining structures, Energiya, Moscow, 160 p.

64. Maslov, N.N., 1935. Problems in Geotechnical Investigations, Svirstroy Publications, Leningrad, Vol. IV, 177 p.

65. Maslov, G.N., 1940. Thermal stressed state of concrete mass taking into account the creep of concrete, Trans. Research Institute of Hydrotechnical Engineering, Vol. 28, pp. 175-188

66. Maslov, N.N., 1952. Some new principles in estimation of the stability of slopes and embankments, Proc. Res. Conf. Leningrad Civil Engineering Institute, Leningrad, pp. 40-42

67. Maslov, N.N., 1982. Fundamental of Engineering Geology and Soil Mechanics, Vysshaya Shkola, Moskow, 511 p.

68. Matsui, T., Abe, N., 1988. Verification of elasto-viscoplastic model of normally consolidated clays in undrained creep, Numerical methods in geomechanics, Innsbruck, pp. 453-459

69. Meschyan, S.R. 1995. Experimental rheology of clayey soils, Geotechnika 13, A.A. Balkema Publishers, Rotterdam, Netherlands, 448 p.

70. Meschyan, S.R., 1974. Mechanical properties of soils and laboratory methods for their determination, Nedra, Moskow, 192 p.

72. Mesri, G., 1973. Coefficient of secondary compression, Journal of the geotechnical engineering division, ASCE, Vol. 99, No. SM1, Proc. paper 9515, pp. 123-137

73. Mesri, G., Choi, Y.K., 1979. Discussion: Strain rate behavior of Saint Jean-Vianney clay, Canadian geotechnical jour., Vol. 16, No. 4, pp. 831-834

74. Mesri, G., Choi, Y.K., 1981, Discussion: A method for estimating the consolidation of a normally consolidated clay of same age, Soils and foundation, Vol. 21, No. 2, pp. 131-134

75. Mesri, G., Febres-Cordero, E., Shields, D.R., Castro, A., 1981. Shear stress-strain-time behaviour of clays, Geotechnique, Vol. 31, No. 04, pp. 537-552

71. Mesri, G., Godlewski, P.M., 1977. Time- and Stress-Compressibility Interrelationship, Journal of the geotechnical engineering division, ASCE, Vol. 103, No. GT5, Proc. paper 12910, pp. 417-430

76. Mesri, G., Rokhsar, A., 1974. Theory of Consolidation for Clays, Journal of the geotechnical engineering division, ASCE, Vol. 100, No. GT8, Proc. paper 10740, pp. 889-904

77. Mezger, T.G. 2002. The Rheology-Handbook, Hannoprint, Hannover, Germany, 252 p.

78. Mitchell, J.K., 1964. Shear resistance of soil as a rate process, Journal of the soil mechanics and foundation division, A.S.C.E., Vol. 90, No. SM1, pp. 29-61

79. Mitchell, J.K., 1993. Fundamentals of soil behaviour, 2nd Edition, John Wiley & Sons, 427 p.

80. Murayama, S., Shibata, T., 1958. On the rheological characteristics of clays, Part I, Bulletin no. 26, Disaster prevention research institute, Kyoto, Japan

81. Murayama, S., Shibata, T., 1961. Rheological properties of clays, Proceedings of the Fifth International Conference on Soil Mechanics and Foundation Engineering, Vol. 1, pp. 269-273

82. Nash, D.F.T., Ryde, S.J., 2001. Modelling consolidation accelerated by vertical drains in soils subject to creep, Geotechnique 51, No. 3, pp. 257-273

83. Navarro, V., Alonso, E.E., 2001. Secondary compression of clays as a local dehydration process, Geotechnique, Vol. 51, No. 10, pp. 859-869

84. Nowacki, E.H.F., 1973. Endimensjonal konsolidering med spennings- og tidsavhengige materialegenskaper, Dr. Ing. thesis, NTH, Norway

85. Naatanen, A., Lojander, M., Puumalainen, N., 1995. Primary and secondary consolidation of Finnish clays, Compression and Consolidation of Clayey soils, Yoshikuni&Kusakabe (eds), Balkema, Rotterdam, pp. 719-724

86. O'Reilly, M.P., Brown S.F., Austin, G., 1988. Some observation on the creep behaviour of a silty clay, Int. conference on rheology and soil mechanics, edited by Keedwell M.J., ISBN 1-85166-273-1, pp. 44-58

87. Oka, F., Adachi, T., Mimura, M., 1988. Elasto-viscoplastic constitutive models for clays, International conference on rheology and soil mechanics, edited by Keedwell M.J., ISBN 1-85166-273-1, pp. 12-28

88. Physica Messtechnik GmbH, 2001. Universal Software US200, Operating Instructions, Printed in Germany

89. PLAXIS Manual, 2002, A.A. Balkema Publishers, Rotterdam, Printed in the Netherlands

90. Potts, D.M., Zdravkovic, L., 1999. Finite element analysis in geotechnical engineering, Theory, Thomas Telford Publishing, ISBN: 0 7277 2753 2, 440 p.

91. Reiner, M., 1963. Deformation and flow, An introduction to rheology, Gosstroyizdat, Moskow, 381 p.

92. Sandven, R. 1990. Strength and deformation properties of fine grained soil obtained from piezocone tests, Ph.D. thesis, Institutt for Geoteknikk, NTNU, Trondheim,

93. Schmidt, M. 2000. The determination of the preconsolidation pressure for Norwegian quick clay, Diploma thesis, NTNU, Trondheim, 134 p.

94. Shirtliffe, C.J., 1972. Thermal Resistance of Building Insulation, Canadian Building Digest, IRC, http://irc.nrc-cnrc.gc.ca/cbd/cbd149e.html

95. Singh, A., Mitchell, J.K., 1968. General stress-strain function for soil, J. Soil Mech. and Found. Div., Proc. ASCE, SM 1, pp. 21-46

96. Singh, A., Mitchell, J.K., 1969. Creep potential and creep rupture of soils, Proc. 7. Int. Conf. on Soil Mech. and Foundation Eng., Vol. 1, Mexico, pp. 379-384

97. Smith, R.E., Wahls, H.E., 1969. Consolidation under constant rates of strain, Journal of Soil Mech. Fdns Div. Am. Soc. Civ. Eng., Vol. 95, No. SM2, pp. 519-539

98. Suklje, L. 1978. Stresses and strains in non-linear viscous soils, Int. Journal for numerical and analytical methods in geomechanics, Volume 2 no. 2 April-June, John Wiley&Sons Ltd., Printed in UK, pp. 129-158

99. Suklje, L., 1957. The analysis of the consolidation process by the isotaches method, Proc. 4th Int. Conf. Soil Mech., London, Vol. 1, pp. 200-206

100. Svanø, G., 1986. Eindimensjonal tøyning som funksjon av effektivspenning og tid, SINTEF report no. STF69 F86010, Division of Geotechnical Engineering, Norway, Trondheim, 26 p.

101. Svanø, G., 1986. Program KRYKON, documentation and manual (The "Soft clay deformation" project.), STF69 F86017, SINTEF, Trondheim, Norway

102. Svanø, G., Christensen, S., Nordal, S., 1997. A soil model for consolidation and creep, Bulletin 29, NTNU, Norway, pp. 269-272

103. Tadesse, S., 2000, Behaviour of saturated sand under different triaxial loading and liquefaction, Ph.D. thesis, NTNU, Trondheim, 166 p.

104. Taylor, D.W., Merchant W.A. 1940. A theory of clay consolidation accounting for secondary compression, Journal of Mathematics and Physics, Vol. 19, pp. 167-185

105. Ter-Stepanian, G., 1975, Creep of a clay during shear and its rheological model, Geotechnique, Vol. 25, No. 2, pp. 299-320

106. Terzaghi, K., Peck, R.B., 1967. Soil Mechanics in Engineering Practice, 2nd ed., Wiley, New York

107. Terzaghi, K.T., 1923. Die Berechnung der Durchlassigkeitsziffer des Tones aus dem Verlauf der Hydrodynamischen Spannungserscheinungen, Sitz, Akademre der Wissenschaften, Mathematishnatur Wissenschaftliche, Klasse, Vienna, Austria, Part IIa, Vol. 132, pp. 125-138

108. Terzaghi, K.T., 1925. Erdbaumechanik auf bodenphysikalischer grundlage, Franz Deuticke, Leipzig und Wien, 399 p.

109. Vaid, Y.P., 1988. Time dependent shear deformation of clay, International conference on rheology and soil mechanics, edited by Keedwell M.J., ISBN 1-85166-273-1, pp. 123-138

110. Vermeer, P.A., Neher, H.P., 1999. A soft soil model that accounts for creep, Beyond 2000 in computational geotechnics - 10 years of PLAXIS, Balkema, Rotterdam, pp. 1-13

111. Vermeer, P.A., Stolle, D.F.E., Bonnier, P.G., 1998. From the classical theory of secondary compression to modern creep analysis, Proc. 9th International Conf. Comp. Meth. and Adv. Geomech., Wuhan, China, Vol. 4, pp. 2469-2478

112. Virdi, S.P.S., Keedwell, M.J., 1988. An interpretation of some observed effects of temperature variation on soil behaviour, Int. conference on rheology and soil mechanics, edited by Keedwell M.J., ISBN 1-85166-273-1, pp. 355-371

113. Virdi, S.P.S., Keedwell, M.J., 1988. Some observed effects of temperature variation on soil behaviour, Int. conference on rheology and soil mechanics, edited by Keedwell M.J., ISBN 1-85166-273-1, pp. 336-354

114. Vulliet, L., Desai, C.S., 1989. Viscoplasticity and finite elements for landslide analysis, Proceedings of the Twelfth int. conference on Soil mechanics and foundation engineering, Rio de Janeiro, pp. 801-806

115. Walker, L.K., 1969. Undrained creep in a sensitive clay, Geotechnique, Vol. 19., No. 4, pp. 515-529

116. Wissa, A.E.Z., Christian, J.T., Davis, E.H., Heiberg, S., 1971. Consolidation at constant rate of strain, Journal of Soil Mech. Fdns Div. Am. Soc. Civ. eng., Vol. 97, No. SM10, pp. 1393-1413

117. Yasuhara, K., Hirao, K., Ue, S., 1988. Effect of long-term K_0 consolidation on undrained strength of clay, Int. conference on rheology and soil mechanics, edited by Keedwell M.J., ISBN 1-85166-273-1, pp. 273-287

118. Zienkiewicz, O.C., 1971. The finite element method in engineering science, McGraw-Hill, 522 p.

Appendix 1 Interpretation of Triaxial tests data

A1.1 Introduction

All the triaxial tests performed by the author were evaluated according to the standard way contained area correction after consolidation, area correction during shearing, correction of the influence of weight of top cap and loading ram (piston correction) and membrane correction. Microsoft Excel sheets prepared by Shaoli Young based on the work of Tadesse [103] were used for the interpretation of triaxial shearing tests with 1:1 specimens. Overview of the evaluated parameters together with the used corrections can be found in the following sections.

A1.2 Evaluated parameters

For the evaluation of the performed triaxial shear tests the following parameters were computed from the measured data summarised in Table A1–1.

Output parameters - drained test			Output parameters - undrained test		
Axial force	P	[kN]	Axial force	P	[kN]
Time	t	[s]	Time	t	[s]
Cell pressure	σ_3	[kPa]	Cell pressure	σ_3'	[kPa]
Pore pressure	u	[kPa]	Axial deformation	δ_1	[mm]
Axial deformation	δ_1	[mm]	Volumetric deformation	ΔV	[cm^3]

Table A1–1:Overview of the output parameters from the triaxial drained and undrained tests.

Effective principle stresses σ_i',

$$\sigma_i' = \sigma_i - u, \quad i = 1, 2, 3 \tag{A1.1}$$

effective volumetric stress p′,

$$p' = \frac{\sigma_1' + 2 \cdot \sigma_3'}{3} \tag{A1.2}$$

deviatoric shear stress q,

$$q = \sigma_1 - \sigma_3 = \sigma_1' - \sigma_3' \tag{A1.3}$$

shear stress τ,

$$\tau = \frac{q}{2} = \frac{\sigma_1 - \sigma_3}{2} \tag{A1.4}$$

axial strain ε_1,

$$\varepsilon_1 = \frac{\delta_1}{H_0} \tag{A1.5}$$

volumetric strain ε_v,

$$\varepsilon_v = \frac{\Delta V}{V_0} \tag{A1.6}$$

and shear strain ε_q,

$$\varepsilon_q = \frac{3}{2} \cdot (\varepsilon_1 - \varepsilon_3) \tag{A1.7}$$

where H_0 is the initial height of the specimen, u is pore water pressure, V_0 is the initial volume of the specimen, ε_3 is horizontal strain, σ_1 and σ_3 are total principle stresses and σ_1' and σ_3' are effective principle stresses.

A1.3 Area correction after consolidation and during shearing

Because of the change of the area of the sample during consolidation and shearing, the area corrections have to be applied in order to obtain accurate results. In the other words the area corrections are necessary for general routine procedure of the evaluation of triaxial shearing tests. One can find different area corrections depending on the type and shape of the specimen and the type of the failure mechanism. Several types of area corrections are given in [9, 42, 43].

Two sizes of the specimens were used by the author for the performed study - 1:1 (50x50mm) and 1:2 (50x100mm) samples. For both types of the specimens only one type of area correction was applied after consolidation,

$$A_c = A_0 \cdot \frac{1 - \frac{\Delta V}{V_0}}{1 - \frac{\Delta V}{3 \cdot V_0}} \tag{A1.8}$$

In contradiction to the previous correction two different area correction during shearing were used for the 1:1 and 1:2 specimens in the case of the drained triaxial test. The "barreling" correction (increasing area due to axial strain) was chosen for 1:2 specimens. The "barreling" correction for the drained test is given by the equation,

$$A_{drained} = A_c \cdot \frac{1 - \frac{\Delta V}{V_c}}{1 - \varepsilon_a} \tag{A1.9}$$

In the case of the drained 1:1 sample the following area correction was applied,

$$A_{drained} = A_c \cdot (1 - 2 \cdot \varepsilon_r + \varepsilon_r^2) \tag{A1.10}$$

where

$$\varepsilon_r = \frac{1}{2} \cdot (\varepsilon_v - \varepsilon_a) \tag{A1.11}$$

For the undrained triaxial tests, the "new" area of the 1:1 and 1:2 samples during shearing was computed according to the following equation,

$$A_{undrained} = A_c \cdot \frac{1}{1 - \varepsilon_a} \tag{A1.12}$$

A1.4 Piston and membrane correction

For the evaluation of the total normal stress σ_1 the correction of the influence of weight of top cap and loading ram (piston correction) was used in the following form,

$$\sigma_1 = \frac{P - \sigma_{cell} \cdot A_p + W_p + W_c}{A} + \sigma_{cell} - p_b \tag{A1.13}$$

where P is the axial force, σ_{cell} is the cell pressure, A_p is the area of the loading ram (piston area), W_p is the weight of the loading ram in kN, W_c is the weight of the top cap in kN, p_b is the back pressure and A is the corrected area during shearing.

The effect of membrane to the shear behaviour of the triaxial specimen depends on its elastic properties and its initial diameter and thickness. A lot of types of the membrane correction can be found. Detailed description of this correction can be found in [9] or [42]. The following equations were used by the author.

For the membrane correction of the axial stress $\Delta\sigma_a$,

$$\Delta\sigma_a = \frac{-4 \cdot t_0 \cdot E_m}{d_i} \cdot \left(\varepsilon_a + \frac{\varepsilon_v}{3}\right) \tag{A1.14}$$

and for the correction of the radial stress $\Delta\sigma_r$,

$$\Delta\sigma_r = \frac{-4 \cdot t_0 \cdot E_m}{3 \cdot d_i} \cdot \varepsilon_v \tag{A1.15}$$

where d_i is the initial diameter of specimen, t_0 is the initial thickness of the rubber membrane, and E_m is the modulus of elasticity of the rubber membrane at 10% extension.

Appendix 2 Evaluation of Triaxial creep tests on Glava clay

A2.1 Characterisation of the performed tests

Test no.	Depth [m]	Type of the sample	Type of the test	Consolidation pressure p_c'
1. (a, b, c)	9.48	1:1	ICD-C	100 kPa
2.	9.25	1:2	ICU-C	200 kPa
3.	9.1	1:1	ICU-C	200 kPa
4.	9.2	1:1	ICU-C	200 kPa
5.	9.6	1:1	ICU-C	Overconsolidated sample 200-400-800-600-400-200 kPa
6. (a, b, c)	9.42	1:2	ICD-C	100 kPa
7. (a, b)	9.35	1:2	ICD-C	200 kPa
8. (a, b)	9.58	1:2	ICD-C	Overconsolidated sample 100-200-400-700-400-200 kPa
9. (a, b, c)	9.1	1:2	ICD-C	Overconsolidated sample 100-200-400-200-100 kPa

Table 7–1:List of deviatoric creep tests under triaxial compression on Norwegian Glava clay performed by the author.

A2.2 Undrained deviatoric creep tests under triaxial compression

Test no.	Type of the sample	Degree of shear mobilisation at the start of the creep, f	Primary creep		Secondary creep	Duration of the creep [days]
			ε_{cp} [-]	r_{1s} [-]	ε_{cs} [-]	
2.	1:2	0.61	0.0400	168.5	-	9
3.	1:1	0.52	0.0074	543.4	0.02	9
4.	1:1	0.63	0.0100	294.5	0.03	4
5.	1:1	0.9	0.0127	163.7	0.01	3

Table 7–2:Evaluation of the undrained deviatoric creep tests under triaxial compression with the Norwegian Glava clay performed by the author.

a) Stress paths of effective stresses.

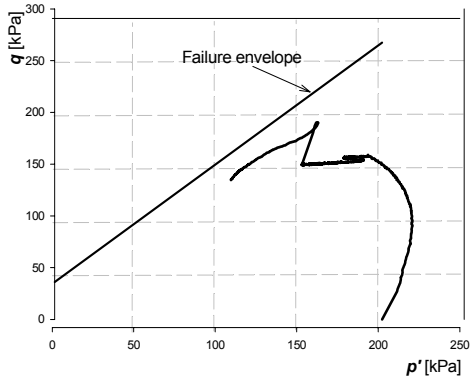

b) Deviatoric stress q vs. axial strain ε_1.

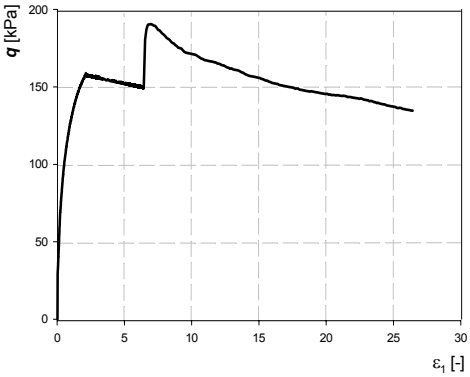

c) Pore pressure u vs. axial strain ε_1.

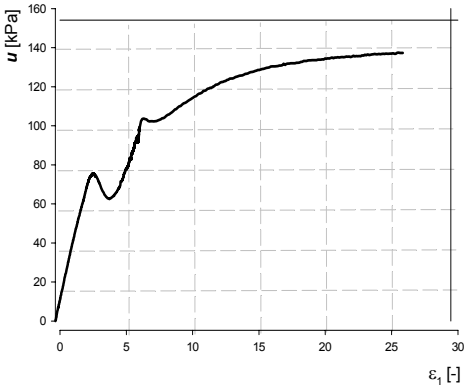

d) Development of the creep vertical strain

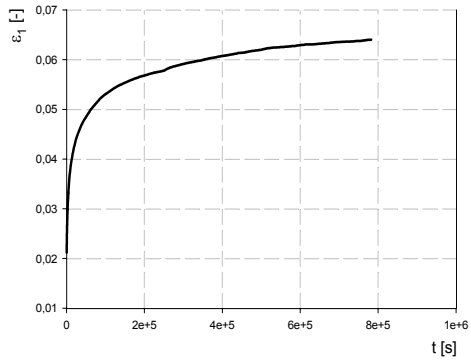

e) Development of the pore pressure with

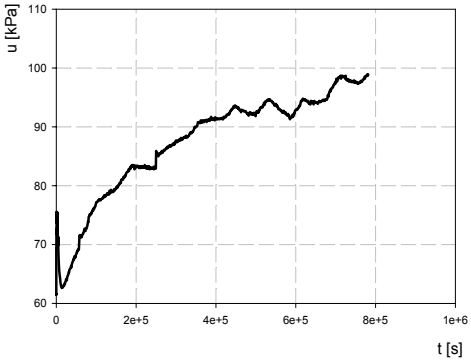

Figure A2–1: Undrained triaxial test no. 2 - representation of the general and deviatoric creep behaviour.

a) Stress paths of effective stresses.

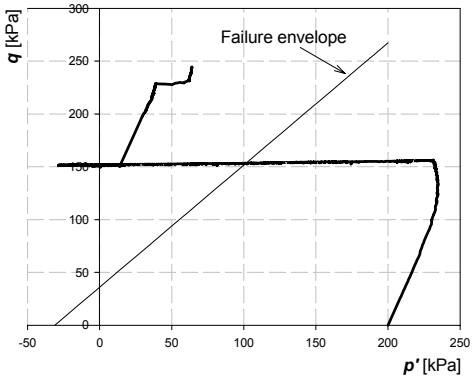

b) Deviatoric stress q vs. axial strain ε_1.

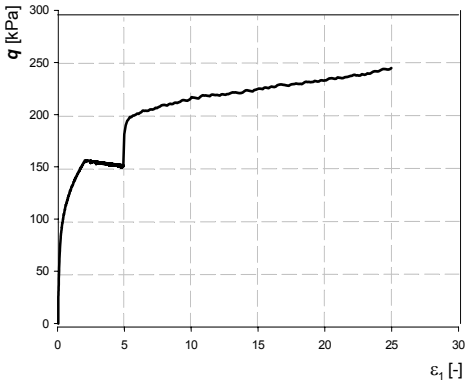

c) Pore pressure u vs. axial strain ε_1.

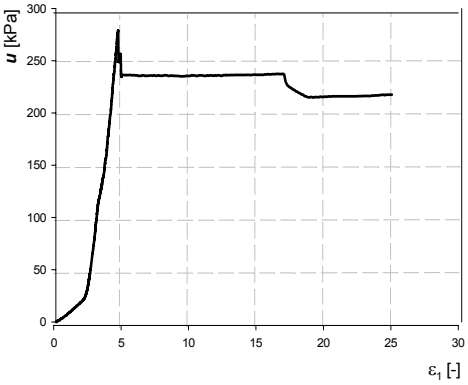

d) Development of the creep vertical strain with time for the creep phase

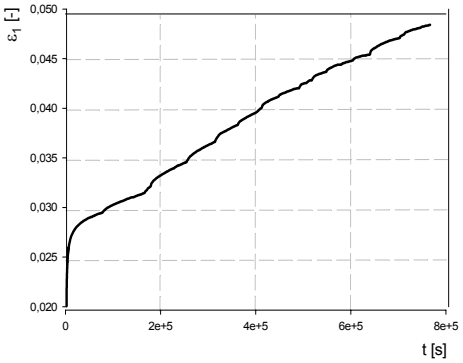

e) Development of the pore pressure with time for the creep phase

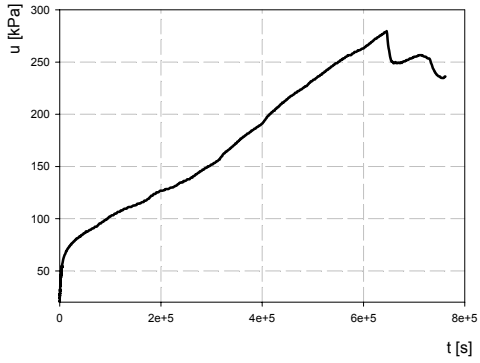

Figure A2–2: Undrained triaxial test no. 3 - representation of the general and deviatoric creep behaviour.

a) Stress paths of effective stresses.

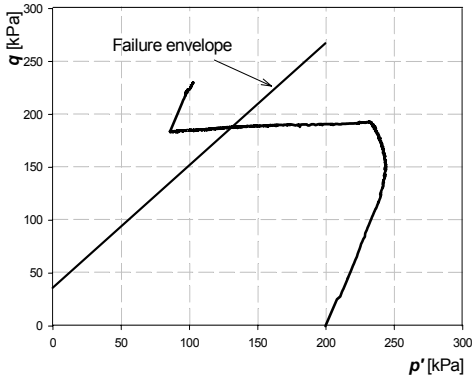

b) Deviatoric stress q vs. axial strain ε_1.

c) Pore pressure u vs. axial strain ε_1.

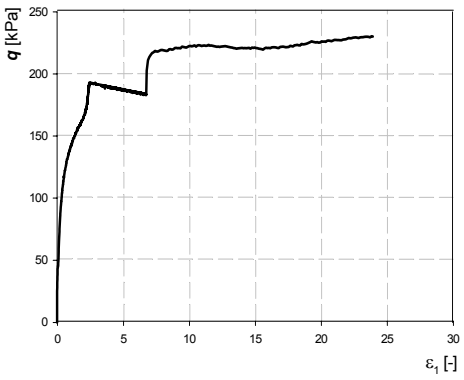

d) Development of the creep vertical strain with time for the creep phase.

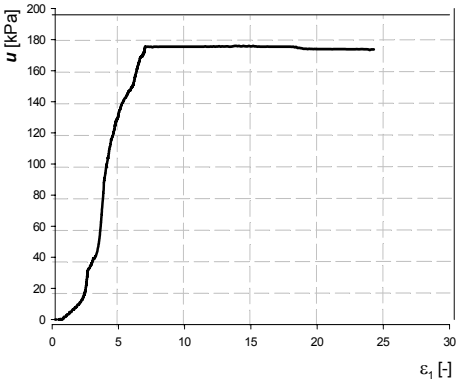

e) Development of the pore pressure with time for the creep phase.

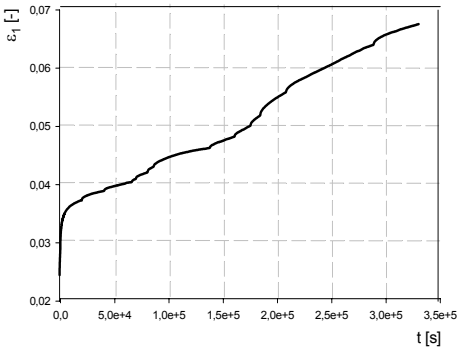

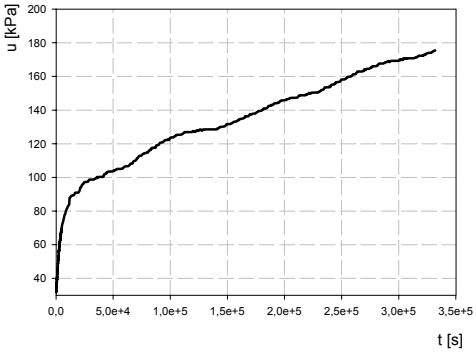

Figure A2–3: Undrained triaxial test no. 4 - representation of the general and deviatoric creep behaviour.

a) Stress paths of effective stresses.

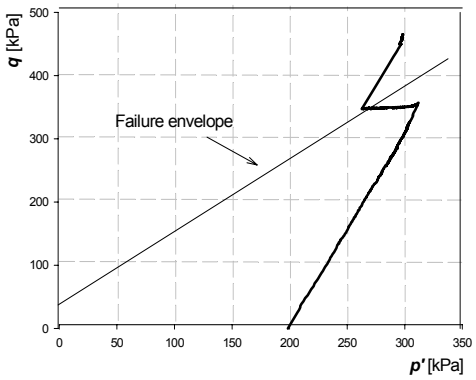

b) Deviatoric stress q vs. axial strain ε_1.

c) Pore pressure u vs. axial strain ε_1.

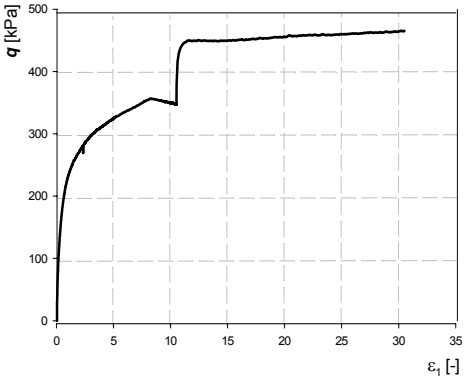

d) Development of the creep vertical strain with time for the creep phase.

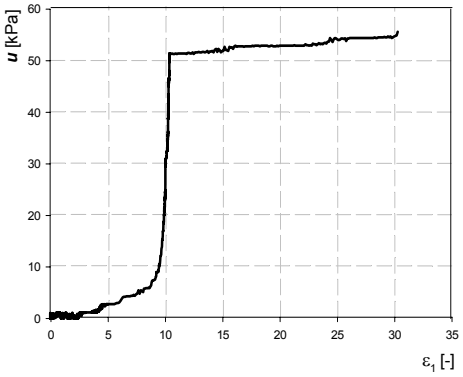

e) Development of the pore pressure with time for the creep phase.

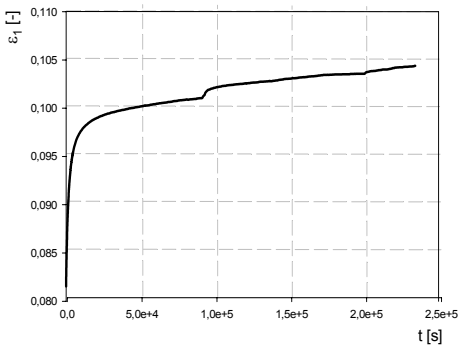

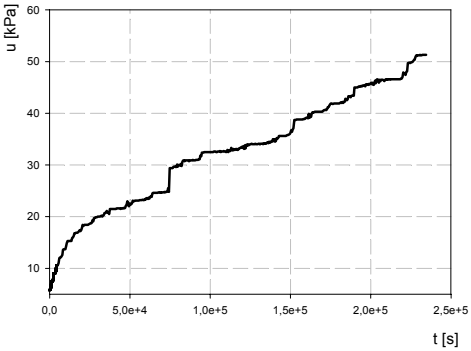

Figure A2–4: Undrained triaxial test no. 5 on over-consolidated Glava clay - representation of the general and deviatoric creep behaviour.

A2.3 Drained deviatoric creep tests under triaxial compression

Test no.	Degree of the shear mobilisation in the start of the creep, f	Volumetric creep		Deformation creep		Duration of the creep [days]
		ε_{vc} [-]	r_{sv} [-]	ε_{1c} [-]	r_{1s} [-]	
1a.	0.31	0.01	305.3	0.004	1029.2	1.5
1b.	0.64	0.015	185.6	0.0054	799	2
1c.	1.1	0.017	28.33	0.0084	486.9	3.5
6a.	0.56	0.027	18.2	0.01	472.6	2
6b.	0.68	0.03	89.7	0.02	259.3	3
6c.	0.76	0.003	268	0.02	151.2	2
7a.	0.53	0.028	28.2	0.017	452.2	6
7b.	0.69	0.036	23.6	0.025	296.8	9
8a.	0.53	0	-	0.0031	2139	1.5
8b.	0.7	0.005	572	0.01	641	3
9a.	0.4	0.0129	11	0.0021	4014	5
9b.	0.66	0.0045	779	0.0064	918.9	2
9c.	0.8	0	-	0.02	397.4	12.5

Table A2–1:Evaluation of the drained deviatoric creep tests under triaxial compression with Norwegian Glava clay performed by the author.

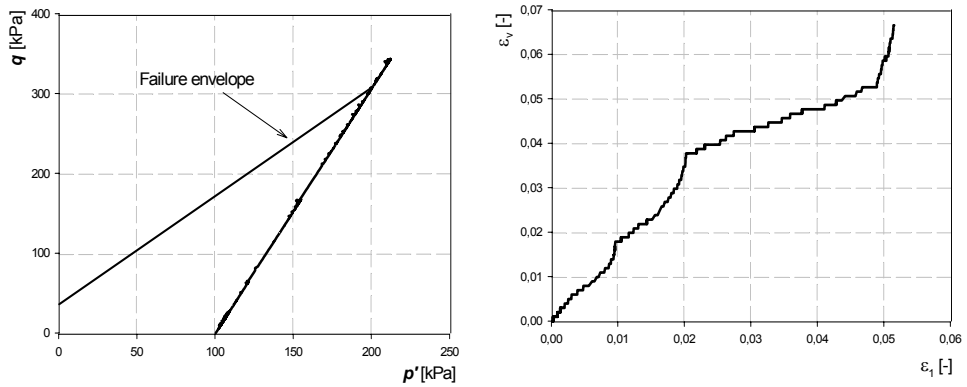

Figure A2–5: Drained triaxial test no. 1a - representation of the general behaviour.

a) Deviatoric creep behaviour - test no. 1a.

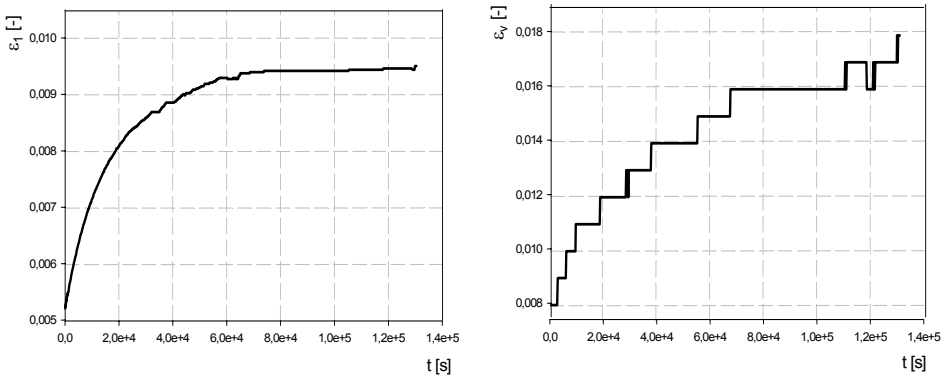

b) Deviatoric creep behaviour - test no. 1b.

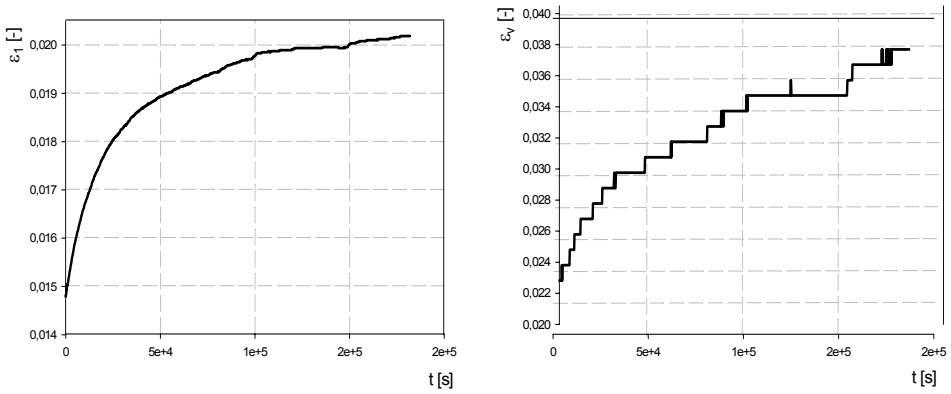

c) Deviatoric creep behaviour - test no. 1c

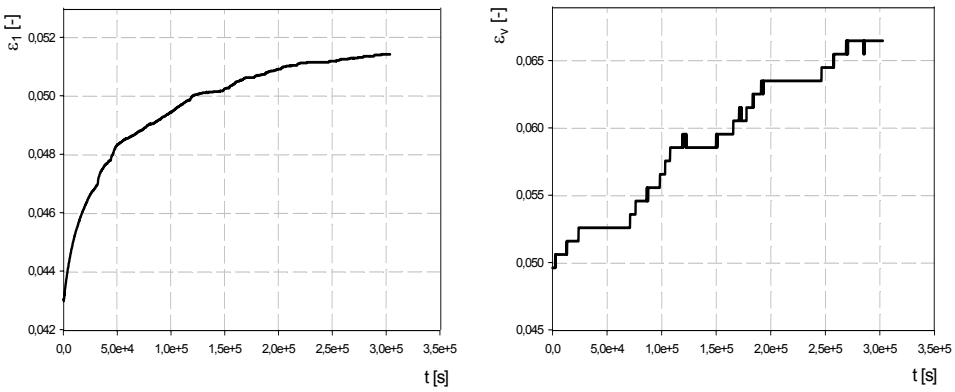

Figure A2–6: Representation of the drained deviatoric creep tests no. 1a, b, c.

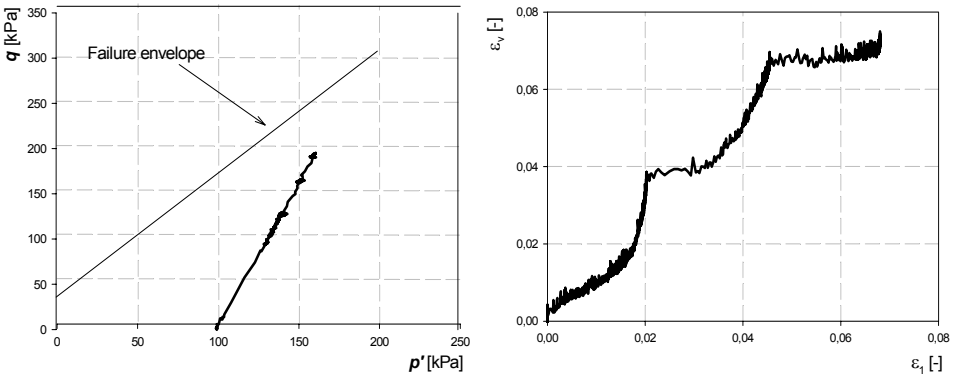

Figure A2–7: Drained triaxial test no. 5 - representation of the general behaviour.

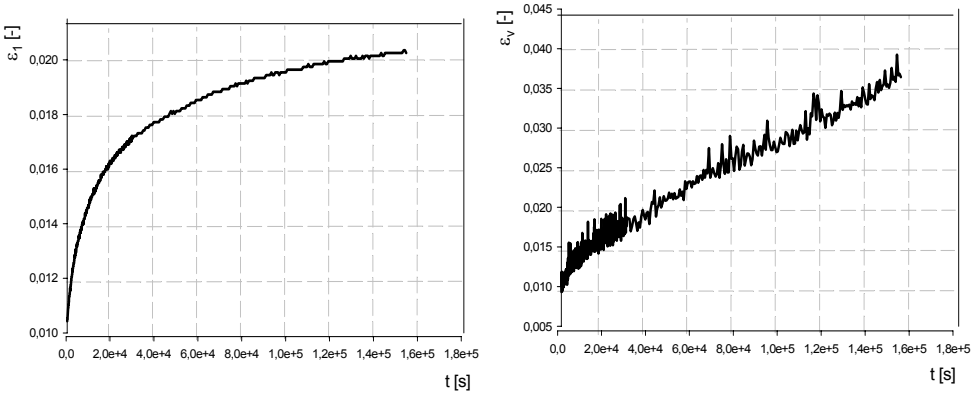

Figure A2–8: Representation of the drained deviatoric creep test no. 5a.

a) Deviatoric creep behaviour - test no. 5b.

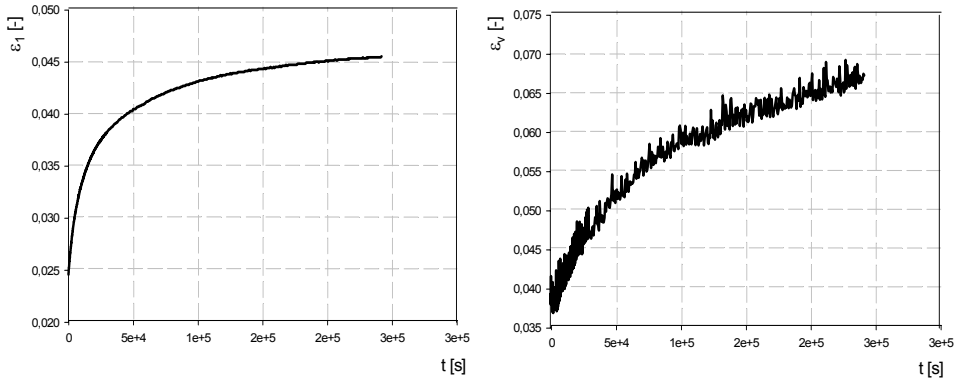

b) Deviatoric creep behaviour - test no. 5c.

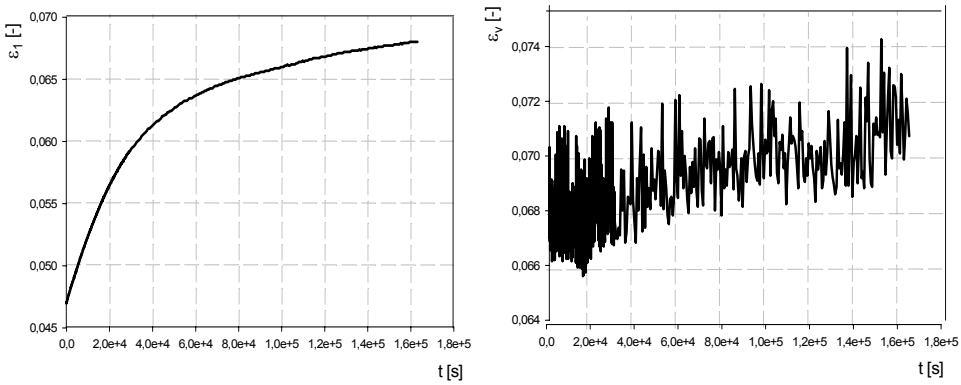

Figure A2–9: Representation of the drained deviatoric creep tests no. 5 b, c.

a) General behaviour of the test no. 6.

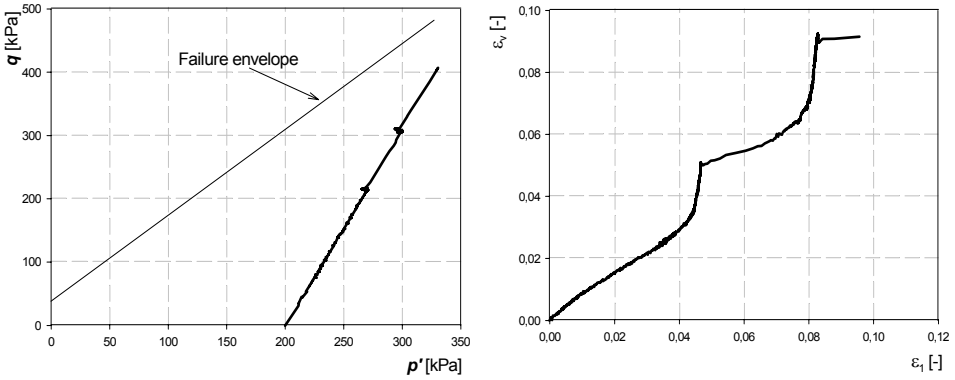

b) Deviatoric creep behaviour - test no. 6a.

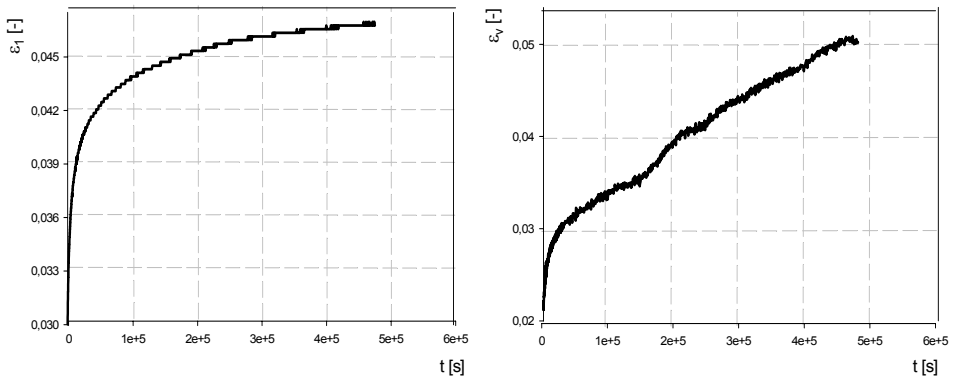

c) Deviatoric creep behaviour - test no. 6b.

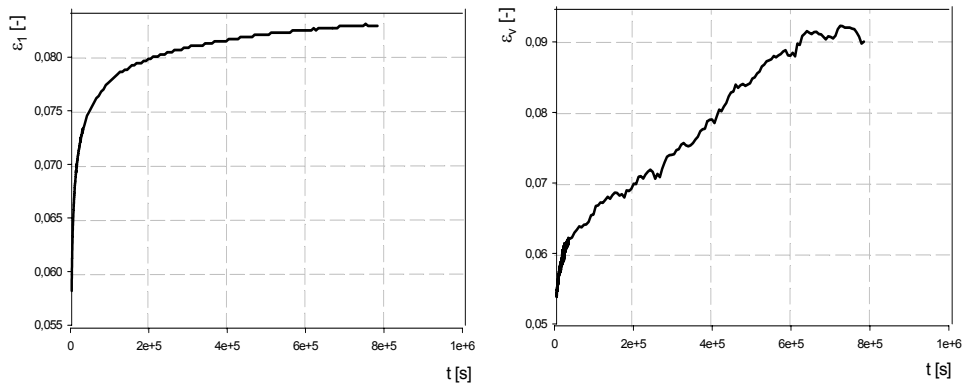

Figure A2–10: Drained triaxial test no. 6 - representation of the general and deviatoric creep behaviour.

a) General behaviour of the test no. 7.

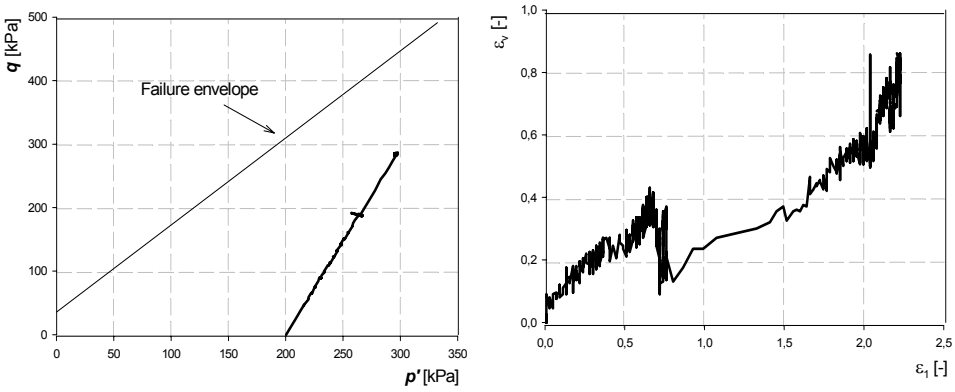

b) Deviatoric creep behaviour - test no. 7a.

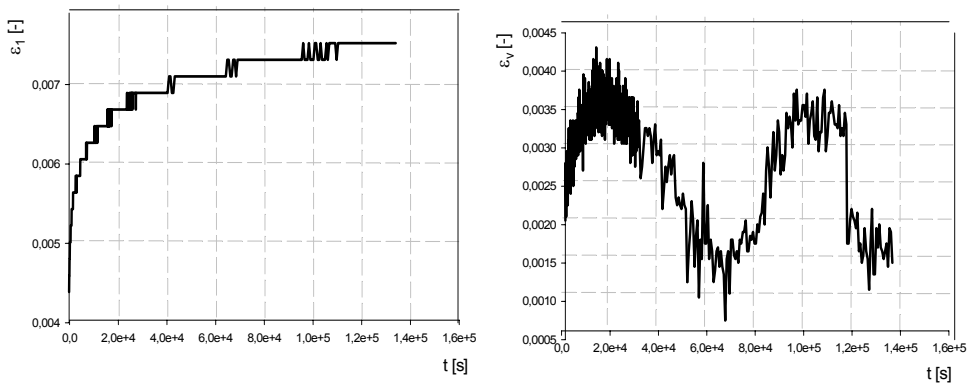

c) Deviatoric creep behaviour - test no. 7b.

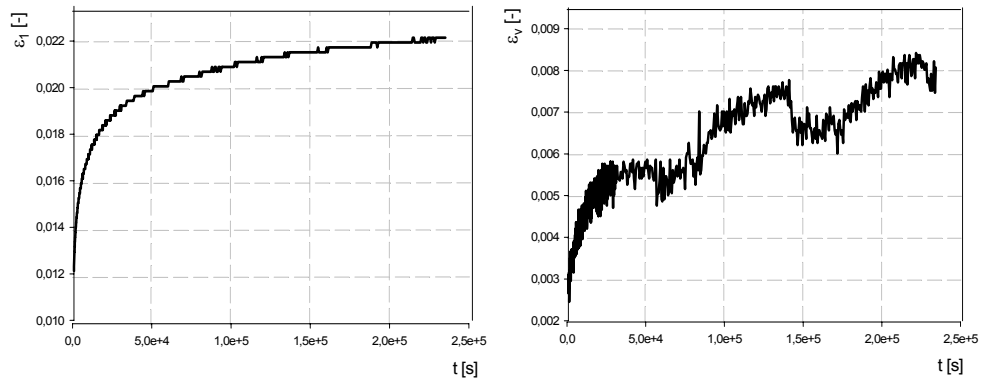

Figure A2–11: Drained triaxial test no. 7 on over-consolidated Glava clay - representation of the general and deviatoric creep behaviour.

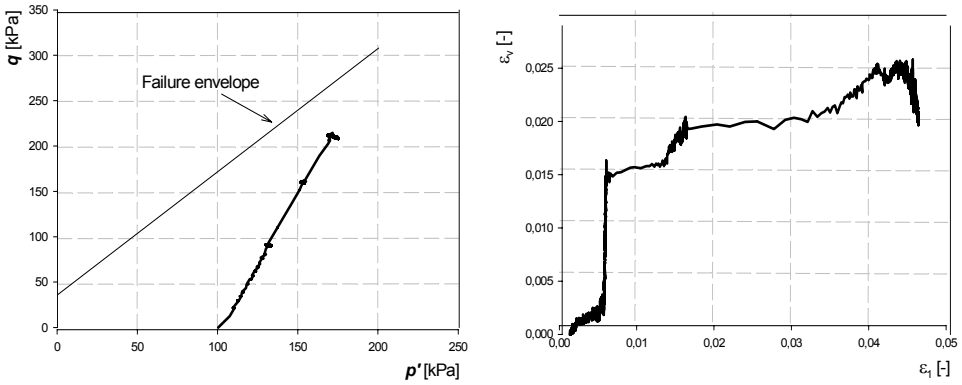

Figure A2–12: Drained triaxial test no. 8 on over-consolidated Glava clay - representation of the general behaviour.

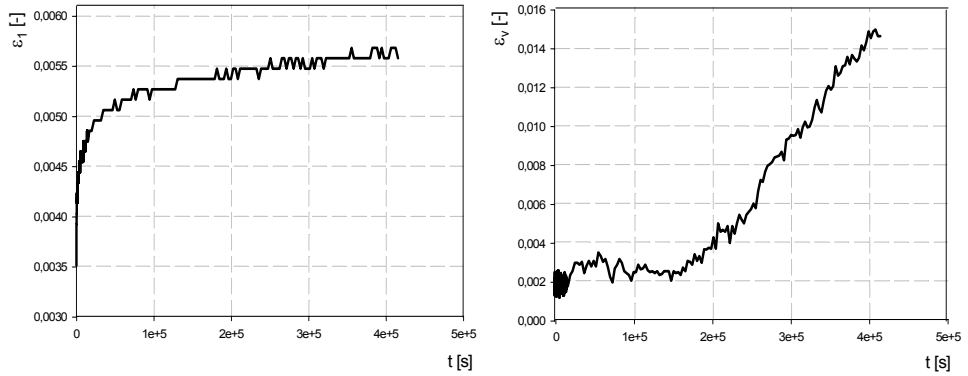

Figure A2–13: Representation of the drained deviatoric creep test on over-consolidated Glava clay no. 8a.

a) Deviatoric creep behaviour - test no. 8b.

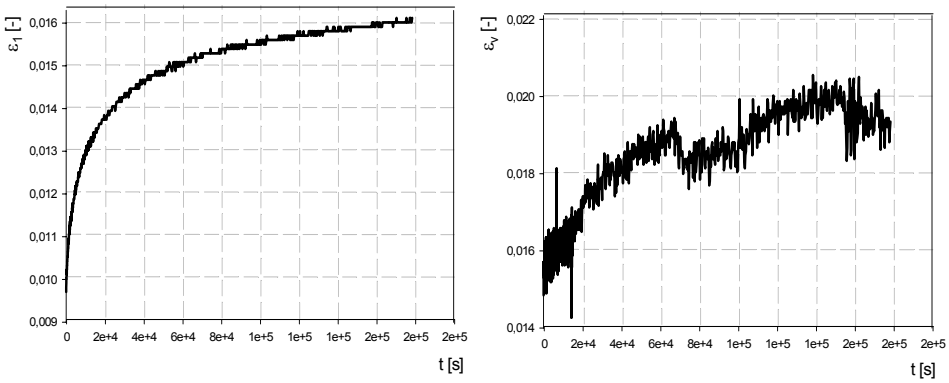

b) Deviatoric creep behaviour - test no. 8c.

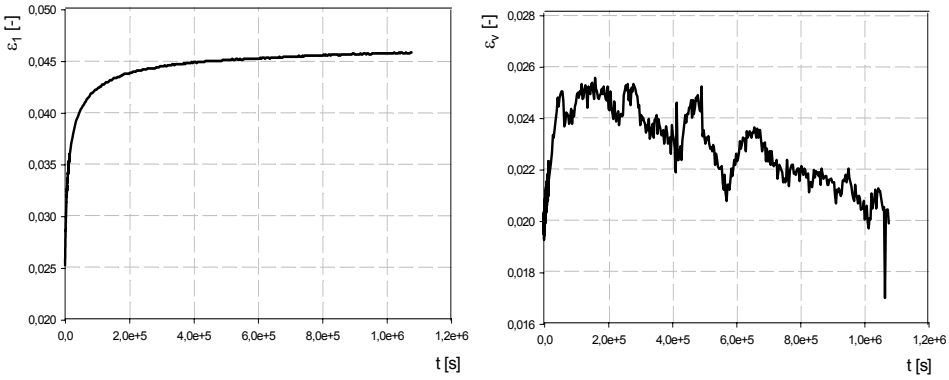

Figure A2–14: Representation of the drained deviatoric creep tests on over-consolidated Glava clay no. 8b, c.